

Research Programme of the Research Fund for Coal and Steel

Technical Group TGS3 "Casting, reheating and direct rolling"

Minimizing NOx emissions from reheating furnaces

J. Niska
MEFOS – Metallurgical Research Institute AB
Metallvägen 2, SE-974 37 Luleå, Sweden

B. Kaufmann
Voest-Alpine Stahl
Voest-Alpine Strasse 3, AT-4020 LINZ, Austria

M. Mörtberg
Air Liquide
1 Chemin de la Porte des Loges, FR-78354 JOUY EN JOSAS, France

S. Marta Almeida
ISQ
Av. Prof. Cavaco Silva Nº 33, Talaide, PT-2780 920 PORTO SALVO-OEIRAS, Portugal

E. Malfa, U. Zanusso
CSM
Via di Castel Romano 100/102, IT-00128 ROMA, Italy

H-P. Gitzinger
VDEh-BFI
Sohnstrasse 65, DE-40237 DÜSSELDORF, Germany

J. M. Fernandez
Fundacion Labein
Cuesta de Olabeaga 16, ES-48013 BILBAO, Spain

M. Fantuzzi, C. Mori
Techint
Via De Marini, 53, Torre Shipping, IT-16149 GENOVA, Italy

RFS-PR-03005

1 September 2003 to 28 February 2007

Final Report

TABLE OF CONTENTS

Page

ABSTRACT	6
1 FINAL SUMMARY	7
1.1 OBJECTIVES	7
1.2 COMPARISON OF THE ACTIVITIES WITH THE WORK ACCOMPLISHED	7
1.2.1 WP1 - LABORATORY AND PILOT TRIALS FOR AIR COMBUSTION (WITH LOW NOX BURNERS)	7
1.2.2 WP 2 - MODELLING OF NOX IN INDUSTRIAL FURNACES AND FROM BURNERS WITH VALIDATION TRIALS	8
1.2.3 WP 3 - MEASUREMENT OF NOX AND OTHER POLLUTANTS AND REVIEW OF NOX ABATEMENT TECHNIQUES	8
1.2.4 WP4 - NOX IN OXY-FUEL COMBUSTION	9
1.2.5 WP5 - MINIMISING NOX EMISSIONS BY HIGH TEMPERATURE REDUCTION (HTR)	9
1.3 DESCRIPTION OF ACTIVITIES AND DISCUSSION	10
1.3.1 WP1 - LABORATORY AND PILOT TRIALS FOR AIR COMBUSTION (WITH LOW NOX BURNERS)	10
1.3.2 WP 2 - MODELLING OF NOX IN INDUSTRIAL FURNACES AND FROM BURNERS WITH VALIDATION TRIALS	11
1.3.3 WP 3 - MEASUREMENT OF NOX AND OTHER POLLUTANTS AND REVIEW OF NOX ABATEMENT TECHNIQUES	12
1.3.4 WP4 - NOX IN OXY-FUEL COMBUSTION	13
1.3.5 WP5 - MINIMISING NOX EMISSIONS BY HIGH TEMPERATURE REDUCTION (HTR)	14
1.4 CONCLUSIONS	15
1.5 EXPLOITATION AND IMPACT OF THE RESULTS	16
2 SCIENTIFIC AND TECHNICAL DESCRIPTION OF THE RESULTS	17
2.1 WP 1 - LABORATORY AND PILOT PLANT TRIALS FOR AIR COMBUSTION	17
2.1.1 TASK 1.1. TESTING OF LOW NOX BURNER DESIGNS	17
2.1.2 TASK 1.2. OTHER LOW NOX COMBUSTION TECHNIQUES	36
2.1.3 TASK 1.3 TEST WITH FLAMELESS REGENERATIVE COMBUSTION LOW NOX BURNER (CSM)	39
2.1.4 SUMMARY	48
2.2 WP 2 - MODELLING OF NOX IN INDUSTRIAL FURNACES AND FROM BURNERS WITH VALIDATION TRIALS	48
2.2.1 TASK 2.1. INTEGRATING CHEMKIN AND INTERACTIONS WITH CFD	48
2.2.2 TASK 2.2. DEVELOPMENT AND ADAPTATION OF CFD MODEL	50
2.2.3 TASK 2.3. MODELLING FOR NOX REDUCTION STRATEGIES	50
2.2.4 TASK 2.4. MODEL VALIDATION AND REFINEMENT WITH DATA FROM REHEATING FURNACE	50
2.2.5 TASK 2.5. GENERALISED MODEL PREDICTING NOX (TECHINT)	85
2.3 WP 3 - MEASUREMENT OF NOX AND OTHER POLLUTANTS AND REVIEW OF NOX ABATEMENT TECHNIQUES	94
2.3.1 TASK 3.1: MEASUREMENT OF NOX CONCENTRATION	94
2.3.2 TASK 3.2: MEASUREMENT OF THE CONCENTRATION OF OTHER POLLUTANTS	96
2.3.3 TASK 3.3: MEASUREMENT OF FLUE GAS CHARACTERISTICS	98
2.3.4 TASK 3.4: NOX ABATEMENT TECHNOLOGY	99
2.4 WP 4 - NOX IN OXY-FUEL COMBUSTION	100
2.5 WP 5 - MINIMISING NOX EMISSIONS BY HIGH TEMPERATURE REDUCTION /HTR	114
2.5.1 TASK 5.1 INVESTIGATION OF THE PARAMETERS OF HTR	114
2.5.2 TASK 5.2. OPTIMISATION OF HTR USING CFD	120

3	ECONOMIC ANALYSIS AND CONCLUSIONS	130
3.1	OXY-FUEL VERSUS AIR COMBUSTION IN NEW FURNACES	130
3.2	OXY-FUEL REVAMPING OF FURNACES	131
3.3	CONCLUSIONS	132
4	LIST OF FIGURES	134
5	LIST OF TABLES	138
6	LIST OF REFERENCES	140

ABSTRACT

Primary NO_x reduction with low NO_x burners can be considered the Best Available Technology (BAT) for steel reheating furnaces. In fact, the results of testing and modelling flameless low NO_x burners for both high temperature air combustion (e.g. Techint TSX and VTS-NFK HRS burners) and oxy-fuel combustion (Air Liquide ALROLL-S burner) indicated that much lower NO_x emissions are possible than with traditional flame burners. This gives new opportunities to the steel industry to reduce the environmental impact of traditional furnaces, and the great potential for energy savings and reduced emissions with this technology are worth further investigations in the new RFCS project CO2RED.

NO_x emissions are strongly dependent on not only the type of furnace and equipment, but also the operational conditions (for example, the excess air, furnace temperatures and combustion air temperature). Therefore the low NO_x burner trials were made varying these major operational parameters. Reducing the excess air reduced the NO_x in general for all the types of burners tested, which is useful up to the process limitations (CO emissions, etc.) and process control accuracy (as flow measurements). Oscillating combustion gave modest NO_x reductions. Secondary NO_x removal with high temperature reduction (HTR) competes with SNCR as an alternative for NO_x removal method with ammonia after the combustion chamber, with both methods having their special advantages and disadvantages.

The NO_x predictions using FLUENT were lower than experimental data for dilute and flameless combustion, but reasonably good predictions were possible for conventional flame burners (e.g. for the furnace at Voestalpine). More complex reaction models using CHEMKIN were not successful in accurately predicting NO_x. NO_x could be predicted using an empirical neural network based program called NANO_x for NO_x in reheating furnaces.

1 FINAL SUMMARY

1.1 Objectives

The objective of this project is investigate methods to reduce NO_x emissions from steel reheating furnaces while maintaining good fuel efficiency and low CO levels for both air combustion and oxy-fuel combustion. Installation of low NO_x burners or equipment on a large steel reheating furnace can be an expensive process change, so this project helps inform steel mills about how to choose the best low NO_x system for their application and give recommendations for what other techniques could help reduce NO_x emissions. In the past, the main obstacle to reach both low NO_x and good energy efficiency had been the conflict between air preheating, the most widely used measure to increase furnaces efficiency, and the resulting increase in the NO_x emissions. Therefore increasing the energy efficiency requires technology to reduce NO_x emissions relative to traditional burners in reheating furnaces. In fact, thermal NO_x formation is controlled by flame temperature, oxygen concentration in the reaction zone and by residence time of the combustion products in the high-temperature zone of the flame. Staged combustion (air and fuel), internal flue gas recirculation (IFGR) and partially premixed combustion are techniques used in the design of present Low NO_x natural gas burners in several industrial sectors (power, petrochemical, glass, ceramic, cement). Recent developments in the basic understanding of flameless combustion [1,2,3], and progress of pilot demonstration work [4,5,6] have opened new perspectives for innovative firing technology in the steel industry.

Good results have been reached not only for reheating furnaces equipped with regenerative burners, [7,8,9,10] but also for more traditionally furnaces equipped with central recuperator [11,12,13]. This research project has included the testing and modelling of several low NO_x burner designs for both air combustion and oxy-fuel combustion, plus industrial furnace modelling, developing an empirical model of NO_x in steel reheating furnaces called NANO_x and investigating a new secondary NO_x removal technique called “high temperature reduction” or HTR.

Methods for NO_x reduction include the evaluation of new equipment, as new low NO_x burners, and modifications of the existing equipment. Implementation of new technology offers the benefits of lower emissions which gives a lower environmental impact, which are objectives specified under category Steel 3. The research work is divided into five work packages involving investigations into methods for reducing NO_x both with practical experimentation in industrial furnaces and pilot equipment, and with theory and modelling.

1.2 Comparison of the activities with the work accomplished

In this section, a comparison is made with the various tasks in the original work packages. A description and discussion of a sample of some of the project results are given in the next section.

1.2.1 WP1 - Laboratory and pilot trials for air combustion (with low NO_x burners)

Task 1.1. Testing of low NO_x burner designs (MEFOS, BFI, CSM)

Activity planned was to test several different low-NO_x-burner designs in a laboratory or pilot furnace while varying the operational conditions, for example, the air-fuel stoichiometry, furnace temperature, burner firing rate, and the air and fuel temperatures. The tests will give data about the NO_x emissions to examine and evaluate. This was accomplished by testing low NO_x burners in pilot furnaces at all 3 partners in this WP, while varying the operational conditions. BFI investigated the Hennig burner, MEFOS the VTS-NFK burner and CSM the Techint and Hauck burners.

Task 1.2. Other low NO_x combustion techniques (MEFOS)

MEFOS planned to test other interesting techniques for reducing NO_x with existing burners in MEFOS pilot furnace. One technique which was to be tested was oscillating combustion, in which the burner is fired above and below a stoichiometric fuel to air ratio to reduce the flame temperature. This was done in MEFOS chamber furnace. Oscillating combustion gave a relatively a small reduction in NO_x. Another technique investigated was flameless combustion produced by fuel lancing or direct fuel injection (DFI) by modifying the traditional burner at MEFOS. The tests confirm the very low NO_x

emissions of the flameless technology, which is available in commercial burners tested in this project, such as the VTS-NFK HRS burner and Techint TSX burner.

Task 1.3. Tests with flameless regenerative combustion low NO_x burners (CSM)

CSM planned to test a commercial flameless regenerative low NO_x burner, including guidelines for their installation in a reheating furnace, and a comparison of different types of burners to understand their differences in NO_x abatement efficiency. There was difficulty obtaining the Bloom burner selected as representative of the state of the art for this technology, so tests were made with an FBB regenerative burner at CSM. The tests investigated the effect of different fuels as NG (BFI and CSM) and COG (BFI) together with the effect of the combustion chamber geometry and size. A comparison of the data obtained from the FBB burner trials with the data in the literature for regenerative burners using flameless combustion with combustion air preheated to 1000 °C confirms the superiority of flameless combustion for minimizing NO_x.

1.2.2 WP 2 - Modelling of NO_x in industrial furnaces and from burners with validation trials

Task 2.1. Integrating CHEMKIN and interactions with CFD (LABEIN)

Calculating NO_x formation based on the chemical kinetics of combustion using CHEMKIN was planned in this WP. A reaction scheme proposed by LABEIN was tested by CSM for modelling the TSN and TSX burners (GRI Mech 3.0). LABEIN tested the ÅA reaction scheme for modelling oxy-fuel combustion. These schemes can simulate the reaction of gaseous mixtures that contain C1-C2 hydrocarbons, including the conversion of NO_x via thermal, prompt, N₂O-intermediate, and fuel mechanisms. The temperature and velocity field obtained are close to those obtained with the simple 2-step mechanism, moreover the NO_x emissions were overpredicted for the GRI mechanism.

Task 2.2. Development and adaptation of CFD model (LABEIN, VA, MEFOS, BFI plus CSM)

CFD models were planned at LABEIN, Voestalpine, MEFOS and BFI for use in predicting NO_x. All partners developed CFD models, plus CSM made CFD models for the Techint burners. Some modelling results are given in the next section and a complete review in the full report in the appendix.

Task 2.3. Modelling for NO_x reduction strategies (LABEIN)

Modelling for NO_x reduction strategies was planned at LABEIN. Technical support was given to Voestalpine in their reheating furnace modelling.

Task 2.4. Model validation and refinement with data from reheating furnace (All WP partners)

The data collected from the trials in the other WPs and the trials at Voestalpine were to be compared with the modelling results to validate the models. NO_x measurements were made in for the tests at all the partners in this WP, including species and temperature traverses of the CSM pilot furnace. The NO_x predictions using the FLUENT NO_x model were lower than the experimental results for flameless combustion, but approximately correct for NO_x in flames in the work at Voestalpine. Modelling NO_x with a pdf NO_x model gave too high NO_x predictions.

Task 2.5. Generalised model predicting NO_x (Techint)

Techint planned to develop and test an empirical NO_x model. This was accomplished using neural networks which were trained on NO_x data from reheating furnaces. The final version of the neural networks analysis was carried out in cooperation with the DIBE (Dipartimento di Biofisica ed Elettronica) of the University of Genova. The final NANO_x model was implemented including the new theoretical algorithms developed with DIBE.

1.2.3 WP 3 - Measurement of NO_x and other pollutants and review of NO_x abatement techniques

Task 3.1. Measurement of NO_x concentration (All WP partners plus AL)

The objective of this work package task was to perform NO_x concentration measurements, during the trials performed within the scope of this project, and supply relevant and reliable data that allowed subsequent modelling work. All the partners in this WP were involved in NO_x measurements. Table 1

presents the measurements performed by ISQ during NOx project for various trials. Plus Air Liquide made NOx measurements during the WBF trials at MEFOS.

Table 1. Measurements performed by ISQ and measured pollutants.

Partner	Date	Place	Measured pollutants
Voest-Alpine	February 2005	Slab reheating furnace no 6	NOx, CO, CO2, O2 and SO2
CSM	March 2005	Pilot furnace during tests with the Hauck TRIOX burner	NOx, CO, CO2, O2 and SO2
BFI	January 2006	Experimental HTR combustion chamber	NOx, CO, CO2, O2, SO2, TSP and heavy metals
CSM	December 2006	Pilot furnace	NOx, O2

Task 3.2. Measurement of the concentration of other pollutants (ISQ, VA, MEFOS)

Other combustion gas pollutants were also of interest, so other gases as CO, and NH3 or ammonia were of interest. The ammonia slip was measured for the HTR trials at BFI as presented in WP5. The CO concentrations were typically measured together with the NOx and oxygen concentrations for the burner trials. Heavy metals were also of interest, and these were measured at BFI for coke oven gas.

Task 3.3. Measurement of flue gas characteristics (ISQ)

The flue gas characteristics were to be measured in the industrial trials at Voestalpine. Industrial trials were made at Voestalpine in 2005 and pilot trials at BFI.

Task 3.4. NOx abatement technology (MEFOS plus ISQ)

A review of NOx abatement technology was planned for primary and secondary NOx reduction. ISQ joined this task and drafted a review available as an appendix. Installation of low NOx burners are one of the best primary NOx reduction methods for obtaining a large reduction in NOx, with low operating costs. Secondary NOx removal with ammonia in SCR or SNCR can give large reductions in NOx, but with higher operating costs than low NOx burners.

1.2.4 WP4 - NOx in oxy-fuel combustion

Task 4.1. Furnace adaptation for full oxy-firing (AL, MEFOS)

Conversion of the continuous walking beam furnace (WBF) at MEFOS to 100 % oxy-fuel firing was planned. This was accomplished by the installation of ALROLL-S oxy-fuel burners and a SAFMATIC furnace control system from Air Liquide.

Task 4.2. Trials and low-NOx oxy-combustion technology evaluations (AL, MEFOS plus BFI)

Trials with oxy-fuel combustion were planned with different operating parameters to investigate both NOx emissions and the reheating performance of oxy-fuel combustion. This was done in two series of trials in which the NOx was found to be very low for these new ALROLL-S burners and the furnace capacity was increased (see the discussion). BFI joined this task with tests of the oxy-fuel burner with other fuels in their furnace.

Task 4.3. Furnace air leaks control (AL, MEFOS)

Air infiltration was thought to be a potential problem, so a task written to allow time to solve it. The problem of air infiltration was solved by increasing the furnace pressure and using a frequency controller for the exhaust fan, so more advanced solutions to the problem were not required. Originally it was thought that modifications to the charging or discharging door system could be required.

1.2.5 WP5 - Minimising NOx emissions by high temperature reduction (HTR)

Task 5.1. Investigation of the parameters of the HTR procedure on an experimental combustion chamber (BFI, ISQ)

Pilot scale trials with the HTR procedure were planned at BFI, and these were done together with emission testing by ISQ. There were difficulties getting the equipment to initially perform properly, including the selection of a proper mixing device for the ammonia and the exhaust gases.

Task 5.2. Optimisation of HTR by using CFD calculation results (BFI plus LABEIN)

CFD analysis was proposed as a method for analysing how to optimise the HTR process. A simpler approach was found to be the use of CHEMKIN reactors in research together with LABEIN to analyse the HTR process.

Task 5.3. Scale up and calculation of the HTR procedure for a reheating furnace (BFI)

Retrofitting existing furnaces with HTR was proposed as a method to reduce NOx with low investment and operating costs. An estimate was made for the NOx reductions and the costs of the HTR process. The HTR process competes with conventional SNCR with the use of ammonia to remove NOx, and both secondary NOx removal techniques have their advantages and disadvantages discussed in this report.

1.3 Description of activities and discussion

1.3.1 WP1 - Laboratory and pilot trials for air combustion (with low NOx burners)

A comparison was made of the NOx emissions of the different burners tested and other techniques in this WP and with working conditions representative of modern reheating furnaces equipped with central recuperator. The results clearly indicate that flameless burner technology is presently the Best Available Technology (BAT) for primary NOx reduction technology. This can be demonstrated with the series of trials from CSM, BFI and MEFOS. The Techint TSN10, Techint TSX12 and Hauck TRIOX 2008 lateral burners were all tested at CSM, the Hennig burner at BFI and the VTS-NFK HRS burner at MEFOS. They can be classified as proposed in Table 2: A traditional flame burner (Hennig), a burner with air staging operating with a flame (Hauck TRIOX with 60/40 mode), burners with high impulse air jets that dilute the combustion air or give IFGR (Techint TSN and Hauck TRIOX with 90/10 mode) and burners that can operate in the flameless combustion regime (Techint TSX and VTS-NFK HRS). This is shown in Figure 1. The NOx increases with the excess oxygen for all these types of burners, but the flameless burner is the best of these burner designs for equivalent operating conditions.

Table 2. Classification of side burners for reheating furnaces equipped with a central recuperator.

.....-1980 1990-2000 2000- ???

Traditional Flame Burner		High impulse burner		Flameless burner	
<ul style="list-style-type: none"> ● Light up at cold furnace ● On / off & modulation ● Anchored Flame 		<ul style="list-style-type: none"> ● Light up at cold furnace ● On / off & modulation ● Lower NOx emissions 		<ul style="list-style-type: none"> ● Flame AND Flameless ● Light up at cold furnace ● On / off & modulation ● Ultra Low NOx emissions ● Flameless Turn down 	
<ul style="list-style-type: none"> ● No air staging ● <u>Visible & Stable Flame</u> 		<ul style="list-style-type: none"> ● Separate air /fuel staging ● <u>Diluted combustion</u> 		<ul style="list-style-type: none"> ● Coupled staging (air & gas) ● <u>Flameless Combustion</u> 	
<ul style="list-style-type: none"> ● Single air piping ● NO valve on hot air 		<ul style="list-style-type: none"> ● Double air piping ● Valve on hot air 		<ul style="list-style-type: none"> ● Single air piping ● NO Valve on hot air 	

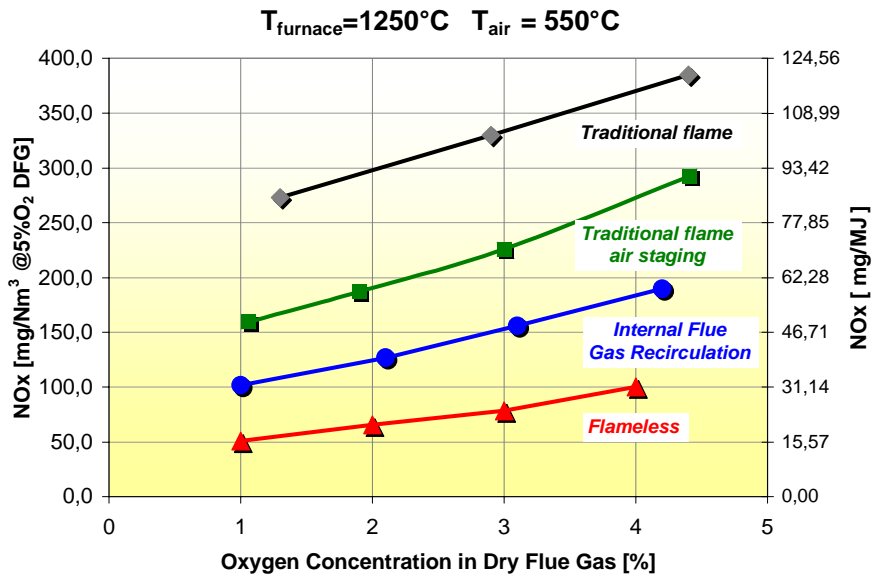


Figure 1. Typical NOx emissions from side burners for reheating furnaces equipped with a central recuperator based on the research at CSM.

1.3.2 WP 2 - Modelling of NOx in industrial furnaces and from burners with validation trials

NOx modelling was done with CHEMKIN, FLUENT and a new empirical model called NANOx. The use of the FLUENT NOx model generally predicted lower NOx than the experimental measurements for low NOx burners. An example of a comparison between calculated and measured NOx is shown in Figure 2 for the TSN burner at CSM, which shows an increase in NOx for both experiments and modelling with increasing excess oxygen and furnace temperature. The NOx predictions were always lower than expected, which confirms the limitation of the FLUENT NOx model in the case of diluted combustion. In summary, FLUENT can predict the NOx variation trends, but an accurate quantitative NOx value cannot be expected.

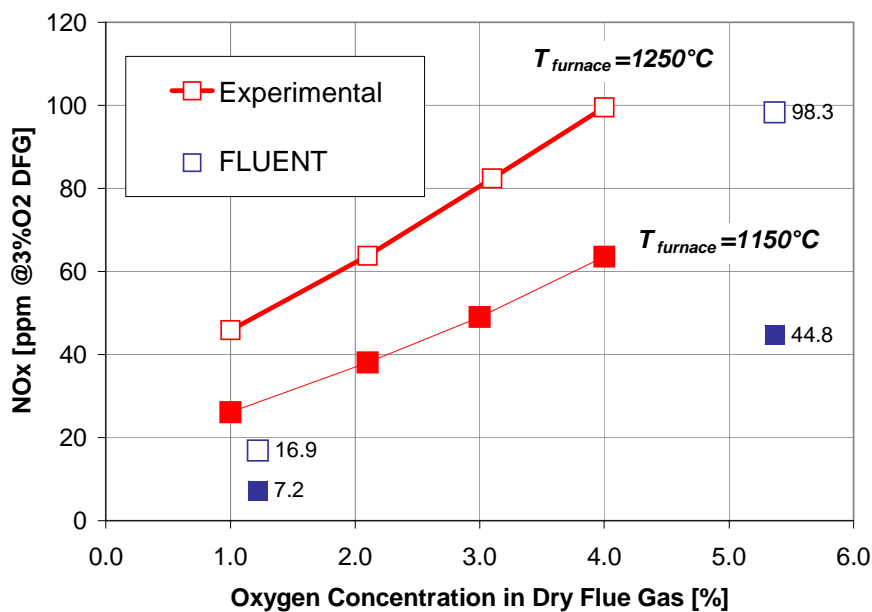


Figure 2. TSN burner NOx emission: experiment vs. modelling.

One way to overcome the limitation in the NO_x prediction by CFD was to correlate the peak furnace temperature calculated with CFD together with the experimental NO_x measurements, assuming most of the NO_x is due to thermal NO_x. This gave a curve with better fit to the experimental NO_x data than the CFD calculations.

The NO_x calculated for the oxy-fuel burner was also typically lower than experimental results, with the added problem of how to best simulate the infiltration of air. Without the presence of air and nitrogen there is essentially no NO_x possible oxy-propane combustion, since both the propane and oxygen have essentially no nitrogen. Natural gas can have nitrogen. The NO_x was typically low, for example, the NO concentration in flue gases with natural gas was calculated to be 17 ppm (on a dry basis), which is equivalent to 1.1 mg/MJ with a burner load of 100 %. In the experimental trials with natural gas for those conditions, the minimum NO_x obtained was on the order of 4 mg/MJ, which is 4 times more than predicted by the simulation.

1.3.3 WP 3 - Measurement of NO_x and other pollutants and review of NO_x abatement techniques

The measurement data was typically included in the other WPs. Both chemiluminescence and non-dispersive IR adsorption (NDIR) gave good NO_x measurements during the various trials.

The literature review in task 3.4 is available as a separate report, with a summary is given in the long description of the results and in Table 3.

Table 3. NO_x reduction (average %) for selected techniques with their advantages and disadvantages.

Abatement technique (% NO _x reduction)	Advantages	Disadvantages
Low Excess Air (5-15 %)	Lower fuel costs Easy to implement	Limited NO _x reduction Risk for smoke
Reburning of NO _x (30-60 %)	No catalysts required gives lower costs than SCR	Fuel rich reburn zone required
External flue Gas Recirculation (FGR) (30-50 %)	Usable with other NO _x controls No new burners Moderate investment cost	Lower fuel efficiency Flame instability and soot formation sometimes
“Flame” or staged low NO _x Burners (40-60 %)	Low operating costs	Capital costs of new burners Staged LNB are best for gas firing
Flameless low NO _x burners (WP1 up to 80 %)	Low operating costs Better temperature uniformity	Capital costs of new burners and equipment
Combustion tempering (20-25 %)	Water injection has low capital costs and can be combined with SNCR	Higher fuel costs
Burners Out Of Service or biased (10-15 %)	Simple to implement	High CO from fuel rich burners
SNCR (45-70 %)	Simple installation and operation Low operating costs versus SCR	NH ₃ slip and slow reaction rates versus SCR Proper temperature and % O ₂ required
SCR (75-95 %)	High NO _x reduction	High costs Optimum temperature window required
High temperature reduction (HTR) (up to 60 % see WP5)	Simple installation and operation Low operating costs versus SCR	Reducing atmosphere required

The goal of this project was to investigate methods for NO_x reduction which would maintain a good fuel efficiency and still have low CO or noxious emissions. Some effective NO_x reduction methods do not meet this goal, including combustion tempering with water injection and external flue gas recirculation. Flameless low NO_x burners meet the project goal of providing low NO_x with good energy efficiencies. There are several post-combustion low NO_x technologies which can be used that also meet this goal, including SNCR and HTR), but these require the use of a chemical to reduce the NO_x which adds to the operating costs but they can have lower capital costs than low NO_x burners. The overall costs of NO_x reduction required need to be considered for a specific installation, so that a combination of NO_x reduction methods given in the table above can give the overall lowest total costs (investment costs and operating costs).

1.3.4 WP4 - NO_x in oxy-fuel combustion

The ALROLL-S oxy-fuel burner utilizes a combination of staged and separated jets injection of the fuel and the oxygen to give low NO_x, and it has a large flexibility and can be used with several types of gaseous and liquid fuels. The ALROLL-S burner was tested firing propane in the WBF at MEFOS and firing natural gas and coke oven gas in the experimental furnace at BFI.

A comparison of the NO_x and O₂ levels for the air combustion and the oxygen combustion were made. The results indicate a significantly higher NO_x emission level during the air combustion case compared to the oxygen combustion case. During the air case an average of 83 mg/MJ was measured as compared to 12 mg/MJ during the oxygen case. Figure 3 shows a detailed analysis during a shorter time period of the flue gas sampling. The graphs reveal the sensitivity of the oxy-burners for air infiltration. An immediate effect can be distinguished on the concentration graphs. In this figure the CO₂, O₂ and the NO_x are presented. The data shows clearly the influence of the charge and discharge of slabs, thus the opening and closing of the furnace doors, with the associated air leakage in to the furnace. During stable operation the NO_x levels reached 9 mg/MJ of fuel input with the furnace doors closed. During the sampling period the oxygen concentration in the flue gases was 6 % and the CO₂ concentration on an average 58 %.

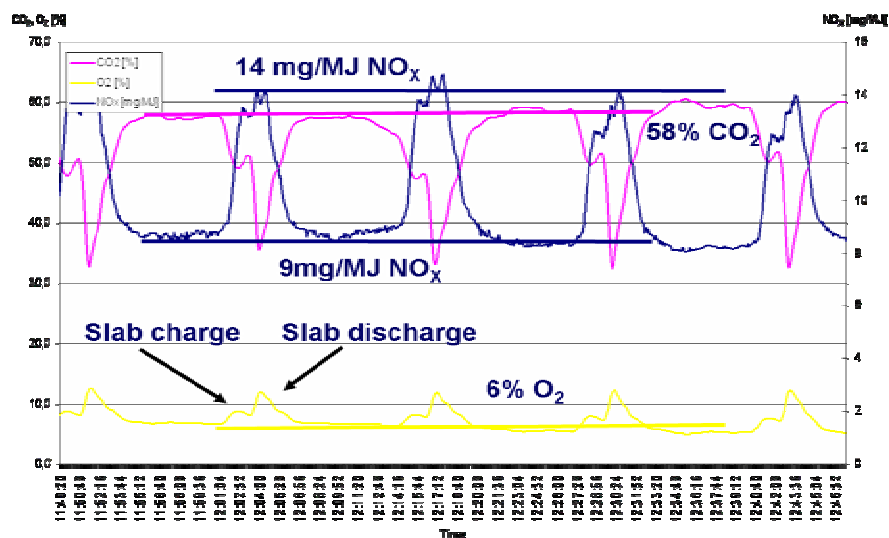


Figure 3. NO_x, CO₂ and oxygen in the flue gases sampling during oxy-fuel trial in the WBF.

Some of the results of tests at BFI with the ALROLL-S burner are shown in Figure 4, which shows the NO_x data in mg/MJ for natural gas with a burner load of 100 %. The NO_x emissions were measured for various oxygen concentrations in the flue gases and furnace temperatures. The NO_x levels in both 80 % and 100 % burner power with natural gas gave NO_x under 10 mg/MJ for all the cases examined during the natural gas trials. The NO_x levels with similar trials using coke oven gas gave NO_x under 20 mg/MJ for all the examined cases. The higher NO_x emissions with COG versus natural gas were anticipated due to the nitrogen content of the fuel. The NO_x levels increased with increased air infiltration, as expected.

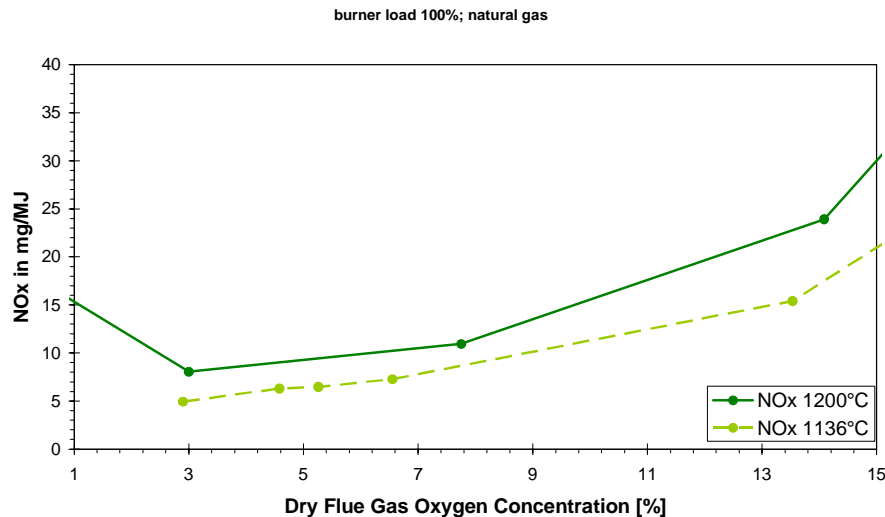


Figure 4. NO_x with the ALROLL-S burner at BFI firing natural gas (note that for oxy-fuel the NO_x is reported in mg NO_x/MJ).

1.3.5 WP5 - Minimising NO_x emissions by high temperature reduction (HTR)

All experiments with HTR were done at BFI inside their experimental furnace. Measurements were performed inside the furnace chamber at P1; after ammonia addition at P2 and in flue gas before stack at P3. Extensive tests were done at various flue gas temperatures and types of additive injection. Figure 5 shows the results of the measurements of the efficiency of the HTR method with nozzle injection of the additive using 2 lances, a flue gas temperature of 1000 °C and different additive amounts chosen. A static mixer leads to a fast and homogeneous mixing of the additive and flue gases in the area of the HTR zone. The NO_x concentration decreases after additive injection - for all marginal conditions - with an increasing amount of additive. The very high NO_x reduction that can be achieved at over-stoichiometric additive amounts (mol ratio > 1.2) cannot, however, be technically used. Unfortunately, new NO_x is produced by the reaction of the excess additive and oxygen of excess air in the post-combustion area that is always needed with staged combustion for prevention of CO emissions.

The ammonia slip measured was negligible in all tests at or below 1 mg/m³. The NO_x concentrations in the area of the stack were only slightly dependent on the amount of additive and when converted to ppm NO_x at 0 % oxygen, and they amounted to around 75 % of the NO_x- concentration in the combustion chamber. Figure 6 summarizes the results of all the measurements and compares the NO_x emissions for air-staged combustion (mol ratio=0) with the reduced NO_x emissions that can be achieved by using the high temperature reduction procedure at various additive amounts (molar ratio). The procedure can be used over a wide range of temperatures (at least 1000 °C to 1200 °C and higher) and achieves its greatest efficiency with a slightly over-stoichiometric use of additive (molar ratio approx. 1.2). Based on initial NO_x emission values of 380 to 460 mg/m³, the tests proved that the emissions could be reduced to 250 or 300 mg/m³. This corresponds to a mean NO_x reduction of 35 %. Based on the original initial NO_x emission value (670 mg/m³) of the test furnace in combination with the staged combustion - which decreases the initial emission value about 35 % - a total reduction of 60 % was achieved.

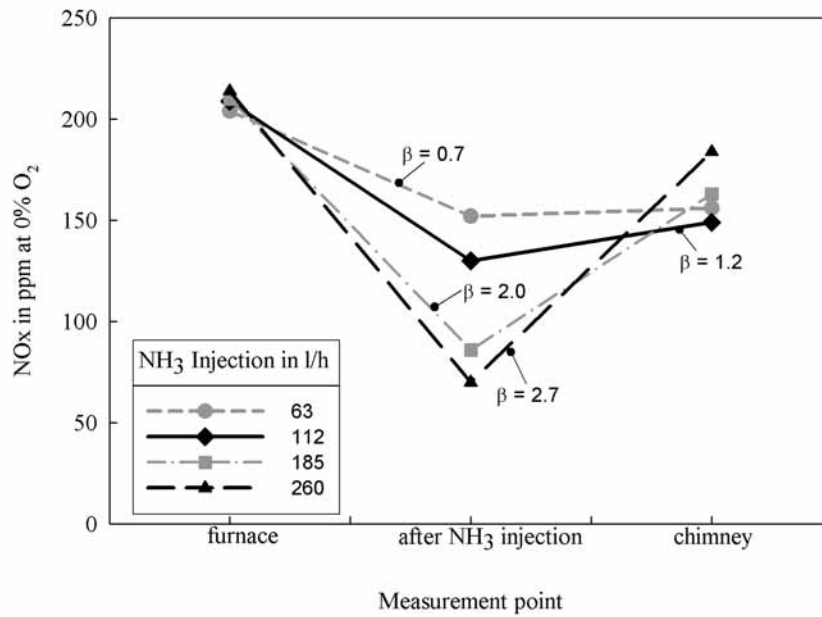


Figure 5. Effect of the high temperature reduction and the post combustion at different additive molar ratios ($\beta = \text{NH}_3 / \text{NO}$) for the additive injection with two lances at 1000 °C.

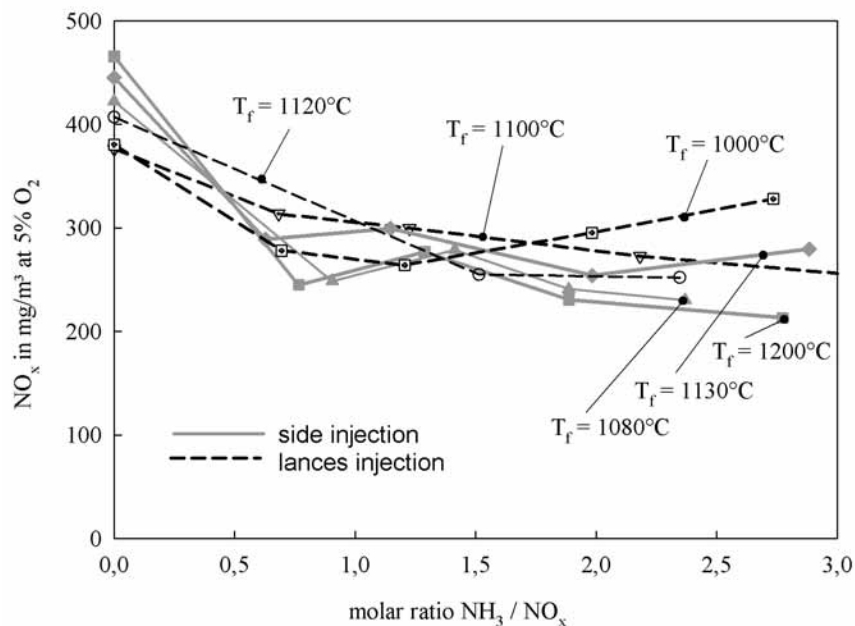


Figure 6. Summary of the total high temperature reduction results (furnace-chimney) with different temperatures and molar ratios.

1.4 Conclusions

Primary NO_x reduction methods in the furnace offer NO_x reduction with low operating costs. Flameless low NO_x burners for both high temperature air combustion and oxy-fuel combustion were tested and modelled to give much lower NO_x than traditional flame burners, and thus give the potential for energy savings and reduced emissions. Flameless high temperature air combustion burners tested were the Techint TSX and VTS-NFK HRS burners, and for flameless oxy-fuel combustion, the Air Liquide ALROLL-S burner. Flameless technologies provide the best available technologies (BAT) for low NO_x burners and primary NO_x reductions. Legislation in Europe should allow for the use of mg NO_x/MJ as an alternative to concentration in mg NO_x/Nm³ to limit the maximum NO_x emissions for oxy-fuel combustion, since the concentration of NO_x can be much higher in the exhaust gases of oxy-fuel combustion than air combustion, yet the mg NO_x/MJ, or tons of NO_x per year or grams of NO_x/ton steel can be lower than air combustion.

Other primary NO_x reduction methods as lower excess air combustion and oscillating combustion were also tested. Reducing the excess air will reduce the NO_x in general for all the types of burners tested, which is useful up to the process limitations (CO emissions in the exhaust gases or surface quality problems due to adhesive scale) and process control accuracy (by flow measurements or gas analysis). Oscillating combustion gave modest NO_x reductions. Secondary NO_x removal with high temperature reduction (HTR) competes with SNCR as an alternative for NO_x removal method with ammonia after the combustion chamber, with both methods having their special advantages and disadvantages.

1.5 Exploitation and impact of the results

The presence of three industrial partners (Voestalpine, Air Liquide and Techint) together with the five research centres (ISQ, CSM, MEFOS, BFI and LABEIN) makes exploitation of the results and commercialization important. Plus, each of the partners have had the opportunity to exploit the results of their own work within their own organisations. This exploitation has included the selection of the specific items used in the research and the focus: MEFOS chose a low NO_x propane burner from VTS-NFK, since furnaces in the Nordic countries typically use oil or propane and VTS is a Swedish company, CSM chose low NO_x natural gas burners from Techint which is a large Italian manufacturer of furnaces and burners, and BFI chose low NO_x natural gas burners from FBB and Hennig which are German companies. The results then can help the local manufacturers to either market a high performance burner, or improve their product to make it more competitive with other burners. The results of the Techint burner tests at CSM could be used for marketing purposes by Techint. Techint was not only a burner supplier for the project, but Techint also developed a neural network based NO_x model for reheating furnaces called NANO_x. The NANO_x program and the problem of predicting NO_x for new furnaces is of commercial interest when Techint supplies new furnaces. The combination of new low NO_x burners (TSN and TSX) and stricter NO_x regulation makes predicting NO_x an important issue in furnace proposals.

The furnace modelling at Voestalpine has included the evaluation of NO_x emissions and reheating with alternative fuels or alternative firing modes, which can help the company to choose the best solution for limiting emissions in a cost effective way. Air Liquide tested a new oxy-fuel burner design in MEFOS WB furnace, called the ALROLL-S burner. This was the first continuous reheating furnace with 100 % firing with these new oxy-fuel burners, and they performed very well, with low NO_x emissions even with the presence of air infiltration. The results of the oxy-fuel trials were presented at conferences and are useful for marketing this new oxy-fuel technology [14-16]. ISQ and LABEIN performed supporting roles for the investigations of new technology by the other partners. ISQ helped other partners with emission measurements, and LABEIN with modelling work. BFI tested the new HTR concept for NO_x reduction, and LABEIN supported the work with modelling. The HTR process is not yet used commercially, so pilot investigations are important to future applications.

Today the steel industry has the opportunity to adopt innovative firing technologies, developed and manufactured in Europe, which considerably reduce NO_x and the environmental impact of high temperature combustion based on flameless combustion technology, with the Techint TSX burners and Air Liquide ALROLL-S burners. Flameless low NO_x HRS burners are also manufactured in Europe by VTS as a licensee of NFK. Flameless technology combined with regenerative or oxy-fuel technology provide also a method for both energy saving and CO₂ reduction, which is worth further investigations in other research projects.

2 SCIENTIFIC AND TECHNICAL DESCRIPTION OF THE RESULTS

This project is divided into 5 work packages (WPs) as describe earlier in the summary. WP1 is for the testing of burners and combustion systems, which is supported by modelling in WP2 and emission analysis in WP3. WP2 has additional experimental activity with the modelling of a full scale reheating furnace at Voestalpine and empirical NOx emission modelling at Techint. WP 4 focuses on testing low NOx oxy-fuel burners developed by Air Liquide in combustion trials at MEFOS. WP5 investigates a secondary NOx removal method, called High Temperature Reduction (HTR) at BFI.

2.1 WP 1 - Laboratory and pilot plant trials for air combustion

2.1.1 Task 1.1. Testing of low NOx burner designs

Burner selection has been an activity in Task 1.1 for the partners in this WP. At CSM, information obtained from literature or manufacturers for Low and Ultra Low NOx direct fire burners suitable for reheating furnaces process (see Table 1) was used to select the Techint TSN and Hauck TRIOX recuperative burners for testing at CSM Combustion Lab. The NFK HRS burner design as manufactured by VTS AB was chosen by MEFOS for burner trials. The Bloom burners were of interest at both BFI and CSM, but Bloom was not willing to supply burners for testing, therefore BFI chose burners from FBB and Henning.

This data likewise shows that burners with the flameless combustion mode give the lowest NOx. The data in this table come from both the literature and this research project, and are only meant to be samples of the operating conditions possible, and not limitations for these burner designs. Design data for furnace installations should be obtained from the respective burner manufacturers.

Table 4. Examples of some low NO_x burners with some typical NO_x levels firing natural gas for various furnace temperatures and combustion air temperatures.

Manufacturer	Burner	NO _x reduction technique	Nominal capacity in kW	Temp. Furnace (°C)	Temp. Air (°C)	NO _x typ. (mg/Nm ³ @ 5 % Oxygen)
Recuperative						
FBB Engineering	TriX 100	Air staging / IFGR	130 to 20000			
Hans Hennig	HG-SBLN	Air staging / IFGR	150 to 14000	1250	400-550	200-380
Bloom	Cyclops	Air staging / IFGR	900-5000	1400	450	110
Hauck	TRIOX	Fuel staging/ flameless	1700 1000	1040 1250	38 550	30-40 65-155
North Amer.	Magna-Flame	Lean premix/ IFGR (LNI)	300 to 6000	1050-1300	55-479	25-120
Techint	TS	Flame	750-8000	1280	450	195
	TSN	IFGR/ dilute flame	800-6500	1250	450	72-127
	TSX	flameless	800-6500	1150-1250	450-520	36-64
WS	Rekumat	FLOX	12-80	900-1200	450-650	55-180
Regenerative						
FBB Engineering	TriX 100	Air staging / IFGR	130 - 8,000	1150 1250	850-1000 900-1150	150-350 150-600
North Amer.	TwinBed II	Lean premix/ IFGR (LNI)	800-1,130			
VTS-NFK	HRS	IFGR/ flameless	175-4650	1250	1000	100-200
WS	Regemat	FLOX	40-200			
Bloom	LumiFlame	Air staging/ IFGR	100-10000			

Low NO_x burners at CSM

The main role of CSM inside the project has been to perform trials with very low NO_x burners available on the market to better understand their performances and provide information to form guideline for primary NO_x abatement in the steel reheating furnaces. In particular the focus has been on side burners working with combustion air pre-heated by central recuperator and localised regenerative system. CSM contribution to mathematical modelling was not originally included in the project. However, to overcome the constrains due to the confidentiality of the burner geometry, CSM agreed to perform CFD modelling of two burners as installed at CSM furnaces using FLUENT code. It was agreed to use part of the man-months originally assigned at CSM in WP3 (task 3.1 & 3.4) for this purpose. The goal has been to:

- understand the fluid dynamics and its effects on combustion process inside the furnace;
- assisting in the designing of experimental programs and interpretation of measured data;
- calculation of NO_x emission with FLUENT post-processor and reduced model developed by LABEIN.

Information, obtained from literature or manufacturers, for state of art direct fire side burners suitable for reheating furnaces process based on air preheating by central recuperator have been summarised in Table 4 together with experimental data from this project. This data confirm that different combustion

techniques are presently adopted in the design of natural gas very low NO_x burner: staged combustion (air and fuel), internal flue gas recirculation (IFGR) and flameless oxidation. The main goal is, in any case, to minimize the NO_x emission by controlling the flame temperature, the oxygen concentration in the reaction zone and the residence time of the products of the combustion in the high-temperature zone of the flame.

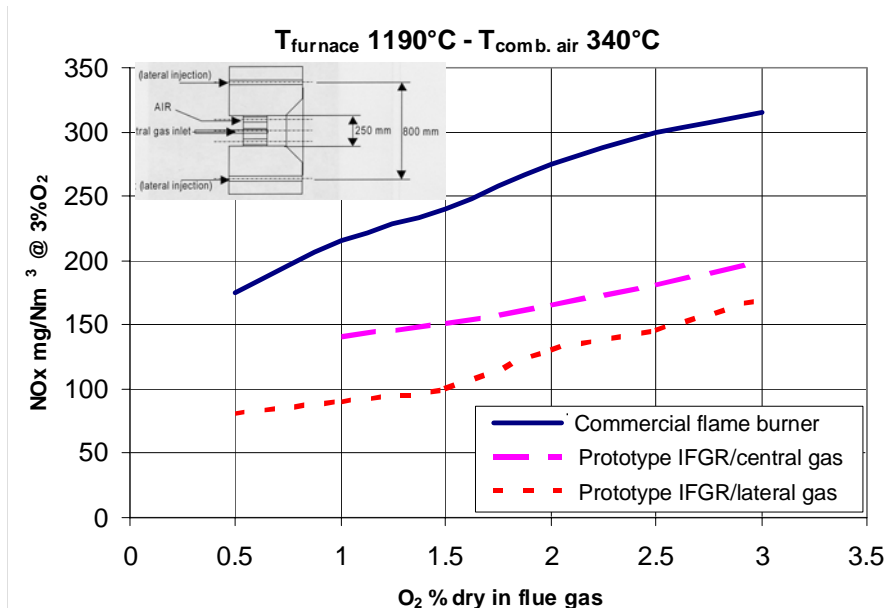


Figure 7. Effects on NO_x emission of different combustion techniques [17].

The different NO_x emission levels, reported in relation to the different combustion techniques, are in good agreement with the data obtained in previous CECA project [17] (Figure 7) for prototype burners. Based on these considerations Techint FlexyTech[®] TSN, Hauck TRIOX and Bloom Cyclops were selected, at the beginning of the project, as representative of Best Available Technology for primary NO_x reduction in reheating furnaces process based on air preheating by central recuperator.

Techint TSN and Hauck TRIOX were tested at the CSM Combustion Laboratories in the frame of this NO_x-RF project, while characterisation test of the Bloom Cyclops burner was not possible due to the decision of Bloom Engineering's management to not supply the burner in spite of a signed confidentiality agreement. During the development of NO_x-RF project, the Techint TSX burner was launched on the market. Certification tests, performed at the same facility (CSM Modular furnace) with the same instrumentation and procedure, have made available to the project by Techint. At the beginning of June 2004 Techint, that is partner of this project, has transferred to the CSM, on a free basis, the TSN burner (Figure 8) working at nominal power of 1500 kW and at the maximum air preheating temperature of 550 °C.

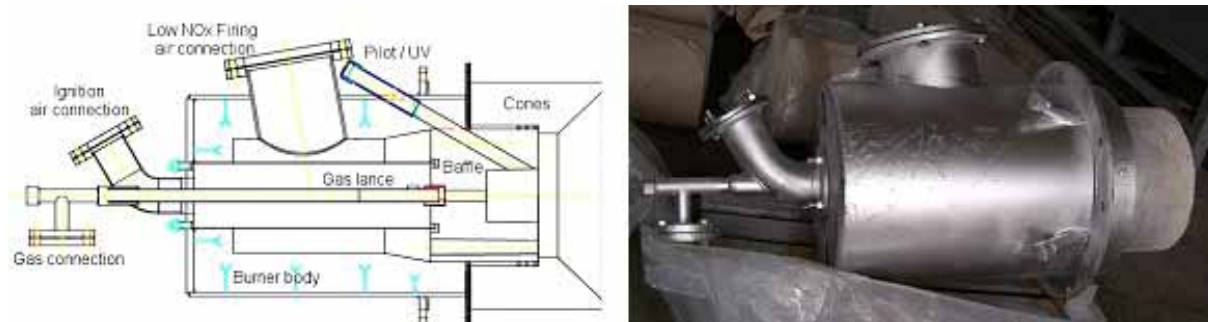


Figure 8. Techint TSN burner as delivered to CSM.

The TSN geometry was designed with the aim of delaying as much as possible fuel and air mixing, in such way that oxygen dilution with the waste gas can take place and the temperature peak of traditional burner is reduced with positive effect on NO_x formation even if a flame is present. The burner was designed with two operational modes with a shut off valve switches from the two operating conditions:

with internal air for ignition and first heating of the furnace. The internal air connection is feed with cold or preheated air with a dedicated piping. A small pilot or spark is needed in order to light the burner; with external air for Low NOx firing. This condition can take place only if furnace temperature is higher than auto-ignition temperature of the fuel used. The auto-ignition temperature is the temperature at which gas/air mixture spontaneously ignites, i.e. without an external source of ignition. The auto-ignition temperature is function pf pressure and composition of the gas. If furnace temperature decreases until this value safety logic is implemented in order to switch operation from Ultra Low NOx firing to Ignition firing.

Based on experience gained with TSN Techint developed, in collaboration with CSM, a new burner based on flameless technology with the goal to reach very low NOx emissions. In September 2004 this burner has been launched on the market with the name of FlexyTech® TSX burner (see Figure 9 and Table 5 summarises the main differences between TSN and TSX burners). Since Techint is partner of NOx-RF project data of 2 MW FlexyTech® TSX Burner certification test performed at CSM combustion facility have made available to the project. The TSX burner is a coupled staged burner, which operates with internal air staging and external gas staging. Air staging is achieved through optimisation of baffle geometry, without any mechanical part. TSX has two running modes:

- with internal gas (flame mode) the burner generate a anchored flame well detected by UV emissions that allows to heat up the furnace;
- with external gas (flameless mode) the burner works in flameless conditions producing very low NOx emission. The burner can operate in this condition when the furnace temperature is over auto-ignition temperature of combustible.

Table 5. Techint TSN vs. TSX burner.

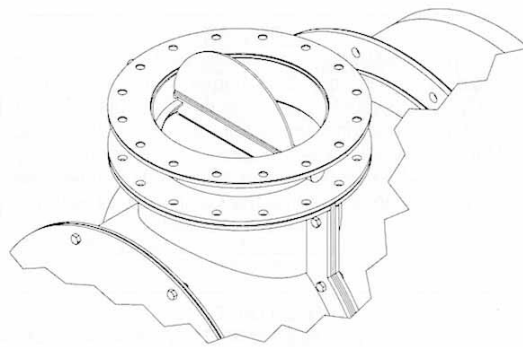
TSN Burner 	TSX Burner 
<ul style="list-style-type: none"> • Light up at cold furnace • On / off running & modulation • Lower NOx emissions 	<ul style="list-style-type: none"> • Flame AND Flameless running • Light up at cold furnace • On / off running & modulation • Ultra Low NOx emissions • Turn down in Flameless mode
<ul style="list-style-type: none"> • Separate air staging • Flame dilution 	<ul style="list-style-type: none"> • Coupled staging (air & gas) • Flameless Combustion
<ul style="list-style-type: none"> • Double air piping • Valve on hot air 	<ul style="list-style-type: none"> • Single air piping • NO Valve on hot air

The Hauck TRIOX 2008 burner was bought and delivered to CSM at the end of December 2005. The main characteristic of the burner are summarized in Table 6. The TRIOX utilizes an air-staged design for very low NOx emissions when firing with low excess air in furnace environments with temperature up to 1480 °C. The burner has two mode of operation, 60 % of air through external slots and 40 % through internals holes (60/40 mode) required for low temperature start-up or operation below 870 °C, and 90/10 or Invisiflame® mode for very low NOx operation above 870 °C. Transition between modes is accomplished via a switching valve (see Figure 9). More details about the burner are available in official Hauck data sheet.

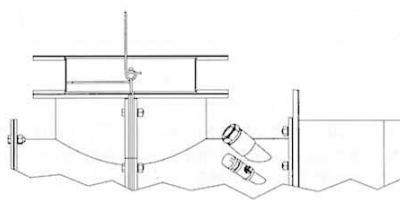
Table 6. Hauck TRIOX 2008 Series burner capacities.

	BURNER MODEL							
	1006		2006		1008		2008	
BURNER SPECIFICATIONS – HIGH FIRE	BURNER STATIC INLET AIR PRESSURE OF 1990 Pa							
Combustion Air Temp. (°C)	15.5°C		482°C		15.5°C		482°C	
Operating Mode	60/40	90/10	60/40	90/10	60/40	90/10	60/40	90/10
Max. Input @ 5% Excess Air (kW)	PENDING				1,610	1,440	1,030	890
Max. Air Flow @ 1990 Pa (nm ³ /hr)					1,610	1,440	1,030	890
Min. Input @ Max. Air Flow (kW)					66	66		
Max. Excess Air (%)					2,450	2,180		
Air Press. @ Switching Valve (Pa)					2,090	2,460	2,240	2,510
Burner Gas Inlet Press. (Pa)					1,740	1,290	920	750
Flame Length @ Max. Input (mm)					3,660	N/A	3,050	N/A
Flame Dia. @ Max. Input (mm)					760	N/A	760	N/A
Stage 1 & 2 Air Static Press. (Pa)					1,990	124	1,990	100
Stage 3 Air Static Press. (Pa)					1,590	1,990	1,490	1,990

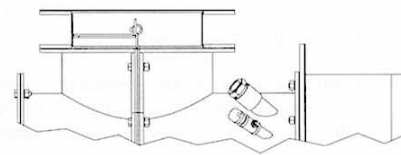
TriOx-9



SWITCHING VALVE
ALIGNMENT TO BURNER BODY



60/40
OPERATING MODE



90/10
OPERATING MODE

Figure 9. Switching valve for Hauck burner.

The experimental test matrix is shown in Table 7, has been defined in agreement with other partners with the goal to perform the complete characterization of the side burner for the typical operative condition in industrial reheating furnaces.

Table 7. Test matrix for burner characterisation.

	Start-up	Turn down										Heat-flux		
Test 1	Range of stability for pilot													
Test 2		P=100%, Tf=1150°C											Low-Nox regime T air=520°C O2=2%	
Test 3			P=100%, Tf=1250°C											
Test 4				P=80%, Tf=1150°C										
Test 5					P=80%, Tf=1250°C									
Test 6						P=60%, Tf=1150°C								
Test 7							P=60%, Tf=1250°C							
Test 8								P=100%, Tf=1150°C						
Test 9									P=100%, Tf=1250°C					
Test 10										P=80%, Tf=1150°C				
Test 11											P=80%, Tf=1250°C			
Test 12												P=60%, Tf=1150°C		
Test 13														P=60%, Tf=1250°C
Test 14														P=100%
		Low-Nox regime T air=520°C					Low-Nox regime T air=450°C							
		Variable parameters O2=1-4%					Variable parameters O2=1-4%							

Industrial scale tests have been performed at CSM Combustion Laboratory in Dalmine at Modular Furnace # 1 (Figures 10-11). The main characteristics are:

- Cross Section: 2 m x 2 m
- Length: variable (3 m, 4.5 m, 6 m, 7.5 m)
- Thermal input up to 2.5 MW
- Water cooled lances to control process temperature
- Air preheating up to 600 °C

The modularity of the CSM furnace allows one to maintain a similar power density and ratio between the flame length and the distance to the furnace walls for the pilot furnace relative to industrial reheating furnaces, especially walking beam furnaces, even with different burner sizes. The validity of the NOx measurements made in CSM's modular furnace has been demonstrated by the good agreement of the experimental data with results from industrial furnaces recently built by Techint, equipped with both the TSN [24] and TSX [25] burners. Moreover, the need to maintain a similarity in the geometry between pilot furnaces and industrial furnaces has been shown by the better accuracy in the NOx results measured for the FBB regenerative burner at CSM than BFI relative to the NOx results obtained by the manufacturer in industrial applications.

The walls and roof are made of a steel construction, thermally insulated with ceramic fibres ($T_{MAX} = 1350$ °C). The roof is equipped with several thermocouples in order to monitor the temperature profile. Heat density in the Modular Furnace can be adjusted by controlling the fuel input and by varying the internal volume. The heat extraction is monitored by measuring the temperature rise and mass flow rate of cooling water. A pressure transducer is used to monitor the furnace pressure that is controlled by air cooled butterfly valves at the flue gas exit. For the measurement of flue gas composition a ceramic suction probe, installed at the exit of the furnace, is linked to an analysis system by an heated line. Flames can be visualised by a camera mounted on the furnace back wall, just in front of the burner while detailed in-flame measurement can be performed through the probe ports on both side of the furnace walls using the IFRF suction pyrometer.



Figure 10. External and internal view of CSM's modular furnace.

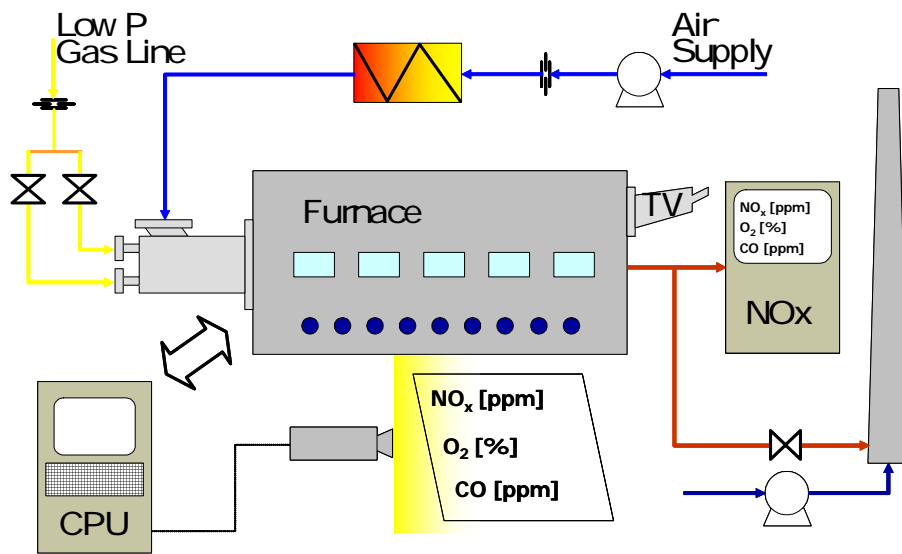


Figure 11. CSM's modular furnace schematics.

The installation of TSN and TRIOX burners on CSM's Modular Furnace # 1 has required to adapt the air and gas piping, to modify the front furnace wall to install a proper connection flange and the refractory inside the furnace making the burner quarl as recommended by burner supplier. Figure 12 the final installation of the TRIOX and TSX in the experimental furnace at CSM.



Hauck TRIOX burner as delivered @ CSM

Techint TSX burner as delivered @ CSM

Figure 12. Photos of the TRIOX and TSN burners mounted on the furnace.

A comparison can be made between the Techint TSN, Techint TSX and Hauck TRIOX burners. Two different operation modes are evident for all the three burners:

flame mode: 60/40 operation mode for TRIOX, internal air for TSN and internal gas for TSX;

low NO_x mode: 90/10 operation mode for TRIOX, external air for TSN and external gas for TSX.

Figure 13 shows the different “flame” structure corresponding at these two modes for TRIOX and TSX burners. The view inside the furnace in the different phases of TSN operation are reported in Figure 14.

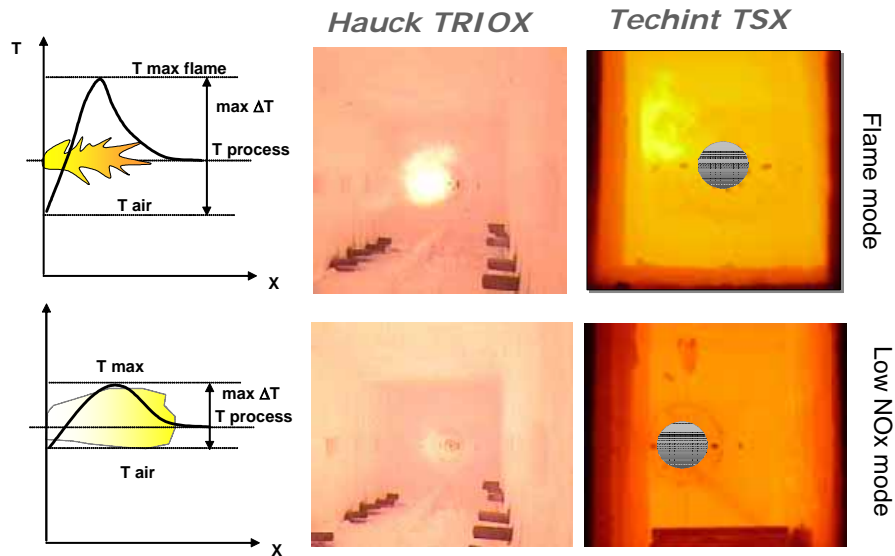


Figure 13. Different burner modes operation.

An important observation during the test is related to UV flame detector. In the case of the TSN and TRIOX burners, the UV alarm is inactive for all the operative conditions. On the contrary during the operation of TSX the UV “views” the flame only when the burner operates with central gas injection while with lateral gas (low NO_x mode) the UV alarm is always active. This indicates that, also for low-NO_x mode, the intensity of OH-radicals is sufficient high in case of TSN and TRIOX burners to allow for the detection of a flame stabilized at the burner tip. This confirms the experimental observation obtained with laser induced fluorescence, Figure 15 [18]: in flame mode the combustion is stabilized at the burner tip and the intensity of the OH-radicals is much higher as at flameless-mode, which indicates a higher reaction intensity and temperature. In flameless-mode the flame is not burner stabilized and the reaction starts far from the front of the burner tip producing an evenly distributed intensity at the reaction zone.

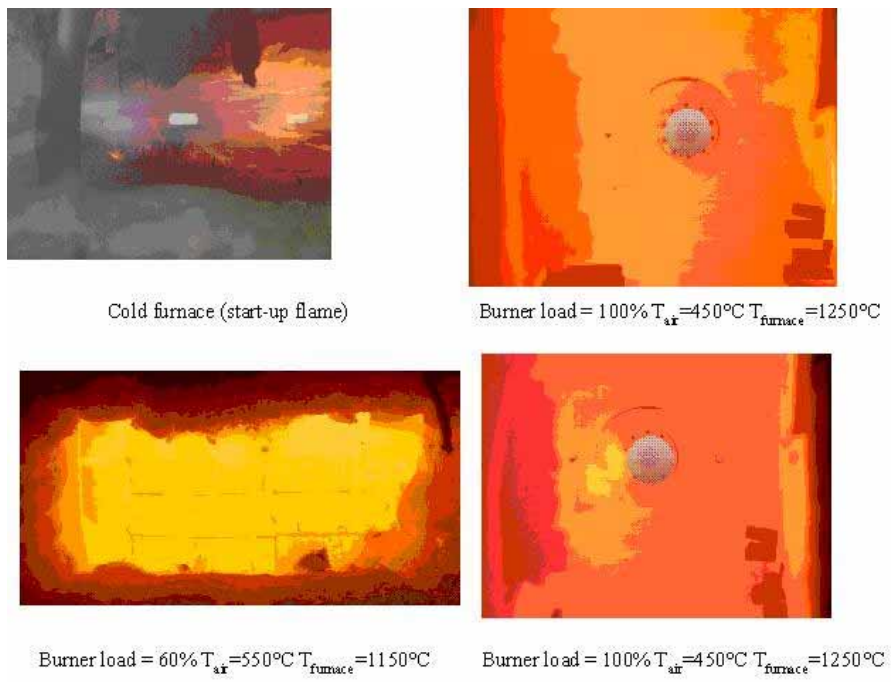


Figure 14. TSN flame for different burner operating conditions.

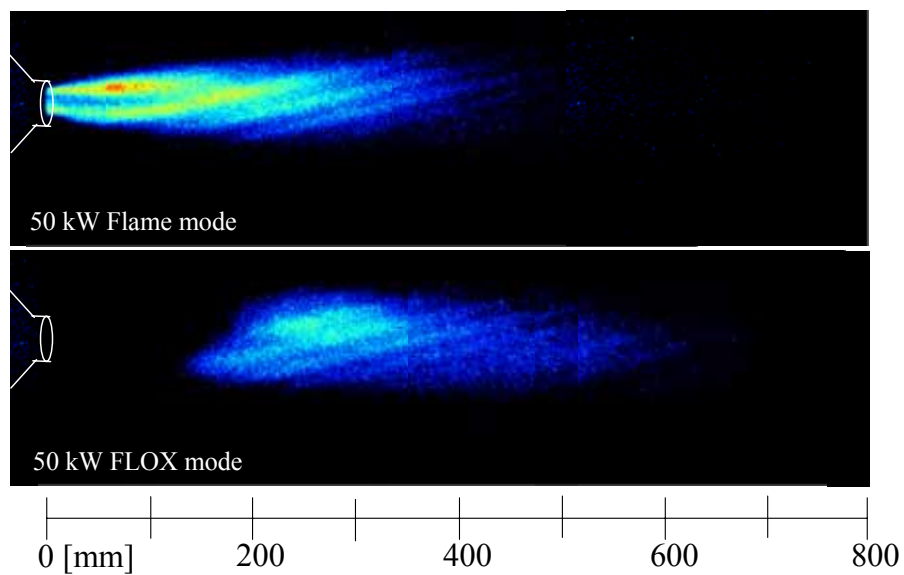


Figure 15. Laser induced fluorescence for OH-radicals at flame and flameless mode [18].

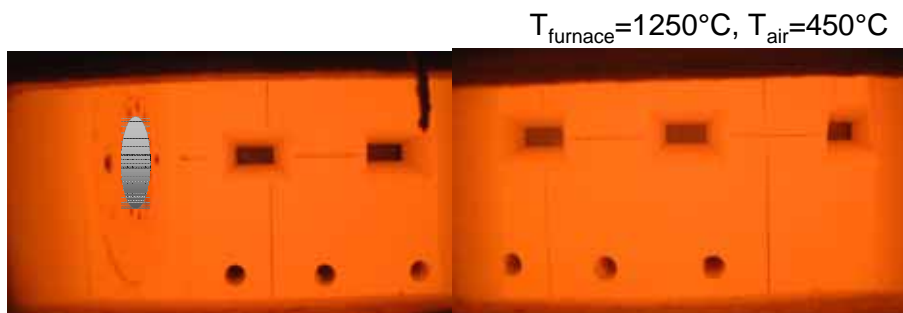


Figure 16. TSX reaction zone in Low-NOx mode.

Based on this indication only the combustion regime generated by TSX burner can be strictly classified as flameless one (Figures 15-16). The effect of different combustion regime on NO_x emission is clearly shown in Figures 17-18, where the performances of the three side burners (TSN, TSX and TRIOX) at working conditions representative of reheating furnaces process are reported (see the test matrix of Table 7). The concentration of NO_x in the flue gas for the TRIOX burner is 35 % higher for the 60/40 than 90/10 operating mode and in the worst test condition, 100 % nominal power, highest furnace temperature (1250 °), highest combustion air temperature (520 °C) and highest concentration of the oxygen in flue gases (4.5 %), the NO_x rises up to 292mg/Nm³@5%O₂DFG. It means that this burner when operated in the flame mode produces a concentration of nitrogen oxides comparable with the traditional “flame” type of burners that presently equip the reheating furnaces [19]. On the contrary, for the 90/10 operation mode, when the TRIOX run in the “invisible flame condition”, NO_x emissions are reduced by 35 % for all the conditions reaching emission well under the legislation limits. The NO_x concentration measured for TSN working with internal air (low NO_x mode) are very close that of TRIOX in 90/10 mode.

In all the test conditions, the emission level of TSX burner are about 50 % lower then TRIOX and TSN burners working in low NO_x mode, giving a clear indication that flameless combustion can be considered the present Best Available Technology for primary NO_x reduction technology in reheating furnaces equipped with central recuperator. Two important observation are related:

- the negligible effect of burner load on NO_x emission for all the three burners. The limit of the turn down at 40 % is due to the difficulty to maintain the furnace at the target temperature (1250-1150 °C) with limited power, not to the limit of the burners itself;
- the relative small effect of combustion air temperature on NO_x emission level: this is mainly related to high quantity of hot gas recirculated in the furnaces due to the high impulse jets that characterise all three burners.

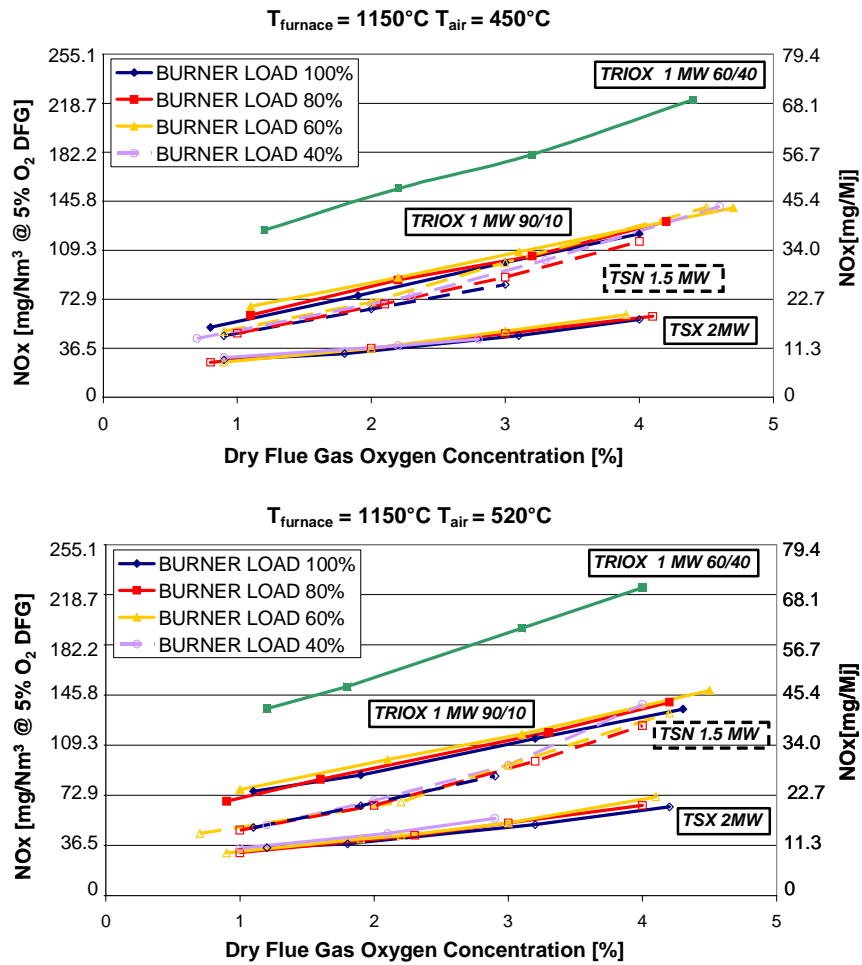


Figure 17. NOx emission of Hauck TRIOX, Techint TSN and TSX burners at 1150 °C furnace temperature and different preheated air temperature and burner load.

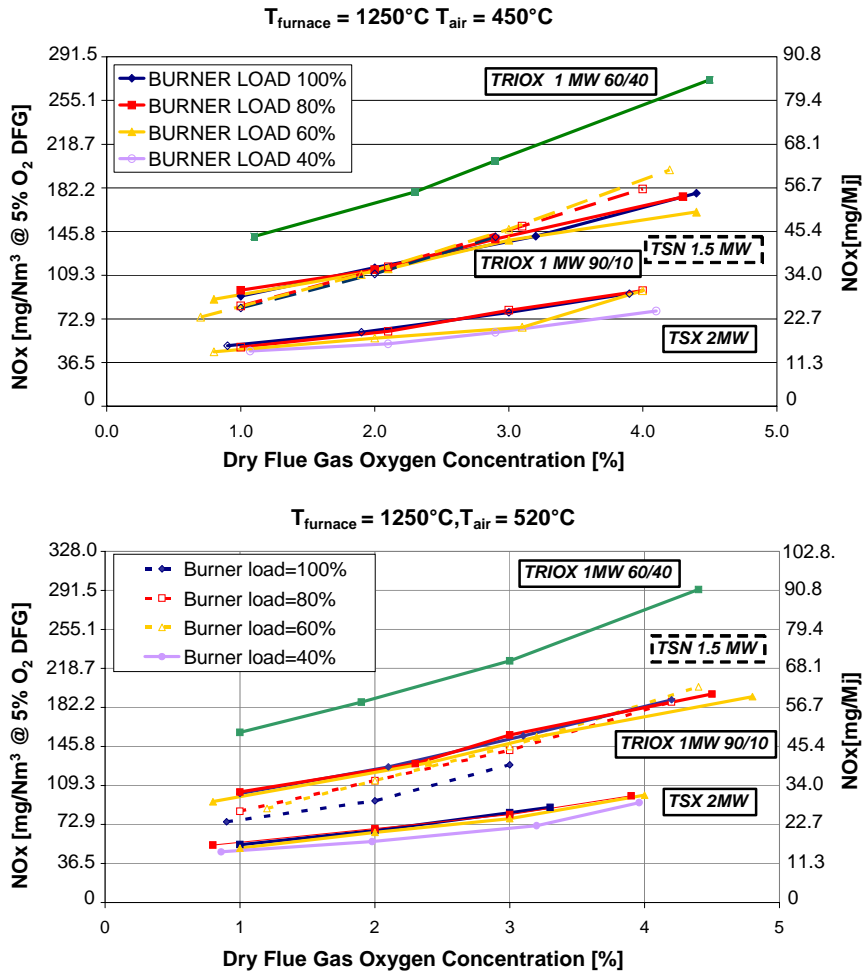


Figure 18. NOx emission of Hauck TRIOX, Techint TSN and TSX burners at 1250 °C furnace temperature and different preheated air temperature and burner load.

In addition to measurement of NOx, O2 and CO in the flue gases, tests were made by using the IFRF suction pyrometer. The profiles of temperature and composition were evaluated at 0.6, 2.1 and 3.6 m from the burner tip for the Hauck TRIOX burner (90/10 operating mode) with 100 % burner load. The temperature trend measured by pyrometer is illustrated in Figure 19 and the species in Figure 20.

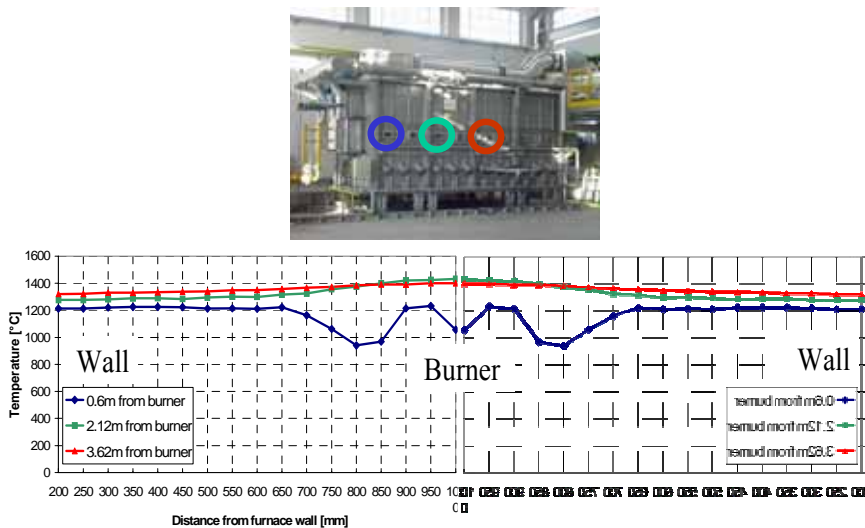


Figure 19. Temperature profiles for the TriOx burner 90/10 operating at 100 % of the thermal capacity (1 MW) at the average temperature of 1250 °C.

The temperature peak is rising with the distance from the burner, passing from about 1200 °C to about 1400 °C. The low temperature measured in the furnace is due to the higher recirculation of flue gases, however the absolute value can be effected by measurement errors (i.e. alignment of probe with the fluctuating jets).

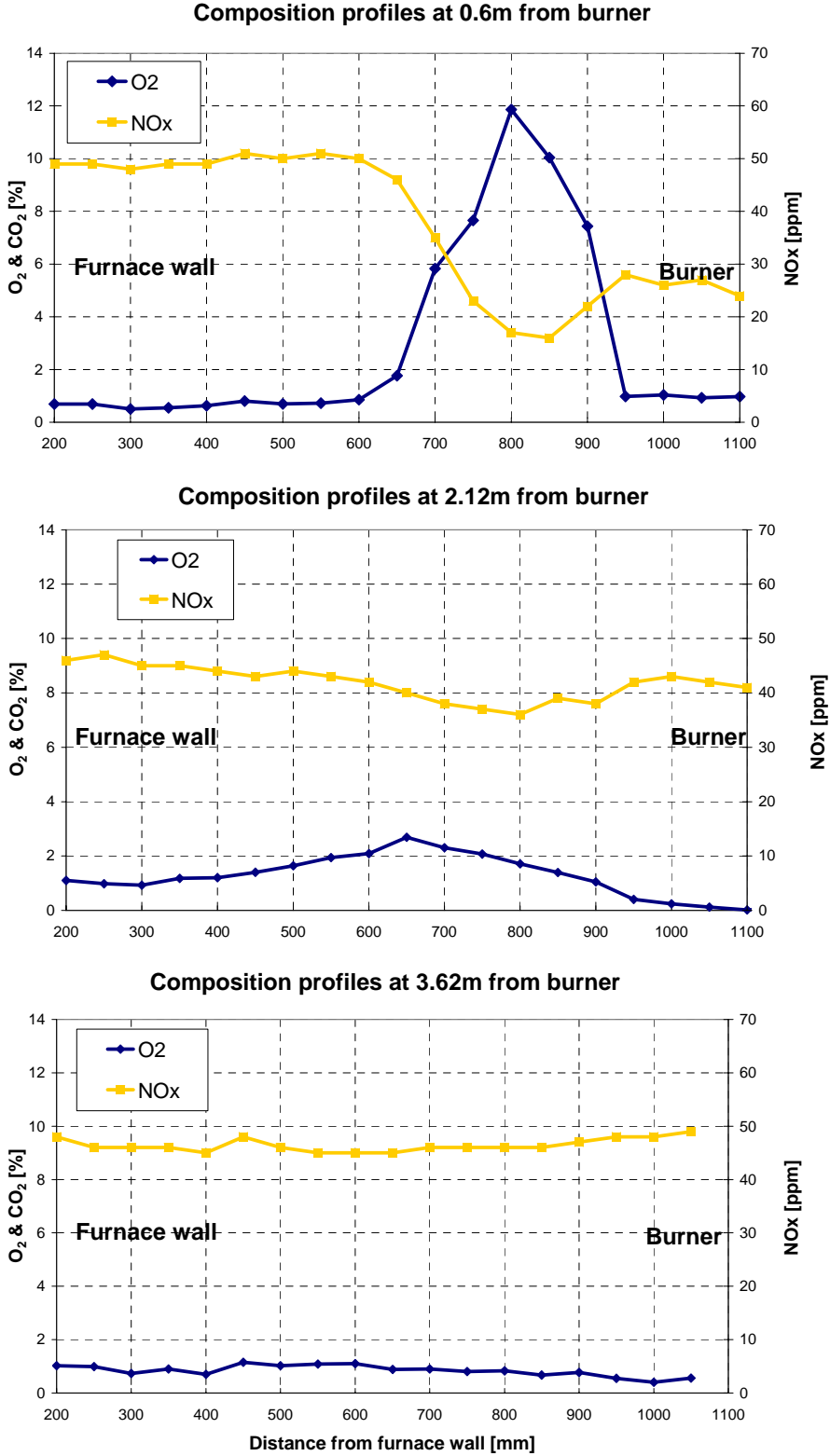


Figure 20. Composition profiles for the TRIOX burner operating at 100 % of the thermal capacity (1 MW) at furnace temperature of 1250 °C and combustion air of 550 °C.

Low NO_x burners at MEFOS

MEFOS made trials with a low NO_x burner from VTS-NFK with air preheating in a muffle furnace. The furnace has 4 tubes and the HRS burner from VTS AB (Nyköping) developed by NFK (Japan) was selected (see the technical data in Table 8).

Table 8. Supplier based technical data for the NFK-VTS low NO_x burner.

Parameter	VTS HRS burner (advanced honeycomb heat exchanger)	Older designs (with ceramic ball heat exchangers)
Exhaust heat recovery	85 %	70 %
Air preheat with a 1300 °C furnace	>1200 °C	up to 900 °C
NO _x in exhaust gases with no fuel N ₂ and <1350 °C furnace	<60 ppm	----
Pressure loss	<1 kPa	>3 kPa
Relative size of the heat exchanger	1 (reference)	5

Source: "NFK-VTS Combustion System", VTS AB, Nyköping, Sweden, www.vts.nu

The VTS burner uses separate fuel and air injection ports to reduce flame temperatures, and NO_x levels, similar to the N. American Twin Bed II burner. The separate injection of fuel gas and air into the combustion chamber is called "Low NO_x Injection or LNI" by N. American. The lance for the fuel is not directly warmed up by hot air with separate injectors. This is especially helpful during the use of high preheated air by means of regenerative heat recovery, which was simulated at MEFOS with the use of a muffle furnace for preheating air.

A NFK-HRS model DL-2.5 low NO_x burner rated for 300 kW firing propane was purchased from VTS who manufactured the burner in Europe as a NFK burner licensee. The burner was installed in MEFOS chamber furnace at the end of the furnace above the flue gas outlet in the same position as the existing dual fuel burner. The burner has two modes: A F1 mode in which the propane is mixed with the hot air in the central air port and a F2 mode in which the propane is injected using 2 nozzles placed the sides of the central air port using the principle of dilute combustion or direct fuel injection to give flameless combustion. Therefore trials were made with both a high NO_x flame mode (F1 mode) and low NO_x flameless mode (F2 mode). The F1 mode permitted testing the principle of oscillating combustion with high NO_x and the presence of a flame (see Task 1.2). The propane was pulsed using electrically controlled on/off valves to switch the fuel flow with the goal of a cycle of about once per second through a high flow or through a low flow restrictor in a system built by NOAB.

The burner power could be adjusted with a water cooled steel plate which was connected to a Scylar hot water power monitor designed for a up to 300 kW and 150 l/min water flow. The NO, CO and oxygen were measured with a Kane-May Quintox extractive gas analyser with NO_x calculated as 1.05 times the NO concentration (or NO₂ = 0.05 x NO). A new ABB furnace controller with a zirconia oxygen analyser was designed to give automatic excess oxygen control.

An electrically heated muffle furnace was used to produce hot air with temperatures up to 1000 °C, so the insulation between the muffle furnace and the VTS-NFK burner was improved for these trials. The pipe insulation used for the DFI combustion trials reported earlier had much lower combustion air temperatures, so thicker insulation was required. The 253 MA high temperature pipe was insulated with about 8 layers of 25 mm fibre insulation. It was not possible to operate the VTS-NFK burner at the rated power. Neither the F1 nor the F2 mode would give a sufficient propane flow rate to produce the rated burner power of 300 kW. The burner was typically operated with a light load of 40-70 kW with the a water cooled plate, and about 4-6 Nm³/hr propane (which corresponds to 104 to 156 kW at 26 kW/Nm³/hr). Expansion of the piping between the muffle furnace and the burner caused hot air to leak at the joint where the hot air pipe entered the burner adapter housing. Therefore the hot combustion air was also limited, and all the burner operating conditions could not be tested.

The NFK-HRS burner from VTS performed well in the F2 flameless mode. The NO_x levels were always below the 70 mg/MJ standard for all the conditions tested with furnace temperatures from 1150-1250 °C, combustion air temperatures from 450-1000 °C and excess oxygen concentrations of 1-5 % (dry analysis). The best results were for the lowest furnace temperatures, least air preheat and the lowest oxygen concentration, which gave under 15 mg/MJ (see Figure 21). Raising the furnace temperature to 1250 °C and excess air gave up to about 65 mg/MJ (see Figure 22). Stable combustion was difficult to obtain in the furnace, so that the set point or desired furnace temperatures and combustion air temperatures are reported. The temperatures were typically within 15 °C of the set point temperature. The oxygen concentration could also vary from the set point levels, but the actual oxygen analyses were used together with the NO_x concentrations to calculate the NO_x in mg/MJ.

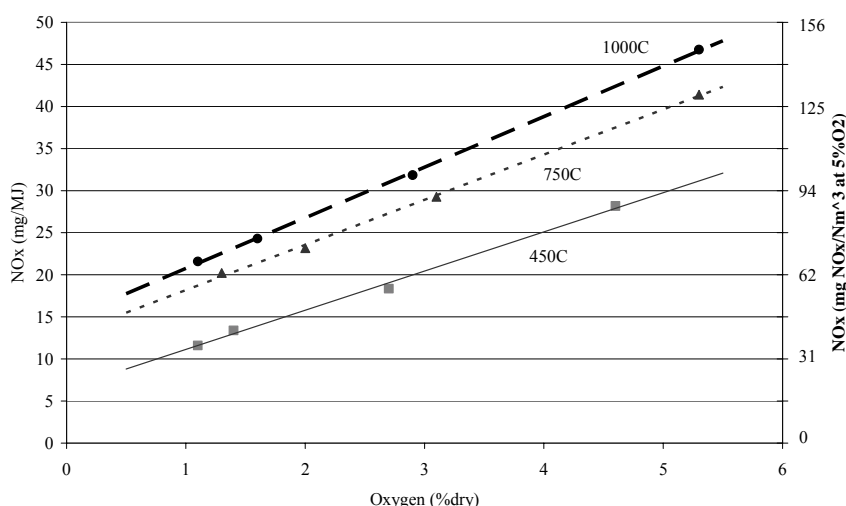


Figure 21. NO_x emissions for the VTS-NFK HRS burner in the flameless F2 mode with a 1150 °C furnace and varying the excess air and combustion air temperatures.

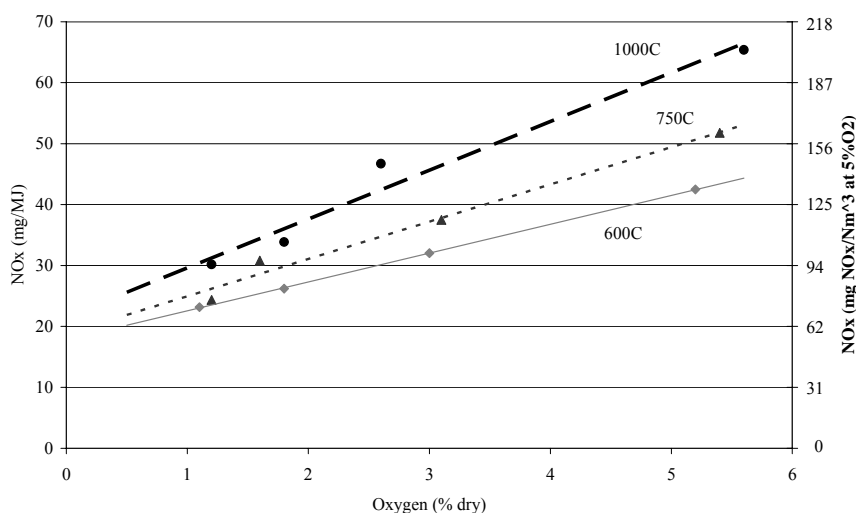


Figure 22. NO_x emissions for the VTS-NFK HRS burner in the flameless F2 mode with a 1250 °C furnace and varying the excess air and combustion air temperatures.

Low NO_x burners at BFI and tests of Hennig HG-SBLN side burner

In January 2007 Hans Hennig has delivered a Hennig HG-SBLN side burner to BFI. The burner has a nominal capacity of 320 kW and was designed for an air preheating of 400 °C. Because of the delay in the research project, a Low-NO_x-burner from serial production had to be used. Burner for higher air preheating and Super-Low-NO_x-burner are also part of Hennig's product field. Figure 23 shows the installation at BFI test rig. The pilot furnace, a steel construction with ceramic fibre insulation, has a length of 8 meters and a cross section area of 1 m² (1 m x 1 m). Several cooling plates and pipes are available in order to control the furnace temperature at a constant level. The furnace pressure is

adjustable by a butterfly valve in the chimney. Different fuels, like natural gas, coke oven gas and blast furnace gas are available through the connection with the piping of a steel mill. The furnace temperature is measured with 8 ceiling thermocouples along the complete length of the furnace. The furnace has more than 40 sampling points at the side wall, in the waste gas flue with recuperator and in the stack. The flue gas composition (CO₂, O₂, CO, NO_x) and temperature can be measured by sampling with suction probes and high velocity thermocouples. The air preheating was done with a central air preheating system, heated by four radiant tubes with self recuperative burners (left side in Figure 23). For this preheating system, the air preheating temperature required is adjustable with an automatic controller.

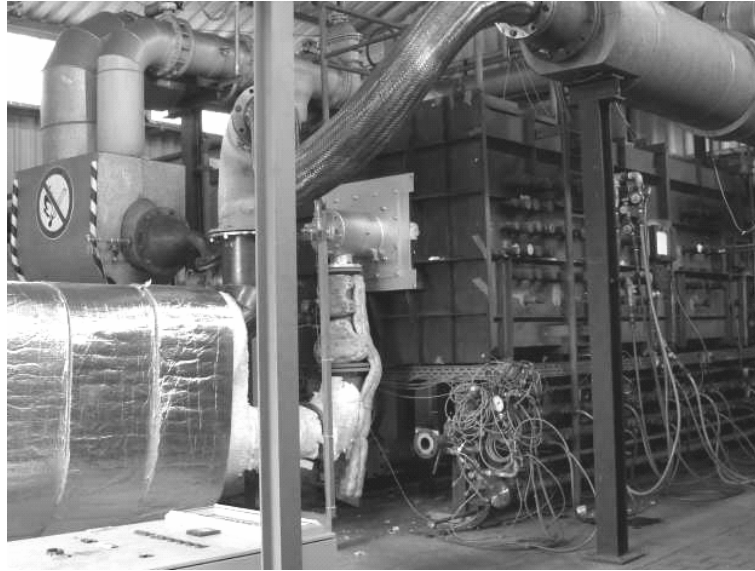


Figure 23. Installation of the Hennig SBLN side burner at the BFI experimental combustion chamber.

The tests with the side burner were done with the standard test air preheating temperatures (in this project) of 450 °C and 550 °C plus additional tests with the design air preheating temperature of 400 °C. Tests were made at furnace temperatures of 1150 °C and 1250 °C, excess oxygen levels of 1 to 4 % and burner loads of 100 % and 50 %. The burner lighted up reliable with both a cold (20 °C) and hot (1250 °C) furnace. The CO emissions was negligible for all of the test conditions. The detailed NO_x emission results with natural gas are shown in Figures 24-26 and following. The emission values increase with increasing air and furnace temperature and increasing excess oxygen level as expected. The lowest emission value at 1250 °C furnace temperature, 400 °C (design-) air temperature and 1.3 % oxygen was 198 mg/m³ (all emission values in mg/m³ dry flue gas were calculated for STP and at 5 % excess oxygen). This corresponds to 62 mg NO_x per MJ energy input. At an air temperature of 450 °C the NO_x emission is round about 20 mg/m³ higher in comparison with an air temperature of 400 °C.

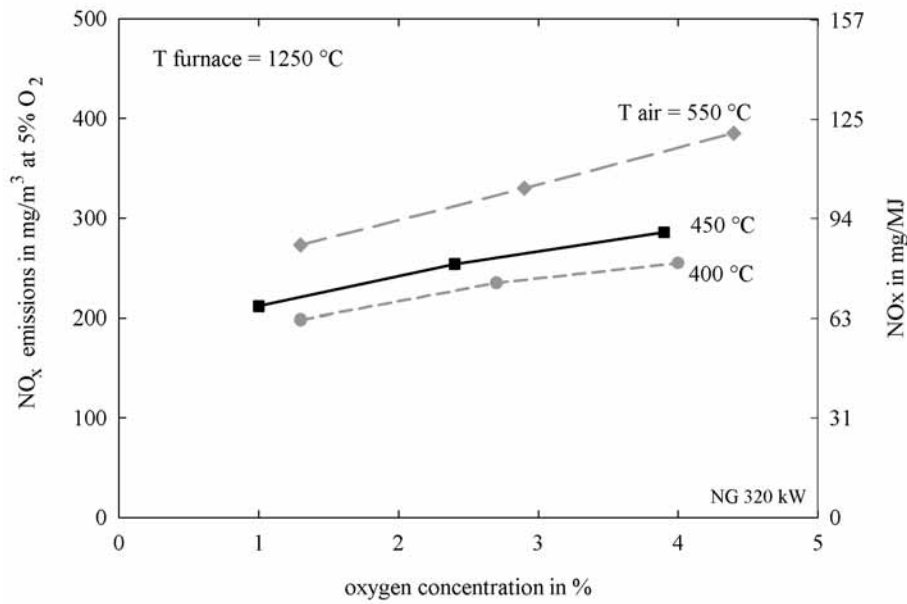


Figure 24. NOx emissions for the Hennig SBLN side burner tested at BFI varying the combustion air temperature at a burner load of 100 % and 1250 °C furnace temperature.

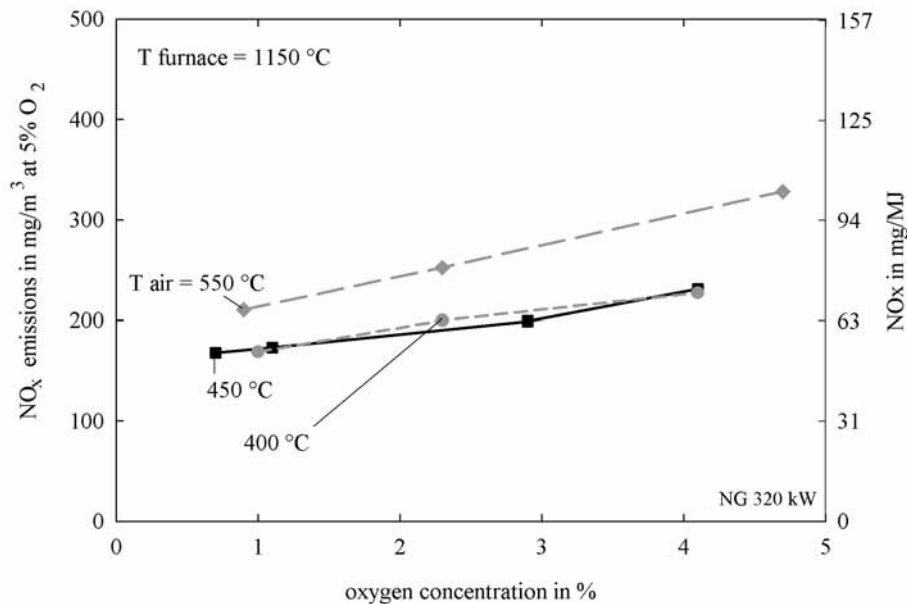


Figure 25. NOx emissions for the Hennig SBLN side burner tested at BFI varying the combustion air temperature at a burner load of 100 % and 1150 °C furnace temperature.

At a furnace temperature of 1150 °C (Figure 25) the lowest NOx emission value at 450 °C air temperature and 0.7 % oxygen was 168 mg/m³. When the burner load is reduced the emissions are nearly unchanged. Figure 26 shows the test results with a burner load of 50 % (160 kW). Additional tests with coke oven gas (COG) were made in order to investigate the influence of the kind of fuel. COG is a by-product of coking plants and often used as a cheap substitute for natural gas at reheating furnaces. The composition and the properties of COG are much different to natural gas. Table 9 shows the gas compositions and important properties.

Table 9. Gas composition and properties of natural gas and coke oven gas at BFI.

	unit	natural gas	coke oven gas
H2	%	-	64.2
CO	%	-	8.0
CH4	%	86.9	21.2
C2H6	%	8.4	0.30
C3H8	%	2.0	0.01
C4H10	%	0.39	0.01
C5H12	%	0.03	-
C6H6	%	0.01	0.07
CO2	%	1.3	1.5
N2	%	0.95	3.4
O2	%	-	0.17
HCN	mg/m ³	-	450
NH3	mg/m ³	-	77
calorific value	MJ/m ³	38.8	16.5
density	kg/m ³	0.83	0.40
air requirement	m ³ /m ³	10.36	3.98

The main differences between the combustion of COG and natural gas are based on the flame velocity and the chemically combined nitrogen content in the fuel. The much higher flame velocity of COG is caused by the high hydrogen content. Hydrogen has a maximum flame velocity of 2.65 m/s. The flame velocity depends on the excess air coefficient and has a maximum in the substoichiometric range. Methane, main component in natural gas, has a maximum flame velocity of 0.35 m/s. The higher flame velocity in COG causes a minor premixing of fuel and air with flue gas before the reactions start. This causes a higher flame temperature and greater thermal NO_x formation.

The chemically combined nitrogen in the COG consists of ammonia (NH₃) and a higher content hydrocyanic acid (HCN). These nitrogen compounds have to be distinguished from any molecular nitrogen contents in fuels. Molecular nitrogen contents in fuels have the same effect on combustion like nitrogen in the combustion air and only leads via the thermal NO_x formation to a higher NO_x emission. The chemically combined nitrogen compounds are an additional nitrogen source for the formation of NO_x. A nearly complete conversion from NH_i (-radicals) to NO_x is well known from premixed flames.

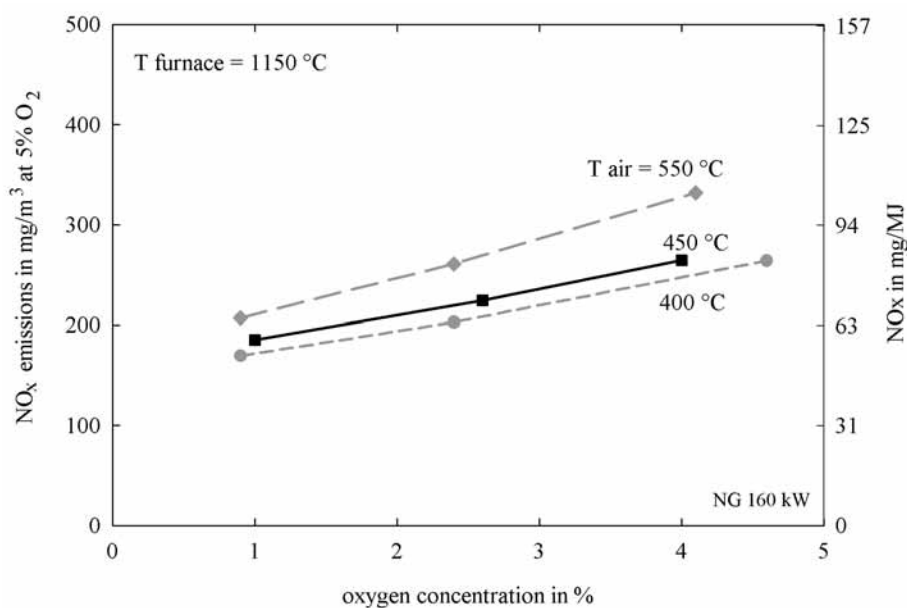


Figure 26. NO_x emissions for the Hennig SBLN side burner tested at BFI varying the combustion air temperature at a burner load of 50 % and 1150 °C furnace temperature.

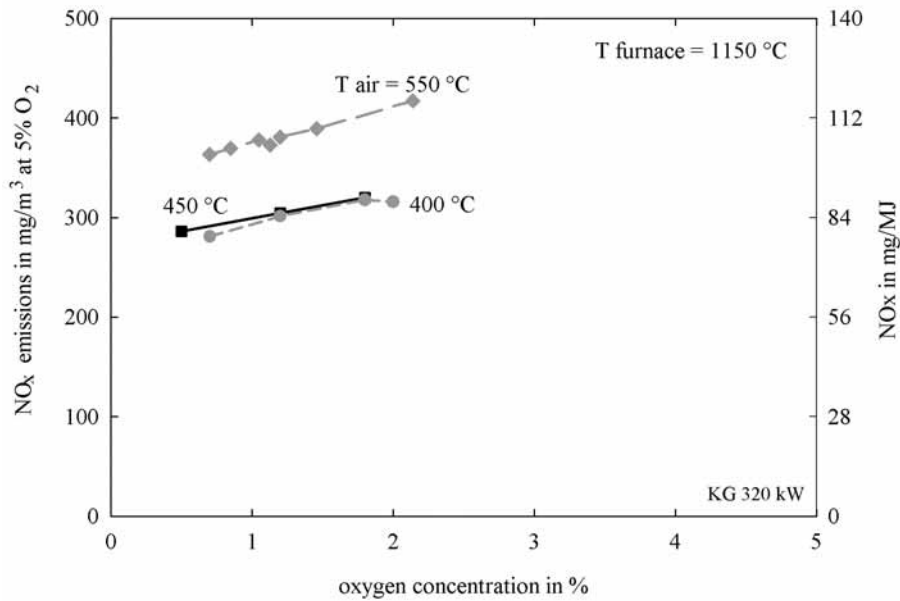


Figure 27. NOx emissions for the Hennig SBLN side burner tested with coke oven gas at BFI varying the combustion air temperature at a burner load of 100 % and 1150 °C furnace temperature.

The detailed NOx emission results with COG are shown in Figure 27. The emission values increase with increasing air temperature and increasing excess oxygen level in the same kind as at the combustion of natural gas. The lowest emission value at 1150 °C furnace temperature, 400 °C air temperature and 0.7 % oxygen is 281 mg/m³. This corresponds to 88 mg NOx per MJ energy input. At an air temperature of 550 °C the NOx emission is round about 80 mg/m³ higher in comparison with an air temperature of 400 °C. Figure 28 shows a comparison of the emission levels of COG and natural gas. For an air temperature of 450 °C the emissions of COG are round about 130 mg/m³ higher. The higher emission level is caused - as mentioned - by a higher flame temperature and the chemically combined nitrogen in the COG. For an estimation of the nitrogen conversion, it was calculated for COG:

450 mg HCN per m³ fuel react to 148 mg NOx per m³ dry flue gas at 5 % oxygen
 and
 77 mg NH₃ per m³ fuel react to 40 mg NOx per m³ dry flue gas at 5 % oxygen

In the case of a complete conversion an additional NOx formation of 188 mg/m³ would result. The difference between the emissions at combustion with COG and natural gas are approximately 133 mg/m³ at an air temperature of 450 °C. Considering the higher NOx formation on account of the higher flame temperature the conversion of chemically combined nitrogen in the COG has to be lower than 71 % (see Figure 28). For 550 °C air temperature a maximal conversion of approximately 88 % can be calculated. For more exact calculations and especially much lower NOx emissions at combustion of fuels with chemically combined nitrogen, such as COG and oil, more applied research is needed.

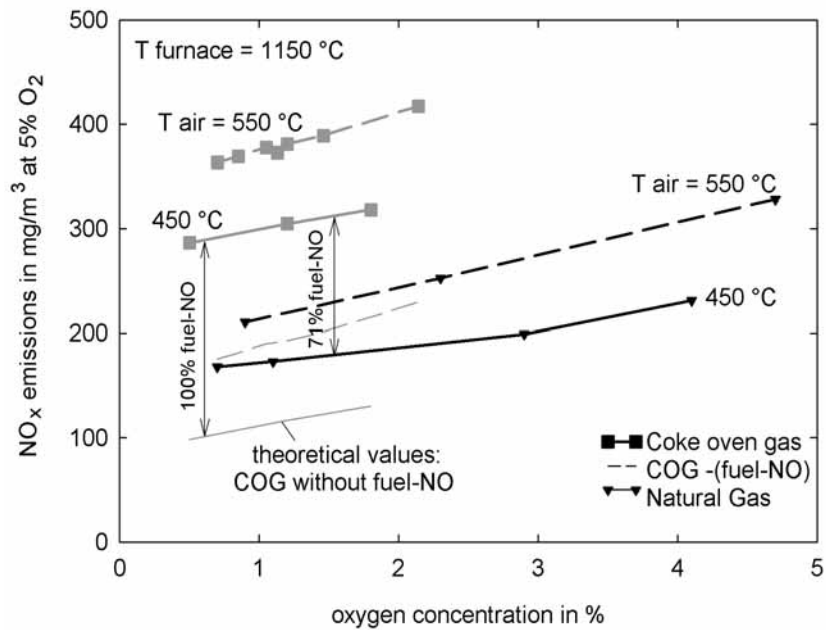


Figure 28. Comparison of NO_x emissions for the Hennig SBLN side burner tested with coke oven gas and natural gas at BFI varying the combustion air temperature at a burner load of 100 % and 1150 °C furnace temperature.

2.1.2 Task 1.2. Other low NO_x combustion techniques

MEFOS has investigated "Oscillating Combustion Technology" (or OCT). OCT is a simple method to reduce NO_x from gas burners using either air or oxygen as the oxidant. OCT was developed by Air Liquide and the Institute of Gas Technology (IGT). The fuel supply is oscillated at a few hertz with a valve on the gas line to the burner to give alternately fuel rich and fuel lean combustion. This is said to reduce the NO_x by up to 70 %, and be applicable to steel reheating furnaces. The equipment required for a burner is quite simple, consisting of a valve, a valve controller, and software to drive the controller.

Oscillating combustion was tested for combustion in both the F1 or flame mode and F2 flameless mode with the VTS-NFK burner at MEFOS. The NO_x reduction was best for the conditions with the highest NO_x. For example, oscillating combustion in the F1 mode for 450 °C combustion air and a 1150 °C furnace gave only a slight improvement as shown in Figure 29. The flow data was logged every second, but the NO_x was logged every 10 s with a delay time both for the volume of the furnace and extraction and cooling of the exhaust gases to the analyser. Undesirable oscillations in the excess oxygen due to the control system for the excess air to the furnace caused additional variations in the NO_x. If the NO_x is evaluated when the system was at 2 % oxygen, then the NO_x before and after the trial was about 365-370 ppm and about 355 ppm during the oscillating combustion. The sampling delay time, etc. cause a delay also before the NO_x concentrations rise after the fuel oscillations stop.

The benefits of oscillating combustion for the F1 mode with higher NO_x conditions with a 1200 °C furnace and 600 °C combustion air are shown in Figure 30. The technique appears to give a greater reduction in NO_x with a lower percent excess oxygen in the furnace. The cycle times and the magnitudes of the fuel flow changes were not optimized, since rather simple flow oscillation equipment was used and many other burner parameters were also studied. The oscillating combustion process is expected to be better for commercial flow oscillation equipment, but it is not expected to perform as well as low NO_x burners.

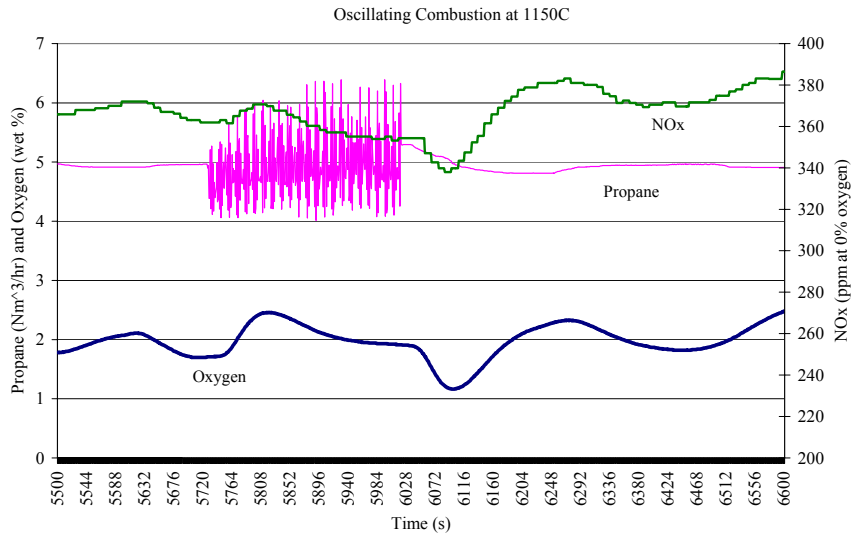


Figure 29. Tests with oscillating combustion in the F1 central flame mode with a 1150 °C furnace and 450 °C air in the chamber furnace at MEFOS.

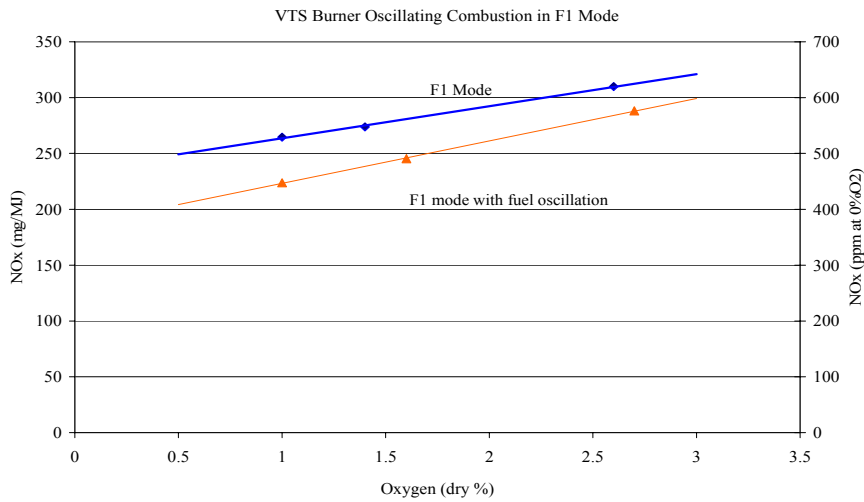


Figure 30. Tests with oscillating combustion in the F1 central flame mode with a 1200°C furnace, 600 °C combustion air and a 40 kW load at MEFOS.

North American Manufacturing Co. has described low NO_x burners which use what they call Low NO_x Injection “LNI” or Direct Fuel Injection “DFI” to give flameless combustion in their TwinBed™ II burners [22]. The second term is more descriptive of the technique used, so it is used to describe the following tests with this technology. Cain, et.al. have described the effect of varying the furnace temperature, fuel injection angle, injector placement, air preheat temperature, etc. in a series of tests with the DFI or LNI technology [22]. The fuel injection is on the outside of a central air inlet, and the fuel jets are placed so that the fuel meets the air jet some distance from the burner outlet. This DFI concept can be applied to reduce NO_x for combustion in general, for example, they also report that the same DFI technology can be used to give low NO_x oxy-fuel combustion in their HiRam™ Oxy-LNI burners [22]. Other burner manufacturers have their application of the same concept. The separate injection of fuel and hot air is the not only used in the North American Mfg. TwinBed™ II burners, but also in other commercial burners including the VTS-NFK HRS and TSX low NO_x flameless burners. This technology is relatively new. DFI originated from the results of research at Tokyo Gas in the beginning of the 1990s in which low NO_x emissions were found when the injection ports for air and fuel were separated. The DOE in the USA stated that “one of the key performance targets for industrial combustion systems of the next decades” [23] will be the improvement of this technology.

Tests were made with fuel lances for separate injection of fuel and air to give direct fuel injection (DFI) combustion in MEFOS chamber furnace. The existing TABO burner was modified so that hot air could be injected through a centre pipe and fuel with lances on opposite sides of the air pipe (see Figure 31). Commercial steel nozzles were mounted on the ends of lances that entered the furnace through holes in the existing furnace brick. The fuel entered at an angle so that the fuel stream centreline meets the air about 0.5-1 meter from the furnace wall.

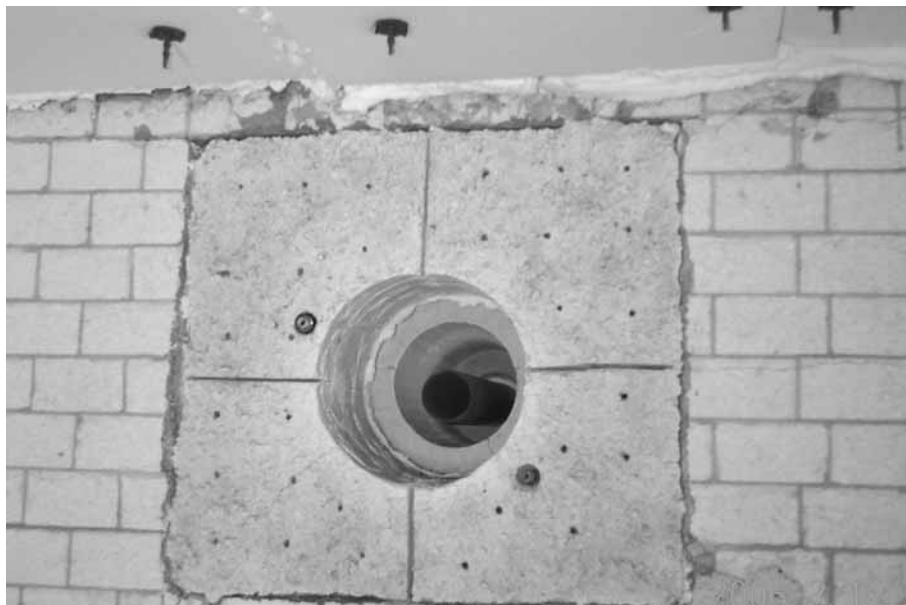


Figure 31. Burner geometry for the separate air and fuel injection trial at MEFOS. The black centre pipe is for hot air injection and the two small nozzles are for propane injection.

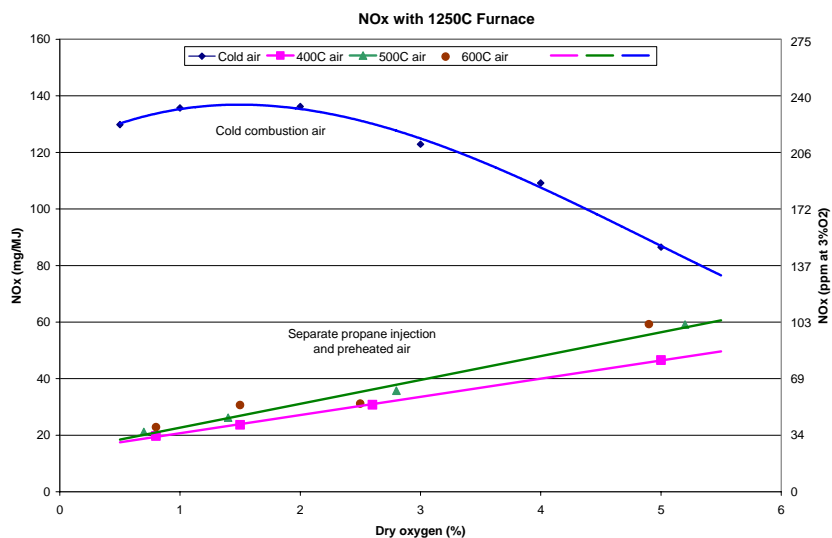


Figure 32. NOx with separate propane injection at 1250 °C with preheated air compared with NOx for cold air with a premix burner in MEFOS chamber furnace.

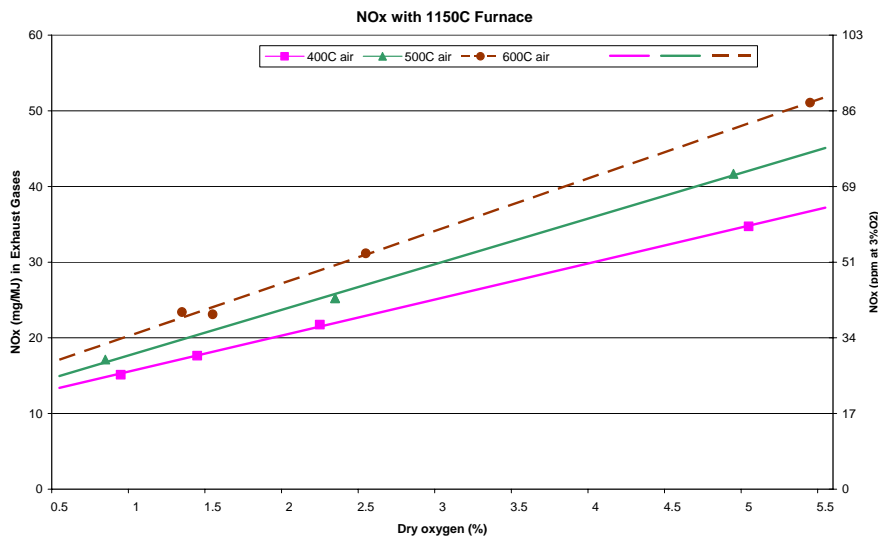


Figure 33. NOx with separate propane injection at 1150 °C and preheated air in MEFOS chamber furnace.

The chamber furnace at MEFOS does not have any heat recovery, so air was electrically heated in a muffle furnace. The air preheat system has been described in earlier project reports. The original TABO type TG751-300 burner was designed only for 300 Nm³/hr of cold air (about 330 kW). Cold air is beneficial for minimizing NOx, but the nozzle mix burner gives relatively high NOx levels.

Trials were made firing propane with a furnace temperature of 1150 and 1250 °C and with air preheated to 400, 500 and 600 °C in an electrically heated muffle furnace. The furnace was preheated to over 750 °C before using the DFI modified burner, since separate injection of fuel and air should not be used with a cold furnace. NOx levels were measured with Kane-May portable gas analyser with electrochemical measurement cells for O₂, CO and NO. The instrument uses a correction factor of 1.05*NO=NOx. The NOx with the furnace at 1150 °C with 1 % dry oxygen in the combustion gases was at or below about 20 mg/MJ (34 ppm NOx corrected to 3 % oxygen) for all air preheat temperatures, rising to about 25 mg/MJ (43 ppm NOx) when a furnace temperature of 1250 °C (see Figures 32-33). The NOx levels increased when increasing the air preheat temperature, increasing furnace temperatures and increasing excess oxygen. A comparison of the NOx with original burner firing cold combustion air is shown with the data at 1250 °C. Note that the NOx levels with cold combustion air can approach the NOx levels with the low NOx DFI technique at about 6 % dry oxygen in the exhaust gases, since the cold air reduces the flame temperature. The fuel nozzles oxidized during the trials changing the fuel injection hole geometry and giving a limited nozzle lifetime. The equipment was intended for only short-term trials, so commercial direct fuel injection technology, flameless burners or burner manufacturer expertise should be used when modifying steel reheating furnaces.

In summary, a lower furnace temperature, lower air preheat temperature and less excess oxygen generally will give lower NOx for the same burner design. The flameless combustion burner designs have shown the best performance, for example the Techint TSX or VTS-NFK HRS burners for air combustion with a central recuperator or regenerator. The NOx emission curves for specific burner trials were compared using both mg NOx/Nm³ at 5 % excess oxygen and in mg NOx/MJ, since oxy-fuel combustion in WP4 should be compared with air combustion only with NOx referred to the energy input and not the exhaust gas concentration.

2.1.3 Task 1.3 Test with flameless regenerative combustion low NOx burner (CSM)

This task is directed at studying regenerative burners, which operate in on/off cycles instead of continuously “ON” as for central heat recovery plus a portion of the exhaust gases typically are exhausted without heat recovery to control the furnace pressure. In Europe research has been performed and burners based on flameless and ceramic regenerator are applied in relative small scale (up to 300 kW) [20]. Recently research project has been sponsored by CORUS to characterise the NFK HRS

burner at IFRF [21] and recently two pair of the NFK-HRS-DL9 burner have been installed in the one of the CORUS pusher type reheating furnaces at the Llanwern Works in the United Kingdom. However, technical design solutions for large plants still is behind other countries, and no European burner manufactures offer very low NO_x regenerative burner of the largest sizes (up to 5 MW). Based on these considerations, and taking into account the availability of IFRF results for NFK burner trials with natural gas, the regenerative burner manufactured by Bloom Engineering was selected for testing. However characterisation tests were not possible due to the decision of Bloom management to not supply the burner in spite of signed confidentiality agreement. During 2005 a new German company, FBB, offered the opportunity to test in the frame of NO_x-RF project the prototype of new regenerative burner with nominal capacity of 600 kW, named FBB TriX 100-10/16 (Figure 34) at both CSM and BFI . This burner is characterised by the use of a new foam regenerator system, but it was not a flameless combustion burner.

The installation of FBB TriX 100 burners on CSM's Modular Furnace # 1 has required adapting the air and gas piping, to modify the front furnaces wall for installing the couple of burners (Figure 35). Moreover, since a high percentage of combustion products (60-80 %) have been sucked directly by the burner, the original connection to the stack has been closed and a new extraction point of smaller diameter opened on the top of the furnace (Figure 36). Unfortunately this caused that the furnace pressure could not be regulated.

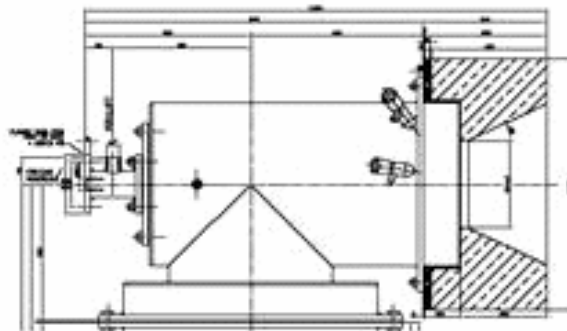


Figure 34. FBB TriX100 burner as received at CSM.

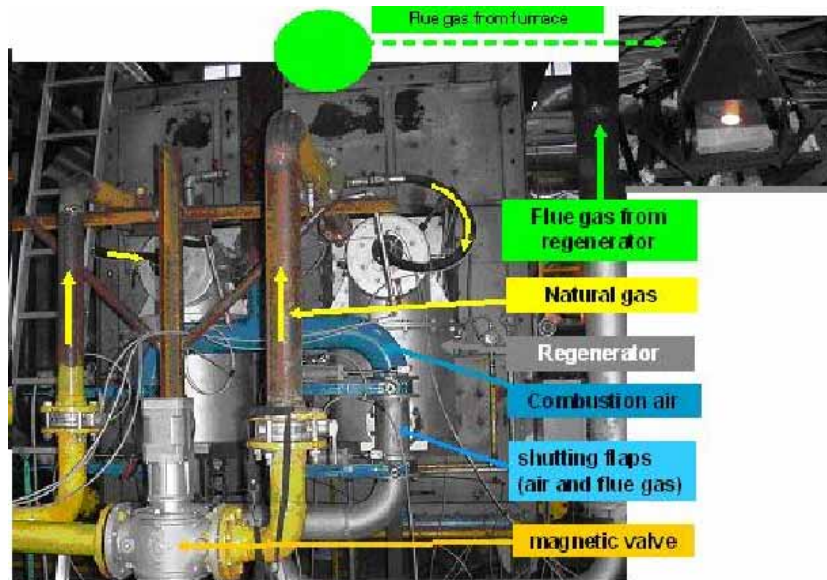


Figure 35. FBB TriX100 installation at CSM Modular Furnace # 1.

The burner has been tested at a nominal firing power (600 kW), calculated as the flow rate of natural gas multiply by lower heating value of the fuel, for two different furnace temperatures (1250 °C and 1150 °C). The NO_x emission has been measured in the furnace, by CSM, and at the exit of the regenerator, after the shutting flaps, by ISQ. The two measurements, if referred to the same value of excess O₂ (some air infiltration through the flaps has been detected) are very close.

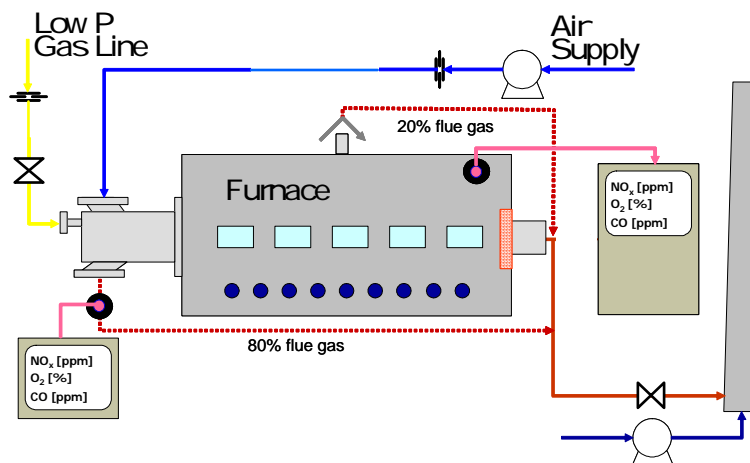


Figure 36. CSM Modular furnace schematics after FBB burner installation.

NO_x emissions, as a function of O₂ concentration in dry flue gas, increase with R, the ratio between flow rate of flue gas from regenerator and the combustion air, for both the furnace temperatures (Figures 38-39). This is because R is related with the temperature of preheated combustion air (Figure 40). In fact, fixed the furnace temperature, NO_x in Figures 35-36 can be also read as a function of temperature (Table 10):

Table 10. Furnace temperatures and recycle ratio R.

	T _{furnace} = 1150 °C	T _{furnace} = 1250 °C
R → T _{air}	0.6 → 825 °C	0.6 → 900 °C
	0.7 → 925 °C	0.7 → 1000 °C
	0.8 → 1000 °C	0.8 → 1100 °C
		0.9 → 1150 °C

The level of NOx emission is higher than BAT side burners (flameless). This is not justifiable only by higher combustion temperature. The main reason of high NOx emission is that the FBB burner shows a stable and attached flame in all the operation range. In fact, looking at Figure 37, the NFK/VTS (flameless combustion) tested at the same level of air preheated temperature (1000 °C) shows a significant lower level. The CO in the flue gas has been found negligible in all tests conditions confirming a very good combustion inside the furnace. Moreover inversion time do not effect the NOx emissions.

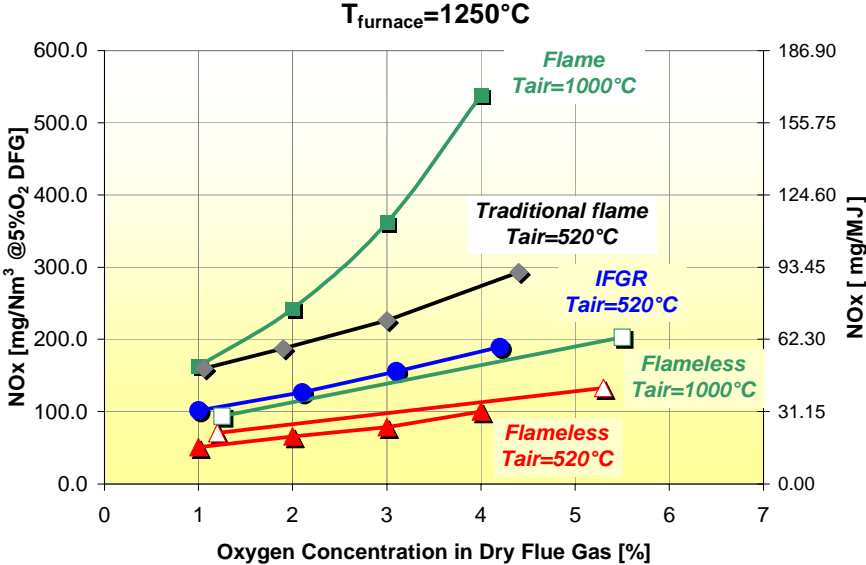


Figure 37. NOx emission for different combustion technology and different combustion air temperature. Data for the NFK HRS burner with flameless combustion at 1000 °C is from the IFRF tests.

The structure of combustion regime is also confirmed by the wide range of air and natural gas flow rates permissible during the ignition phase.

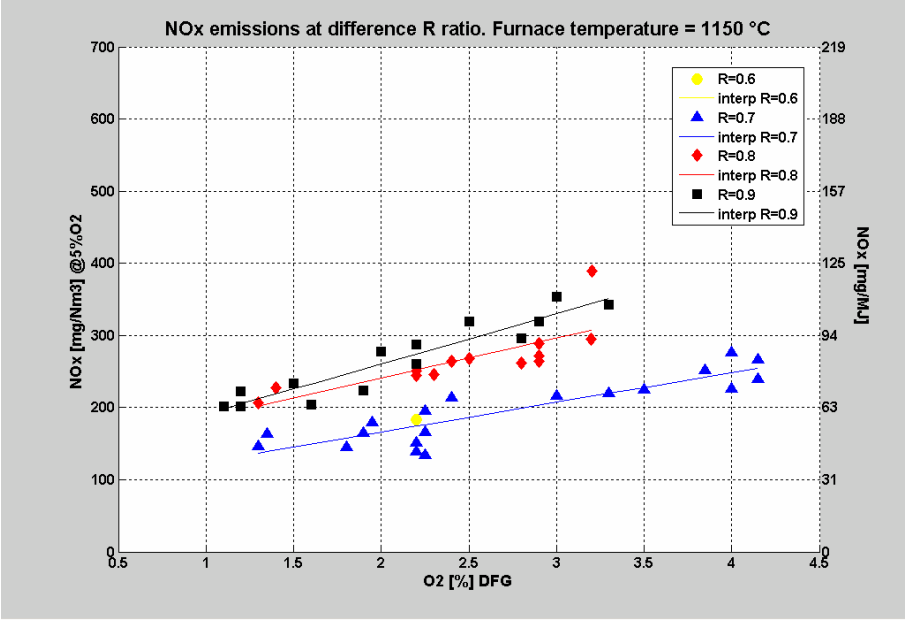


Figure 38. NOx emissions at various R ratios with a furnace temperature of 1150 °C.

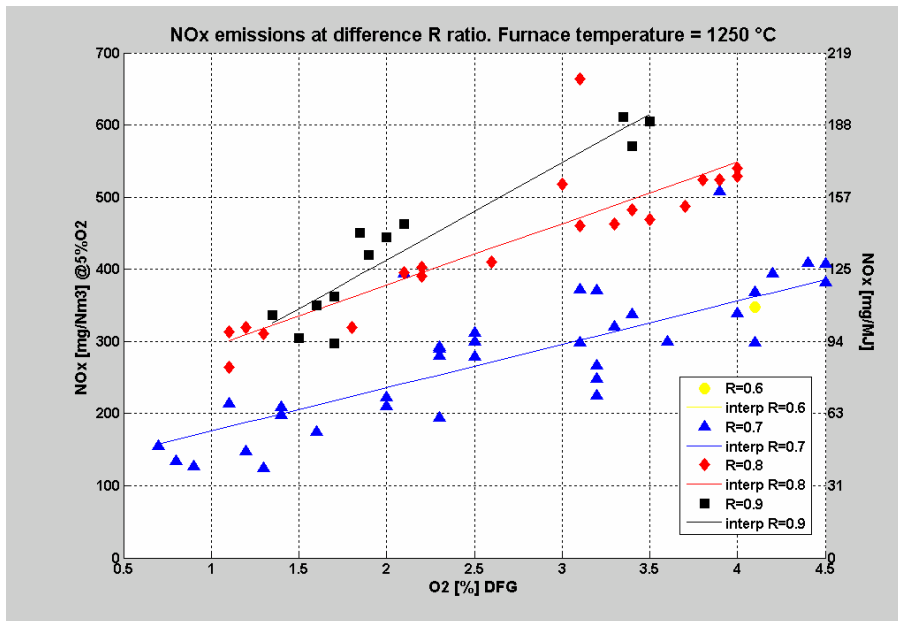


Figure 39. NOx emissions at various R ratios with a furnace temperature of 1250 °C.

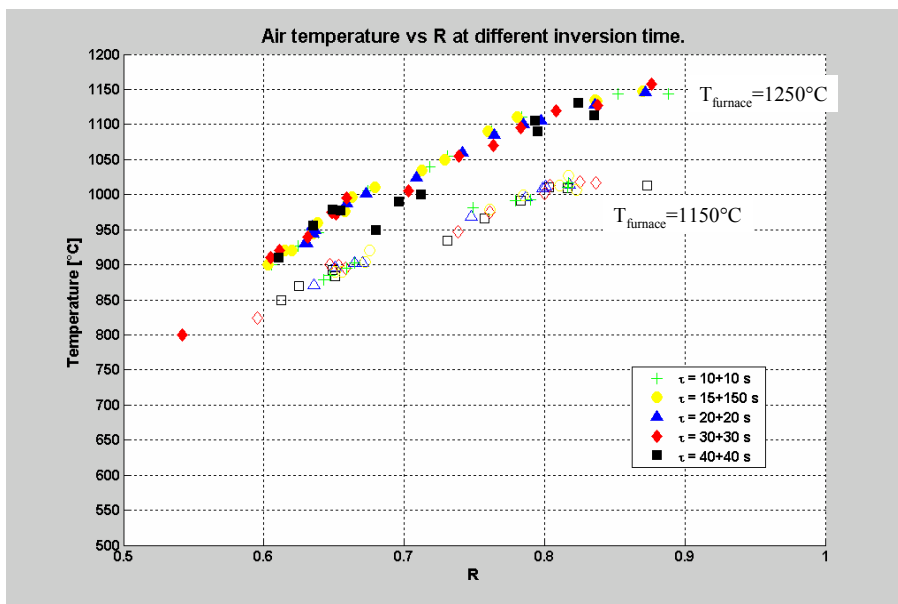


Figure 40. Air temperature versus R for various cycles.

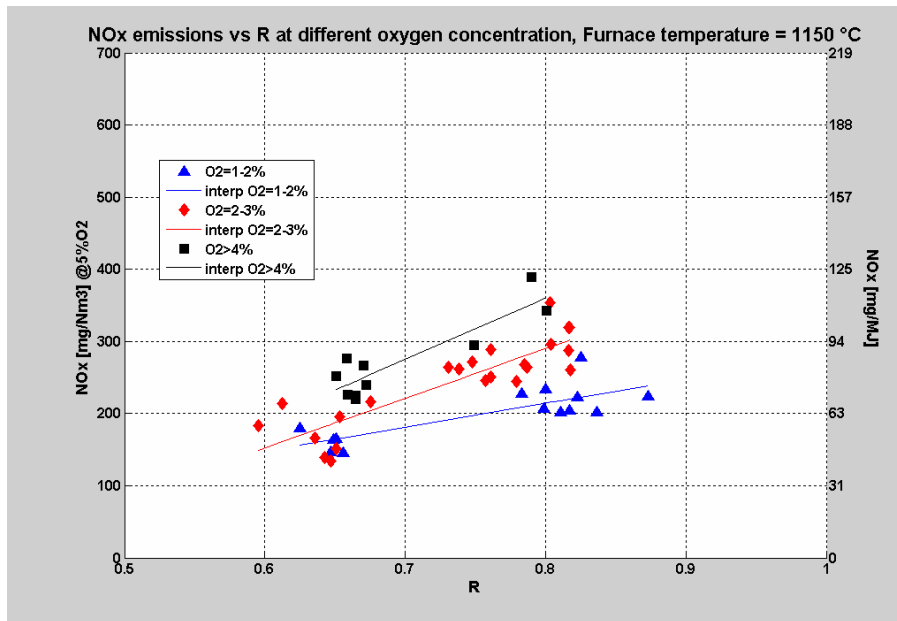


Figure 41. NOx emissions for various R ratios and oxygen concentrations at 1150 °C.

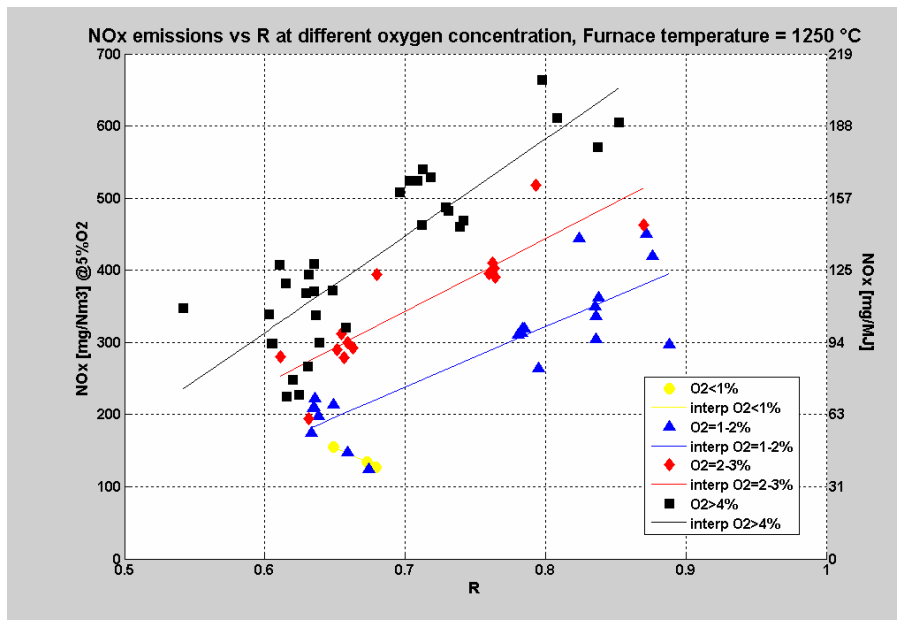


Figure 42. NOx emissions for various R ratios and oxygen concentrations at 1250 °C.

When evaluating the performance of the foam regenerator, a high efficiency of air preheating has been observed, that is, with a high R the air temperature is 100 °C lower than furnace temperature (Figure 40). This produce a increase of furnace efficiency respect to the standard recuperator technology up to 80 % (Figures 43-44).

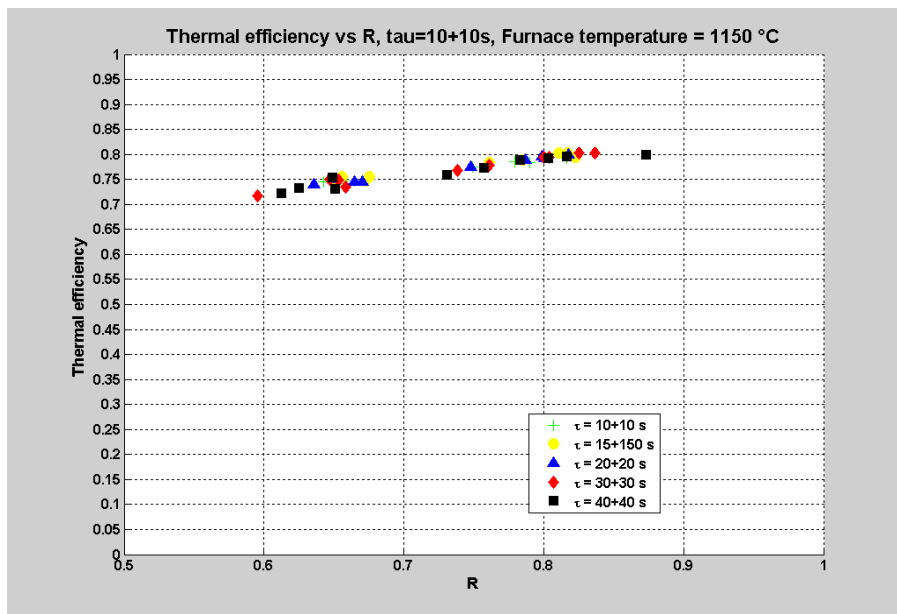


Figure 43. Thermal efficiency versus R for a furnace at 1150 °C (left side figure).

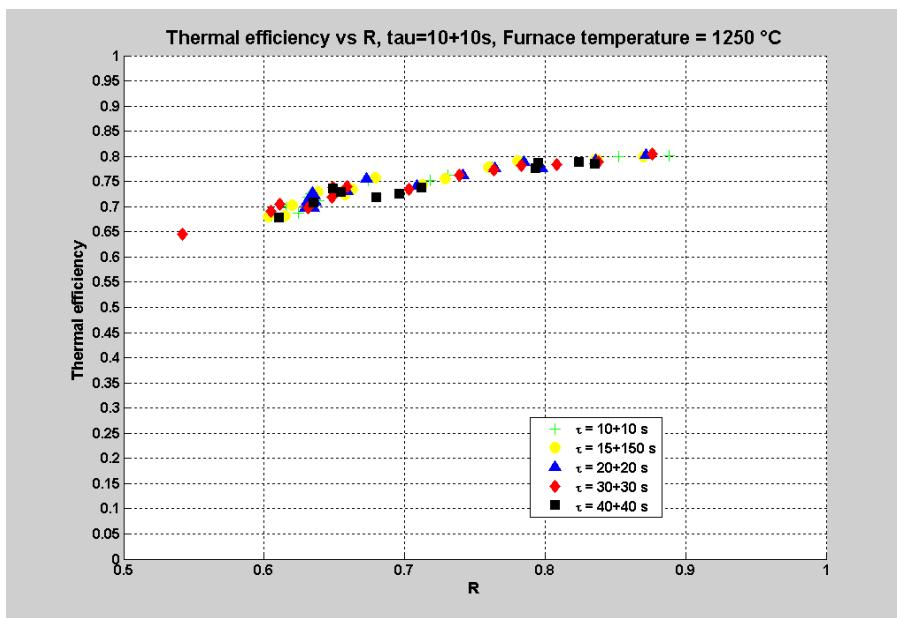


Figure 44. Thermal efficiency versus R for a furnace at 1150 °C (right side figure).

This high thermal efficiency has been obtained with regenerator pressure losses (Figure 45) between the honeycomb and ball one, however the dimensions used for the FBB regenerator are higher in comparison with an equivalent regenerator based on the honeycomb geometry.

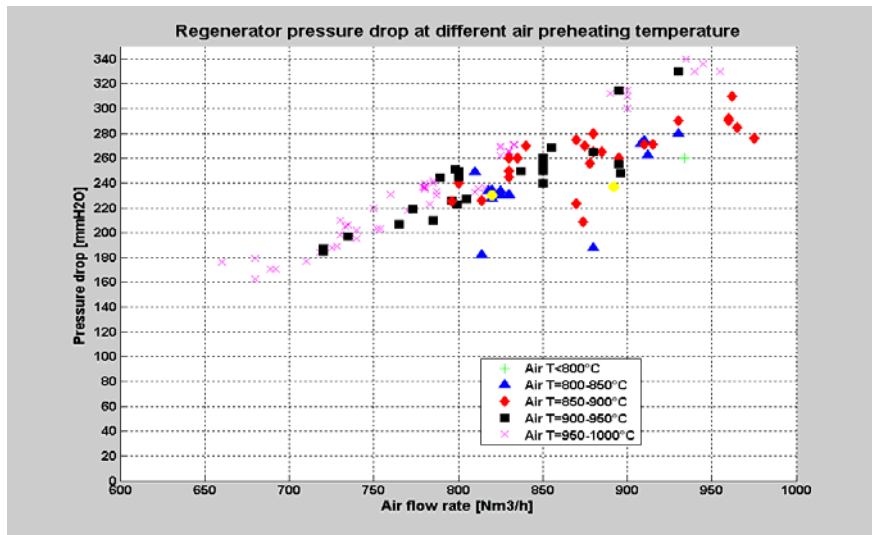


Figure 45. Pressure drop in regenerator.

The same FBB burners tested at CSM were also tested at BFI. The two burners were faced mounted at BFI because of the small cross section area (1 m x 1 m) of the combustion chamber. Figure 46 shows the scheme of the installation of the two regenerative burners at the burner test rig. For the installation extensive alterations were needed. In former time only single burners were tested at the test rig inside of the hall. The waste gas flue on one end of the combustion chamber that leads to the stack (top right in Figure 46) was largely closed with fireproof fibre blocks to prevent any radiation influence on the burner below. The flue gas flow through this flue was choked with a control butterfly valve in the flue gas line (\varnothing 500 mm). On account of existing leaks in the control butterfly valve and flue duct, the flue gas amount that could be extracted through the regenerators - to maintain a combustion chamber excess pressure and avoid the infiltration of air - was limited to around 80 % of the theoretical flue gas amount.

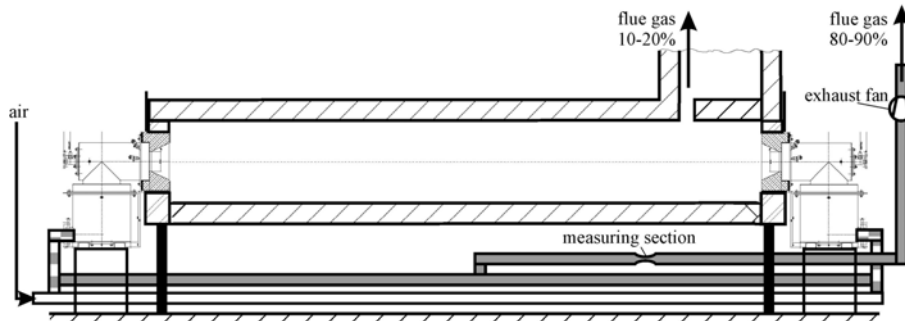


Figure 46. Scheme of the installation of the FBB TriX regenerative burners at the BFI burner test rig.

Outside of the hall new piping for combustion air and fuel was mounted for the second burner. For the exhaust of the flue gas through the regenerators a exhaust fan with flue gas piping was needed. The switching for an alternating air- and flue gas- flow through the regenerators was accomplished by four butterfly valves. The piping was mounted symmetrically for both burners, so that the same volumetric flow rate could be obtained for both burners without any pressure control. The flue gas flow rate of both regenerators was measured by one measuring section in the common flue pipe (see Figure 46). This was the initial heating of the burner, so it was carried out at a low heat-up velocity over a period of 40 hours up to around 1250 °C. This largely avoided a damage to the burner firing blocks through cracks. The same burners were later sent for a second series of tests at CSM.

Figure 47 shows the thermal behaviour of a regenerator at nominal and very long switching time. The air and flue gas temperatures in the regenerator were measured with high velocity thermocouples. A high air pre-heating of around 125 K below the combustion chamber temperature was achieved at the nominal switching time of 40 seconds. The fluctuations in temperature of the regenerator material (both top and base) were very low with these conditions. This proves to be a good size for the regenerators

with only minor thermal cycling stresses in the material. The flue gas piping after the regenerators could not be used for emission sampling on account of combustion air leaks in the switching flaps. A measuring point on the regenerator base was thus used for the analysis. On account of the cyclic operation of the burner the medium alternates at this point between combustion air and flue gas. No sufficiently constant emission values could be measured with a cycle time of 80 seconds. An extended burner running time of two minutes each (cycle time four minutes) was thus set for the measurements of the emission values. The measured concentration values hereby remained constant for a period of approximately one minute.

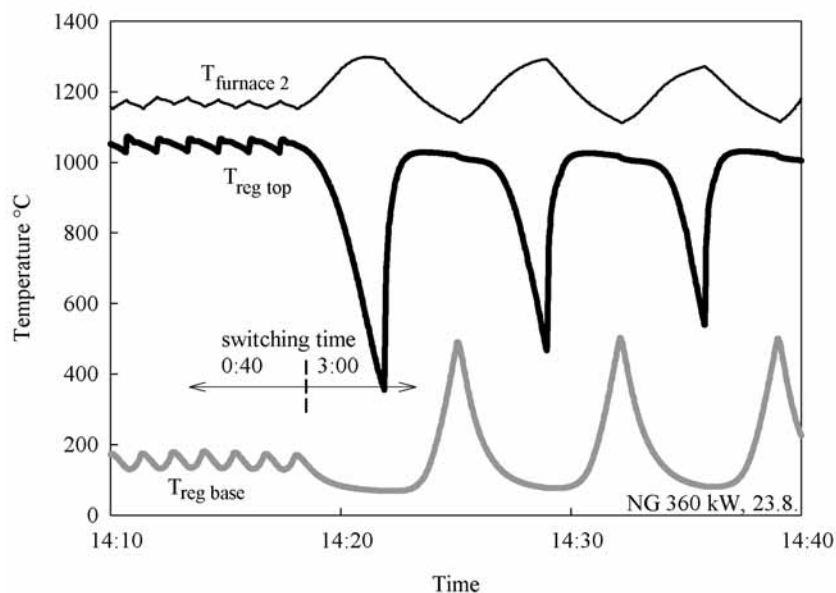


Figure 47. Temperature fluctuation in the furnace and inside of the regenerator top and base (air or flue gas temperatures) at different switching times.

Unexpected high NO_x emission values were the results of the measurements - both for natural gas and coke oven gas. The search for possible reasons by numerical calculations (see WP 2) led to the problem of very small recirculation areas in the furnace near the burner mouth. This caused a very quick heat up of the flue gas in the furnace and prevented the minimization of the flame temperature by dilution with the flue gases. The temperature in the combustion chamber was measured with 8 ceiling thermocouples. Figure 48 shows the increase of temperature in the combustion chamber during a burner's running time. The temperature in the area near the burner increased by around 200 K. So the NO_x values measured were not representative for this regenerative burner. The tests were repeated at CSM in a much bigger combustion chamber, which gave lower and more representative NO_x emission values. A result of this first analysis one can conclude that there is a need for a large cross-sectional area in the furnace around the burner mouth. The mounting of Low-NO_x-burners should ensure a distance of more than 300 mm between the burner mouth and a furnace wall or a next burner.

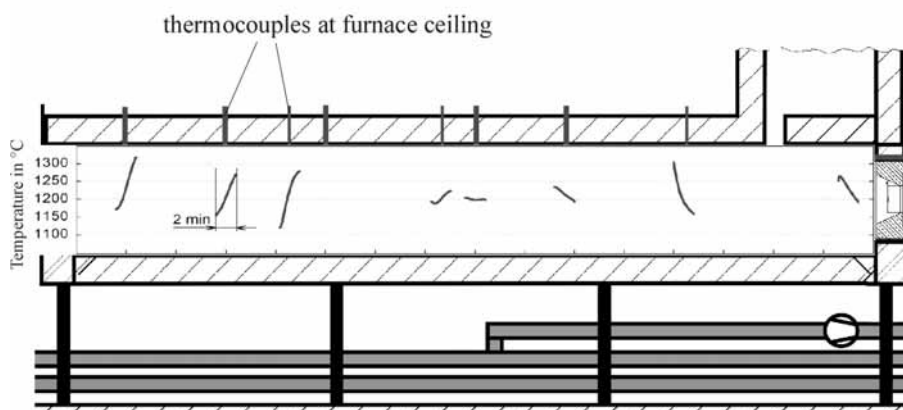


Figure 48. Temperature fluctuation over the length in the BFI combustion chamber during a half cycle at the operation of one regenerative burner (on the left side).

2.1.4 Summary

Flameless low NO_x burners are superior to conventional burners with visible flames, but there are both advantages and disadvantages to consider for the new technology. Table 11 summarises some of the factors to consider when installing flameless technology both air combustion in WP1 and oxy-fuel combustion in WP4.

Table 11. Advantages and disadvantages of flameless low NO_x burners for air and oxy-fuel combustion.

Advantages	Disadvantages
Flameless air combustion burners	
Reduction of NO _x of up to 80 % with respect to conventional flame burners.	Higher pressure for gaseous fuel than conventional burners. This could be less of a problem for NG than COG and BFG.
Minimum investment for revamping with easy installation, and little impact on the flue gas extraction system.	Need of logic for switching from flame to flameless and vice-versa, for example, based on thermocouple signals and not from traditional flame detectors.
No additional operating cost as far as concerns fuel and air.	Additional maintenance operation for valves: minimal if only the gas valve mode is switched.
Flameless oxy-fuel burners	
Very low NO _x in mg/MJ are possible (12 mg/MJ in the WBF trials).	Air leakage has to be minimized to optimise NO _x emissions, which can mean additional equipment.
Energy saving relative to reheating furnaces with central recuperators.	Additional operating cost to supply the oxygen.
Higher furnace productivity relative to air combustion.	Need for new burner control and safety equipment, e.g., for switching from flame to flameless and vice-versa.
Reduction of equipment cost for new furnace, e.g. shorter furnace possible.	Higher pressure for gaseous fuel than conventional burners. This could be less of a problem for NG than COG and BFG.
Less flue gases make CO ₂ recycling easier.	

2.2 WP 2 - Modelling of NO_x in industrial furnaces and from burners with validation trials

2.2.1 Task 2.1. Integrating CHEMKIN and interactions with CFD

Combustion processes are governed by reacting flows, mostly the flows can be considered to be non-compressible, and where the understanding of the interplay between the fluid transport, heat transfer and chemistry is essential for the development of new combustion techniques to improve industrial processes. Chemical kinetics has an important role in determining the final composition of flue gases for combustion, but is not the only factor to be taken into account, because turbulence is also crucial in the combustion process. Finally, the chemical composition for the mix of gases is a function of the kinetic constants for the reactions taking place in the mixing, but they are also a function of the mixing rate of the different species. So, the products of the reactions depend on the initial species, the reactions occurring and the way species are mixed.

Nitrogen chemistry is particularly challenging, since there are a large number of reactions and intermediate species describing nitrogen oxides (NO_x) formation and reduction. Generally speaking, there are three primary sources of NO_x formation in combustion processes, which are well documented: Thermal NO_x, fuel NO_x and prompt NO_x. Thermal NO_x formation is highly temperature dependent, and it is recognized as the most relevant source of NO_x when combusting natural gas under normal conditions. Fuel NO_x tends to dominate during the combustion of fuels, such as coal, which have a significant nitrogen content, particularly when burned in combustors designed to minimise thermal NO_x. The contribution of prompt NO_x is normally considered negligible.

As mentioned earlier, the NO_x kinetics are very complex, and different mechanisms have been developed and are still under development during the last years. Some of those kinetics mechanisms, which have been used in the frame of this project are briefly describe below.

The Kilpinen 97 mechanism involves 57 species in 353 elementary gas-phase reactions (see Kilpinen 97 mechanism (see <http://www.abo.fi/fak/ktf/cmc/research/index.html>) [27-29]. Sub-mechanisms are included for oxidation of C1-C2 hydrocarbons, HCN, and NH₃, as well as for interactions between hydrocarbons (CH_i, HCCO) and nitrogen species (NO, NH_i, N₂). The scheme is based on the mechanisms of Glarborg [27,28] and Miller and Glarborg [29]. The mechanism Kilpinen 97 is used for the CHEMKIN model. The Kilpinen 97 mechanism is the result of an upgrade of Kilpinen 92 done in 1997 and it includes 353 reactions between 57 species. The upgrade comprised the revision of many kinetic constants, as well as the introduction of new reactions involving the species N₂H₃, N₂H₄, HONO, NO₃, H₂NO, NCN, C₂N₂, and HNNO. In the simulations with Kilpinen 97 mechanisms, the thermodynamic properties of most of the species involved were deduced from the Sandia Chemkin Data Base (www.ca.sandia.gov). The basis of the two Kilpinen mechanisms has been validated over the years against a body of experimental data, and found to be satisfactory for describing the nitrogen reactions under a variety of combustion conditions. Kilpinen 92 represents the first generation mechanisms developed at Åbo Akademi University since the late 1980s. All these mechanisms have been based on the mechanisms of Glarborg and co-workers (1986, 1991, 1993, 1994, 1995a, and 1995b) and Miller and Bowman (1989). The Kilpinen 92 model involved 253 elementary gas-phase reactions between 49 species. It included the oxidation sub-mechanisms for C1-C2 hydrocarbons, HCN, NH₃, and the sub-mechanisms describing the interactions between hydrocarbon (CH_i, HCCO) and nitrogen (NO, NH_i, N₂) species.

GRI-Mech 3.0 (www.me.berkeley.edu/gri_mech/) is an optimized mechanism designed to model natural gas combustion, including NO formation and reburn chemistry. It is the successor to version 2.11, and another step in the continuing updating evolution of the mechanism. It is to be noted that the important reactions of NH₂+NO leading to thermal De-NO_x processes are not included in the GRI-Mech 3.0, which could be one reason for the over estimation in the NO_x predictions obtained when implementing this mechanism.

The scheme ÅA mechanism [30] is a gas-phase detailed chemical kinetic scheme involving 60 species in 371 elementary gas-phase reactions. There are 57 species and 353 reactions which are the same as in the scheme formerly released on this website as Kilpinen 97 (K97), while the remaining 3 species and 18 reactions are taken from a scheme recently developed at Princeton University (PU). The scheme K97 can simulate atmospheric and pressurized processes at high temperatures, but it does not account for oxygenated compounds, such as methanol.⁴ The 18 reactions from the scheme PU include a subset for the oxidation of methanol (CH₃OH) as based on the work by Li et al., and it can simulate the oxidation of methanol at high temperatures.

The Scheme ÅA was developed for the simulation of gaseous mixtures that contain C1-C2 hydrocarbons, CO, H₂, and CH₃OH in the combustible portion. The ÅA Scheme can also simulate the fate of nitrogen pollutants, including the conversion of NO_x via thermal, prompt, N₂O –intermediate, and fuel mechanisms. In its current state of development, the AA Scheme can be used especially (but not exclusively) for simulating the combustion and pyrolysis of biomass-derived gases at atmospheric and pressurized conditions.

CHEMKIN is a software tool for solving complex chemical kinetics problems. It is used worldwide in multiple processing industries and for combustion problems. It was originally developed at Sandia National Laboratories and is now developed at Reaction Design (see: <http://www.reactiondesign.com>). CHEMKIN solves thousands of reaction combinations to develop a comprehensive understanding of a particular process, which might involve multiple chemical species, concentration ranges, and gas temperatures. The computational capabilities of CHEMKIN allow for complex chemical reactions to be studied in detail, including intermediate compounds and trace compounds. CHEMKIN allows for a more time-efficient investigations of potential new processes compared to direct laboratory investigations. One limitation of CHEMKIN is that it assumes the reaction vessel has a relatively simple geometry, whereas sometimes this is not the case. For that reason, CFD programs are better able

to account for geometric complexity, at the expense of being more limited in their treatment of the underlying chemistry of the reactive process being studied.

The High Temperature Reduction (HTR) process described in WP5 was solved by means of CHEMKIN reactor network, since the geometry is easy to simplify. A reactor network was used to describe the ammonia or urea injection, and the results of the prediction of the NO_x concentration in the flue gases can be calculated.

Fluent CFD software describes NO_x formation and reduction chemistry, with an additional NO_x model for the prediction of thermal, prompt and fuel NO_x formation. But the mechanisms of NO_x formation and reduction have been obtained from laboratory experiments, using laminar premixed flame or shock-tube studies, where molecular diffusion conditions are well defined. For industrial processes, the combustion is highly turbulent, with fluctuations in temperature and species concentration that influence the characteristics of the flame. Fluent uses the Probability Density Function (PDF) approach [26] to model the mean turbulent reaction rate, which has proven very useful in the theoretical description of turbulent flow. The basis of the non-premixed modelling approach, in which chemical kinetics schemes previously defined are included, is that under a certain set of simplifying assumptions, the instantaneous thermochemical state of the fluid is related to a conserved scalar quantity known as the mixture fraction. If a secondary stream (another fuel or oxidant, or a non-reacting stream) is included, the fuel and secondary mixture fractions are simply the elemental mass fractions of the fuel and secondary streams, respectively. The sum of all three mixture fractions in the system (fuel, secondary stream, and oxidizer) is always equal to 1: In mathematics, a probability density function (PDF) represents a probability distribution in terms of integrals. Formally, a probability distribution has density f , if f is a non-negative Lebesgue-integrable function $\mathbb{R} \rightarrow \mathbb{R}$ such that the probability of the interval $[a, b]$ is given by:

$$\int_a^b f(x) dx \quad (\text{Eq. 1})$$

for any two numbers a and b . This implies that the total integral of f must be 1. Conversely, any non-negative Lebesgue-integrable function with total integral 1 is the probability density of a suitably defined probability distribution. Intuitively, if a probability distribution has density $f(x)$, then the infinitesimal interval $[x, x + dx]$ has probability $f(x) dx$. Informally, a probability density function can be seen as a "smoothed out" version of a histogram: if one empirically samples enough values of a continuous random variable, producing a histogram depicting relative frequencies of output ranges, then this histogram will resemble the random variable's probability density, assuming that the output ranges are sufficiently narrow.

The equations governing turbulence and chemical kinetics describe the instantaneous relationships between mixture fraction and species fractions, density, and temperature under the assumption of chemical equilibrium. The FLUENT prediction of the turbulent reacting flow, however, is concerned with prediction of the averaged values of these fluctuating scalars. How these averaged values are related to the instantaneous values depends on the turbulence-chemistry interaction model. FLUENT applies the assumed-shape probability density function (PDF) approach as its closure model when the non-premixed model is used. The Probability Density Function, written as $p(f)$, can be thought of as the fraction of time that the fluid spends in the vicinity of the state f . The use of these modelling tools are described in the other sections of this report.

2.2.2 Task 2.2. Development and adaptation of CFD model

2.2.3 Task 2.3. Modelling for NO_x reduction strategies

2.2.4 Task 2.4. Model validation and refinement with data from reheating furnace

These three tasks overlap, so the report will discuss these tasks by work done by the partners instead of dividing the modelling into many pieces that can be difficult to follow. For example, industrial furnace

modelling was only done at VA, oxy-fuel modelling of WP4 trials was only at LABEIN, while CSM, BFI and MEFOS made CFD models of NO_x formation based on the pilot trials in WP1.

The CFD calculations have been made using the FLUENT code. The NO_x model implemented in FLUENT uses rate models developed at the Department of Fuel and Energy, The University of Leeds, England as well as from the open literature. The formation of thermal NO_x is determined by a set of highly temperature-dependent chemical reactions known as the extended Zeldovich mechanism. The rate constants for these reactions have been measured in numerous experimental studies, and the data obtained from these studies have been critically evaluated by Baulch et al. [31] and Hanson and Salimian [32]. The expressions for the rate coefficients are based on the evaluation of Hanson and Salimian. The "prompt NO_x" formation was based on Fenimore work [33]. This model performs well for NO_x formation in flames, but it was found to underestimate the NO_x formed for lower temperature flameless combustion.

Oxy-fuel modelling at LABEIN

A CFD model of the oxy-fuel burner was made using only half of the BFI furnace geometry. Even when the geometry has two planes of symmetry, the physical model has only vertical symmetry. Therefore, half of the combustion chamber has been modelled. For modelling purposes, two meshes have been employed: one of tetrahedrons and another structured mesh using hexahedrons.

First step in CFD modelling consists of simplified chemistry combustion, with the Eddy Break Up combustion model. It is also possible to make a very simplified study which only considers flow solution, not taking into account the combustion. With both cases, the convergence for the meshes was tested and it was concluded that the mesh of hexahedrons, which in theory must work better, gave instead a worse result. That seems to be due to the bad aspect ratio in some of the cells, derived from the huge difference in scales from the order of millimetres in the inlets of fuel and comburent oxygen to on the order of meters in the combustion chamber. In such cases, a tetrahedral mesh or a mesh consisting in multiple zones with differences in the mesh resolution can work better.

From the first results of the CFD calculations, the temperature and flow field were obtained, so that, an approach in terms of reactor network is possible. The easiest network consisting of a unique reactor, taking the averaged values for turbulence, temperature and the other parameters involved in the combustion can be used in the description. A more realistic reactor network can be made after the flow details are obtained.

The tetrahedral mesh consisted of 800000 cells, which in the case of the complete geometry corresponds to 1600000 cells. Figure 49 describes the tracks from the fuel injection, where re-circulations are negligible. In Figure 50, re-circulations from secondary oxygen injection are shown, being similar to those obtained for primary oxygen injection.

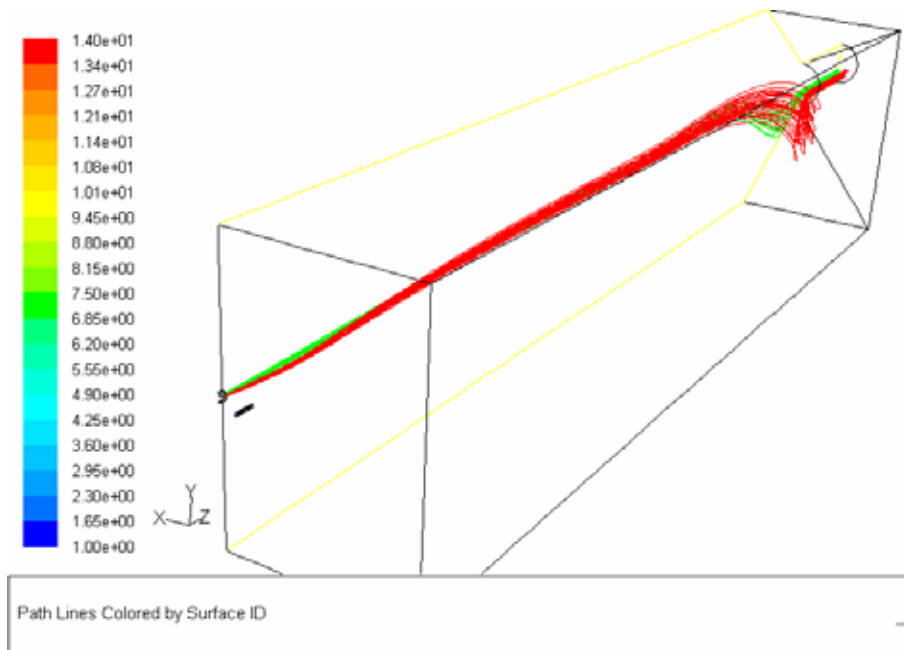


Figure 49. Path lines from fuel injection for the oxy-fuel burner model.

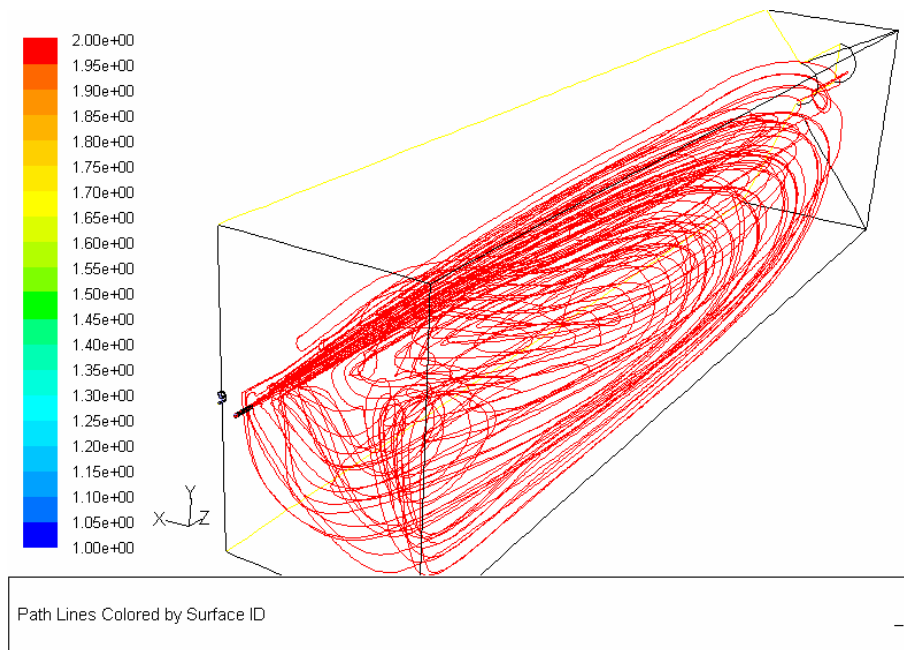


Figure 50. Path lines from secondary oxygen in combustion chamber.

When combustion occurs with pure oxygen instead of air, the origin of NO_x is greatly reduced, because nitrogen from air is not allowed and nitrogen oxide production is greatly reduced. The origin of nitrogen oxide in this case is due to two sources: air leaking into combustion chamber or nitrogen present in the fuel. Fuels employed in steelmills, as Natural Gas or Coke Oven Gas contain some nitrogen in their compositions. Air leaks into furnaces can be reduced increasing operating pressure of the furnace, but is very difficult to control for an unsteady process when doors or other openings are being opened. In a theoretical model with propane and oxygen combustion, without air leaks, no NO_x production is obtained in the furnace. That was modelled in a preliminary furnace chamber simulation, with the Eddy Break Up (EBU) model of combustion, for which combustion occurs by mixing instead of chemical kinetics. This was mostly to understand the flow and select the most appropriate of the meshes. EBU model also trends to over predict temperatures and it is not suitable for the purposes of this study.

Probability Density Tables (PDF) have been generated for each of the simulations run. Those PDF tables are unique for each composition of fuel and oxidizer, and also for the conditions in which the combustion occurs. A model with propane and oxygen was tried. Air leaks have been calculated from the exhaust gas composition, taking into account the presence of nitrogen in the furnace gases due to air infiltration. The problem in trying to modelling those leaks in terms of chemical kinetics is due to a Fluent limitation with PDF tables with 2 streams. Here, a secondary oxidizer stream of air must be included, apart of the stream of pure oxygen calculated for the 100 % oxy-fuel combustion. In this case, Fluent only allows the kinetic equilibrium option for PDF tables, which for simplification considers species equilibrium in the flow. The results in terms of nitrogen oxides concentration goes towards a clear over-estimation of NO_x, resulting in thousands of ppm. In conclusion, for model purposes of air leaks, the PDF model is not suitable.

Natural Gas and oxygen combustion modelling without considering air leaks is done with the PDF table based on the ÅA mechanism for the experiments at BFI. The exact composition is the one shown with the BFI experimental data in WP 1. To implement the mechanism, a simplification of the C₃₊ fraction (that is, hydrocarbons of 3 or more carbons) to C₂ was necessary. The model of radiation used has been P1, with participation of gases in radiation by means of a function of averaging radiation coefficients with molecular composition in each cell of the domain. Turbulence was modelled by means of K-epsilon model. Combustion was modelled with PDF with flamelets. As mentioned before, used grid was of tetrahedrons. The numerical solution used the segregated solver, implicit linearization and 2nd order schemes. The problem is a steady one with no time dependence. Inlets are considered as mass flow inlets, and the outlet as a pressure outlet. The wall has fixed temperature. With the above boundary conditions and combustion model, the results for the gas temperatures are shown in Figure 51.

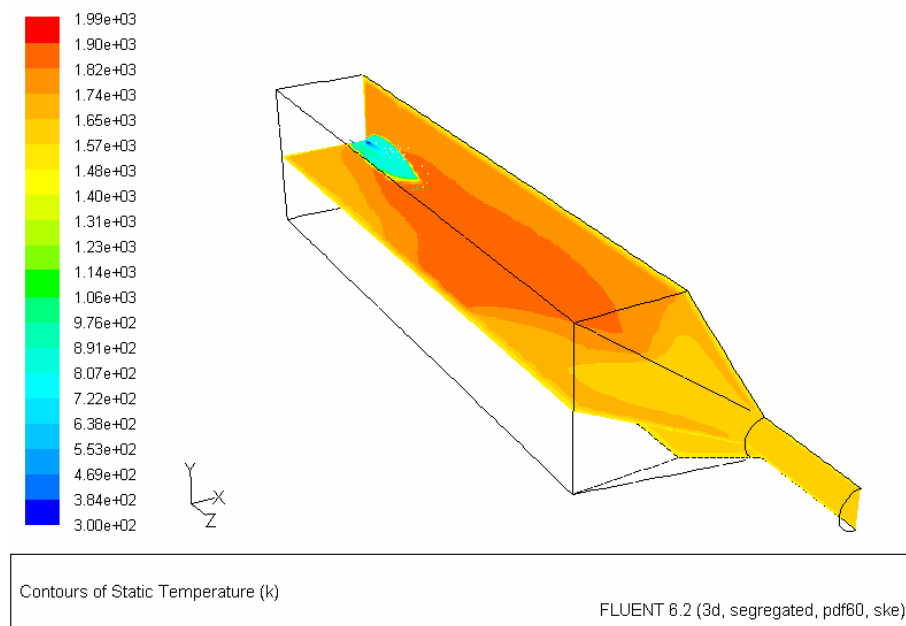


Figure 51. Temperature profiles (in K).

There is also present a NO distribution from the burner using the same assumptions, with a resulting NO concentration in flue gases of 17 ppm (on a dry basis), which is equivalent to 1.1 mg/MJ for Natural Gas combustion with a burner load of 100 % (see Figure 52). In the experimental trials for those conditions, the minimum NO_x obtained was on the order of 4 mg/MJ, which is 4 times more than predicted by the simulation. The differences of both cases could be because of transient effects and air infiltrations are not taken into account by simulation. There is also a more minor effect due to the modelling of only NO formation instead of the sum of all nitrogen oxides, which gives an error on the order of 5 %. Therefore the NO_x based on the simulations can be considered as a theoretical minimum not possible under industrial conditions. A more complex and real simulation must include soot formation, and its interaction with radiation, because that affects the mechanism of NO_x formation.

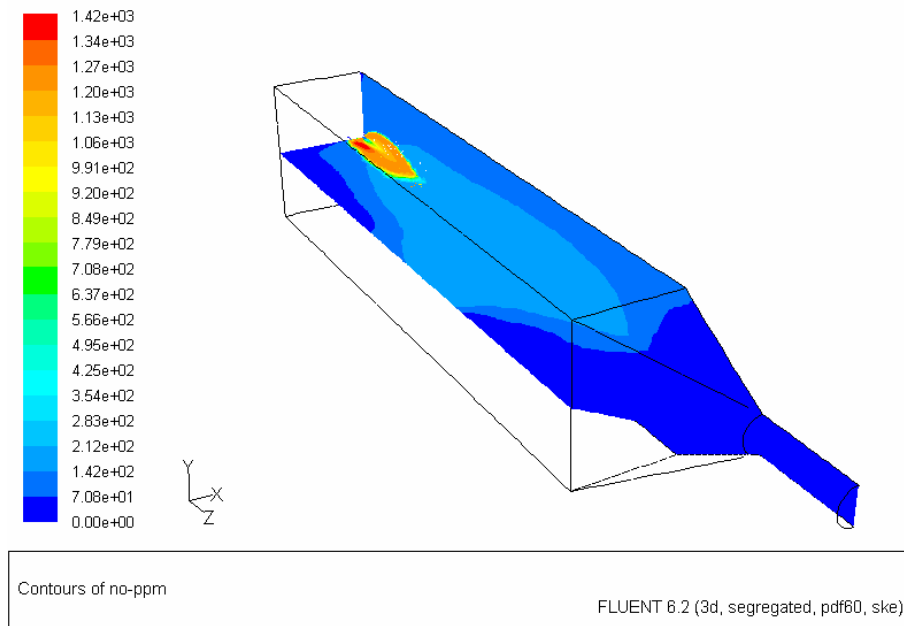


Figure 52. NO distribution for the oxy-fuel burner (ppm on a dry basis).

Modelling the Techint TSN and TSX burners at CSM

CSM’s contribution to WP2 was not originally included in the project. However, to overcome the constraints due to the confidentiality of the Techint burner geometry, CSM agreed to perform CFD with the man-months originally assigned at CSM for WP3 (task 3.1 & 3.4) for modelling Techint TSN and TSX burner as installed at CSM furnaces using FLUENT code. Use of geometry details for the simulation of Hauck TRIOX was not allowed by confidentiality agreement signed with Hauck. The goals of simulation work has been to:

- understand the fluid dynamics and its effects on combustion process inside the furnace;
- assisting in the designing of experimental programs and interpretation of measured data;
- calculation of NO_x emission with FLUENT post-processor

Table 12 summarises the main features of the CFD set-up at CSM developed after investigations dedicated to select: The turbulence model which is able to overcome the well known problem of “round-jet/planar-jet anomaly” [37,38]; and the simplest combustion model to be used in industrial applications for representing the diluted combustion reactive flows [39,40].

Table 12. CFD model parameters at CSM.

Physical model and reaction scheme	
Flow	Reynold Average Navier-Stokes (RANS) Compressible ideal gas
Turbulence	Wilcox k- Ω
Species	CH ₄ , O ₂ , CO ₂ , CO, H ₂ O, N ₂
Reaction scheme	Two steps CH ₄ + 3/2 O ₂ --> CO + 2H ₂ O CO + 1/2 O ₂ --> CO ₂
Chemistry	Eddy-dissipation/Arrhenious (Westbrook&Drives)
Numerical approach	
Grid Type	Hybrid
Solver	Segregated, cell centred finite volume based
Linearization	Implicit
Discretization of non liner terms	Second order up-wind scheme
Boundary Conditions	
Inlet	Mass flow rate
Outlet	Pressure outlet
Walls	Temperature

Modelling of TSN burner at baseline condition

FLUENT™ code (release 6.1.18) has been used first for simulating the combustion process inside CSM’s Modular Furnace equipped with TSN burner working at base line operative conditions: $MFR_{NG} = 147 \text{ Nm}^3/\text{h} @ 25 \text{ }^\circ\text{C}$ and $MFR_{air} = 1475 \text{ Nm}^3/\text{h} @ 450 \text{ }^\circ\text{C}$. The following assumption has been adopted in the build-up of the CFD model (see Figure 53): Symmetry for a cylindrical furnace (36° sector), fixed wall temperatures, emissivity of furnace walls ($\epsilon=0.83$), fuel: 100 % CH_4 and $T_{process} = 1250 \text{ }^\circ\text{C}$. To mesh the 36° sector 108 000 cells are used which are equivalent at about 1000000 for the complete configuration.

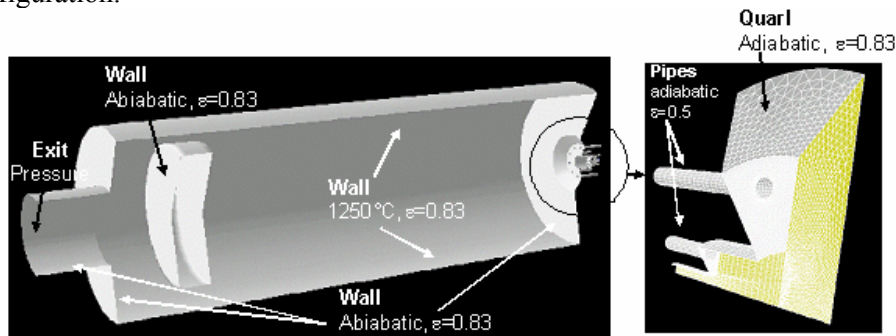


Figure 53. Geometry and boundary condition for TSN simulation.

The first simulations were performed with a Wilcox 98 $k-\omega$ turbulence model [41]. Damage to the refractory at the exit duct of the furnace observed in the preliminary burner tests, confirms the high velocity and high temperature of the jet predicted. The possibility to use a refractory wall to avoid overheating has been investigated, however this can cause some influence on the flue gases recirculation pattern and its local intensity, which has been shown by a simulation (Figure 54). To avoid any modification of this important parameter that dominates for dilute combustion processes, it was decided to increase modify the maximum length of the CSM Modular furnace #1 from 6 to 7.5 m for the final experimental campaign.

Table 13. Arrhenius reaction rate parameters.

	Ak	Ea [J/kmole]	a	b
Set 1				
CH ₄	5.01E+11	2.00E+08	0.7	0.8
CO	2.24E+12	1.70E+08	1	0.25
Set 2				
CH ₄	1.50E+07	1.26E+08	-0.3	1.3
CO	2.24E+12	1.70E+08	1	0.25

In a second set of simulations, the effect of the standard $k-\epsilon$ turbulence model, the model adopted by some of the other partners for the modelling of diffusion flames generated by traditional burners (flame burner), on the thermo and fluid dynamic field has been investigated. The superior ability to reproduce the behaviour of round jets by Wilcox 98 $k-\omega$ turbulence model has been confirmed (Figure 55); the shorter jet predicted by the $k-\epsilon$ turbulence model, in fact, contradicts the experimental observation. The sensitivity at the kinetics used in the Finite-Rate/ Eddy-Dissipation model [42] has been also investigated. However, since in the case of the TSN burner, the combustion process is mainly dominated by mixing, the use of two different sets of Arrhenius reaction rate parameters for the two step global reaction scheme (Table 13 [43]), have not a relevant effect. They are essential only to reproduce the physical situation in a small zone close to the burner tip where Dankohler number (i.e. the ratio between Arrhenius and Eddy dissipation rate) is less than 1 (Figure 56).

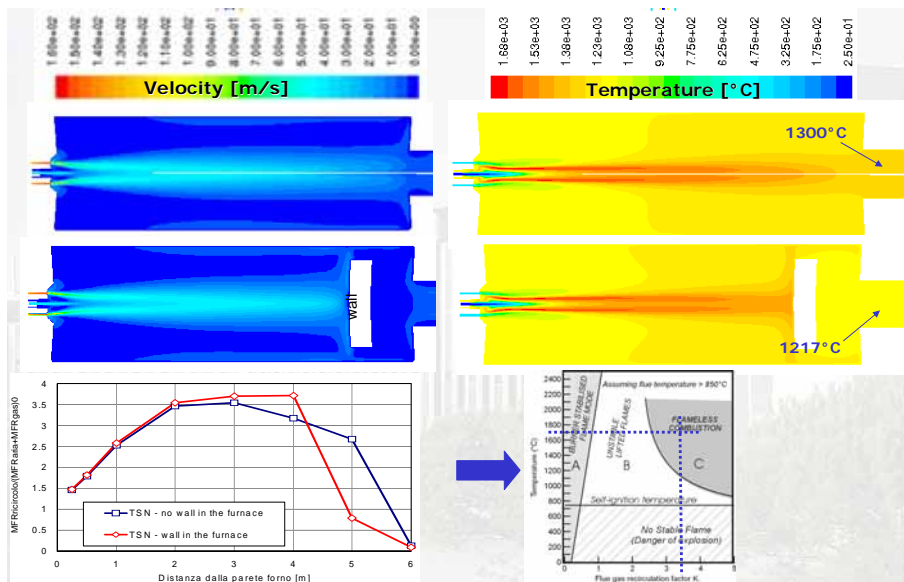


Figure 54. Effect of an obstacle (wall) inside the furnace on recirculation rate ($k-\omega$ model).

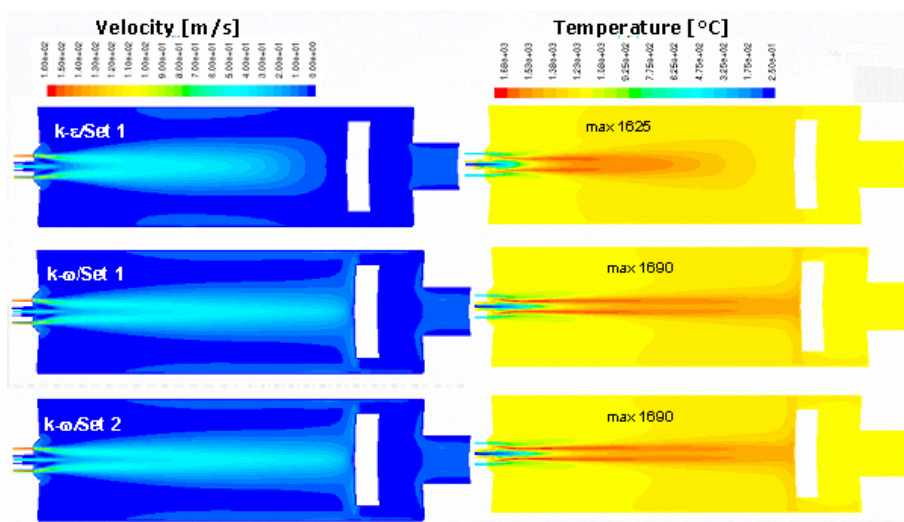


Figure 55. Results of TSN simulation for different turbulence models and Arrhenius rates.

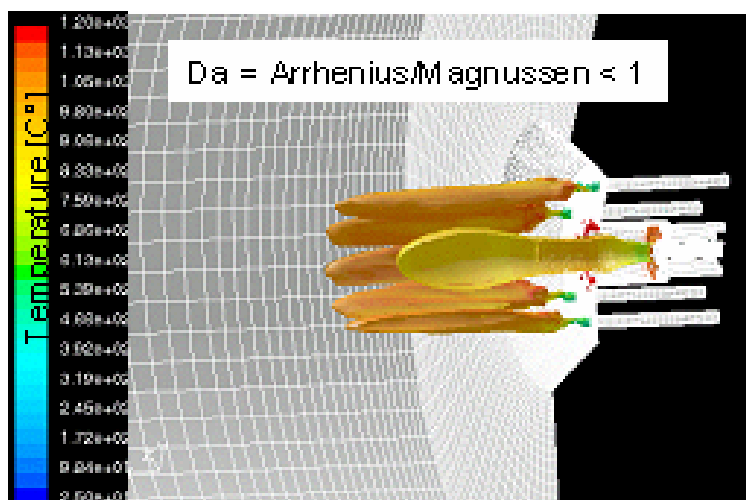
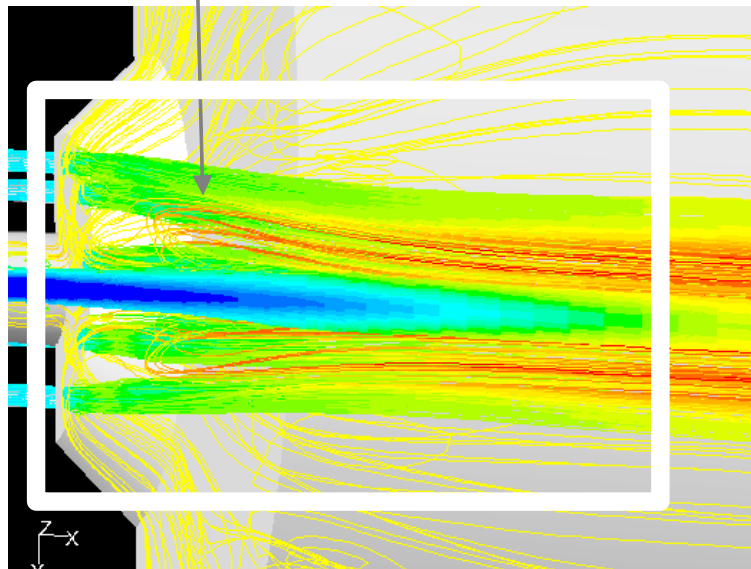


Figure 56. Iso-surface with $Da=1$ coloured by temperature.



Flame visualization inside CSM furnace



Path lines coloured with temperature

Figure 57. Near burner zone.

In general, the simulations confirm that the TSX burner geometry was designed with the aim to dilute as much as possible the oxygen in the furnace with combustion gases (that is, to give a high recirculation value as in Figure 54). This allows the reduction of the peak combustion temperature in comparison with traditional burners, which gives a positive effect on the NO_x formation. A diluted flame, however exists; Figure 57 shows the behaviour near the burner that, in good agreement with observations during the characterisation test, of a flame starting just inside the quarl.

FLUENT™ code (release 6.2.16) has been used for simulating the combustion process inside CSM's Modular Furnace equipped with TSX12 burner working at different conditions (Table 14).

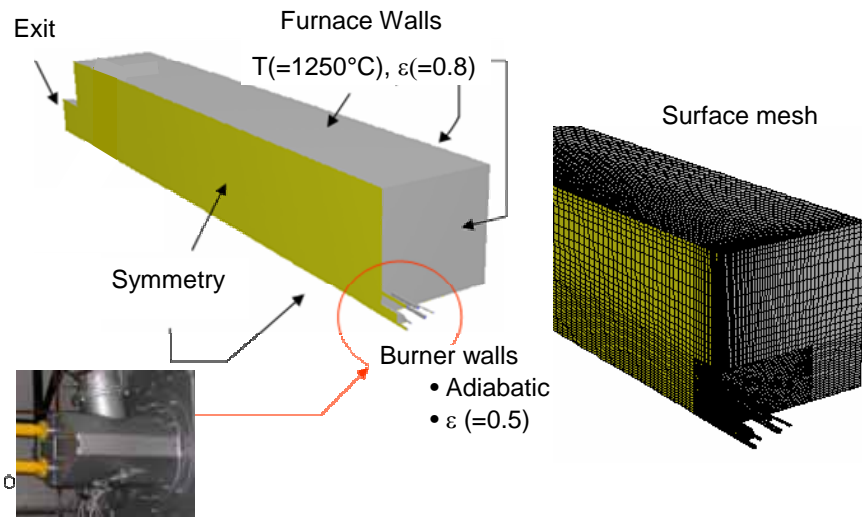


Figure 58. Geometry, boundary condition and surface mesh for TSX simulation.

Table 14. Conditions used at CSM for testing the TSX burner.

	MFR		O ₂ DFG	T _{furnace}	T _{air}
	Air (Nm ³ /h)	NG (Nm ³ /h)	%	°C	°C
Condition 1	2011	200	1.25	1250	450
Condition 2	2186	200	3	1250	450
Condition 3	2395	200	4	1250	450
Condition 4	2011	200	1.25	1250	520

The general description of the burner is object of other section of this report, as well as the CSM's Modular Furnace combustion chamber. Due to the confidentiality requested by Techint no further details about the TSX burner geometry are reported herein. The furnace dimensions used in the simulation are 2 x 2 x 7.5 m, corresponding at that used in the experimental campaign. The following assumption has been adopted in the build-up of the model (Figure 58): Double symmetry (45° sector), fixed wall temperatures, fixed emissivity of furnace walls ($\epsilon=0.83$) and the natural gas fuel is composed of 100 % CH₄. To mesh the 45° sector 240440 cells were used, which is equivalent to about 1 000 000 cells if the complete burner and furnace were modelled. The same CFD set-up, used in the simulation of the TSN burner was used.

The results of the simulations, in terms of temperature field, in a section of the furnace crossing the burner and natural gas lance are shown in Figure 59. The maximum value of the temperature (temperature peak) is significantly lower than the adiabatic flame temperature of a air/CH₄ mixture with preheated air at 450 °C (2174 °C). This effect is due to the flue gas recirculation by burner jets that produce the dilution of comburent (air) in the furnace (Figure 60.a/b); and the design of the natural gas nozzle that allows the injection of the fuel at distance from the burner tip at which the comburent has the proper level of dilution to operate in the flameless regime (Figure 60.c).

Figures 59-61 summarize the general behaviour of the fluid-dynamics of the TSX burner. The air and fuel jets velocity is close, however the momentum of the air jet is higher than the fuel one. So it is clear that in this situation the fuel jet is even weaker when considering it as a “strong jet – weak jet” problem [44]. In the first 0.3 m downstream, the air and fuel jets flow parallel. From that point on the gas jet is attracted by the air jet, and the jets meet for the first time at about 0.7 m downstream. The path lines that are shown in Figure 60 give some more information about the flow in the near burner zone. Looking at the temperature field the temperature differences in the furnace are relatively small, as envisaged with flameless combustion. The combustion air jet temperature is lower than the furnace temperature, but not so far from the average furnace temperature. The fuel jet is cold compared to the rest, but because of hot flue gas entrainment, the temperature of the fuel/flue gas jet increases quite quickly. The maximum

flame temperature is predicted to be around 1600 °C, which is very low for flames with this level of air preheat of 450-550 °C and it is in good agreement with the adiabatic flame temperature corresponding to the calculated O₂ concentration (recirculation rate) in the near burner zone. This is the result of the large amount of flue gas entrainment in the fuel and combustion air jet, which is one of the main principles of flameless combustion. Moreover since the recirculation ratio (kv) is not affected by variation of the injection velocity, the increase in the peak temperature and shortening of the flame at higher air/NG ratios is related to the increase in the local O₂ concentration. On the contrary, the higher value of the air preheating temperature (450 vs. 520 °C) has not a large effect on the peak flame temperature due to the high recirculation of hot flue gas. The importance of fuel injection is also demonstrated by the

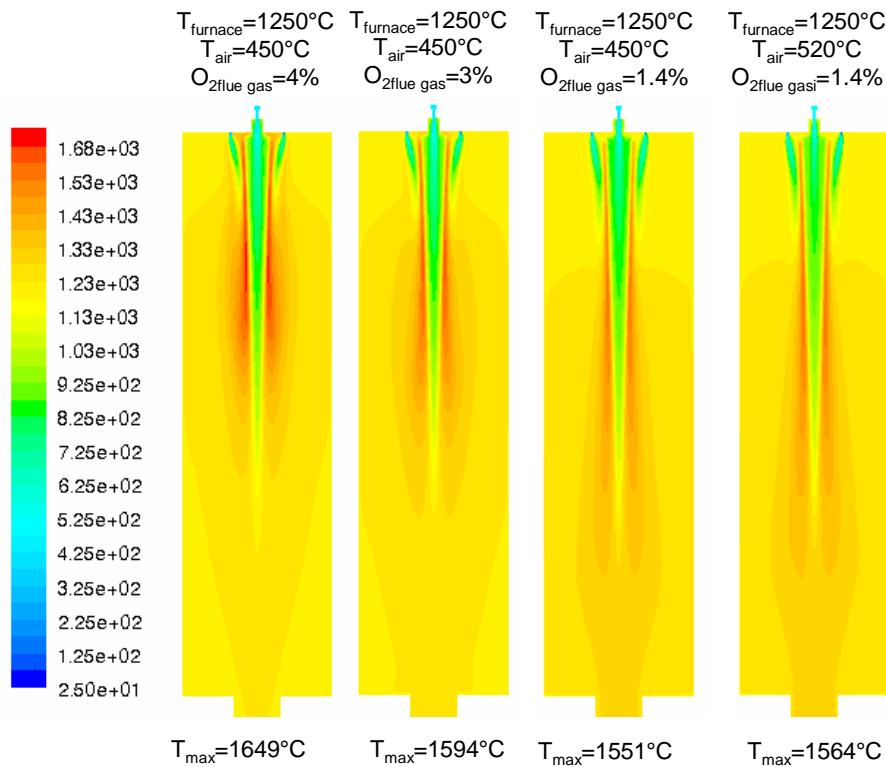


Figure 59. Temperature field generated by Techint TSX burner inside the CSM Modular Furnace.

comparison of the temperature field generated by TSN and TSX burners (Figure 61): the central injection of the fuel means that the fuel reaches the combustor very close to the burner tip where the air flow has a dilution level lower than in the case of the lateral injection in spite of a higher level of recirculation at the centre of the furnace.

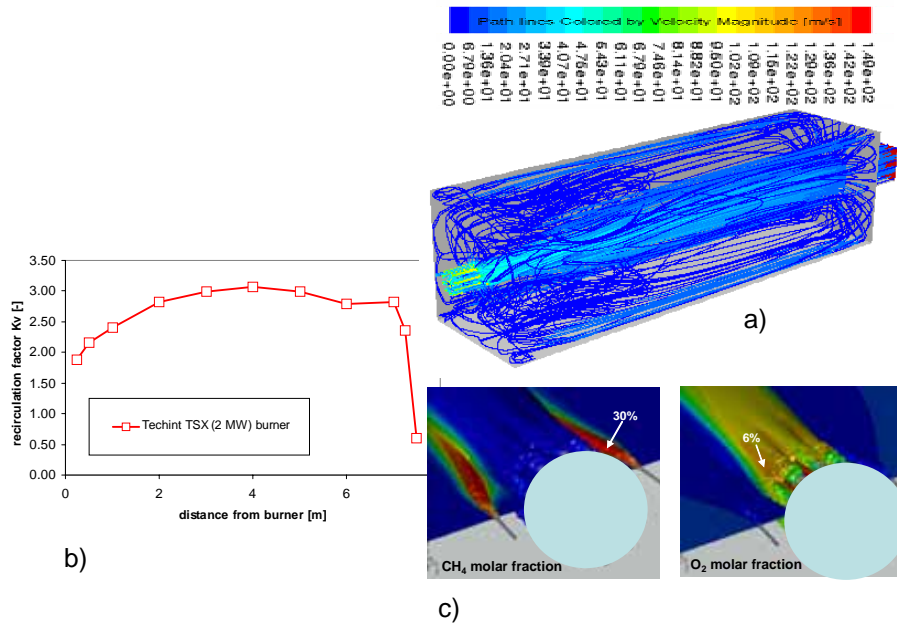


Figure 60. Fluid-dynamic behaviour of TSX burner for the base line condition : $T_{air}=450\text{ }^{\circ}\text{C}$, $T_{furnace}=1250\text{ }^{\circ}\text{C}$, 1.25 % O_2 in DFG.

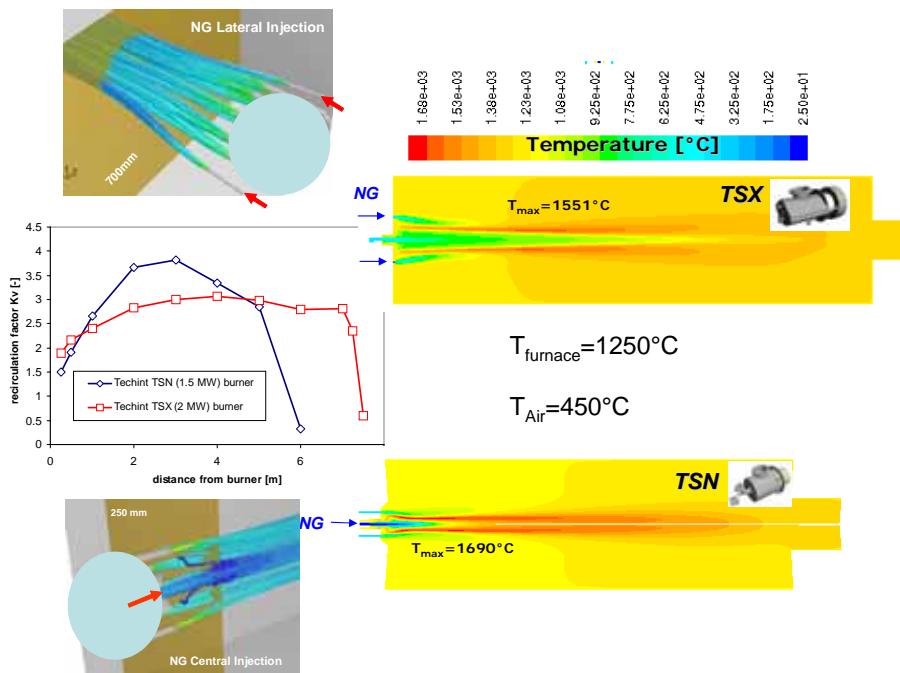


Figure 61. Comparison between TSN and TSX burner combustion behaviour.

Modelling has been done using FLUENT NOx post-processor for calculation of thermal and prompt NOx formation for the TSN burner. To predict NOx emission, transport equation for nitric oxide (NO) concentration have been solved based on the given flow field and combustion solution for four different operating condition of the burner. Contours of temperature and NOx (Thermal plus Prompt) at the different working condition are shown in Figure 62 including maximum temperature and NOx concentration (ppmv dry @3%O2) at the exit of the furnace.

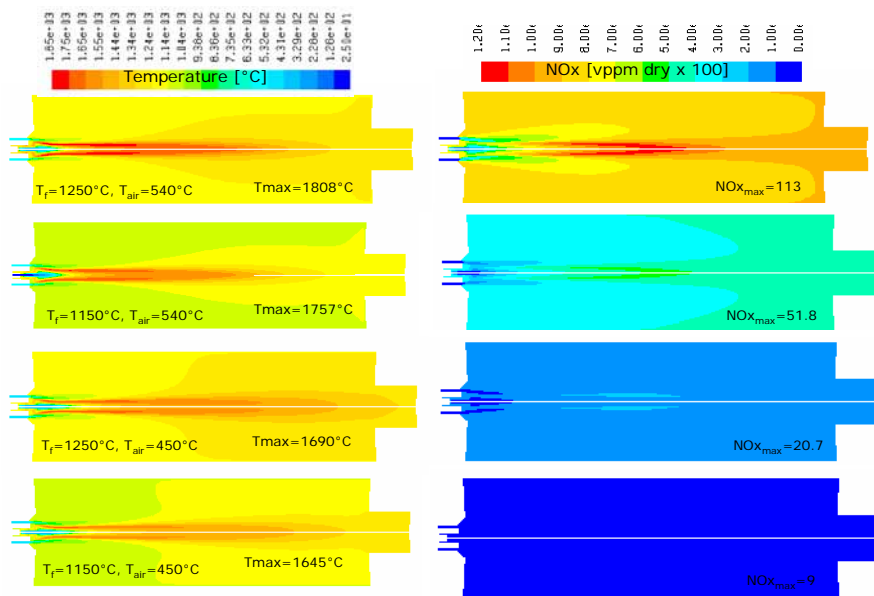


Figure 62. Temperature and NOx (thermal + prompt) field for different working conditions of TSN burner.

Comparison between calculated and measured NOx (Figure 63) confirms the limitation of FLUENT NOx model capability in case of diluted combustion regime: NOx variation trends can be predicted but an accurate quantitative NOx value cannot be expected.

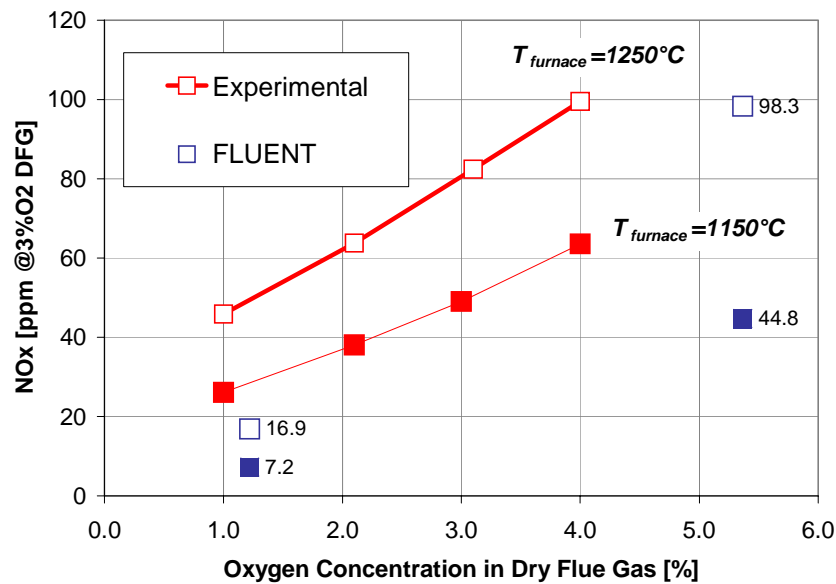


Figure 63. TSN burner NOx emission: experiment vs. modelling.

To overcome the limitation in the NOx prediction pointed out, two different approach has been followed:

- relation between the temperature peak obtained by CFD simulation and NOx measured during the experimental trials. This approach is based on the consideration that in the case of natural gas the main source of NOx is the “thermal NOx” ;
- simulation with the advanced combustion models. Based on literature overview of flameless combustion simulation the flamelet Probability Density Function [45] has been the selected approach. The table based on GRI-Mech 3.0 reduced scheme, as proposed by LABEIN, has been used. GRI-Mech 3.0 is an optimized mechanism designed to model natural gas combustion, including NO formation and reburn chemistry. It is the successor to version 2.11, and another step in the continuing updating evolution of the mechanism.

Figure 64 shows the correlation between the temperature peak obtained by CFD simulation and the NOx measured during the experimental campaign. The blue rhombus are the data from the simulations and tests of TSN and TSX burner operating with process temperature of 1250 °C and at different air/NG flow ratio. The blue line is the exponential interpolation line for these data. The red and green dots correspond at value estimated for TSN and TSX working in the different conditions as summarized in Table 15.

Table 15. NOx measurements and calculated concentrations for trials at CSM.

Burner	T _{air} [°C]	T _{furnace} [°C]	O ₂ DFG [%]	NOx measured [ppm @ 3%O2 DFG]	NOx estimated [ppm @ 3%O2 DFG]	Error [%]
TSN	540	1150	5.3	90 *	81.80	-9
TSN	450	1150	1.25	30	46.21	54
TSX	520	1250	1.25	35	30.57	-13

* extrapolated

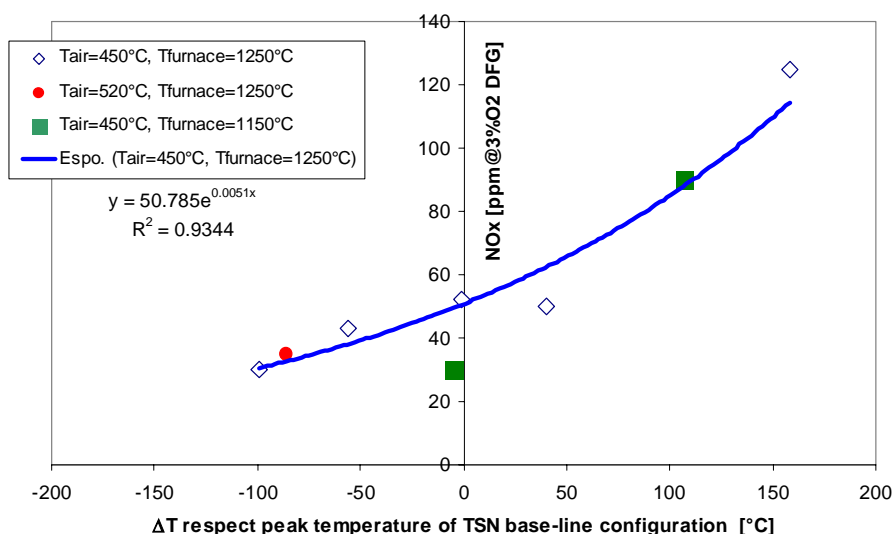


Figure 64. NOx emission for TSN and TSX burner versus peak flame temperature variation.

Based on this consideration CFD simulation of TSX burner, operating at condition 1 of Table 14, with advanced combustion models proposed by LABEIN has been performed to verify if more accurate NOx prediction can be obtained. The results of the simulations performed with PDF table generated by LABEIN, using GRI-Mech 3.0 reduced scheme, are reported in Figure 65 in terms of velocity and temperature field for the horizontal section of the furnace.

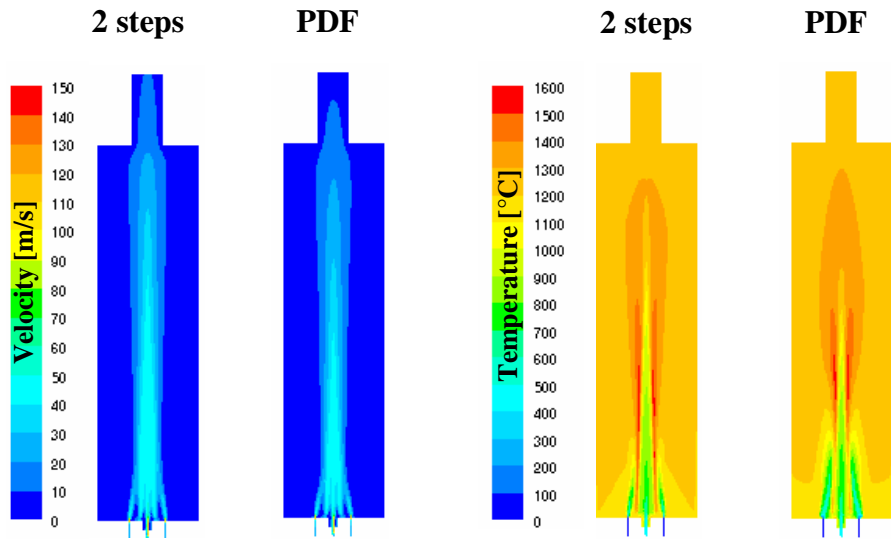


Figure 65. Velocity and temperature and NO_x field for TSX burner with different combustion models.

The comparison between the data obtained using simplified 2 steps reaction scheme with Finite-Rate/Eddy-Dissipation model and the advanced PDF shows a very close correlation in the velocity fields.

Figure 66 show the temperature traverses in the Modular furnace for three sections. At 1.4 m downstream of the inlet, the burner the measurements show a relatively flat temperature profile, which is better predicted by PDF model. The main discrepancies are for both models at the centre of the air jet: it can be concluded that the reason is physical (the temperature of the incoming air is higher than expected) or numerical (under prediction of entrainment of hot gas).

Both the 2 step model and the PDF model predict the increase in the temperature level where fuel and oxidiser meet: the increase is stronger then in the measurements for the 2 step model. It possible also to see that the temperature of the flue gas at the outsides of the furnace is well predicted in the first and last sections and not middle one. This means that the assumption of constant temperature for the furnace wall do not corresponds perfectly at experimental condition. However considering that the prediction of the flue gas temperature is in very good agreement with experimental value for both models (see profile at 7.4) this means that the overall heat balance of the furnace is correctly reproduced.

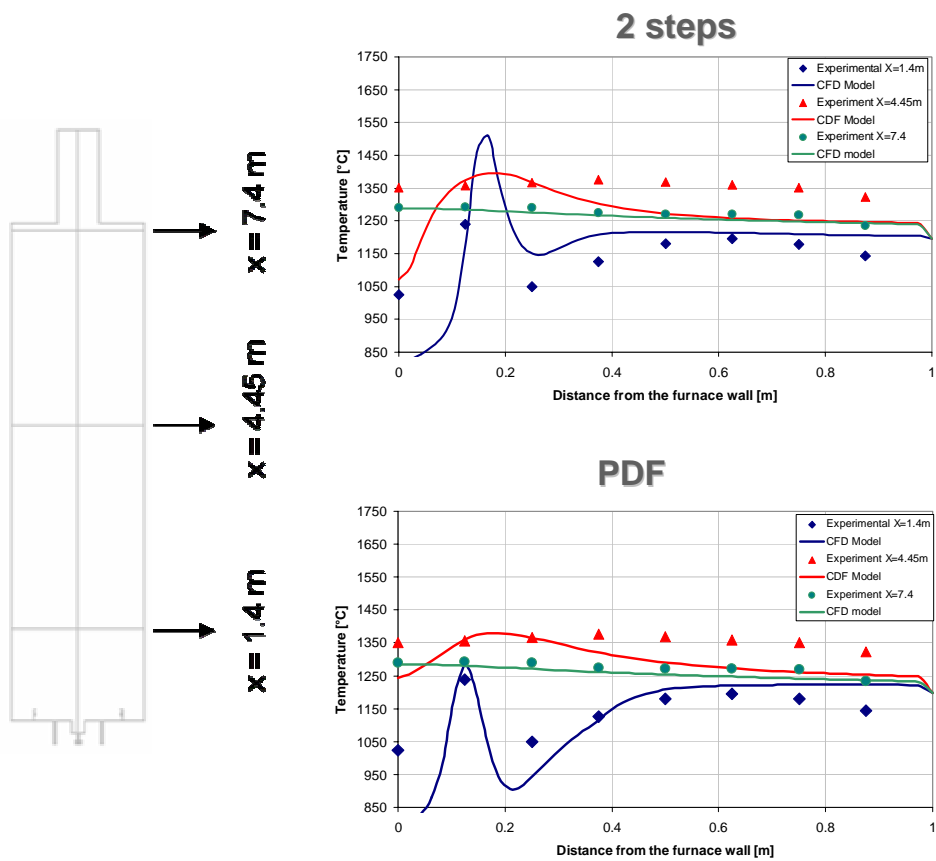


Figure 66. Temperature profiles inside CSM modular furnace in three positions.

Figure 67 shows the oxygen levels in the furnace. Close to the burner, the oxygen concentration in the combustion air jet is very close for the two combustion models as well as the further dropping of the oxygen level along the furnace is predicted. Looking more closely at the fuel jet and the flame area, it can be seen that there is oxygen predicted in the fuel jet, confirming the data obtained in the measurement for a similar configuration [46]. Only the PDF model is able to predict this.

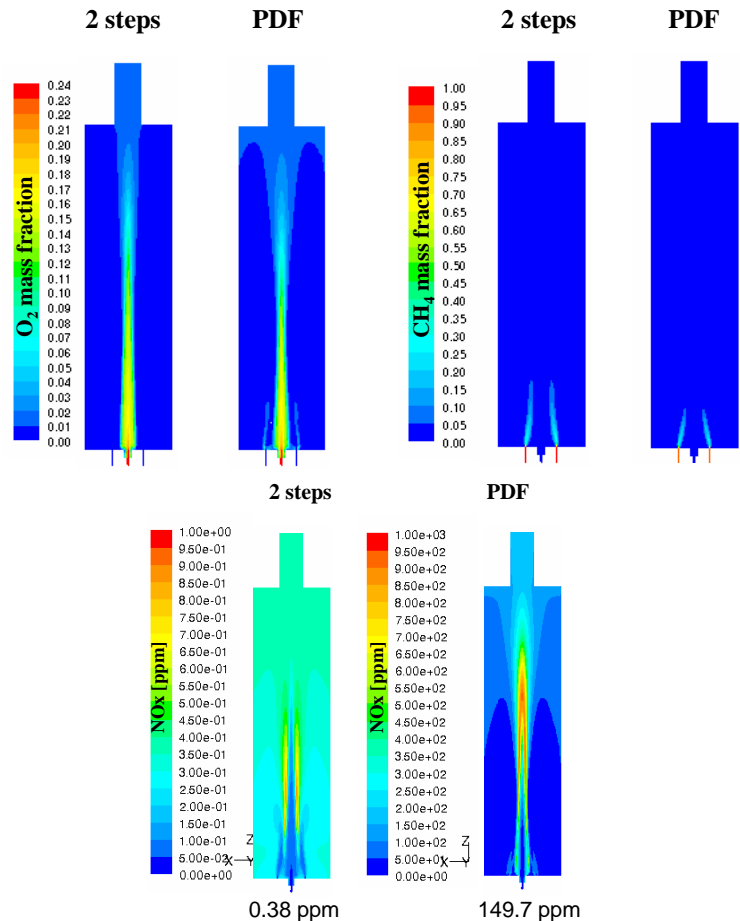


Figure 67. Specie mass fraction and NO_x field for TSX burner with different combustion models.

In spite of very close value of the maximum value of the temperature in the furnaces (temperature peak of 1550 °C) predicted by the two models the value of NO_x calculated differs of order of magnitude (Figure 67). The simulation with Finite-Rate/ Eddy-Dissipation model confirms the non applicability of the FLUENT NO_x model in case of flame temperature lower than 1600 °C, that are typical of flameless regime, while the PDF approach over predicts the NO_x in comparison with experimental values of about 4 times.

Based on this results no further effort to improve the quality of the solution using experimental values for the wall temperature or simulating directly the heat extraction from the water cooled lances. This, in fact, requires the simulation of the full furnace with a relevant increase in the computational time without any evident advantage in term of information relevant for understanding the combustion process inside the furnace and of accuracy of NO_x prediction. On the contrary, it was decided to use the PDF model to the simulation of TSN to verify the applicability in a different combustion regime. Similar results has been obtained: PDF approach over predicts the NO_x in comparison with experimental values by about 5 times (Figure 68).

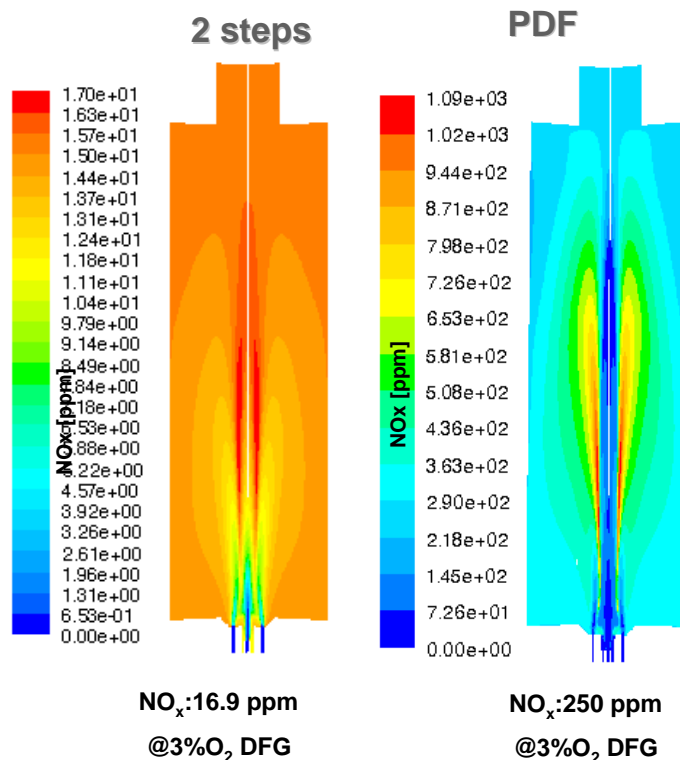


Figure 68. NOx field for TSN burner with different combustion models.

The possibility to compare the results obtained by different partners during the project for different combustion regimes, different fuels and different combustion chambers, with the adopted approach, has allows to identify the guideline for the proper use of commercial CFD code, such as FLUENT, for the simulation of combustion process in the reheating furnaces. Since the best way to model combustion process in a given industrial process, depends not only on the quality of the combustion model, but also on the critical phenomena to be modelled in the specific application different approaches have been investigated.

To overcome the well known "round-jet/planar-jet anomaly", the Wilcox $k-\omega$ turbulence model has been adopted for the simulation of burners characterized by high momentum multiple jets. In this case the traditional $k-\epsilon$ based models (standard $k-\epsilon$ RNG/ $k\epsilon$, ren/ $k\epsilon$) has confirmed to over predict the spreading rate of round jets in comparison with Wilcox 98 $k-\omega$.

Traditional Finite-Rate/ Eddy-Dissipation model with two reactions and more advanced PDF flamelet model have been used by CSM to simulate dilute and flameless combustion. Both models are able to predict the overall air and fuel jet behaviour in the furnace with the corresponding chemical reactions and diffusion processes. The PDF flamelet model seems to give a better prediction of temperature distribution inside the furnace in the case of flameless combustion, even if the maximum temperature level is very close. However both approach are able to predict NOx variation trends but the NOx quantity itself cannot be pinpointed: Finite-Rate/ Eddy-Dissipation model under predict the NOx, vice versa PDF over predict the emissions. In spite of some difference between the CFD model and the measurements the results obtained in the project indicated that CFD can be used an engineering tool to:

- obtain additional information: certain observation or data can only obtained using mathematical modelling technique due to practical limitation of taking measurements on fuel-fired plant;
- reduce the risk: modelling can enable production plant modification to be evaluated minimizing on-site experiments which may cause loss of production;
- reduce the development cost: modelling allows a wider range of design options to be evaluated before testing of new concept;
- reduce the development time: design performance data can be obtained more quickly compared with undertaking experimental on production or prototype plant.

CFD modelling of DFI combustion at MEFOS

A CFD model was made of the DFI trials using the GAMBIT v. 2.1.2 pre-processor and FLUENT version 6.1.22. A hybrid grid model was made for half of the chamber furnace to reduce the mesh size for analysis to 51967 cells. The furnace was divided down the centreline of the air inlet with fuel nozzles assumed to be symmetrically located on both sides of the air inlet. The use of a hybrid mesh allowed for a fine mesh size near the fuel and air outlets and a coarse mesh for the large furnace volume (see Figure 69). The finite rate/eddy dissipation 2 step reaction model, DO radiation model, and the standard $\kappa-\omega$ turbulence model based on the modelling by the other partners as given in Table 16.

Table 16. Physical models and boundary conditions for the CFD model at MEFOS.

Physical models:	
Turbulence	standard $\kappa-\omega$
chemical reaction	finite rate/eddy dissipation
species	6 species CO, H ₂ O, O ₂ , N ₂ , CO ₂ , C ₃ H ₈ plus NO
radiation	DO 4 x 4 angles and 2x2 pixels
pollutant	Thermal and prompt NO
absorption coeff.	WSGGM cell based
gas density	Ideal gas
Numerical approach:	
Grid type	Hybrid 3D
Solver	Segregated, steady
Linearization	Implicit
Discretization	Second order up-wind scheme for momentum and turbulence
Boundary Conditions	
air and fuel inlets	mass flow
exhaust outlet	pressure outlet
wall surfaces	temperature

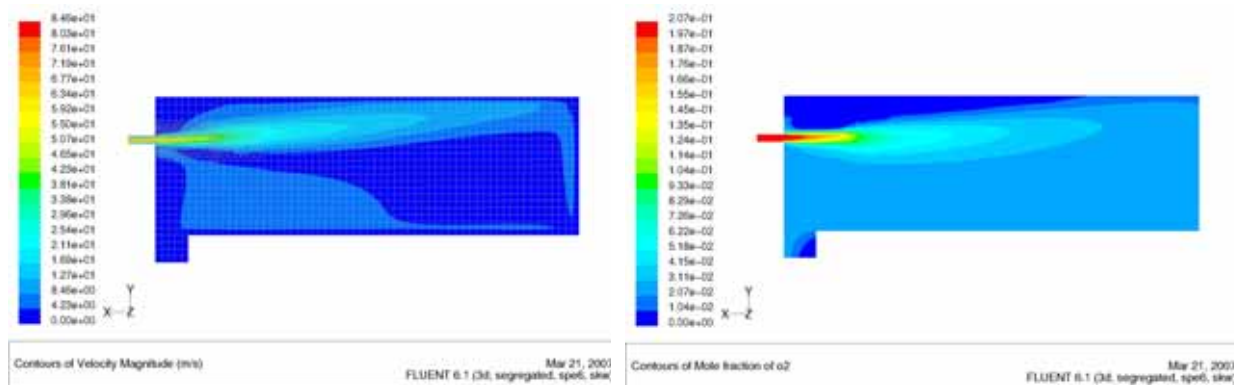
The propane and air flow rates were based on the DFI trials at MEFOS for a furnace temperature of 1250 °C and 500 °C combustion air while varying the excess air. A constant fuel flow rate of 0.00151 kg/s of pure propane was used for all the cases, even if there were some fluctuation in the fuel flow for the experimental conditions. Commercial propane was used in the trials, and it is stated to be at least 95 % pure, with the presence of some higher carbon compounds. The parameters used and results of the CFD calculations are given in Table 17. The final NO and oxygen concentrations were evaluated over the bottom surface of the furnace where there was essential complete combustion, and the peak NO_x and peak gas temperatures were obtained from the histogram summary from FLUENT for not more than 1 cell over this value. The water vapour concentrations are useful for conversion of the CFD data for wet combustion to equivalent dry concentrations for comparison with the experimental NO data. The resulting mesh with gas velocities and oxygen concentrations are given in Figures 69-70.

Table 17. Modelling parameters and results.

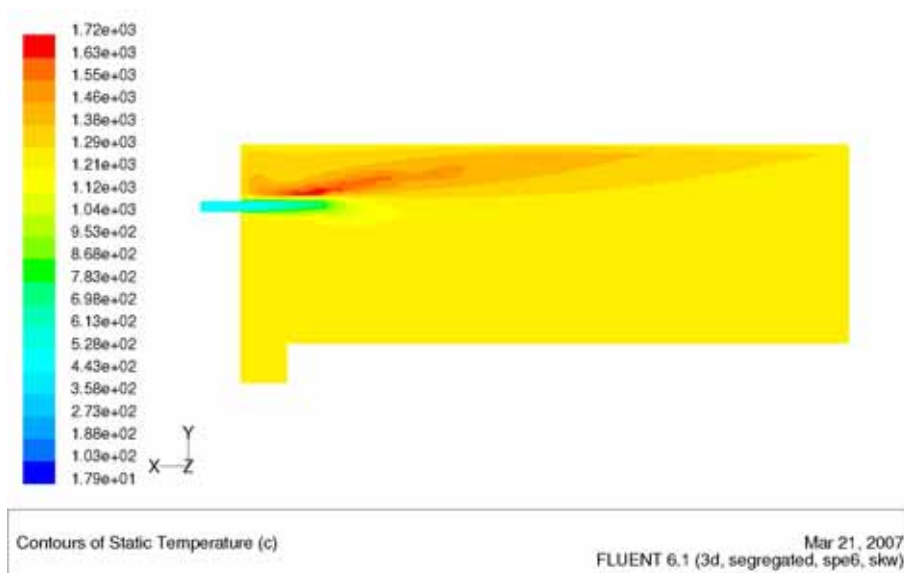
Case	Air flow (kg/s)	Fuel-Air Equil. ratio	Final wet and dry O ₂ (%)	Final H ₂ O (%)	Final NO (ppm)	Peak NO _x (ppm)	Peak gas temperature (°C)
1	0.0236	1.0	0.0 0.0	15.1	0.7	1.1	1641
2	0.0276	0.86	2.57 2.96	13.2	1.4	2.5	1742
3	0.0315	0.75	4.60 5.21	11.6	12.8	15.2	1820

NO_x was modelled using the FLUENT NO_x model for both thermal and prompt NO_x without reburn. The carbon number was 3 for propane, oxygen radicals were assumed to be in equilibrium and hydroxyl radicals in partial equilibrium. The resulting NO_x concentrations were averaged over the bottom of the furnace to avoid erroneous dilution errors due to backflow in the exhaust duct for the CFD model. The average wet NO_x and oxygen concentrations over this surface obtained in the model were corrected to

dry gases using the water vapour concentration. Mole fractions which easily give ppm are standard units in FLUENT and the experimental data was measured in ppm, so the data is given in ppm instead of mg NO_x/Nm³. The highest gas temperatures and NO_x concentrations were calculated to occur at the top of the combustion zone (see Figures 69-71), which would support the work at BFI that a confined region around a low NO_x burner restricts flue gas recirculation and can lead to higher NO_x.



Figures 69a-b. Velocities and oxygen concentrations and NO concentration at the centreline of the burner in the CFD model of the DFI trials in the chamber furnace at MEFOS.



Figures 70. Temperatures at the centreline of the burner in the CFD model of the DFI trials in the chamber furnace at MEFOS for a furnace temperature of 1250 °C, 3 % dry oxygen and 500 °C combustion air.

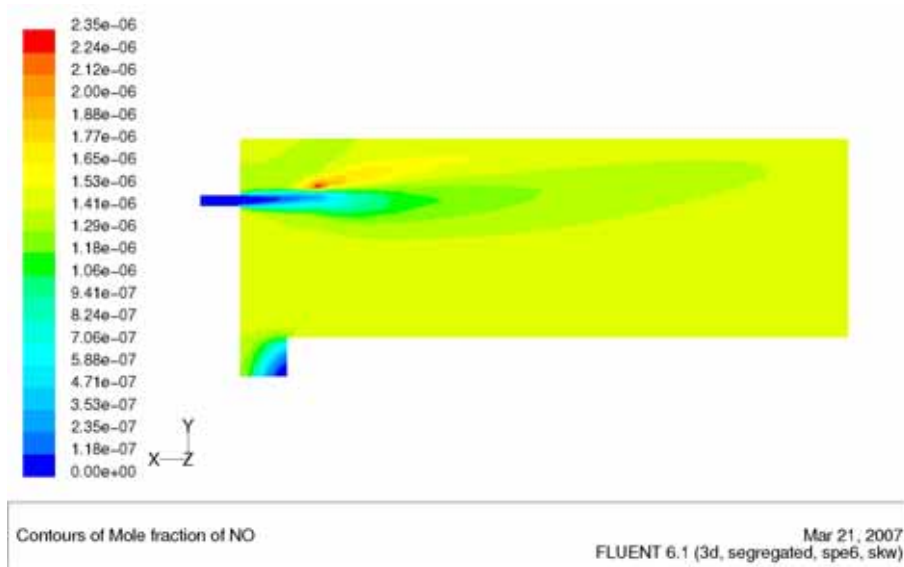


Figure 71. NO concentration at the centreline of the burner in the CFD model of the DFI trials in the chamber furnace at MEFOS for a furnace temperature of 1250 °C, 3 % dry oxygen and 500 °C combustion air.

The NO concentrations calculated with FLUENT can be converted to NO_x in the same manner as the experimental NO concentrations measured during the DFI trials. These two curves are plotted in Figure 71 and the NO_x levels calculated are seen to be much lower than the experimental results. This would indicate that modelling thermal and prompt NO_x is insufficient, and additional reactions are required. A report in the literature stated that N₂O reactions should be included for low combustion temperatures typically of flameless combustion [47]. A request was made to FLUENT support towards the end of the project to include these reactions in the FLUENT NO_x model [48]. This software modification to the FLUENT program can be made, but there was not sufficient project time left to do the work.

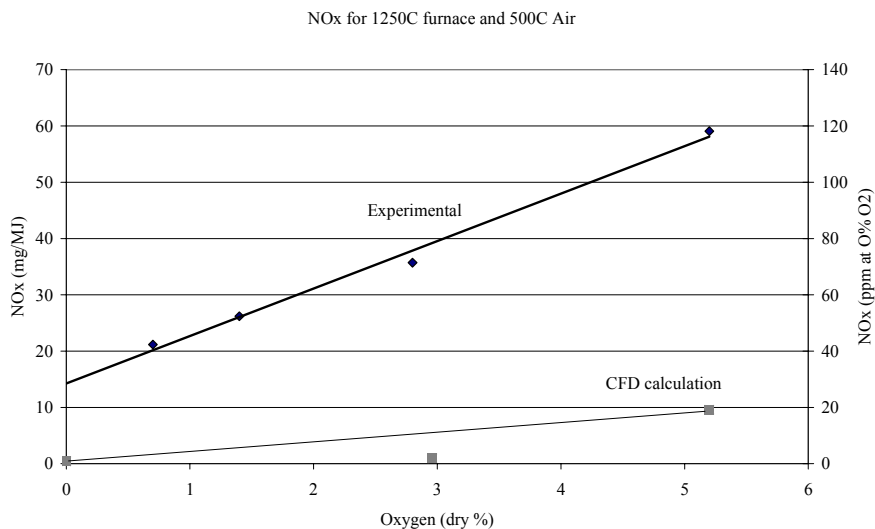


Figure 72. A comparison of the NO_x calculated with CFD versus the experimental results for DFI with 1250 °C furnace, 500 °C combustion air and varying the excess oxygen.

Voestalpine - Modelling the Voestalpine Industrial reheating furnace

In Voestalpine’s Linz plant the hot rolling mill is equipped with two pusher-type reheating furnaces which are identical in construction. A schematic drawing of this furnace-type is presented in Figure 73. Characteristic Data about the furnace are compiled in Table 18.

Table 18. Data for the Voestalpine slab reheating furnaces.

Data of slab heating furnaces 6 and 7

furnace dimensions	outside	inside
length	37 m	<u>34,5 m</u>
width	14 m	13,0 m
slab dimensions	min.	max.
length	2800 mm	12000mm
width	600 mm	1660 mm
thickness	160 mm	350 mm (230 mm)
tubular support construction	6 skids with riders	
energy consumption	390 Wh/kg at 160 °C initial slab temperature	
furnace temperature	max. 1320 °C	
flue gas		
recuperator	cross current flow	
air preheating	350 - 400 °C	
flue temperature before recu.	700 - 800 °C	
flue temperature after recu.	400 - 500 °C	
flue temp. after steam generator	200 °C	

About every 5 minutes a cold slab is pushed into the convective zone and a hot slab is removed from the soaking zone. The gas moves against the direction of the slabs from the soaking zone to the convective zone where before the doors it enters ducts which open at the floor and at the bottom. The flue gas passes a recuperator which heats the air for the burners to about 400-450 °C. After that it passes a steam generator and is led into the funnel with about 200 °C.

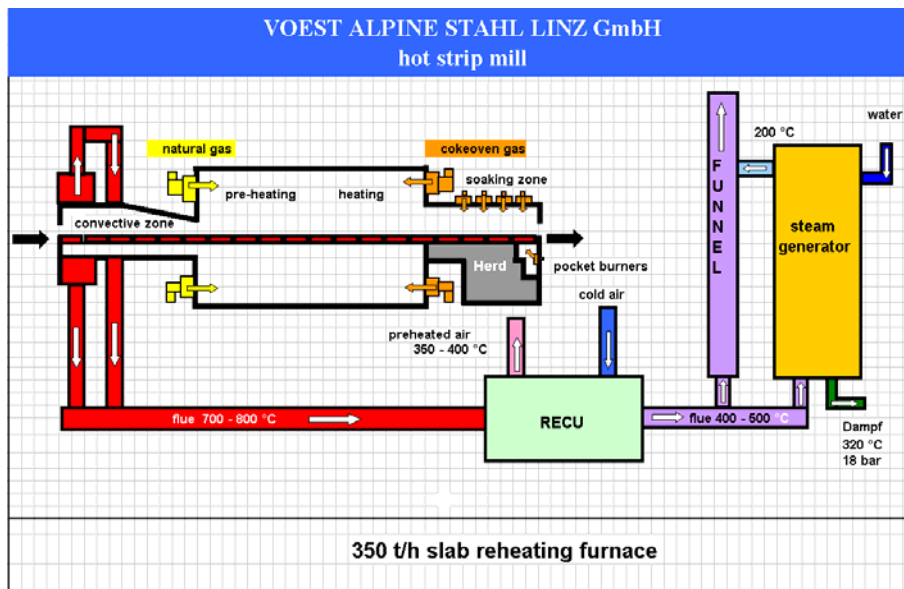


Figure 73. Scheme of the Voestalpine slab reheating furnace.

The burners are assigned in the following way to different zones:

- preheating zone – top: 12 front- side burners, fired by natural gas
- preheating zone – bottom: 8 front- side burners, fired by natural gas
- heating zone – top: 12 front- side burners, fired by coke oven gas
- heating zone – bottom: 8 front- side burners, fired by coke oven gas
- soaking zone: 30 ceiling-burners, fired by coke oven gas
- holding zone: 10 ceiling-burners, fired by coke oven gas

Figure 74 shows the full geometric furnace model. It is evident that the burners with their nozzles for gas and air need a much finer resolution than most other parts of the furnace. This is a serious challenge for grid generation and evidently must lead to a grid consisting of a very large number of cells if not really crude grid interfaces are used. In order to make the grid and the computational work load more manageable it was therefore decided to use the symmetry plane and to model only one half of the furnace. Figure 75 shows the grid in this furnace- half. This grid consists of 1.2 million cells, uses grid interfaces at the burner outlets and still has very different cell sizes at both sides of the grid interfaces. In another step towards simplification was to cut out a slice of the furnace to give a model with a width of 1/8 of that of the whole furnace. This slice contains respectively 1.5 burners in the upper preheating and heating zones, 1 burner in the lower preheating and heating zones and should contain 1.25 roof-burners in each row of the soaking and holding zone. As a quarter of a burner cannot be modelled realistically, only one burner was used in each row, therefore the number of roof burners is in reality 25 % higher than in this model. This reduced furnace model could be meshed without grid interfaces and Figure 76 shows some details about the grid in the neighbourhood of the burners.

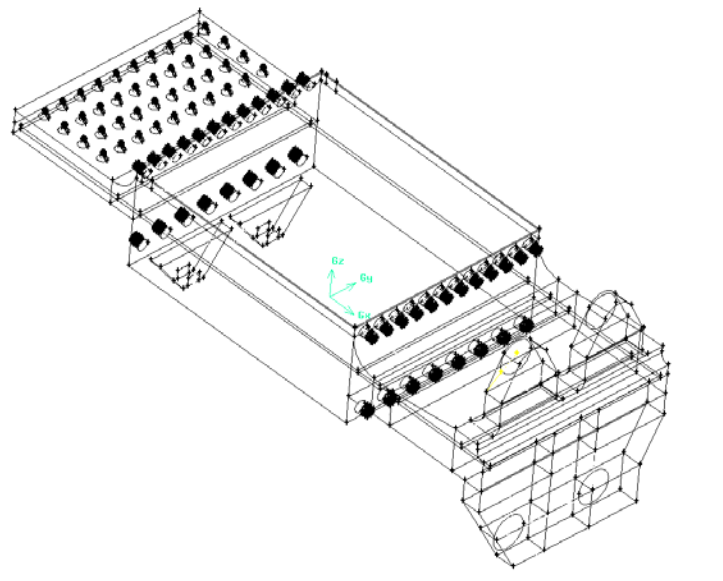


Figure 74. Full geometric furnace model.

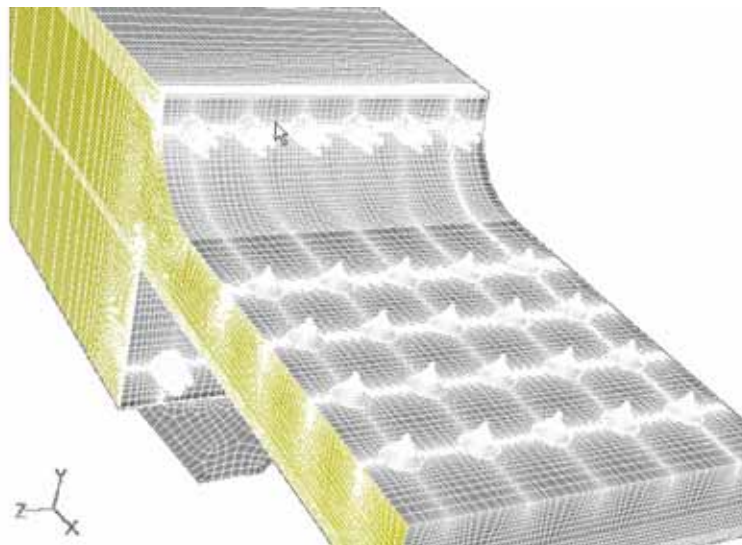


Figure 75. Grid for the model of half furnace at Voestalpine.

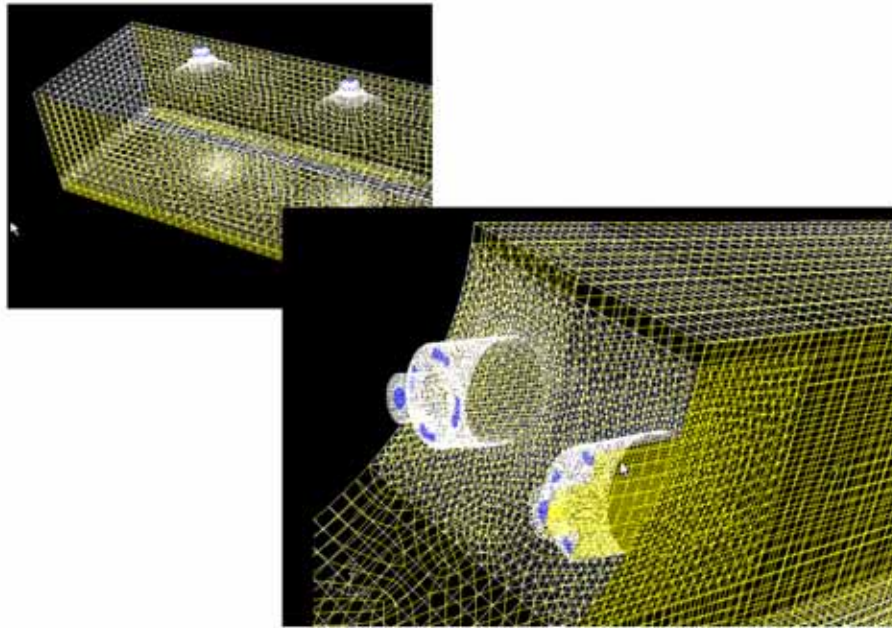
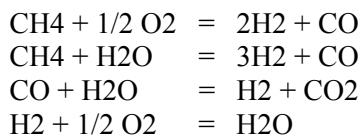


Figure 76. Grid details of the 1/8 furnace model.

The gas phase was defined as a mixture material consisting of the following species:

CO, CO₂, CH₄, H₂, O₂, H₂O, N₂.

The following is a summary of the reactions that were taken into account of in the model:



The reaction rates were modelled by the finite rate/eddy dissipation model in FLUENT. The concentration exponents and Arrhenius parameters used are displayed in Table 19:

Table 19. Arrhenius- Rates and rate (concentration) exponents for the reactions. The parameters are based on data from the project partner CSM.

Reactions	Rate Exponents reactants		Arrhenius		
	1st	2nd	Factor	Ea [J/kmol]	T-Exponent
CH ₄ + 1/2 O ₂ = 2H ₂ + CO	0.5	1.25	4.4E+11	1.2558E + 8	0
CH ₄ + H ₂ O = 3H ₂ + CO	1	1	3.0E+08	1.2558E + 8	0
CO + H ₂ O = H ₂ + CO ₂	1	1	2.79E+09	8.372E + 07	0
H ₂ + 1/2 O ₂ = H ₂ O	0.25	1.5	6.8E+15	1.6744E + 8	-1

The Discrete Ordinates (DO) radiation model was used with an absorption coefficient calculated by FLUENT (WSGGM-domain-based), a scattering coefficient of 1E-05/m assuming isotropic scattering and a refractive index of 1. Turbulence was modelled using the standard k-ε with enhanced wall treatment. The FLUENT NO_x-model was used with the options thermal and fuel NO_x, specifying equilibrium for the [O] model. Fuel NO_x is accounted for in coke oven gas with HCN and NH₃, the N mass fraction in the coke oven gas is set to 0.00037, the conversion rate to unity and the ratio HCN: NH₃ is 77: 23.

Some time has been spent in the attempt to simulate the complete flow- combustion and thermal problem in the model of the 1/8 furnace with an instationary calculation simulating the movements of the slabs by the moving-grid feature in Fluent. This meant that a region of the computational grid containing the slabs was defined as moving and during the calculation this region was actually moved

through the furnace, starting from a position completely outside of the furnace. It soon turned out however, that this procedure was extremely time consuming, the computational time needed to pass the slabs from the entrance to the exit amounted to about one week on a fast single processor Linux workstation. The result depicted the situation to be expected if a cold furnace is started with full power and run for two hours with full slab load – not really a realistic situation and therefore the slab temperatures were notably colder than what is known from regular operation.

As it did not seem to be realistic to extend the unsteady simulation until a steady thermal state has been reached in the furnace, the need grew urgent to develop a steady formulation for the problem. Fortunately, this could be obtained by using the moving reference method also implemented in Fluent. In this approach, the zone with the slabs is not actually moved, but the solver uses equations corresponding to a moving reference frame in this part of the grid. Thus the heat conduction equation in the slabs can be made to have the form of steadily moving slabs – still a stationary problem. This approach at last made it possible to solve the complete flow, combustion and thermal problem for the situation of stationary moving slabs and to obtain reasonable results.

In order to be able to compare the influence of different operational variants on NO_x and on energy efficiency, it was decided to modify the boundary conditions of the standard-case used for model-calibration in such a way that the lambda was 1.05 for all the zones. The corresponding new burner flow-rates are listed in Table 20. The analyses of the air and of the two gases are displayed in Table 21a-c.

Table 20. Gas and air flow-rates of the burners in the reference-case with Lambda = 1.05 in all the zones. If more than 1 burner is modelled, then the flow-rate is the sum over all the burners in this zone of the model.

	Gas type	Nr. of burners in model	gas flow kg/s	air flow kg/s
upper preheating zone	natural	1.5	0.0670	1.187
lower preheating zone	natural	1	0.0735	1.304
upper heating zone	coke oven	1.5	0.0395	0.578
lower heating zone	coke oven	1	0.0521	0.763
roof burner (soaking zone)	coke oven	3.75	0.0061	0.089
roof burner (holding zone)	coke oven	1.25	0.0049	0.072

Table 21.a. Simplified analysis of air, b: simplified analysis of natural gas and c: simplified analysis of coke oven gas.

simplified analysis air		simplified analysis natural gas		simplified analysis cokeoven gas	
	concentration vol.-%		concentration vol.-%		concentration vol.-%
CH ₄	0.000	CH ₄ (+C _n H _n)	98.39	H ₂	60.7
O ₂	20.950	N ₂ (+Ar+Rest)	1.3	CH ₄ (+C _n H _n)	27.3
CO ₂	0.033	CO ₂	0.28	CO	6.4
H ₂ O	0.937	O ₂	0.03	N ₂	3.3
N ₂	78.080	H ₂ O	0	CO ₂	2
				O ₂	0.3
				H ₂ O	0

Lower calorific values for the fuel gases:

Hu natural gas: 9920 Wh/m³ STP
 Hu coke oven gas: 4949 Wh/m³ STP
 Hu blast furnace gas: 1115 Wh/m³ STP

In coke oven-gas the fuel-NO_x producing components NH₃ and HCN are found in the following quantities: HCN 500 mg/m³ at STP and NH₃ 150 mg/m³ STP.

Case 1: Standard case with $\lambda = 1.05$

Figure 2.30 shows the gas temperature in the furnace. The wall temperatures and the temperature profiles at the slab surfaces are found in Figure 78. Figure 79 illustrates the flow situation in the preheating (right side) and heating zone. Velocities larger than 10m/s are omitted for sake of clarity. It is clearly seen that each of the burners produces a large scale swirl reaching deep into the furnace. As had to be expected, the velocities are higher in the upper furnace as the gas from the roof burners flows only in the upper zones and the velocities increase from the heating to the preheating zone as all the gas has to leave by the convective zone at the right, which is not equipped with burners. By far the lowest velocities exist in the lower heating zone where no flue gases from any other burner passes.

Figure 80 shows the NO distribution calculated in the furnace. It is evident that the roof burners in the soaking and holding zones produce the largest NO concentrations, but this is not really important since the gas input into these zones is much less than 1/10 of the other zones.

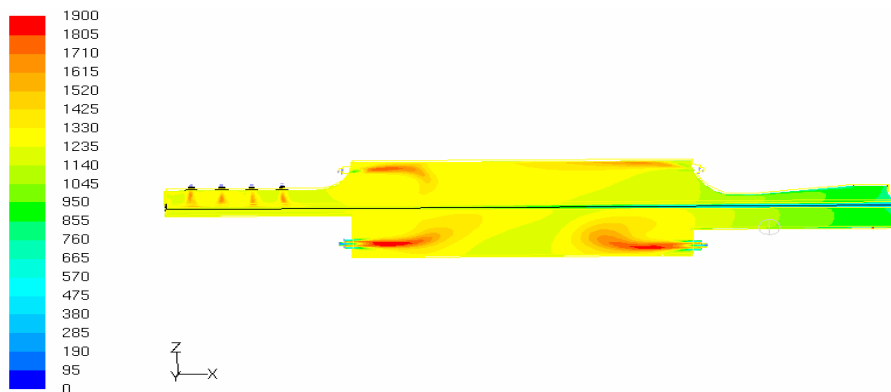


Figure 77. Reference case: Gas- temperature in the furnace (note, the figure was compressed on the z-axis).

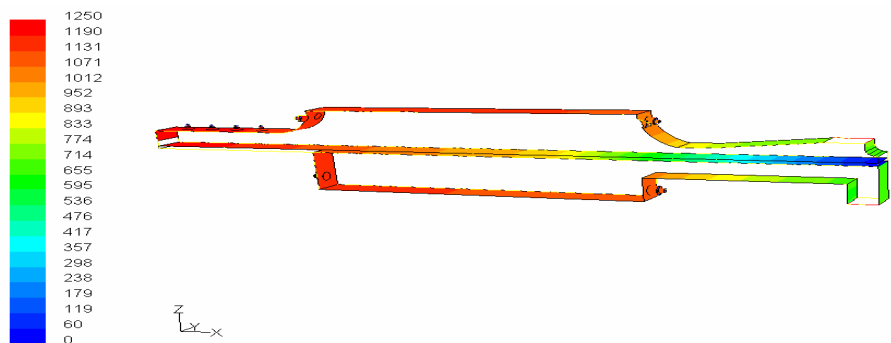


Figure 78. Inner wall temperatures of the furnace (note, the figure was compressed on the z-axis).

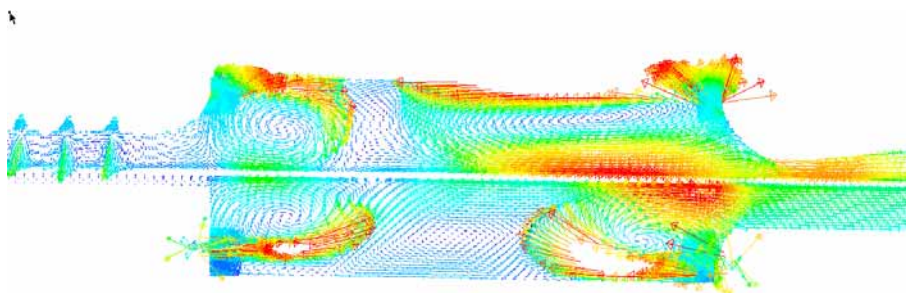


Figure 79. Velocities in a plane crossing the burners of the lower preheating and heating zones. Vectors corresponding to velocities larger than 10 m/s have been omitted for clarity.

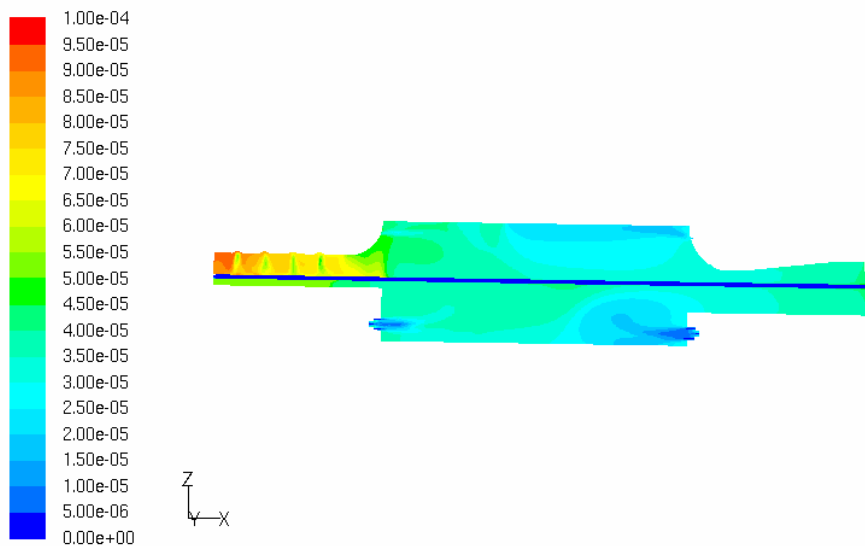


Figure 80. NO volume fraction in the reference case.

After this model had been validated against the available furnace data the confidence in the numeric model was large enough to investigate changes in furnace operation and even alternative burners and their impact on steel and NO_x production. In all these cases, the flow rates of the gases were chosen such that the total energy input as measured by the net calorific value remained the same as in the reference case if not otherwise specified. The net calorific values were used for the natural gas, coke oven gas and blast furnace gas were 9.920, 4.949 and 1.115 kWh/Nm³ respectively. Tables 22-23 show the calculated NO_x in flue- gas and the slab- temperatures for the various cases evaluated.

Table 22. NO_x in the flue gas calculated for various modes of operation for the furnace.

NO _x	ppm dry	mg/Nm ³ @3%	mg/Nm ³ @5%	mg/MJ
Reference conditions (Case 1)	153	288	256	75.1
100 % coke oven gas (Case 2)	208	388	345	90.4
Blast furnace gas (Case 3)	0.0063	0.0113	0.0100	0.0042
Preheat zone power reduction (4.1)	189	357	317	91.3
All zones power reduction (4.2)	140	261	232	66.1
ON-OFF (Case 5)	209	385	342	98
Air-staging burners	76	142	126	35

Table 23. Slab temperatures for various modes of operation for the furnace.

Slab temperatures °C	furnace entrance	furnace exit
Reference case	364	1204
100 % coke oven gas	364	1176
Blast furnace gas	364	895
Preheat zone power reduction	364	1214
All zones power reduction	364	1203
Air-staging burners	364	1207

Case 2: 100 % coke oven gas

For economical reasons it would be advantageous to use coke oven gas for all of the burners in the furnaces. However it is known that this fuel will increase the NO_x content of the flue gas, therefore it was desirable to predict the amount of NO_x of this operational mode preliminary to any decision to reconstruct the gas supplying system of the furnace. The settings for the gas flows have been chosen such that the total energy input into the furnace measured by the lower calorific would be the same than in the reference case. The following settings for the gas-flows have been applied:

Table 24. Flow rates with 100 % coke oven gas.

	Gas type	Nr. of burners	gas flow	air flow
		in model	kg/s	kg/s
upper preheating zone	coke oven	1.5	0.0713	1.044
lower preheating zone	coke oven	1	0.0783	1.146
upper heating zone	coke oven	1.5	0.0395	0.578
lower heating zone	coke oven	1	0.0521	0.763
roof burner (soaking zone)	coke oven	3.75	0.0061	0.089
roof burner (holding zone)	coke oven	1.25	0.0049	0.072

The NO_x concentration and slab temperatures calculated are given in Tables 22-23. The conclusion is that with coke oven gas in all zones the furnace and slab temperatures would be slightly lower than with the standard mixture of coke oven gas and natural gas. The NO_x concentration is however by about 30 % higher than in the standard case with natural gas in the preheating zone. Not a good perspective, especially if one takes into account that even more gas will be needed to reach the same slab temperature than in the reference case.

Case 3: Blast furnace gas

Blast furnace gas has a rather low usable energy content, but in an integrated steel-plant large quantities of this not very useful gas have to be dealt with. Economically it would therefore be very advantageous to use as much as possible in the slab reheating furnaces, but it is known from theoretical considerations that it will not be possible to reach the slab temperatures desired at the normal production rates with this gas alone. However, to get a feeling of what can be obtained with this gas and what would be the impact of using it, a calculation was done with the assumption that the furnace is fired with 100 % blast furnace gas with the same total lower calorific heat input as in the reference case. The gas-flow settings in Table 25 were used and the BFG analysis in Table 26.

Table 25. Gas flows used in the model with blast furnace gas.

	Gas type	Nr. of burners	Gas flow	Air flow
		in model	kg/s	kg/s
Upper preheating zone	BF gas	1.5	1.095	0.898
Lower preheating zone	BF gas	1	1.203	0.986
Upper heating zone	BF gas	1.5	0.607	0.498
Lower heating zone	BF gas	1	0.801	0.657
Roof burner (soaking zone)	BF gas	3.75	0.094	0.077
Roof burner (holding zone)	BF gas	1.25	0.076	0.062

Table 26. Analysis of blast furnace gas.

Analysis of the blast furnace gas	
	vol.-%
H ₂	5.35
CH ₄	0.81
CO	24.49
N ₂	49.4
C _n H _n	0.08
CO ₂	19.87
O ₂	0
H ₂ S	0
	100

The NO_x concentration and slab-temperatures obtainable with operation with blast furnace gas were calculated to be low (see Tables 22-23). Notwithstanding the fact that the same energy is input, the slab

temperature now amounts only to 895 °C, while the flue gas temperature remains almost unchanged. The NO_x given by the model is practically zero, indicating that the range of validity of this simple NO_x model has been left, but supporting the conclusion that the NO_x concentration would indeed be much lower with this type of gas. The following figure illustrates the temperature in the furnace operated with blast furnace gas.

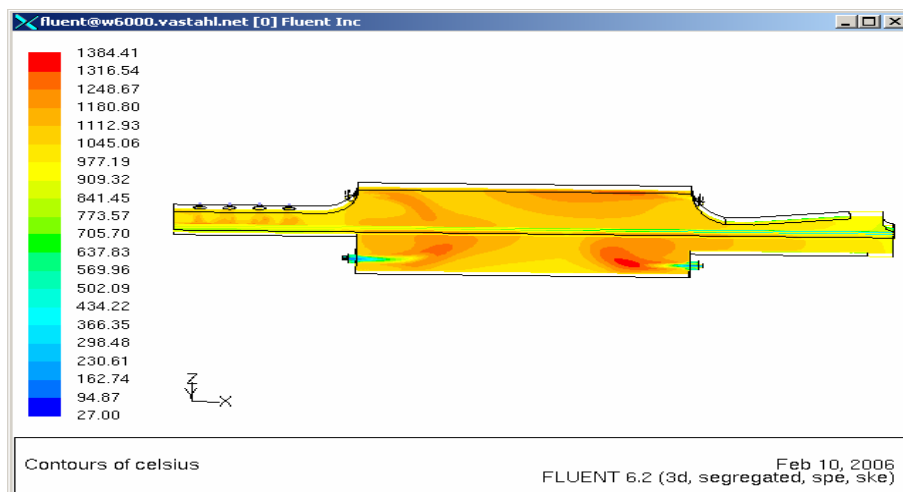


Figure 81. Temperature in furnace operated with blast furnace gas (note, the figure was compressed on the z-axis).

Evidently, the peak temperatures are much lower than with natural gas or coke oven gas, therefore the NO_x production is much lower with blast furnace gas. Unfortunately however the wall temperature, which is critical for heating up the slabs by radiation, is also lower by almost 300 °C. The slab temperature is lower by more than 200 °C as compared with a natural gas or a coke oven gas fired furnace. As the blast furnace gas flow is ten times higher than in the reference case and more would even still be required, if slab temperatures above 1000 °C are needed, it is to be doubted that this huge amount of gas could be handled without changing the construction of the burners.

Case 4: Operation with 70 % of power compared to reference case

During furnace operation periods happen where the load has to be reduced. Optimizing considerations may lead to the request to reduce fuel consumption not in all zones equally, therefore the mathematical furnace model was used to predict the impact of both equal and non-equal reduction on NO_x and on energy efficiency. This task was tackled by considering fuel reduction only in the preheating (natural gas fired zone) as compared with an equal reduction in all zones. The conditions have been chosen as follows:

The total power input by all burners in the reference case is 94 MW, the load of the furnace is 308 t/h in this case. This was compared with a situation where the power input and the throughput were reduced by 30 % to 66 MW and 216 t/h respectively. This reduction was done in two ways:

Power was reduced in all zones by 30 %.

Power was reduced only in the preheating zone, but now by 50 % yielding again a total power reduction in the whole furnace by 30 %.

Only in the preheating zone natural gas is used, in all the other zones the burners are supplied with coke oven gas. It can be seen from Table 22 that reducing the input in all zones will lead to a small decrease of the NO_x concentration in the flue-gas as compared with the reference case. However, if the power-reduction is done only in the preheating-zone, the NO_x-concentration will rise compared with full production. Obviously natural gas contributes less to NO_x formation than coke oven gas.

The effect of power and throughput reduction on the slab temperatures can be seen in Table 27. As was expected, reducing power in all zones does not change the slab temperature if this is accompanied by an equal reduction of the thermal load. It is interesting to note that the slab temperature is 10 degrees

higher if the power reduction is made only in the preheating zone. In an attempt to offer an explanation for this fact, the heat balance of the gas phase in the furnace is displayed in Table 27.

Table 27. Heat balance for the gas phase in the model furnace. It is to be noted that the model furnace is only 1/8 of the real furnace, the power is reduced correspondingly.

	<i>ref. case</i>	<i>70%, only preh. zone reduced Case 4.1</i>	<i>70% all zones Case 4.2</i>
<i>slab temperatures °C</i>	1204	1214	1203
<i>heat flow in gas phase:</i>			
air and gas from burners	702920	480737	470421
flue gas	8123984	6099609	6041738
<i>total heat input from gas phase</i>	<i>8826904</i>	<i>6580346</i>	<i>6512159</i>

It may seem paradoxical that the main input comes from the flue gas, but this is caused by the fact that the enthalpy of the flue gas is negative and FLUENT swaps the sign because the flue gas is leaving the domain. Therefore the enthalpy flows from the burners and from the flue gas have to be added in order to get the total heat input. Table 27 also makes clear that with a power reduction only in the preheating zone the flue gas has less enthalpy (that is a larger absolute value) than in the case of equal power reduction in all zones meaning that more energy is left in the furnace in the first case. The difference in the heat input is 68 kW which is significantly above the heat balance errors of 23 kW and 1.8 kW for the all-zones and only-preheating-zone reduction. It seems that the burners in the preheating zone are slightly less effective because they are nearer to the exit of the flue gas and therefore the hot gas from these burners has the smallest residence time in the furnace.

Case 5: On-Off operation

As an alternative to power reduction by 70 % it was investigated numerically to run with full power (i.e. the power of the reference case) for 70 % of a certain cycle time and to switch off the burners for the rest of the cycle. As this mode of operation requires expensive new gas- and air- control devices, it is very important to simulate this situation mathematically in order to get a realistic prediction of the expected benefits. In this CFD simulation 60 seconds were chosen as cycle time, therefore power on was for 42 seconds and off for 18 seconds. The NOx concentration at the furnace outlet during the on-period is displayed in Figure 82.

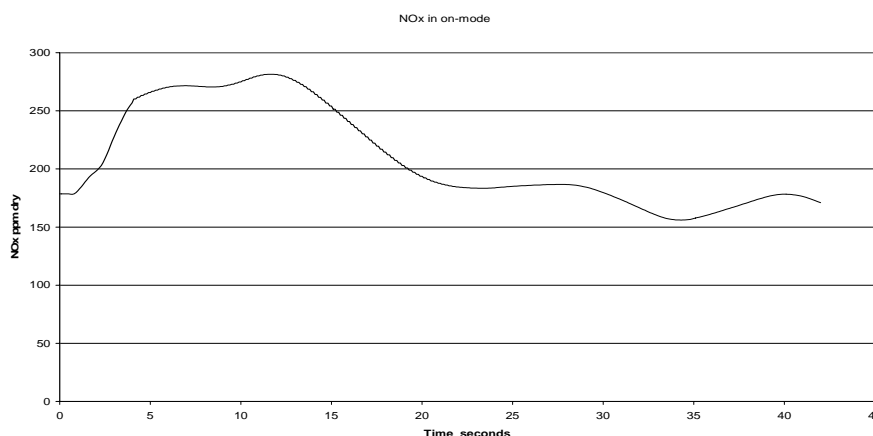


Figure 82. NOx concentration at furnace outlet during burner-on period.

The average NOx concentration during the on-period is 209 ppm. When burners are switched off, virtually no NOx and no flue-gas is produced, the NOx-concentration in the off-state being undefined, strictly speaking. The results of this operational method therefore depend on how the contribution of the off-state is defined. In this evaluation the NOx concentration is determined by averaging the concentrations only in the on-state. If this average concentration is multiplied by the total amount of

flue-gas produced during an on-off cycle it will yield the mass of NO_x generated during one cycle. Table 28 gives the normalized NO_x concentrations with on-off operation:

Table 28. NO_x concentration with on-off operation corresponding to 70 % power and furnace load of the reference case.

	ppm dry	mg/Nm ³ @3%	mg/Nm ³ @5%	mg/MJ
NO_x	209	385	342	98

As compared with 70 % stationary power reduction in all zones, on-off operation is predicted to produce even a larger amount of NO_x under the described conditions. Obviously this unfavourable behaviour is due to the larger NO_x values during the first 15 seconds of the on-mode, see Figure 82. It cannot be excluded however, that changing the switching cycle-time could lead to the expected decrease in NO_x. This should be subject to further investigations.

Case 6: Alternative Burners

One goal of this work was to be able to predict the performance of a certain burner in the environment of an actual industrial furnace. After the proper performance of the CFD calculation with the present comparatively old burners (“first generation”) in the slab reheating furnaces of the Voestalpine hot rolling mill in Linz has been asserted, interest grew to investigate the NO_x reduction achievable with newer burners employing air- staging in the actual environment of the furnaces.

In order to model this behaviour, not more is required than accurate drawings of the geometry of the burners. It turned out, however, that none of the companies constructing and selling burners are willing to give away sufficiently detailed drawings of their burners to a potential customer. As a consequence, it was necessary to rely on burners which actually have been bought. Fortunately, the roughing mill in Linz has also a slab reheating furnace which is equipped with burners using already air-staging from the same supplier than of those older ones in the hot rolling mill. Those burners are designed for about half the nominal power and show considerable differences in construction. Their geometry was placed into the present furnace model and the calculation performed with the operational data of the hot rolling mill, see description of the reference case. The data measured from the roughing mill could not be used to predict the behaviour of these burners in the hot rolling mill’s furnaces, because furnace construction, number and placement of burners and operational mode differ remarkably from the hot rolling mill. The results of these calculations are compiled in Table 22. It is noted that the NO_x concentrations predicted are much lower than in the reference case with the old burners. Still, the reductions in NO_x computed are so large, that the results have to be questioned, whether the reduction is only due to the difference between 1st generation and 2nd generation burners. An investigation of the velocities at the nozzle exits of the burners reveals some remarkable differences, see Table 29.

Table 29. Velocities and corresponding pressure-differences in the reference case and with air staged burners.

	Ref.case				roughing mill burners			
	velocity m/s	density kg/m3	density STP	p-diff mbar	velocity m/s	density kg/m3	p-diff mbar	
upper preheating zone	23	0.587	0.73	1.93	50	0.602	9.13	
lower preheating zone	35	0.433	0.73	4.47	65	0.625	15.42	
upper heating zone	19	0.316	0.4	0.72	34	0.352	2.31	
lower heating zone	23	0.333	0.4	1.06	70	0.358	9.80	

It turns out that the gas- velocities are about two times larger for the newer burners, which is not really surprising as these burners are designed for about half the nominal power than for those at the hot rolling mill. As in the calculation they have been fed with the gas and air flux rates of the hot rolling mill, their simulated situation indicates their behaviour when the load exceeds their nominal power. Evidently, this case is rather favourable for internal flue gas recirculation, which in turn lowers peak flame temperatures and therefore NO_x production. Figure 83 illustrates the somewhat more smooth temperature distribution in the furnace with those burners. The only problem seems to be that the pressure necessary to achieve the desired flow rates will rise be about four times larger than in the reference case.

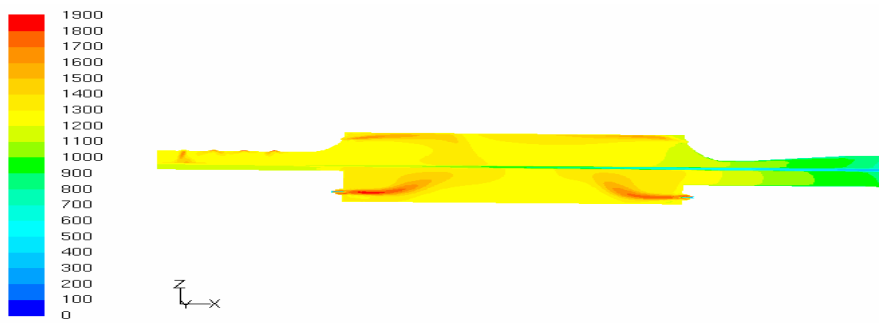


Figure 83. Temperature field in the furnace equipped with air-staging burners (note, the figure was compressed on the z-axis).

The calculation was no more difficult than for the standard case and the result indicates clearly that this kind of burners would help to reduce NO_x in the furnaces at the hot rolling mill. It is somewhat surprising, that burner suppliers neither support their customers if they want to make calculations on their own nor do they offer to perform themselves calculations for the behaviour of their proposed burners within simplified but still basically realistic models of the furnaces of their customers.

Voestalpine Model validation

The standard state used for this model validation was a four hours lasting period of constant operation of both furnaces at the hot strip mill. The gas- and air- flow rates averaged over this period were chosen as boundary values for the numeric model and the results of the calculation were compared with the average temperatures and concentrations of this record in Table 30.

Table 30. Average actual furnace temperatures from reference case compared with results of the stationary calculation.

average furnace temperatures and results of calculation		
	measured	calculated
flue gas	912	912
frontal convective zone	941	962
rear convective zone	970	1012
upper preheating zone	1290	1410
lower preheating zone	1306	1270
upper heating zone	1290	1390
lower heating zone	1245	1250
soaking zone	1269	1270
holding zone	1274	1270

The agreement of the results is excellent in the holding-, soaking and convective zone, and consequently in the flue gas too. In the main zones the temperatures agree still reasonably well in the lower preheating and heating zones, while in the upper zones the actual temperatures are about 100 °C higher than the calculated ones. A possible explanation would be that in the upper zones the positions of the ardometers are more close to the centre of the flame, possibly because the burners are more tightly spaced than in the lower zones (there are 12 burners in each of the upper zones compared to only 8 in the lower zones). The temperature of the slabs after withdrawal from the furnace also fits well: The furnace automation system gives an average temperature of 1191 °C while the calculated temperature of the slabs was 1186 °C. The average gas temperature in the CFD model was 1243 °C and the average furnace wall temperature 1214 °C. Table 31 gives a comparison of the measured and calculated NO_x-values.

Table 31. NO_x in flue gas in standard case.

	ppm dry	mg/Nm ³ @3%	mg/Nm ³ @5%	mg/MJ
NO _x	262	507	451	132.0
NO _x measured		437		

It is noted that the calculated NO_x (taken as NO₂) is larger than the measured one, the difference exceeds even somewhat the standard deviation which is 57. This could be related to the rather high peak flame temperatures in the calculation results which in turn may have been caused by compromises in grid cell shape and size which have been necessary in order to deal with the large scale-differences between the detailer burner geometry and the shape of the furnace interior. The flow rates of the gases and air are summarized in Table 32.

Table 32. Flow rates in the reference case. Indicated are averages over the observed time period.

	<i>natural gas</i>	<i>coke oven gas</i>	<i>air</i>	<i>Lambda</i>
	<i>Nm³/h</i>	<i>Nm³/h</i>	<i>Nm³/h</i>	
<i>Zone1 upper preheating zone</i>	2676		27461	1.08
<i>Zone2 lower preheating zone</i>	2938		28515	1.02
<i>Zone3 upper heating zone</i>		2973	13792	1.06
<i>Zone4 lower heating zone</i>		3923	17908	1.05
<i>soaking zone</i>		458	2485	1.24
<i>holding zone</i>		370	2018	1.25

During their stay in Linz, members from the project partner ISQ was able to measure the NO_x- content in the main zones of one furnace. The mean concentrations derived from these results are given in Table 33. The figures indicate somewhat higher NO_x- concentrations in the lower part of the furnace as calculations have predicted, but they do not show a significant higher NO_x- concentration in the lower heating zone, as calculations have done. It has to be mentioned that the measurements could not be performed simultaneously, but rather only one zone could be investigated at a time, therefore it is not without some problems to compare the values as it is done in Table 33.

Table 33. Measured NO_x in the heating, preheating and convective zones of the Voestalpine slab reheating furnace.

	NO_x [ppm] in zones		NO_x [mg/Nm³] in convective zone	
	measured heating	measured preheating	measured convective	calculated convective
upper	130	110	223	204
lower	160	150	260	279

A direct comparison between calculated and measured NO_x-concentration was attempted for the convective zone. Table 33 also shows the calculated and measured results for the upper and lower convective zone. The calculation was done with the mean gas- and air-inputs during the measuring periods and the indicated measured concentrations are means over the periods. It can be seen that the CFD results are rather close to the measured ones and the trend – more NO_x in the lower convective zone is predicted correctly. In order to determine how well the CFD-model can calculate the temperature of the slabs, a slab was equipped with thermocouples and a water-cooled data acquisition system and pushed together with normal production slabs through the furnace. The mean gas- and air-flows during the residence time of the slab in the furnace was the input to the stationary CFD-calculation and the resulting temperatures at the location of the thermocouples have been compared with the measured ones. The thermocouples were placed at the middle of a 7500 mm long, 1400 mm wide and 207 mm thick slab underneath the side face looking towards the exit-door. Three different depth were chosen for the placement of the thermocouples: 70, 102 and 130 mm from the upper slab-surface. At first sight, there is a big disagreement between calculated and measured temperatures, as can be seen in Figure 84.

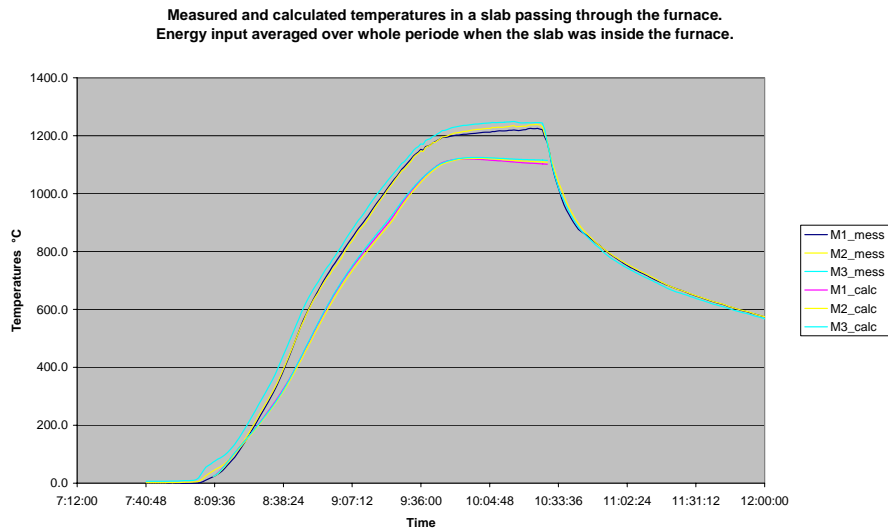


Figure 84. Measured (mess) and calculated (calc) temperatures at different locations in a slab passing through the furnace. Distance of the measuring sites from the surface: M1 130 mm, M2 102 mm, M3 70 mm with a slab thickness of 207 mm.

In an attempt to explain the deviations of the calculated temperatures from the measured ones the time-dependent behaviour of the energy input into the furnace was analyzed more carefully. It was found that while the measuring slab was inside of the furnace, the operation conditions were rather unsteady, the gas- and air- flows in the different zones changing heavily. This is not really a favourable situation for a stationary calculation, but an attempt was made to take this time-dependence into account. The idea was to extend the averaging of gas and air in each zone of the furnace only over that period of time when the equipped slab was in that zone – and not over the whole period when the slab was in the furnace. This is possible because the times when slabs are pushed into and redrawn from the furnace are logged as well as the flow-rates of the gases and of the air. It is therefore possible to track a particular slab through the furnace and to determine the flow-rates in the zone where it stays. The results of this calculation are shown in Figure 85.

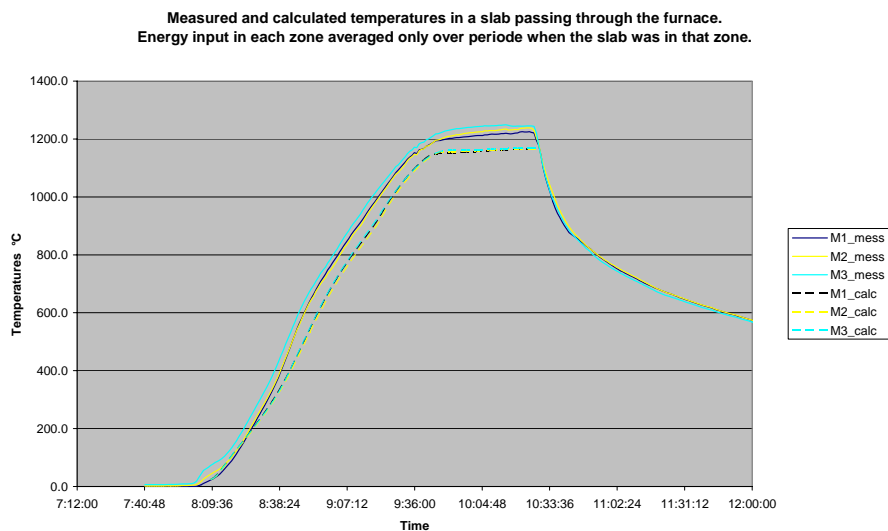


Figure 85. Measured and calculated temperatures at different locations in a slab passing through the surface. For the calculation, the energy input in each zone was averaged only over that period when the slab was actually in that zone.

Figure 85 shows a much better agreement between measured and calculated temperatures. This result shows that also for the slab-temperatures the calculation gives realistic results if the operating conditions of the furnace are implemented properly into the boundary conditions. Of course, an unsteady calculation would have to be preferred for an unsteady operation condition, but this poses yet too heavy requirements on computational time.

BFI - NO_x-Modelling the FBB regenerative burner at BFI

Apart from the experimental investigations at the BFI burner test rig, numerical stationary calculations with the FBB regenerative burner were carried out using the CFD program FLUENT (Version 6.2.16). The aim of these investigations were to prove the CFD capabilities to model thermal and prompt NO_x formation and to compare this with experimental results. A hybrid 3D volume grid was created with the grid generator GAMBIT (Figure 86). A full simulation of the combustion chamber was not carried out in order to reduce the computing time and storage space since the burner has a symmetrical design. Half a combustion chamber was modelled with symmetrical conditions.

Various partial models have to be realised for the mathematical modelling of furnaces. These are based on the flow model to describe the turbulent gas flow processes. A reaction model to calculate the species balance is needed for the chemical conversion. The transport of heat through convection and radiation on the wall and in the gas is taken into account through a heat transfer model. Table 34 summarises the models used for this simulation. The simulation for natural gas was carried out with a methane share of 86.86 Mol.-%. The exact composition can be seen in the previous WP. The burner load was 600 kW with an air ratio of 1.05. Air pre-heating of 1000 °C was assumed. 4 water-cooled plates are installed in the combustion chamber floor to cool the furnace, these were defined in the calculations as areas with a temperature of 35 °C. Calculations were carried out for two furnace temperatures of 1250 and 1150 °C. Figure 87 gives an impression of the flow conditions in the combustion chamber. The burner is characterized through three main air outlets (3 x 120°). Velocities of up to 140 m/s occur at the burner head. In the lower half of the picture two bigger recirculation zones are identified. These recirculation zones are each narrow limited between two (of the three) air flows and the furnace wall. After a short flow path the air flow already leans against the furnace wall. Only a small and short recirculation zone results close to the burner head because of the relative small furnace cross section area. This means that a more intensive reflux could be generated if the furnace would have enough space for bigger recirculation zones. The CO concentrations are detectable up to around half the combustion chamber length. After this a complete burnout was calculated.

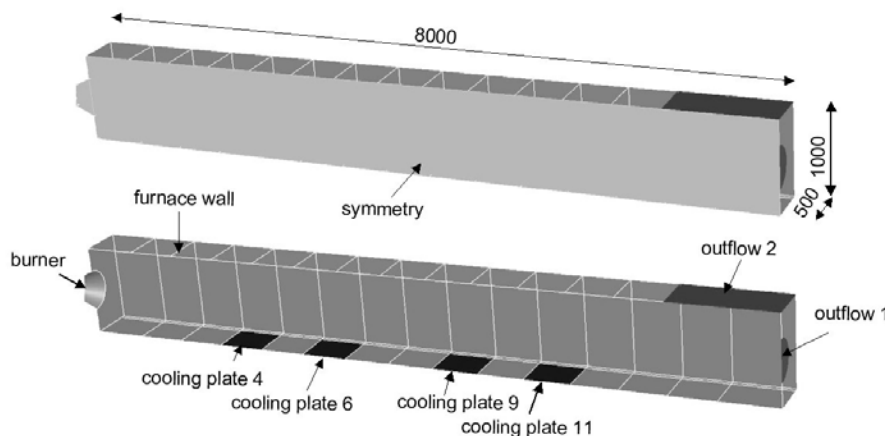


Figure 86. Geometry for the 3D volume grid of the regenerative burner and the furnace.

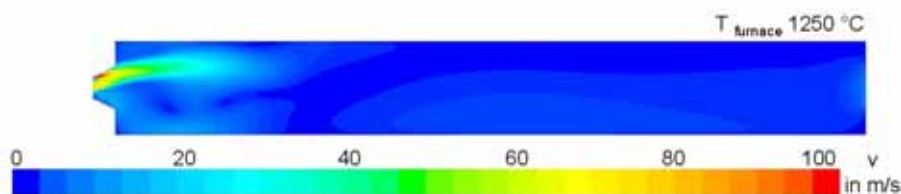


Figure 87. Velocity field generated by regenerative burner inside the BFI combustion chamber.

Figure 88 shows the temperature field for the central section through the combustion chamber. The highest flame temperatures are calculated in the area near the burner, between the air and gas injection nozzles. An even temperature develops in the combustion chamber later on. There is an increased thermal NO_x formation account of the high temperatures in reaction zone (Figure 89), with higher NO

emission values too at higher furnace temperatures. The model calculated well the influence of the different furnace temperatures. The predicted NO values at the stack are 211 mg/m³ at 5 % O₂ for 1250 °C and 168 mg/m³ at 5 % O₂ for 1150 °C furnace temperature. The calculated emission values are the results from the stationary calculation. A comparison with the experimental results is not possible because of unsteady operation of the regenerative burners and the increasing furnace temperature in front of the operating burner while testing at the combustion chamber at BFI, but the same burner was tested at CSM as reported earlier.

Table 34. Physical models and boundary conditions at BFI.

Physical models	
Turbulence	RNG k-ε
chemical reaction	Non-premixed; pdf-mixture
species	Table 13 including CO, H ₂ O, OH, O
radiation	DO 4 x 4
pollutant	Thermal and prompt NO
Numerical approach	
Grid type	Hybrid
Solver	Segregated
Linearization	Implicit
Discretization	Second order up-wind scheme
Boundary Conditions	
inlet	velocity
outlet	out flow
wall	temperature

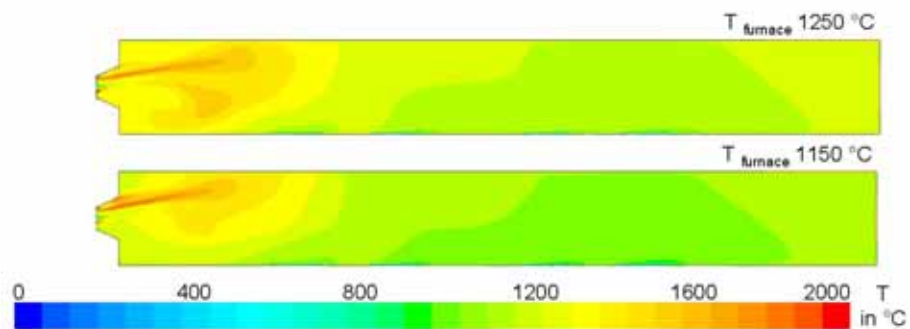


Figure 88. Temperature field generated by regenerative burner inside the BFI combustion chamber.

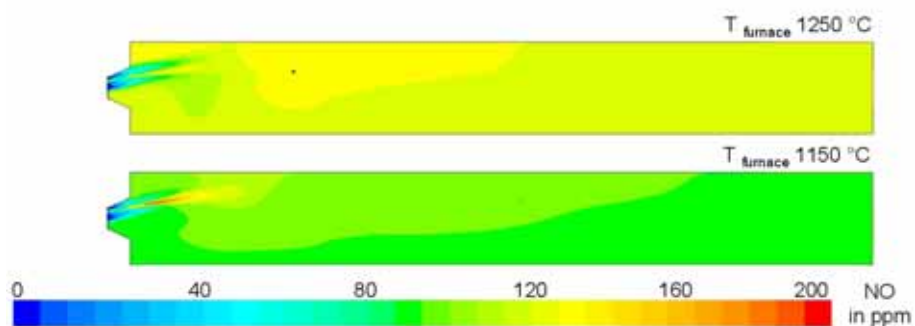


Figure 89. NO field generated by regenerative burner inside the BFI combustion chamber.

2.2.5 Task 2.5. Generalised model predicting NOx (Techint)

The NOx modelling at Techint is divided into the following sections:

- Predicting large and small scale NOx variations from reheating furnaces
- Overview of the analysis methods for predicting small scale NOx variations
- New model version

The multilayer perceptrons and circular back-propagation (CBP) networks architecture are described. An integrated approach to NOx prediction using Vector Quantization and CBP is described with reports from experimental results carried out on the 380 t/h WBF of TKS at Duisburg Beeckerwerth (Germany). The final version of the neural networks analysis was carried out in cooperation with the DIBE (Dipartimento di Biofisica ed Elettronica) of the University of Genova. A special thanks to the professors Paolo Gastaldo and Rodolfo Zunino. A new release of the NANOX model was implemented including the new theoretical algorithms.

Predicting large scale NOx variations

It is well known by the furnace engineers that average NOx emissions large scale variations from reheating furnaces are strongly affected by some main features such as:

discharging temperature (and therefore furnace process temperatures). Passing from 1250 °C discharging temperature, typical of a WBF for slabs on a HSM, to 1150 °C of a WBF for billets, average NOx emissions drop down approx of 15 %. And reaching 1050 °C of a heat treatment WBF for pipes NOx drops down of a further 15 %.

fuel type. A reheating furnace equipped with a combustion system fed by a standard natural gas (HCV 35580 kJ/Nm³) is characterized by NOx emissions lower of approx 40 % than a similar furnace fed by COG (HCV 16750 kJ/Nm³).

burners type. A reheating furnace fully equipped with flameless burners is characterized by NOx emissions up to five times lower than a similar furnace equipped with flame burners (of the same power) operating at the same process temperature.

Table 35 (below) summarizes some reference value of NOx emission from the burners present on the Techint burners catalogue.

Table 35. Typical NOx emissions for Techint burners firing natural gas with a furnace temperature of 1250 °C.

Pos.	Combustion Type	Name	Application	NOx emissions with NG [ppm] (Ref 3% O ₂ Temp= 1250°C)
Side	Flame	TS	Standard side burners for reheating furnaces	110
		TLHS	Side burner for roller hearth furnaces	90
		THS	Side burner for heat treatment furnaces	150
		TSN	Diluted flame side burner for reheating furnaces	60
	Flameless	TSX	Flameless side burner for reheating furnaces	25
		TLX	Flameless side burner for roller hearth furnaces	40
	Flame	TRG	Regenerative side burner for reheating furnaces	70
	Flameless	TRGX	Regenerative flameless burner for reheating furnaces	35
Roof	Flame	TR	Standard roof burner for reheating furnaces	140
	Flameless	TRX	Flameless roof burner for reheating furnaces	30

While the a.m. features affecting the large scale or gross variations lead to identify with coarse (but sometimes useful) precision NO_x emissions it is quite impossible to foresee the small scale or fine variations in NO_x without a mathematical tool.

Overview of the analysis methods for predicting small scale NO_x variations

An overview of some analysis methods for predicting small scale NO_x variations from a reheating furnace was made with various analysis tools including modern techniques of soft computing using a scientific baseline for a connectionist approach. NO_x emissions involve a complex and not yet fully understood phenomenon, in which several undisclosed mechanisms which makes the prediction task quite difficult. Two critical issues inhibit, or at least make impractical, the adoption of conventional approaches such as linear multivariate analysis or correlation-based statistics. First, the lack of an established set of numerical features seems to thwart the straightforward search for an explicit, analytical model. Secondly, nonlinear interactions among the parameters involved ultimately make the application of conventional statistical methods quite unsatisfactory. Incidentally, preliminary tests on the specific problem of NO_x prediction clearly pointed out the ineffectiveness of conventional statistical tools for accurately modelling the phenomenon.

In such a complex scenario, empirical nonlinear models might provide to provide a scientific basis to approach the prediction task using an implicit approach, in which the NO_x-prediction module is parameterized by a set of quantities, whose optimal values must be tuned empirically by using a training set of measured data. The crucial feature of computational-intelligence approaches in this sense is the availability of very powerful models. These models typically combine effectiveness in real-world domains with sound theoretical characterizations and give analytical bounds to the expected accuracy in rendering the relationships within the empirical samples. In the last twenty five years, the literature in the area of Computational Intelligence has been offering a vast variety of approaches, but in fact only a few survived the sort of implicit selection process that filtered out those models that best performed in practical applications. In particular, the most successful paradigms for neural-network based systems seem to have been Feedforward Neural Networks [49], Vector Quantization [50] methods, and, more recently, Support Vector Machines [51]. The former approach best fits those application context in which the observed phenomenon can be modelled in terms of I/O relationship (possibly recursive), and therefore relates to a basic stimulus-response paradigm. Vector quantizers are very useful for data representation and compression applications, hence they best perform when some grouping of empirical data is required, either for further processing or for direct inspections of the data clusters obtained. Support Vector Machines pursue a theoretical approach toward minimizing generalization error, and stem from the classical statistical approach of maximum-margin separation among data; in general, they are most used as classifiers although there are known applications for prediction. In view of all the above features, it seemed a natural conclusion to adopt the Feed Forward approach, and the model of MultiLayer Perceptrons in particular, for tackling the empirical prediction task of modelling NO_x in furnaces.

MultiLayer Perceptrons and Circular Back-Propagation Networks

Feedforward neural networks seem a viable approach to tackle the prediction task mainly because of their proved effectiveness in complex regression applications [26]. In addition, the input-output relationship can be learned empirically and does not need an *a-priori* analytical formulation of the observed phenomenon. Figure 90 shows a classic MLP architecture with two layers of neurons.

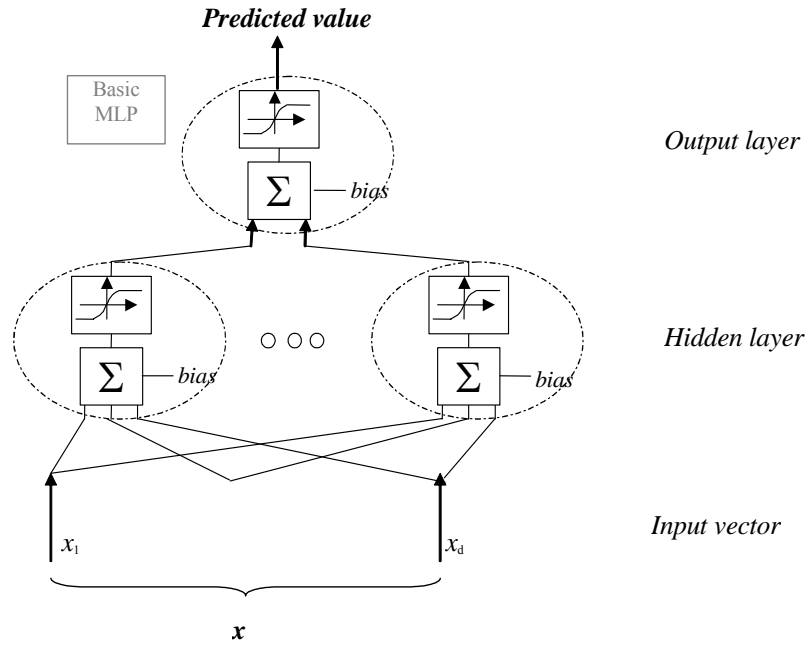


Figure 90. The classical two-layer MLP feed forward architecture.

In the case of MultiLayer Perceptrons (MLPs) [52], that stimulus mapping is attained by arranging several elementary units (‘neurons’) into a layered structure. As the resulting networks do not allow any feedback between layers, they are indeed called ‘feed forward networks. Each neuron performs a simple, nonlinear transformation of weighted inputs; the nonlinearity is usually accomplished by a sigmoidal function, either

$$\text{sigm}(r) = (1 + e^{-r})^{-1} \text{ or } \text{tanh}(r). \quad (\text{Eq. 2})$$

An MLP-based estimator actually implements a series-expansion of the desired input-output relationship, and sigmoids are the basis functions of all terms in the series. The sigmoidal nonlinearity is crucial, as theory proves that such networks can support arbitrary mappings. The typically MLP architecture involves two layers of neurons, as illustrated in Figure 90. A d -dimensional vector, \mathbf{x} , supplies the input feature values. Those quantities connect to an intermediate *hidden* layer, including N_h neurons. First, each hidden neuron weights the input values by a specific set of coefficients; then, it applies a sigmoidal nonlinearity:

$$a_u(\mathbf{x}) = \text{sigm}\left(w_{u,0} + \sum_{k=1}^d w_{u,k} x_k\right); \quad u=1, \dots, N_h \quad (\text{Eq. 3})$$

where $\text{sigm}(r_u) = (1 + e^{-r_u})^{-1}$, $\{w_{u,k}\}$ is the set of coefficients (“weights”) and $w_{u,0}$ is a bias term. The notations r_u and a_u conventionally stand for the ‘stimulus’ and ‘activation’ of the u -th neuron, respectively. The *output* layer provides the assessment response, y , by a similar transformation:

$$y_{\text{MLP}}(\mathbf{x}) = \text{sigm}\left(w'_0 + \sum_{u=1}^{N_h} w'_u a_u(\mathbf{x})\right) \quad (\text{Eq. 4})$$

where $\{w'_u\}$ and w'_0 represent the output coefficients and the output bias, respectively. The set of coefficients $\{w, w'\}$ are called the network “weights” and have to be adjusted during the training process. The basic scheme is usually enhanced by processing the output value by a sigmoidal nonlinearity $\text{sigm}(y_{\text{MLP}})$, as well, which limits the dynamic output range by a clipping effect. So in summary an MLP-based estimator can be regarded as a series-expansion, using sigmoids as a kernel space, of the input-output mapping $y_{\text{MLP}}(\mathbf{x})$. Except for trivial cases, when designing any estimator one

typically has a sample-based formulation of that input/output mapping, described by a training set of input patterns with their expected responses. The degrees of freedom of the nonlinear estimator (Eq. 4) that must be fitted are the depth, N_h , of the series expansion and the weighting coefficients within each neuron. As to the former quantity, there is no established design criterion; however, the literature provides both theoretical and practical criteria to ensure accuracy of prediction performance, while minimizing the risk of over fitting training data. The present research followed a practical approach mainly because of its simplicity and proven effectiveness.

Once the number, N_h , of network neurons is decided, a fitting process must tune the set of their weights, W , in such a way that the network best reproduces the desired input/output mapping. Toward that end, the classical cost function for feed forward networks is the mean square error, E_w , between the desired responses (i.e., the quality scores from human assessors) and the network outputs. Thus, the network-training process is formulated as an optimization problem expressed as:

$$\min_w E_w = \min_w \frac{1}{n} \sum_{s=1}^n [t^{(s)} - y_{\text{MLP}}(\mathbf{x}^{(s)})]^2 \quad (\text{Eq. 5})$$

where n is the number of training patterns, and $t^{(s)}$ is the desired output for the s -th pattern, $\mathbf{x}^{(s)}$. The Back-Propagation algorithm [49] tackles the learning problem (Eq. 5) by a stochastic gradient-descent strategy over the weight space, and for each pattern the algorithm adjusts each weight, w , in the network according to the following strategy:

$$\Delta w = -\eta \frac{dE}{dw} \quad (\text{Eq. 6})$$

Although the derivation step (2.5) is easy for the output layer, the problem is that no target reference is available for lower layers, but the problem is solved empirically and iteratively first by rewriting:

$$\frac{dE}{dw'} = \frac{dE}{dsigm} \frac{dsigm}{dw'} \quad (\text{Eq. 7})$$

for the output layer, then propagating such gradient information as an error to the lower layers. The resulting ‘‘Back-Propagation’’ algorithm eventually also gave its name to the whole neural model; it clearly does not guarantee global convergence but in practice it is very fast and computationally easy to implement. The availability of such an effective tool actually represented the boosting factor to the practical impact of MLPs. To further enhance the convergence speed of the fitting process (Eq. 5), the research presented in this paper adopted an accelerated version [53] of the classical Back-Propagation algorithm.

MultiLayer Perceptrons for the prediction of NOx

In the present approach, the feed forward neural network maps feature-based descriptions characterizing the state of the furnace into a set of scalar values, representing the NOx level. Efficiency requirements (i.e., the storage size of the parameters) and generalization issues (i.e., the NN performance over data not used for training) drive the design of the neural-network model. The ‘‘Circular Back Propagation’’ (CBP) network [54] extends the conventional MLP model by adding one input, but notably increasing the network’s representation effectiveness.

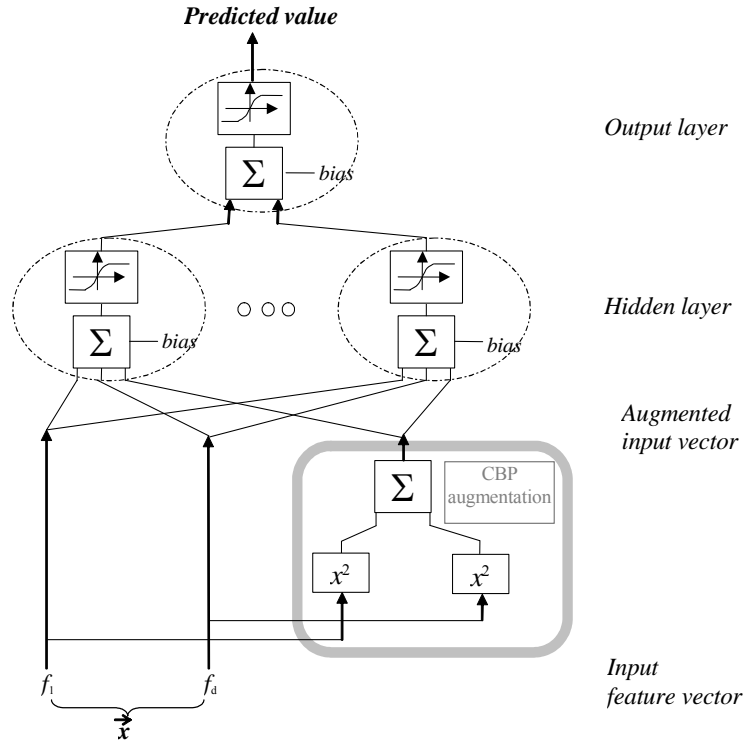


Figure 91. CBP architecture with two layers of neurons.

The CBP architecture involves two layers of neurons, as illustrated in Figure 91. The same d -dimensional vector, \mathbf{x} , used for the classical MLP supplies the input feature values. Likewise, input neurons connect to an intermediate hidden layer of N_h neurons. In the CBP reformulation, each hidden neuron weights the input values by a specific set of coefficients but also includes in the weighted sum the norm of the input vector itself. Then of course the sigmoidal nonlinearity is applied, hence the CBP model formulation affects only the intermediate hidden layer, and can be written as:

$$a_u(\mathbf{x}) = \text{sigm} \left(w_{u,0} + \sum_{k=1}^d w_{u,k} x_k + w_{u,d+1} \sum_{k=1}^d x_k^2 \right); \quad u=1, \dots, N_h \quad (\text{Eq. 8})$$

The last, quadratic term in the argument of the sigmoid represents the additional input to the conventional MLP. The quadratic augmentation does not affect the fruitful properties of the MLP structure, as the gradient-descent back-propagation approach to optimise weights still applies successfully. More importantly, theory has proved [54] that, in classification problems, CBP networks can map both linear and circular separation boundaries; this was not allowed by the straight MLP model, which implied a linear-boundary strategy. Such a feature endows the CBP model with the ability to encompass specific regions of the space in which peculiar treatment is required. The theoretical analysis also showed that such an augmentation does not affect generalization performance, so the ultimate risk of over fitting as a result of the reformulation is negligible. An interesting feature is that the selection of either model (linear or circular) is entirely data-driven and comes from the empirical training process: the selection of a model does not require any *a priori* assumption. Such an adaptive behaviour makes CBP networks suitable for application to problems whose domain structure is obscure.

An integrated approach to NOx prediction using Vector Quantization and CBP

The effectiveness of the feed forward architecture at run time best shows up when the prediction system operates on a data source having the same distribution as the samples used for training. This beneficial generalization power has been thoroughly examined in the literature and also extensively verified in practice, including the present application domain, as will be detailed in the following section. If, however, one assumes to draw empirical data from quite a different sampling situation (e.g., from a different plant, or even from the same plant but under different production cycles), then the statistical distribution of the observed phenomenon changes with respect to training conditions. As a result, some

correction has to be activated to keep track of the mutated situation. Two options usually are available to neural network-designer: the first option is to re-train the original neural network with the new sample population, in order to build a “more general” estimator. Otherwise, one can devote an entirely new neural network to the new sample and use the specific assessor properly when required. Both alternatives have pros and cons.

The former approach maintains a single-estimator structure starting from a previously trained condition, hence once would expect re-training to be easier; at the same time, teaching a common estimator two different phenomena may generate undesirable artefacts. More precisely, collating a unique training set from two samples forces some crosstalk to arise between the two distributions in the weight-adjustment process; this might not be welcome especially if the those samples pertain to two objectively different phenomena.

The alternative approach has the advantage of avoiding spurious interactions among statistical measures, but of course it pays the price of a multiple neural structure that requires some preliminary selection mechanism. Indirectly, a multiplexed neural estimator might increase the risk of over fitting. Nevertheless, such an approach seems not only viable but even recommended when one can prove substantially (i.e. by statistical analysis) that the various sample populations originate from different distributions or belong to different zones in the data space. In view of the above discussion and of the experimental evidence collected on the NOx data during this research, the second approach clearly provided a satisfactory solution to the final estimation architecture. The basic space-spanning mechanism is supported by a Vector-Quantization network; thanks to its unsupervised nature (it does not regard at all emission data but rather the input parameter distribution), the VQ network tries to separate input samples and to identify separate clusters in the original sample. The classical formulation of the VQ training problem can be set as follows. The d -dimensional data space is partitioned by a set of prototypes, $W = \{w_n \in \mathcal{R}^d, n = 1, \dots, N_w\}$, which lie at “significant” positions in the data space; each prototype (“neuron”) covers the samples lying within its associate partition.

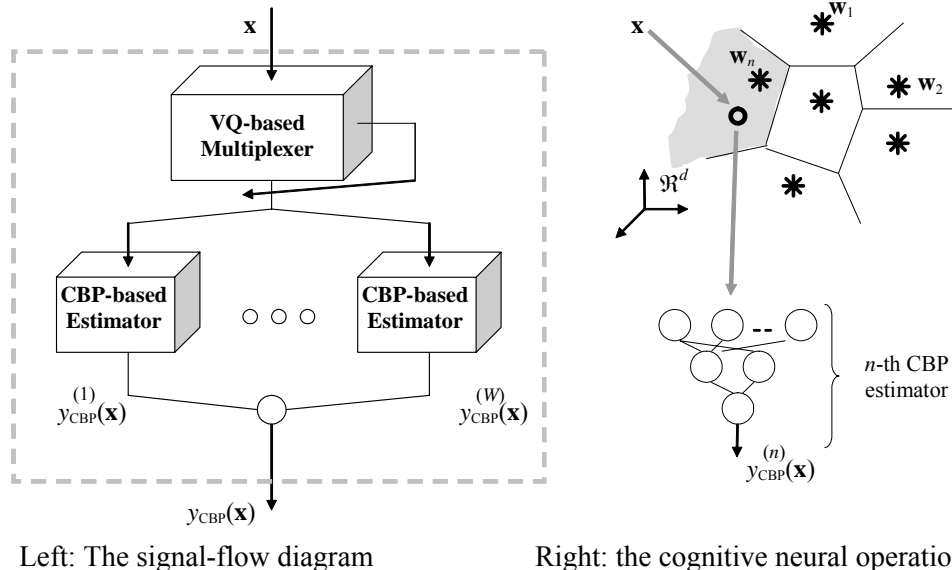


Figure 92. The VQ-based network multiplexing strategy, where the input pattern, x , is detected to belong to the n -th partition of the data space and activates the associated CBP neural estimator.

In any case, the output of the VQ training process is indeed a partitioning of the data space, according to some minimum-distortion criterion in pattern representation. The multiplexed neural architecture takes advantage of that partitioning to build, whenever required by the VQ outcome, a specific CBP estimator for each significant region of the space. The pattern-assignment process eventually drives the multiplexing mechanism, as each incoming pattern that should generate a prediction of NOx emission first enters a VQ classifier that decides which region of space the pattern belongs to; then the system invokes the associated CBP estimator. The overall principle of operation is illustrated in Figure 92.

Testing the NANOx model experimentally

The effectiveness of the proposed neural-based approach has been inspected on a database of patterns collected on the 380 t/h WBF of TKS at Duisburg Beeckerwerth (Germany). The test bed included two different datasets composed by patterns spanning a 16-dimensional feature space: DATASET1 included 8303 patterns, DATASET2 included 11379 patterns. The two datasets were collected on same plant but under different production cycles.

A preliminary experiment was set up to characterize the statistical distribution of the observed phenomenon. To achieve this goal, an unsupervised representation of the space covered by the two datasets was obtained by exploiting advanced VQ techniques [50]. Table 36 presents the results obtained by the clustering algorithm: for each prototype (i.e. cluster), the table reports the number of patterns belonging to the dataset DATASET1 and the number of patterns belonging to the dataset DATASET2. Numerical figures clearly show that the two datasets almost cover two different portions of the feature space: in several cases, the large majority of the patterns in a cluster (i.e. a partition of the feature space) belong to only one dataset (either DATASET1 or DATASET2). Hence, the two dataset are characterized from different statistical distributions, although data were collected on the same plant. According to the approach described in the previous section, two different neural-based predictors have been developed for the two different statistical distributions.

The first estimator addressed the distribution characterized by dataset *DATASET1*. To evaluate the generalization ability of the neural-based estimator, two different experiments has been carried out. In each experimental run, 7303 randomly selected patterns made up the training set for the neural network, whereas the remaining 1000 patterns provided a test set; the latter ones never entered any step of the training process, and served to assess the system generalization performance empirically. Both experiments involved a CBP network with 16 inputs and 5 neurons in the hidden layer.

Table 36. Results of the clustering analysis.

Cluster #	DATASET1 patterns	DATASET2 patterns	Cluster #	DATASET1 patterns	DATASET2 patterns
0	1148	47	15	1	778
1	957	22	16	77	549
2	952	12	17	2	1138
3	866	0	18	8	1041
4	493	80	19	39	722
5	501	8	20	0	489
6	20	731	21	110	143
7	838	4	22	281	0
8	1008	4	23	0	184
9	595	0	24	0	190
10	8	547	25	0	224
11	7	1349	26	0	340
12	15	921	27	0	641
13	3	499	28	0	168
14	102	461	29	4	87

Measuring the generalization error required to compare the NOx values, y , predicted by the neural network with the actual NOx values, t , collected on site. The discrepancies between these quantities were interpreted by different statistical descriptors:

Table 37. Test results on run #1 and run #2.

	$\hat{\mu}_{err}$	s_{err}	$\hat{\mu}_{ err }$
Run #1	-0.29	36.15	23.59
Run #2	-0.53	34.00	23.45

the mean prediction error, $\hat{\mu}_{err}$, between y and t with the associate sample standard deviation, s_{err} ; the mean value of the absolute prediction error, $\hat{\mu}_{|err|}$; Table 37 reports the results obtained with run #1 and #2. Numerical figures show that the neural predictor attained satisfactory performance on both experiments; in both cases, the mean value of the absolute prediction error is smaller than 24, corresponding to an estimation accuracy higher than 99 %. Besides, Figure 93 and 94 present the scatter plots characterizing the results obtained with run #1 and run #2, respectively. The scatter plots give the predicted value of NOx (on the y-axis) versus the actual NOx value (on the x-axis) and confirm the effectiveness of the neural-based approach.

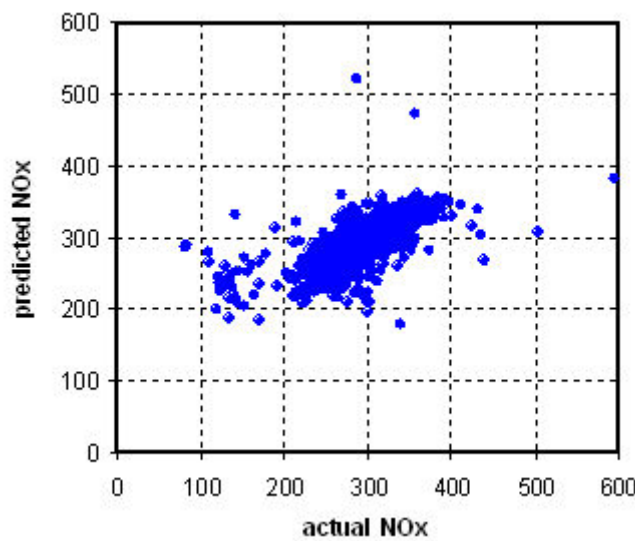


Figure 93. Estimated NOx values versus actual values for run #1.

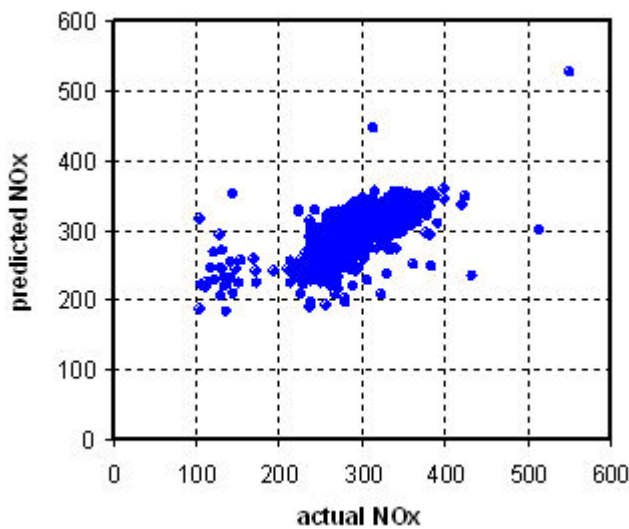


Figure 94. Estimated NOx values versus actual values for run #2.

Table 38. Test results on run #1 and run #2.

	$\hat{\mu}_{err}$	s_{err}	$\hat{\mu}_{ err }$
Run #1	-0.42	21.31	15.61
Run #2	0.48	20.77	15.08

The second estimator addressed the distribution characterized by dataset DATASET2. In this experimental session, each run involved 8879 randomly selected patterns for the training set, whereas the remaining 2500 patterns provided a test set. Both experiments involved a CBP network with 16 inputs and 5 neurons in the hidden layer.

Table 38 reports the results obtained with run #1 and #2. Numerical figures show that the neural predictor attained satisfactory performance on both experiments; in both cases, the mean value of the absolute prediction error is smaller than 15, corresponding to an estimation accuracy higher than 99 %. Besides, Figure 95-96 present the scatter plots characterizing the results obtained with run #1 and run #2, respectively. The scatter plots give the predicted value of NO_x (on the y-axis) versus the actual NO_x value (on the x-axis) and confirm the effectiveness of the neural-based approach.

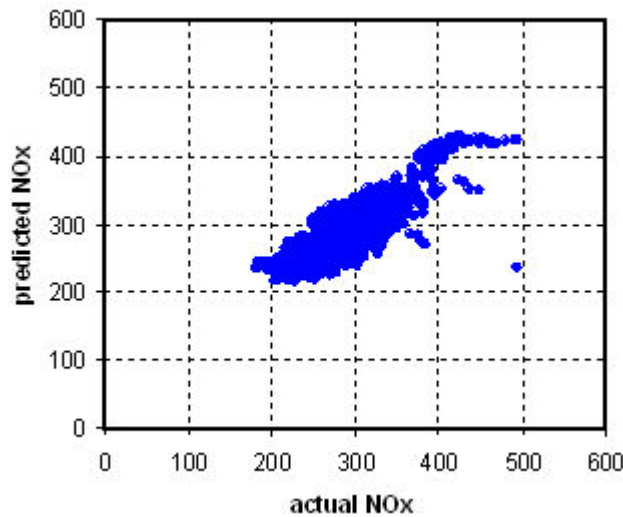


Figure 95. Estimated NO_x values versus actual values for run #1.

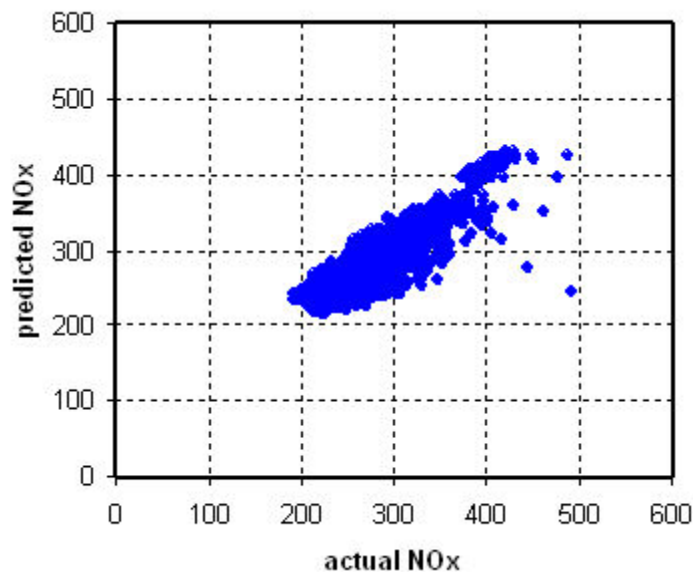


Figure 96. Estimated NO_x values versus actual values for run #2.

2.3 WP 3 - Measurement of NOx and other pollutants and review of NOx abatement techniques

The objective of this work package was to perform NOx concentration measurements, during the trials performed within the scope of this project. Therefore, it supplied a set of relevant and reliable data that allowed subsequent modelling work. Table 39 presents the measurements performed by ISQ during NOx project.

Table 39. Measurements performed by ISQ and measured pollutants.

Partner	Date	Place	Measured pollutants
Voest-Alpine	February 2005	Slab reheating furnace no 6	NOx, CO, CO2, O2 and SO2
CSM	March 2005	Pilot furnace during tests with the Hauck TRIOX burner	NOx, CO, CO2, O2 and SO2
BFI	January 2006	Experimental HTR combustion chamber	NOx, CO, CO2, O2, SO2, TSP and heavy metals
CSM	December 2006	Pilot furnace	NOx, O2

2.3.1 Task 3.1: Measurement of NOx concentration

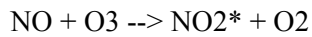
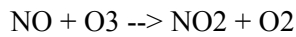
Although nitrogen forms eight different oxides, our principal air pollution interest is in the two most common oxides - nitric oxide (NO) and nitrogen dioxide (NO2). Different measuring techniques can be used to determine NOx concentration. Chemiluminescence and Non Dispersive Infrared Absorption (NDIR) were the techniques adopted during NOx project. Comparing with other traditional chemical techniques, the characteristics of these two methods were considered the most adjusted to the project objectives.

Trials performed during the project demanded NOx measurements during different operating conditions. As the operating conditions changed very quickly, spot measuring techniques were not adequate. In these techniques a grab sample is collected in an evacuated flask containing a dilute sulphuric acid-hydrogen peroxide absorbing solution, and the nitrogen oxides, except nitrous oxide, are measured colorimetrically using the phenoldisulfonic acid (PDS) procedure. Consequently, spot measuring techniques need time to absorb enough quantities of flue gas to allow NOx measurement. Moreover, special sample conditioning is also required after the sampling process.

Chemiluminescence and NDIR provided real time sampling and analysis of NOx, without losing the accuracy and precision. The integration of NOx and other pollutants such as O2, CO2 and CO in the same instrument allowed the acquisition of data for different pollutants for the same time. This fact allowed a better interpretation of the results. Chemiluminescence is recognised as a reference method by European legislation.

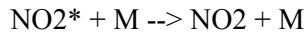
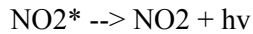
Chemiluminescence

Chemiluminescence has long been recognized as the best practical analytical method for NOx detection in a wide variety of applications. The technology is easily capable of making PPT (parts per trillion) measurements in research settings. Chemiluminescence analyzers are recognized as the only practical choice for ambient air quality monitoring stations, where thousands of units are deployed worldwide to measure PPB (Parts Per Billion) ambient concentrations. Chemiluminescence analyzers are also the overwhelmingly dominant choice in regulatory combustion monitoring systems, especially as emissions regulations become stricter and permissible levels get lower each year. Chemiluminescence NOx analyzers measure NO by routing the sample gas directly to the reaction chamber where it combines with ozone (O3). In the reaction between NO and O3, NO2 is formed, some of which is in an excited (unstable) state. The unstable NO2 molecule emits electromagnetic radiation which is measured as a light by a photomultiplier tube.



NO₂* represents the excited state molecule.

Only about 20 % of the NO₂ that is formed is in the excited state. This NO₂* reverts back to the ground state while emitting electromagnetic radiation.



$h\nu$ represents the radiated emission, which is in the wavelength range between 600-3000 nm, with intensity maximum at approximately 1200 nm. This chemiluminescence signal is detected photo-electrically. When O₃ is present in excess the signal is proportional to the NO concentration of the sample gas. By far, the largest portion of the NO₂* returns to the ground state without radiation emission, due to collisions with other molecules (M). In order to enhance the light yield the pressure in the reaction chamber is reduced. The probability that the NO₂* molecule is deactivated by a collision with another molecule (M) - thus emitting no light - increases proportionally with the reaction chamber pressure. The collision between the NO₂* molecule and another molecule (M) is usually referred to as "quenching". Quenching is an unwanted phenomenon and the extent to which it occurs depends on the character of the colliding molecule (M). For example, H₂O and CO₂ quench NO chemiluminescence more effectively than N₂ and O₂.

In general, NO_x exists as some mix of NO and NO₂, with the relative fractions of these species depending upon a number of factors. NO is the thermodynamically favoured species at high temperatures, which is why it is the dominant species of NO_x in combustion exhausts. NO₂ is the thermodynamically favoured species at low temperatures, making it the dominant species in ambient air. But, the conversion between the species happens extremely slowly at room temperature. While most chemical reactions occur in a small fraction of a second, this conversion takes up to a day under normal atmospheric conditions.

Conversion of NO₂ to NO, necessary to get an accurate reading of total NO_x since only NO can be detected, can be accomplished in a number of ways.

At elevated temperatures, the reaction between NO and NO₂ occurs very quickly, and if the temperature is high enough essentially all NO₂ in a sample can be converted to NO. As the sample cools, the NO_x is temporarily "frozen" as NO since the timescale for conversion back to NO₂ is so long. This is the basis for high temperature thermal conversion. Other converters either try to exploit this basic technique, using catalysts for lower temperature operation, or use a reducing agent that becomes oxidized by stripping one oxygen atom away from NO₂ to convert it to NO. While these strategies lower the required operating temperature of the converter, they introduce catalytic or consumptive materials that are often poisoned, depleted, or reacted unpredictably.

Trials performed by ISQ in Voest Alpine (in Slab reheating furnace no 6), CSM (during tests with the Hauck TRIOX burner and with the Regenerative burner) and BFI (in experimental combustion chamber studying the minimization of NO_x emissions by HTR) used chemiluminescence to determine NO_x concentrations. It was used an automatic gas analyser Horiba PG 250 that uses chemiluminescence (cross-flow modulation) for NO_x measurement (Table 40). The PG-250 is a portable stack gas analyzer that can simultaneously measure up to five separate gas components. The instrument interfaces directly with a laptop computer through an RS-232C interface to record measured values. It includes a built-in sample conditioning system with sample pump, filters, and a thermoelectric cooler.

Non-dispersive Infrared absorption – NDIR

Gaseous materials, except for symmetrical bi-atomic molecules and mono-atomic molecules, normally contain absorption peculiar to the infrared region. There are two types of analyzers using the method of infrared absorption: one is dispersive infrared gas analyzer which irradiates infrared rays having particular wave number, such as produced by a diffraction grating or a prism, to select the infrared rays emitted from light source, to absorption cells and receiving this transmission light with a

photomultiplier and others. The other type is a non-dispersive infrared gas analyzer, with a reference cell sealed with the measuring component or other gases having absorption spectrum identical with the measuring component, and detects the change in the absorption of infrared rays at particular wavelength in a sample cell. To measure the concentration of gases in flue gas this non-dispersive infrared gas analyzer (NDIR) is normally used.

CSM, during tests with the Hauck TRIOX burner and with the Regenerative burner, used the analyzer Fuji Electric Series Z, Model ZKJ. This infrared gas analyzer measures the concentration of NO, SO₂, CO₂, CO and CH₄ contained in sampling gas on the principle that different atomic molecules have an absorption spectrum in the wave band of infrared rays, and the intensity of absorption is determined by the Lambert-Beer law. This analyzer is equipped with a catalytic converter to reduce NO₂ to NO that is measured by NDIR.

In oxy-fuel trials, MEFOS and Air Liquide used the equipment ABB URAS 14. This is a NDIR analyzer that allows the determination of NO_x concentrations. This equipment does not permit the measure of the NO₂, thus only NO. Given the short distance that separates the measurement probe in the chimney and the analyzer, it was assumed that the conversion of NO to NO₂ is not significant and therefore the measured level of NO is equivalent to the NO_x amounts. The analyzer was calibrated daily during the campaign and measurements followed the norm: X 43-300. Voestalpine during trials in furnace 6 and 7 used the equipment Siemens Ultramat 5E that is also a NDIR analyzer that allows continuous determinations of NO_x concentrations.

2.3.2 Task 3.2: Measurement of the concentration of other pollutants

ISQ during trials with Voestalpine, CSM and BFI measured CO₂, CO, O₂ and SO₂ with an automatic gas analyser Horiba PG 250. The PG-250 uses non-dispersive IR detection for CO, SO₂, and CO₂; and a galvanic cell for O₂ measurements. The main specifications of the portable gas analyser HORIBA PG-250 are presented in Table 40.

Table 40. Horiba PG-250 specifications.

Components measured	NO _x /SO ₂ /CO/CO ₂ /O ₂
Analysis principle	NO _x by chemiluminescence (cross flow modulation) SO ₂ /CO/CO ₂ by non-dispersive infrared adsorption O ₂ by galvanic cell
Standard ranges	NO _x : 0-25, 50, 100, 250, 500, 1000, 2500 ppm SO ₂ : 0-200, 500, 1000, 3000 ppm CO: 0-200, 500, 1000, 2000, 5000 ppm CO ₂ : 0-5, 10, 20 vol % O ₂ : 0-5, 10, 25 vol %
Sample gas flow rate	approx. 0,4 L/min
Sample gas condition	temperature - less than 40 °C H ₂ O content - saturated or less at ambient temperature Dust – 0,1 g/m ³ or less Pressure – 0,98 kPa

MEFOS and Air Liquide, in oxy-fuel trials, used the equipment ABB URAS 14 which is a non dispersive infrared (NDIR) analyser that measured CO₂, NO and CO. The URAS 14 continuous NDIR photometer can selectively measure the concentrations of up to 4 components. The analyzer is characterized by higher stability and selectivity. The analyzer features gas-filled opto-pneumatic detectors which have been optimized for each application. This enables higher sensitivity, a wider range of sample components and reduced cross-sensitivity to interfering components. Detector filling corresponds to the gas being measured. This means that the detector provides optimal sensitivity and high selectivity for the component of interest. In oxy-fuel trials O₂ was measured by an ABB Magnos 16. The measuring principles for the Magnos 16 are based on the specific paramagnetic behaviour of oxygen. These analyzers are characterized by a high measurement accuracy and stability. The oxygen concentration in the 3 furnace zones was monitored and controlled during the air

combustion trials using ABB ZFG2 zirconia oxygen probes and ABB ZDT oxygen analyser/transmitters. These units are mounted a tube outside the furnace, so that oxygen analysis can be made at lower temperatures on the furnace gases after cooling.

The NO and oxygen concentrations were measured with a Kane-May Quintox electrochemical analyser for the VTS-NFK HRS burner trials and DFI in the chamber furnace. NOx emissions were also measured with the Airsense Compact mass spectrometer manufactured by V&F Analysetechnik with the VTS-NFK HRS burner trials at MEFOS. The mass spectrometer allowed for the measurement of both NO and NO2, plus oxygen so that the assumption of $NO_x = 1.05 NO$ could be checked. The results for tests with the VTS-NFK burner in the F2 flameless mode with set point values for the furnace at 1250 °C and 600 °C for the combustion air are shown in Figure 97. The NO2 levels were rather low, so NO2 may be absorbed in the water trap used to dry the gases or in condensation in the sample lines. This is shown by the sum of NO+NO2 was less than $NO \times 1.05$. The tests with the mass spectrometer also provided NOx concentrations for comparison with the data from the Quintox analyser given in WP1 for the VTS-NFK HRS burner trials. The mass spectrometer required the use of a reference calibration gas which was purchased from Air Liquide, so the NO levels measured should be more accurate. The results agree reasonably well considering there is considerable variation in the raw NO signal for a specified level of excess oxygen in the figure below. The noise in the data is typical of pilot plant trials and industrial trials, and it can be related to various factors, including deviations from set point temperatures and flow rates.

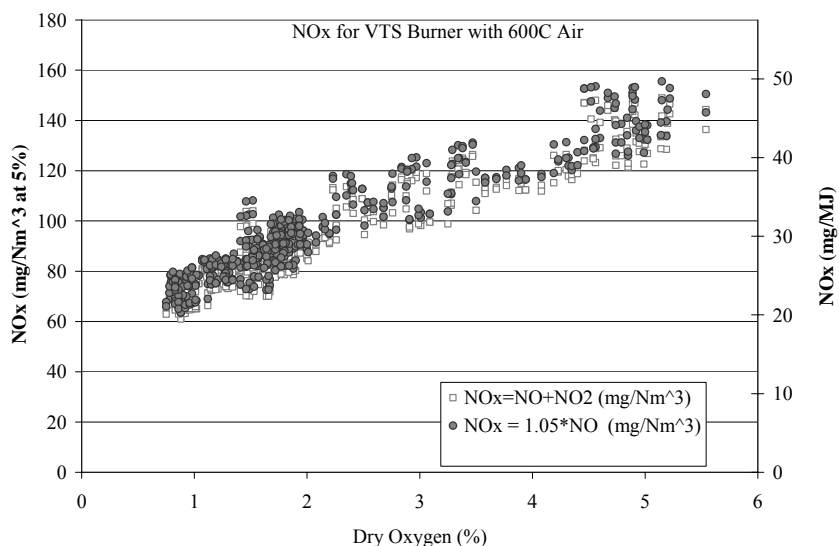


Figure 97. NOx measurements using the mass spectrometer to measure both the NO and NO2 for VTS-NFK burner in the flameless F2 mode with the furnace at 1250 °C and for 600 °C combustion air (March 31, 2006).

Measurements at BFI experimental combustion chamber were performed in January 2006 in order to study the minimization of NOx emissions by High Temperature Reduction (HTR) that uses the ammonia as a secondary abatement technique for reduction of NOx emissions. Apart from NOx, other parameters of interest were also monitored namely NH3, CO2, CO, O2, SO2, TSP and heavy metals. Measurements were performed inside the furnace chamber - P1; after ammonia addition – P2 and in flue gas before stack – P3. The data and discussion are in WP5.

Voestalpine during trials in furnace 6 and 7 used the equipment Siemens Oxymat 5E. This equipment uses the paramagnetic effect of oxygen (Quinke effect) to make small pressure pulses with an electromagnet which are measured to determine the amount of oxygen in a process stream. Measurement can be from 0-100 % oxygen, out of the box. The gas stream never sees the sensor, so corrosive gases are not a problem.

Particles

Total Suspended Particles (TSP) were sampled with a Universal Stack Sampler Anderson, in pre-weighed fibre glass filters maintained at a temperature of 120 ± 14 °C. Isokinetic conditions were assured by controlling the velocity of the effluent and regulating the flux of the collector. After sampling, filters were dried and measured by gravimetry with a precision balance Mettler. TSP were measured according the standard ISO 9096 (equivalent to US EPA5).

Pb, As, Cd, Cr, Fe, Cu, Ni and V

The Universal Stack Sampler Anderson was equipped with a filter to collect metals in solid phase and with impingers to sample metals in gaseous phase. The sampler and the sampling train are shown in Figure 98. Filters were digested with nitric acid and the solution was measured by ICP-MS with a spectrometer Variant Liberty AX. Metals were measured according the standard US EPA12 (Pb) and Modified US EPA12 (As, Cd, Cr, Fe, Cu, Ni and V).

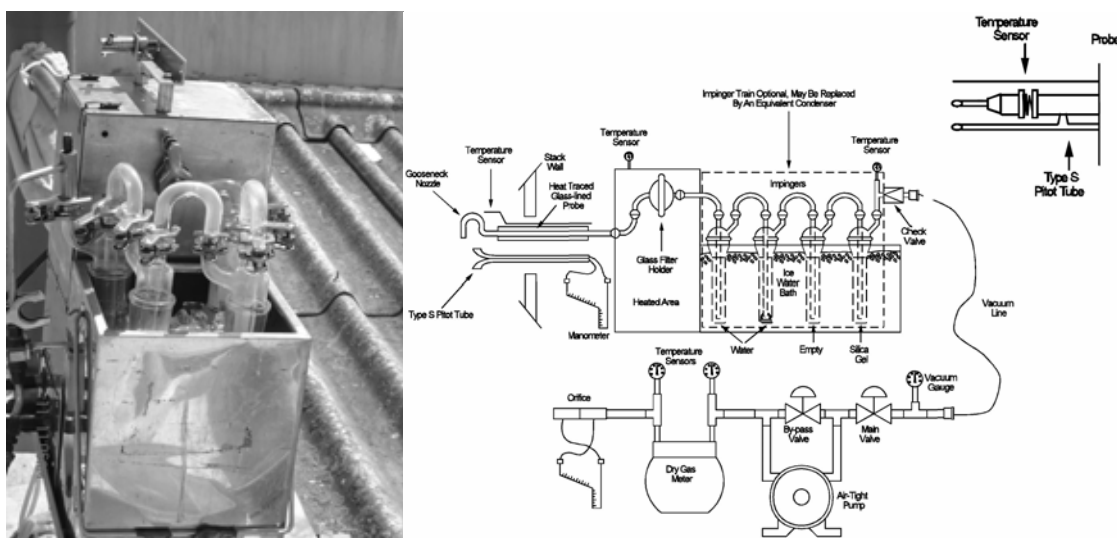


Figure 98. Universal Stack Sampler Anderson, sampling probe and sampling train.

Ammonia

The determination of ammonia was made with a colorimetric methodology using a UV/VIS spectrophotometer (Hitachi U2000).

2.3.3 Task 3.3: Measurement of flue gas characteristics

Flue gas characteristics such as pressure, velocity, flow rate, moisture content and temperature were measured in Voest-Alpine and BFI trials. For the determination of moisture content, a gas sample was extracted from the stack and the gas sample was analyzed with an Orsat for CO₂, CO and O₂ percent.

Velocity and flow rate were measured according EPA method 2. The average gas velocity in the stack was determined from the gas density and from measurement of the average velocity head with a Type S (Stausscheibe or reverse type) pitot tube. Velocity and stack geometry were used to determine the flow rate.

Pressure and temperature were measured with a barometer and a thermopar, respectively.

Techniques for flame temperature measurement

An overview of available methods and techniques for flame temperature measurement was made and is presented elsewhere. These techniques are divided into contact and non-contact techniques. Contact techniques include the well-known thermometers, e.g., glass bulb mercury or alcohol, thermocouples, or resistance thermometers that must be placed in direct contact with the temperature source. Their useful measurement range is -100 °C to 1500 °C. Thermocouples are the most widely used in industry but they are subjected to several potential errors including surface reactions, radiation, stem loss, etc.

Non-contact temperature measurement is the preferred technique for moving, or inaccessible objects; dynamic processes that require fast response; and temperatures above 1000 °C. Infrared temperature sensors are the most widely used. Technology types available include thermal based bolometers, thermocouple or thermopile, and pyrometer or pyroelectric, and optical pyrometers. There are several commercially available infrared pyrometers especially designed for flame temperature measurement, with several temperatures (from 200 °C to 3000 °C) and emissive ranges. Recently developed methods for flame temperature measurement include laser techniques (at present, the most successful method is CARS - coherent anti-Stokes Raman spectroscopy); photothermal refraction spectroscopy; thermographic phosphor and multi-wavelength emission absorption spectroscopy.

2.3.4 Task 3.4: NO_x abatement technology

Abatement technologies are divided into two categories, primary techniques (aiming reduction of NO_x generation) and secondary techniques (aiming reduction of NO_x emissions). Primary techniques are mainly combustion controls that reduce the level of NO_x emissions by altering or modifying the firing conditions under which combustion is achieved. Available techniques include combustion tempering, flue-gas recirculation, flameless oxidation, flame stabilizing, fuel balancing, low excess air, low NO_x burners, off-stoichiometric (or staged) combustion, reburning, reduced air preheat and ultra-low NO_x fuels.

Each of these combustion control technologies have one or more of three primary objectives: lower the flame temperature; create a fuel rich condition at the maximum flame temperature; or lower the residence time under which oxidizing conditions exist. The efficiency of the combustion process and CO emissions are often affected by the implementation of these techniques. In general, primary techniques are the lowest cost approach for obtaining an initial reduction in the uncontrolled NO_x emissions on any stationary furnace.

Secondary techniques are end-of-pipe or post-combustion controls that reduce the level of NO_x emissions. The most popular are selective catalytic reduction (SCR) and selective non-catalytic reduction (SNCR). These technologies convert the NO_x formed during combustion to nitrogen gas. The chemical reactions required to convert the NO_x to N₂ are applied downstream of the combustion zone.

These techniques introduce a reagent into the flue gas stream to selectively react with the NO_x. The reaction may be completed either with or without the use of a catalyst depending on the applied technology. A new technique for NO_x reduction from flue gases is iron filing reduction, following complex adsorption in iron-ethylenediaminetetraacetic acid aqueous solution. With the concept of desulfuration first and denitrification next, this technique has been recently studied at a laboratorial scale using simulated flue gases in a bubble column. Investigations are in progress for other emerging technologies, already starting to be commercially available, such as plasma assisted catalytic reduction, ozone oxidation and adsorption.

Table 41 summarizes the typical NO_x reduction levels reported for several techniques with some selected references from the literature review [55-63]. A complete description of available NO_x abatement technologies was compiled in a document presented in a separately [64].

Table 41. NOx reduction for different abatement techniques [64].

Abatement technique	% NOx reduction (average range)
Low Excess Air	5-15
Reburning	30-60
Induced Flue Gas Recirculation	30-40
Forced Flue Gas Recirculation	40-50
Low NOx Burner (oil & gas)	40-60
LNB/FGR combination	55-65
Close coupled Over Fire Air	30-50
Techniques (continued):	NOx reduction:
Separated Over Fire Air	40-60
Combustion tempering	20-25
Burners Out Of Service	10-15
Fuel Biasing	10-20
Ultra-Low NOx Fuels	Up to 70
SNCR	45-70
SCR	75-95
Iron Filings Reduction	> 90 (laboratorial scale)
Plasma Catalytic Reduction	Up to 94
High temperature reduction	Up to 60 (see WP5)
BioDeNOx	80 (laboratorial scale)

2.4 WP 4 - NOx in oxy-fuel combustion

Two series of trials were made, in the first case an investigation of the Walking Beam Furnace at MEFOS which were done for two conditions, namely, air combustion and full Oxy-combustion firing propane. The second series of investigations were performed at the BFI in Germany where the burner characteristics were investigated with Coke Oven gas and Natural gas as fuel in a test facility for burner evaluation. During the oxygen combustion trials at MEFOS, the gas analysis showed that the NOx emissions and the gas composition in the furnace varied when the furnace doors were opened as a function of the air infiltration. The oxygen case also revealed improved heat transfer characteristics due to the changed furnace atmosphere, which was shown by the increased slab surface temperatures during the oxygen case run. The oxy-combustion trials gave very low NOx emissions at both MEFOS and BFI as reported in previous project reports and at conferences [65,66].

Conversion of MEFOS WBF

The walking beam furnace at MEFOS was converted to oxy-combustion combustion by Air Liquide. A new fuel and oxygen control skid was prepared by Air Liquide, as described in the semester reports. Each regulation zone was independent of the others; with their own thermocouple measurements. The operator adjusts the set point power and an oxygen/propane ratio around stoichiometry with the flow rates for the oxy-combustion trial given in Table 42. The microprocessor totalized the propane and oxygen consumptions for each zone to allow comparison with air cases. During the reference trials a fully automated control and data logging system was used in order to monitor and control the combustion process. During the oxy-combustion trials the furnace was operated with a pressure of 1.2 mmH₂O, compared to a normal operating pressure of 0.5 mmH₂O to help avoid air infiltration.

Table 42. Conditions for the different zones of the WBF.

	Zone 1	Zone 2	Zone 3	Zone 4
Temperature set points	-	1040	1220	1250
Oxygen concentration	-	3,0%	0,1%	0,1%
Oxy-burner zone power		442 kw	357 kw	208 kw
Light fuel oil zone power		402 kw	508 kw	385 kw

During the WBF test series two different kinds of burners were used. In the reference trials, six standard NOx light fuel oil burners type 5424-6/T3-25 from North American were used. The oil burners are part of the original equipment for the WBF when it was commissioned in 1980. The WBF has a Turbomant 48 recuperator for preheating the air. During the oxy-combustion test a modified ALROLL burner was used. In a later series of trials, which was not within the scope of the current research programme the fuel oil air burners were converted to propane air burners for a more straight comparison of the NOx emissions data. In order to reach the same input power only five oxy-combustion burners were used during the oxygen test cases in comparison to 6 burners used for the air trials. In order to reach the target of very low NOx emissions during oxygen combustion a redesigned burner was used during the oxygen combustion tests. The modified ALROLL oxy-fuel burner was called the ALROLL-S-200. The ALROLL-S burner utilizes a combination of staged and separated jets injection of the fuel and the oxygen and has a large flexibility and can be used with several types of gaseous and liquid fuels.

In order to investigate the heat up curves, a slab was equipped with five thermocouples in order to monitor the temperature distribution in the slab during its passage through the furnace. During the trials the walking beam furnace was operated under a relatively long time in order to reach temperature equilibrium. Before the test slab equipped with thermocouples were charged in to the walking beam furnace, the walking beam furnaces was filled with slabs in order to stabilize and to reach steady state conditions. Furthermore, after the test slab had been charged, the charging of slabs continued until the test finished in order to simulate stable operating conditions.

The scale losses were monitored as well for three different steel grades. The different mini-slabs were provided by Rautaruukki to MEFOS, for the composition see Table 43. Before charging the slabs, the weight was measured. The slabs were charged into the furnace during stable operation and heated during oxy- and air combustion respectively. After the heat up the slabs were discharged and descaled. During the experiments the scale losses were recorded for the three different types of test slabs. The values of the different scale losses were very small, and it should furthermore be noticed that during the air-fuel trials the slabs were reused and the formed scale was more adhesive and more difficult to remove, thus indicating a lower scale formation. The mass loss during the oxy-combustion trial was one per cent which is comparable with usual air combustion scale losses (note that adhesive scale reduced the apparent scale loss for air combustion given in Table 4.3).

Table 43. Composition of test slabs.

Alloy /	C	Si	Mn	P	S	Al	Nb	V	Cu	Cr	Ni	Mo
90459A/1	.02	.01	.17	.007	.008	.048	.002	.003	.044	.03	.05	.006
90459A/2	.15	.45	1.52	.009	.008	.032	.019	.004	.039	.04	.04	.004
90459A/3	.00	.03	.15	.011	.003	.046	.002	.010	.012	.03	.04	.003

Table 44. Scale losses during the experiment.

Mini-slab	Oxy-combustion trial				Air-fuel trial			
	Weight, in	Weight, out	Scale loss (kg)	Scale loss %	Weight, in	Weight, out	Scale loss (kg)	Scale loss %
Rauta 1	865,6	855,6	10,0	1,16	856,1	850,1	5,925	0,69
Rauta 2	860,1	851,4	8,7	1,01	851,6	849,1	2,5	0,29
Rauta 3	831,2	822,5	8,7	1,04	822,6	818,1	4,5	0,55

The test campaign was finished successfully and the recorded NOx emissions during oxy-combustion were at very low levels compared to the levels when using regular air combustion. The emissions were in the range 10-20 mg/MJ during full operation with 6 % of oxygen in the flue gases, even during slab charging and discharging, when significant air leakage occurs. Figure 99 and Figure 100 gives the temperature distribution and the reheating curves for the test slabs equipped with thermocouple. The data shows that the slab reached a uniform temperature distribution after three hour and twenty minutes when it was discharged. By a closer study of the slab heating curves, it can be concluded that with the implementation of oxy-combustion one obtains a time benefit of 14 minutes. This shorter reheating time implies a productivity increase of 6.5 %, or a increase in the reheating capacity from 4.25 t/h to 4.53 t/h for the actual walking beam furnace at MEFOS.

Figure 101 combines both the NOx measurement and the entire slab reheating period. The data also show the tuning process of the burners in order to reach stable and optimized conditions. Furthermore, the figure also shows the temperatures of the flue gas in the sampling point and the temperature curve of the test slab during its travel through the furnace.

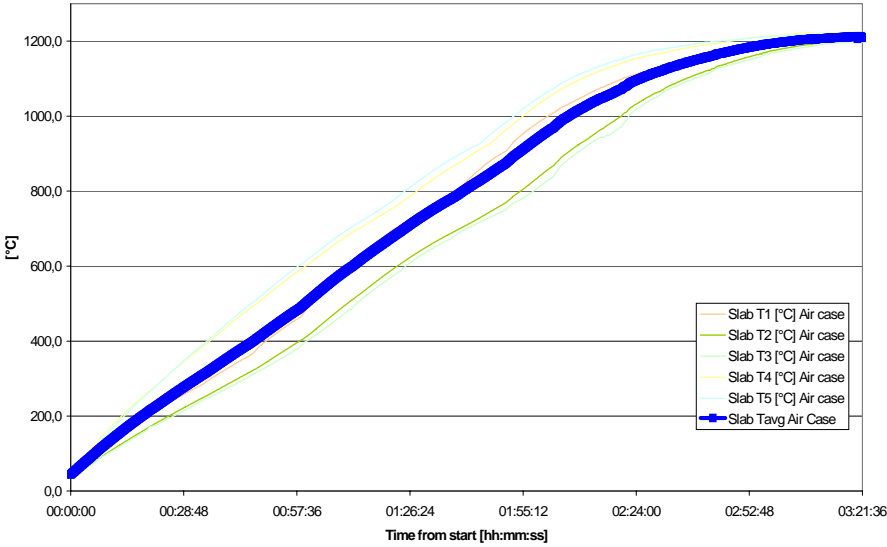


Figure 99. Temperature distribution within test slab during heat up process with air burners.

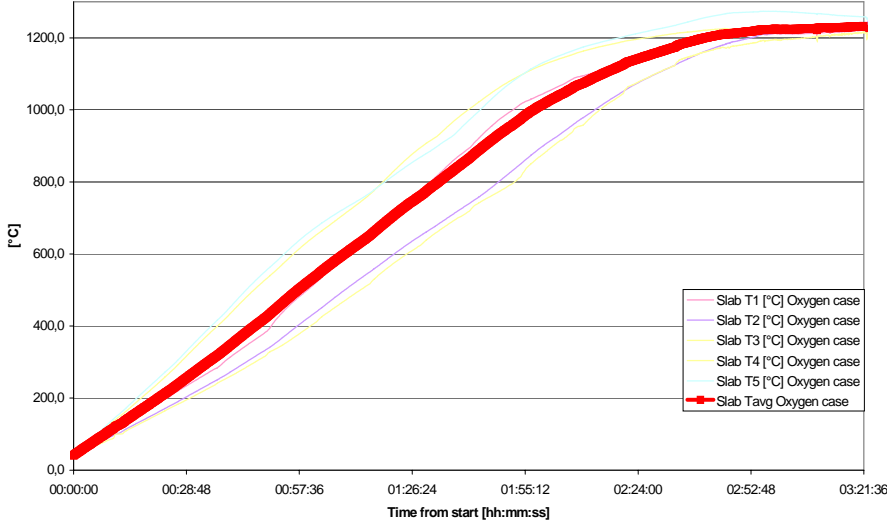


Figure 100. Temperature distribution within test slab during heat up process with oxygen burners.

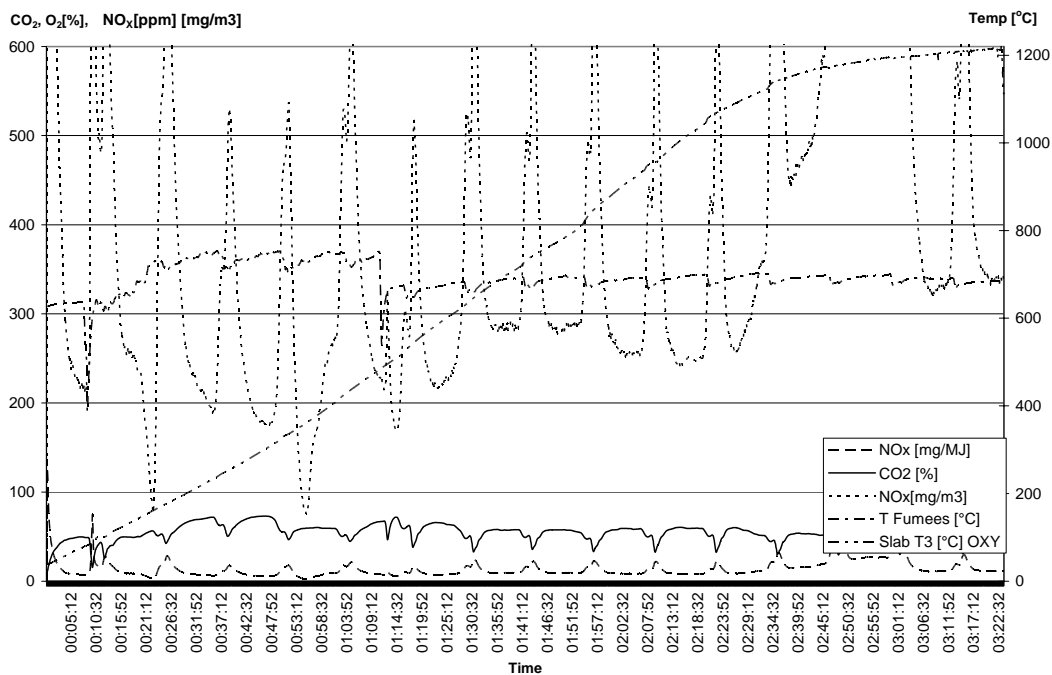


Figure 101. Results from flue gas sampling and flue gas temperature during entire slab heat up process.

A comparison of the NOx and O₂ levels for the air combustion and the oxygen combustion respectively can be seen in the results (see Figure 102 with the scale mg/MJ and Figure 103 for the mg/m³ unit). During the sampling period, the gas measurement probe was mounted in the flue gas channel. The results indicate a significantly higher NOx emission level during the air combustion case compared to the oxygen combustion case. During the air case an average of 83 mg/MJ was measured as compared to 12 mg/MJ during the oxygen case. Figure 104 shows a detailed analysis during a shorter time period of the flue gas sampling. The graphs reveal the sensitivity of the oxyburners for air infiltration. The significant changes of the concentrations of CO₂, O₂ and NOx during the measurement period are related to the opening and closing of the furnace ports for charging and discharging of slabs. An immediate effect can be distinguished on the concentration graphs. In this figure the CO₂, O₂ and the NOx are presented. The data shows clearly the influence of the charge and discharge of slabs, thus the opening and closing of the furnace doors, with the associated air leakage in to the furnace. During stable operation the NOx levels reached 9 mg/MJ of fuel input with the furnace doors closed. During the sampling period the oxygen concentration in the flue gases was 6 % and the CO₂ concentration on an average 58 %.

The maximum temperature difference between the thermocouples mounted in the test slab during the reheating process are presented in Figure 105. The monitored temperatures shows a maximum temperature difference of 290 °C between the surface- and the centre mounted thermocouples for the slab during the oxygen combustion, and a maximum difference of 240 °C during the reheating with air burners. This result shows gives a clear indication of the influence of the changed atmosphere due to the changed combustion conditions when using pure oxygen as oxidizer. The changed atmosphere, with an increased amount of diatomic molecules results in a significantly increased heat transfer to the surface, thus a higher surface temperature of the slab. This offers the possibility to reduce the burner power towards the end of the reheating cycle when slab temperature is equalizing in order to further reduce energy consumption of the walking beam furnace.

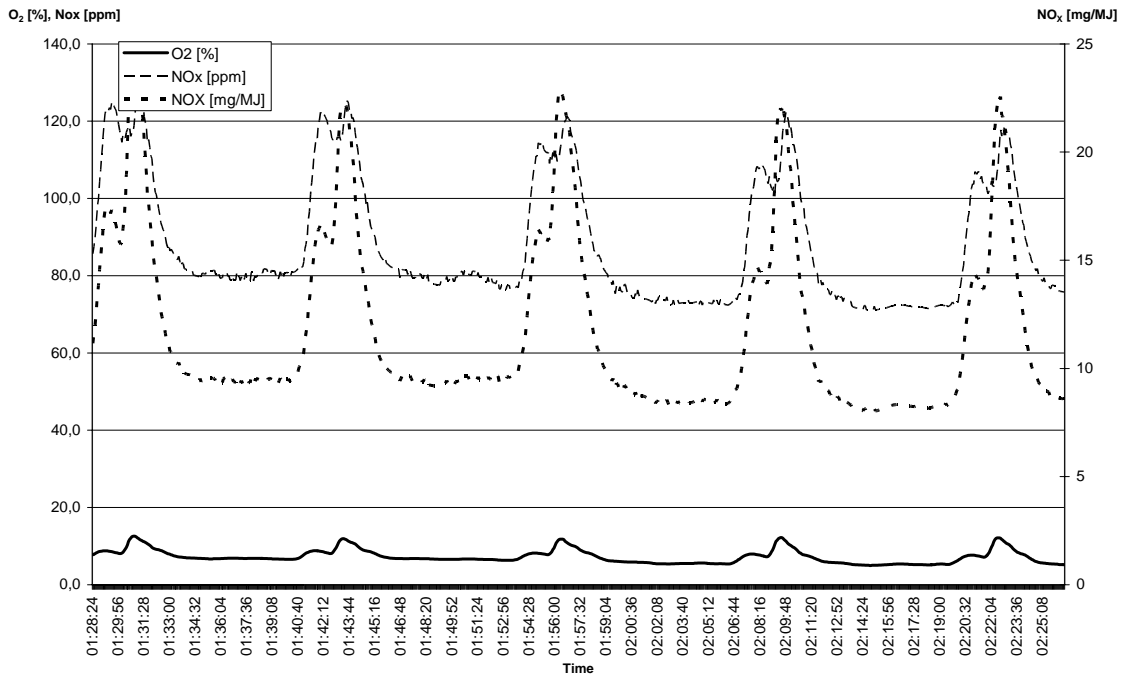


Figure 102. NO_x emissions levels and O₂ levels in flue gas duct during oxygen combustion. [mg/MJ].

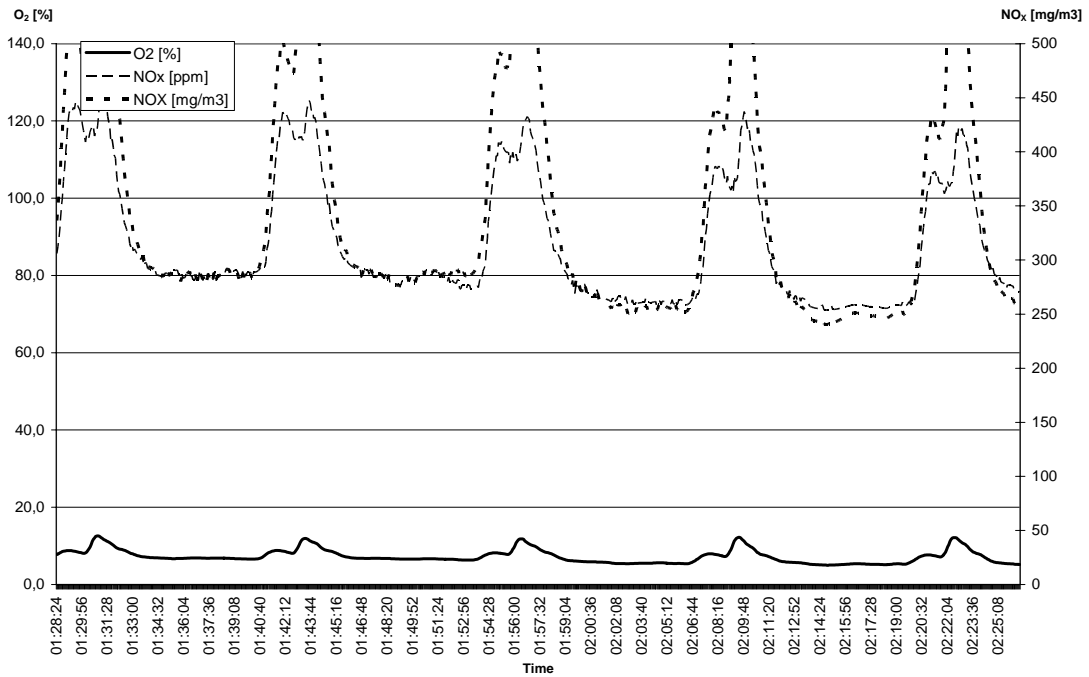


Figure 103. NO_x emissions levels and O₂ levels in flue gas duct during air combustion [mg/m³].

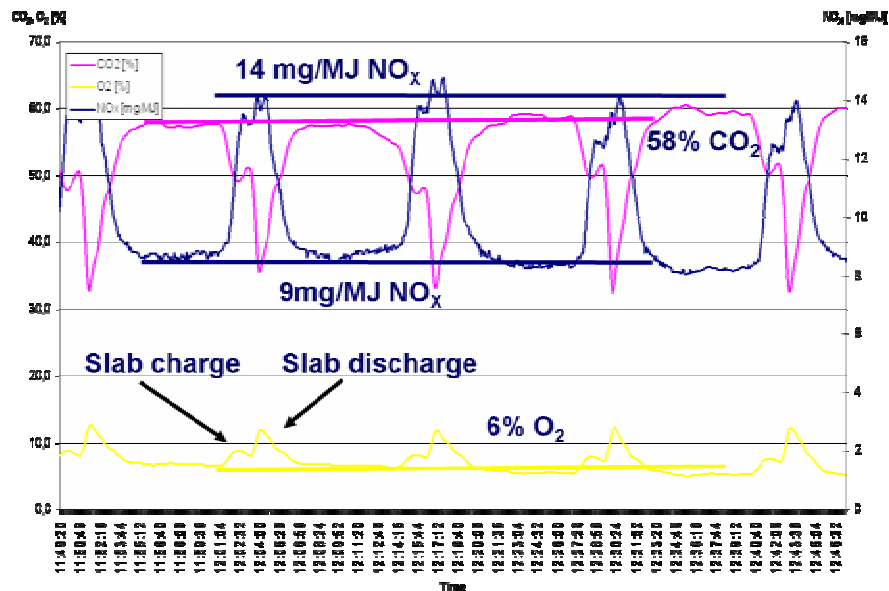


Figure 104. Detail of flue gas sampling during oxygen case.

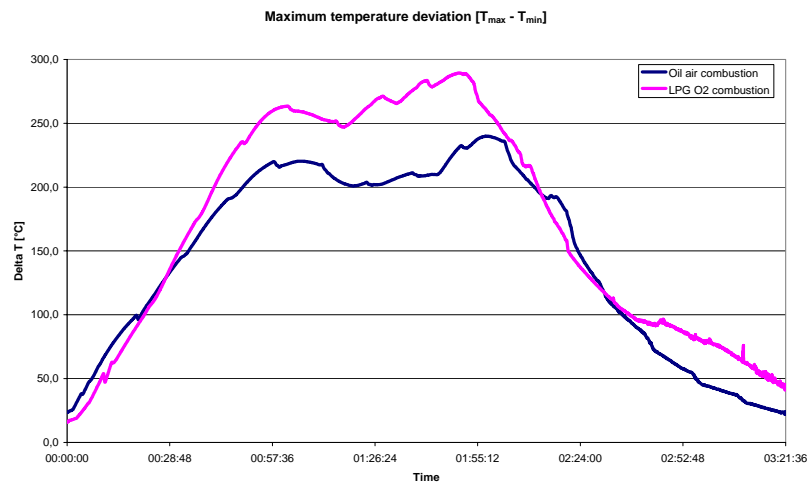


Figure 105. Maximum measured temperature difference in test slab during the two different runs.

Additional investigations with conversion of MEFOS WBF

The previous set of trials was a revamping where the fuel for the air combustion was light fuel oil, but for the oxy-combustion propane and oxygen was used. In order to get a correct comparison of the effect on the NO_x emissions, the energy efficiency and the productivity with a changed heating method from air combustion to oxy-combustion. The objectives of the supplementary test campaign was to convert the walking beam furnace at MEFOS into full oxygen combustion and to demonstrate reduced NO_x emissions during full operation of the furnace compared to operation of the furnace with air burners with the same fuel used throughout all the trials.

The power distribution for the different zones can be seen in Figure 106. Two different kinds of oxy-combustion trials were performed in order to either investigate the possible reduction in the energy consumption when switching to oxy-combustion, or investigation of the maximum possible productivity that was achievable when switching to oxy-combustion. Throughout the experiments the NO_x emissions were monitored, besides the follow-up on fuel consumption, air and oxygen flow rates, temperatures in the furnace, furnace pressure, temperature of the recuperator and the flue gas composition. During the test series two different kinds of burners were used. In the reference trials, standard air-propane burners were utilized and during the oxy-combustion test a modified ALROLL-S burner was used. As described above, the air propane burners were controlled by the SAFMATIC PLC. The air propane burner was a standard air burner, the combustion air was heated in a recuperator to 400 °C.

The ALROLL-S burner utilizes a combination of staged and separated jets injection of the fuel and the oxygen to give low NO_x, and it has a large flexibility and can be used with several types of gaseous and liquid fuels (see WP2 modelling). The WB furnace was during the trials run with an oxygen concentration measured in the three different reheating zones. The furnace temperature was also controlled in the three different zones. The burner power in the three different reheating zones was controlled accordingly to a set zone temperature. The operating conditions with data collected from the furnace monitoring system are presented in Table 45. For the oxygen-propane case the aim was to duplicate the zone temperatures and oxygen concentration as close as possible for the air-propane case in order to measure the reduction of the energy consumption after the switch to oxy-combustion. In the second oxygen-propane case, the intention was to achieve the maximum throughput of load in the furnace with maintained energy consumption.

Table 45. Compilation of actual operating conditions.

Air/Propane			Billet temperature		
	T Wall	T Roof	O2	T centre	T top
ZONE 1	1102	1099	1,5	1226	1245
ZONE 2	1253	1255	0,31		
ZONE 3	1243	1256	0,72		

Oxygen/Propane			Billet temperature		
	T Wall	T Roof	O2	T centre	T top
ZONE 1	1097	1153	1,2	1266	1270
ZONE 2	1252	1265	1,1		
ZONE 3	1256	1284	1,5		

Oxygen/Propane 1,44 increase pull rate			Billet temperature		
	T Wall	T Roof	O2	T centre	T top
ZONE 1	1084	1115	0,96	1230	
ZONE 2	1265	1278	0,22		
ZONE 3	1256	1283	0,74		

In order to monitor the temperature distribution in the billets during the reheating process thermocouples were mounted at the surface and in the centre of the test billets. With help of these thermocouples it is possible to determine the temperature distribution inside the billet in order to certify that there are no drawbacks experienced when changing from air to oxy-combustion. The measurements were repeated for all three experimental cases and the results from the trials are shown in Figure 107. It can be seen that with the oxy-combustion case 1, the heating curve is identical with the heating curve for the air case. During the oxy-combustion case 2, the heating curve shows a faster heat up, which is anticipated since the pull rate was significantly higher. The billets travelled through the furnace for 130 minutes during the oxy case 2, instead of 180 minutes for the air case and the oxy case 1. Although it can be concluded from the graphs, that the billets reached the target temperature during the oxy-combustion case 2, and the equilibrium was reached. Unfortunately there was a thermocouple failure during the second oxy case, as the thermocouple got stuck inside the WBF and consequently broke. Although the final centre temperature was measured with a replacement thermocouple immediately after the discharge of the slab.

A comparison of the NO_x and O₂ levels for the air combustion and the oxygen combustion respectively can be seen in Figures 108-110. During the sampling period, the gas measurement probe was mounted in the flue gas channel. The results indicate a significantly higher NO_x emission level during the air combustion case compared to the oxygen combustion cases. During the air case an average of 80 mg/MJ was measured as compared to 8 mg/MJ during the oxygen case. When comparing the three cases, it can clearly be seen that the oxy-burner is more sensitive of air infiltration than the air burners. The large fluctuations in the NO_x levels when using the oxy-burners comes from the infiltration of air when the discharge or charge doors are opened. The difference between oxy case 1 and oxy case 2 comes from the burner power utilized in the different cases. During the oxy case 1 the burners were running at low power and consequently were more sensitive to the air infiltration. Furthermore, the CO₂

levels during the oxy-combustion cases approached 75-80 % which is very important in order to reduce the NOx formation. The significant changes of the concentrations of CO2, O2 and NOx during the measurement period are related to the opening and closing of the furnace ports for charging and discharging of slabs. An immediate effect can be distinguished on the concentration graphs.

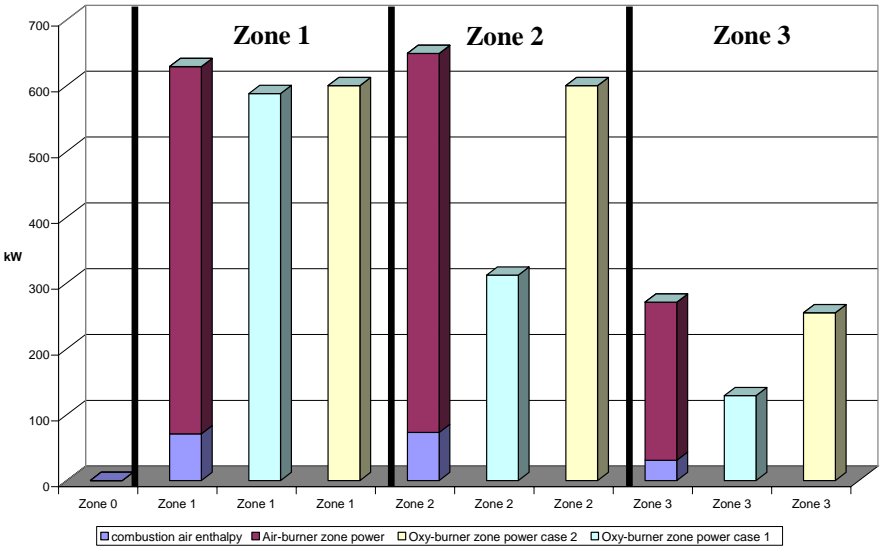


Figure 106. Power distribution in the different zones for the different burners.

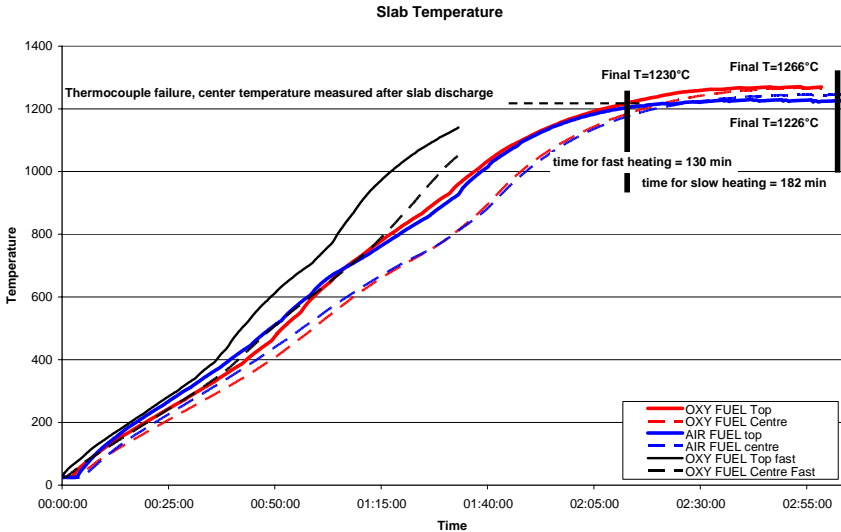


Figure 107. Temperature distribution within test slab during heat up process with air burners.

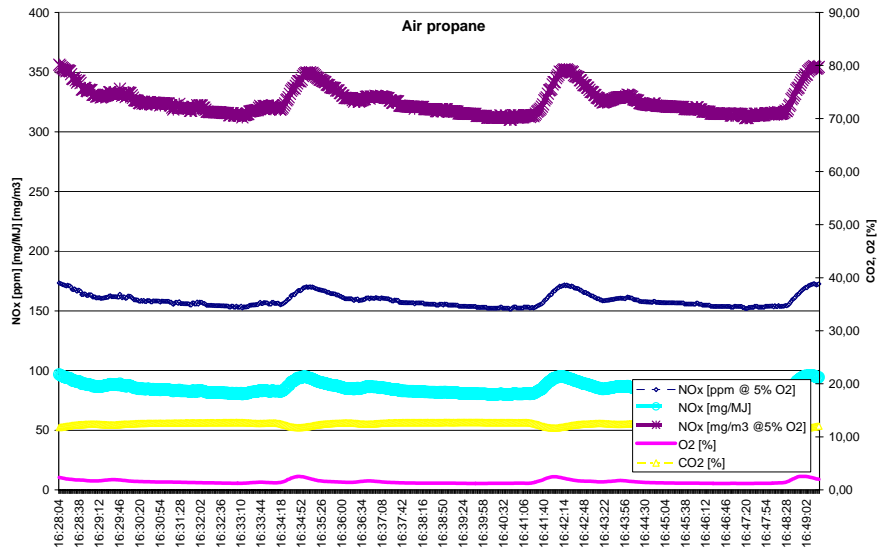


Figure 108. Flue gas composition for the air combustion case.

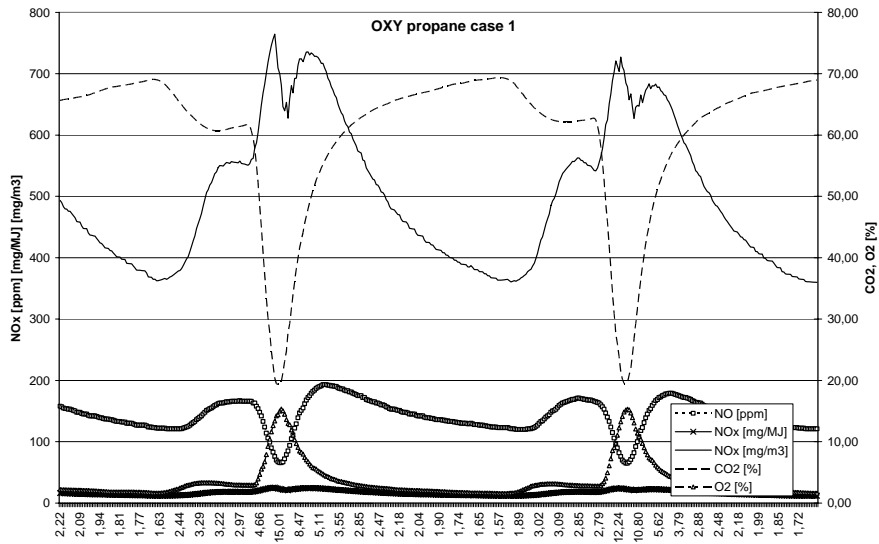


Figure 109. Flue gas composition for the oxy-combustion case 1.

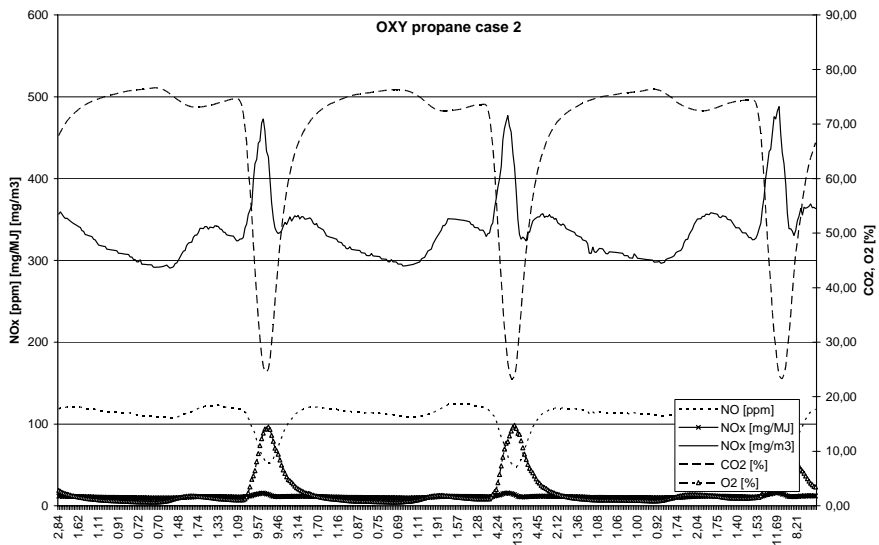


Figure 110. Flue gas composition for the oxy-combustion case 1.

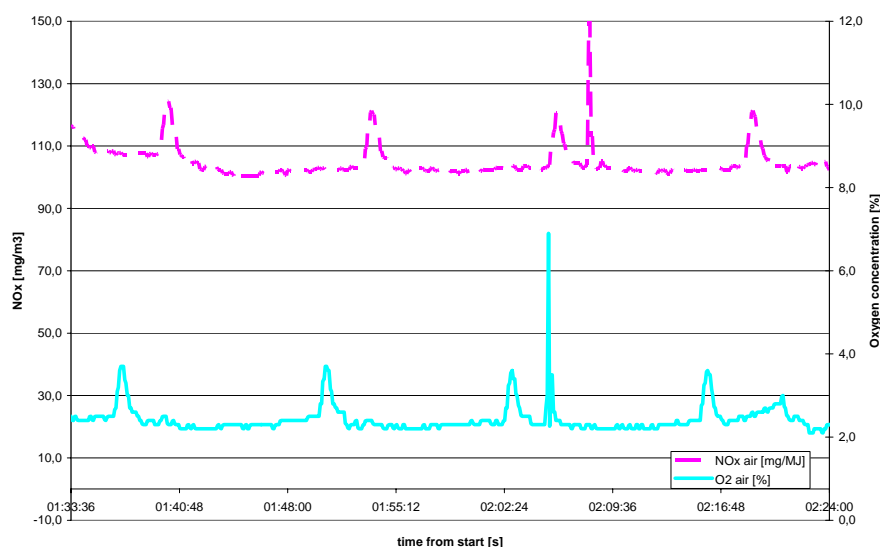


Figure 111. NO+ emissions levels and O2 levels in flue gas duct during air combustion [mg/MJ].

NOx in oxy-fuel combustion, measurement at BFI

The second oxy-combustion test campaign was performed at BFI. The furnace has a thermal capacity of 15 MW. In order to closely control the furnace temperature the furnace load can be controlled by insertion of water cooled probes. Two fuels were tested with an ALROLL-S burner from Air Liquide, natural gas and coke oven gas (COG). The furnace inner dimensions are 1 m x 1 m x 8 m (h x w x l). Furthermore, the furnace pressure was controlled by a damper mounted in the chimney of the furnace. In Figure 112 and Figure 113 some photos of the BFI test stand can be seen, showing the furnace with a left- and right-hand side views as well as the burner. In order to measure the NOx emissions for different fuels, both natural gas and COG were used during the experiments. The burner performance was monitored for the different burner loads of 100 % and 80 %. Furthermore, two different furnace temperatures were used, 1150 and 1250 °C in order to study the influence of the furnace temperature on the NOx. The excess oxygen was also changed during the experiments in order to follow the influence of oxygen. The experimental configurations and the flow rates of the fuel and the oxygen are shown in Table 46. The CO2 level was 60 % during the NG experiments and 55 % during the COG experiments which indicates that there was some air leakage in the test furnace.

Table 46. Experimental configurations and flow rates of fuel and oxygen at BFI.

	Burner Load		Flow rate	Oxygen		Lamda	
				1,00	1,05	1,10	1,15
	%	kW	m ³ /h (N)				
Natural gas	100	500	45,00	97,25	102,11	106,97	111,83
	80	400	36,92	79,77	83,76	87,75	91,74
Coke Oven Gas	100	500	110,89	90,61	95,14	99,67	104,20
	80	400	88,71	72,48	76,11	79,73	83,36

The diagnostic equipment included furnace temperature, fuel and oxygen flow rates and pressure measurements of the furnace in order to monitor the combustion. Furthermore gas sampling analysis with respect to NOx, CO, O2, and CO2 levels in the chimney were performed. The major components in the natural gas were 86.9 % methane, 8.4 % ethane, 2.0 % propane 1.3 % carbon dioxide and 1 % nitrogen with a heating value of 10.84 kWh/m³, while for the coke oven gas the major components were 63.4 % hydrogen, 20.4 % methane, 7.3 % carbon monoxide, 5.2 % nitrogen and 1.7 % carbon dioxide with a heating value of 4.51 kWh/m³.

The test campaign was finished successfully and the NOx emissions recorded during oxygen combustion were at very low levels compared to the levels when using regular air combustion. The results from the measurements are presented graphically in Figure 114 to Figure 121. Figure 114 shows

the NO_x data in mg/MJ for natural gas with a burner load of 100 %. Figure 115 shows the NO_x data in mg/m³ for natural gas with a burner load of 100 %. The NO_x emissions were measured for various oxygen concentrations in the flue gases and furnace temperatures. Figure 116 shows the NO_x data in mg/MJ for natural gas with a burner load of 80 %. Figure 117 shows the NO_x data in mg/m³ for natural gas with a burner load of 80 %. The NO_x levels in both cases are under 10 mg/MJ for all the cases examined during the natural gas trials. Figure 118 and Figure 120 shows the NO_x data in mg/MJ for coke oven gas with burner loads of 100 % and 80 % respectively. Figure 119 and Figure 121 shows the NO_x data in mg/m³ for coke oven gas with burner loads of 100 % and 80 % respectively. The NO_x emissions were measured for various oxygen concentrations in the flue gases and furnace temperatures. The NO_x levels in both cases are under 20 mg/MJ for all the examined cases during the coke oven gas trial. The higher NO_x emissions with COG versus natural gas were anticipated due to the nitrogen content of the fuel. The NO_x levels increased with increased air infiltration, as expected.



Figure 112. A photo of the oxy-burner mounted in the pilot furnace at BFI.



Figure 113. The pilot furnace at BFI.

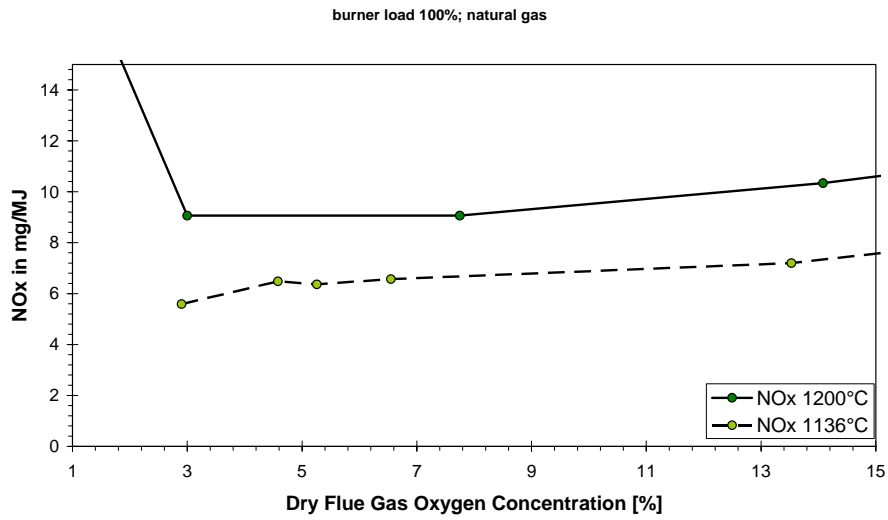


Figure 114. NOx in mg/MJ for Natural gas, 100 % burner load.

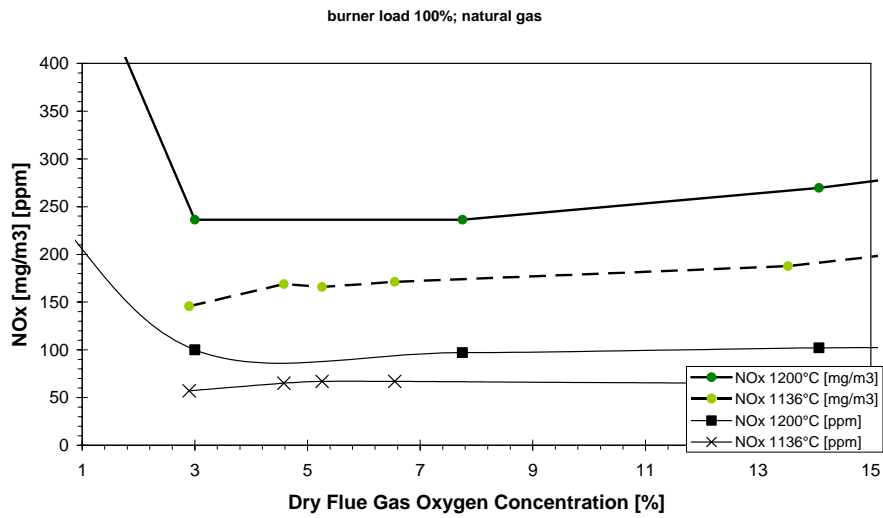


Figure 115. NOx in mg/m³ for Natural gas, 100 % burner load.

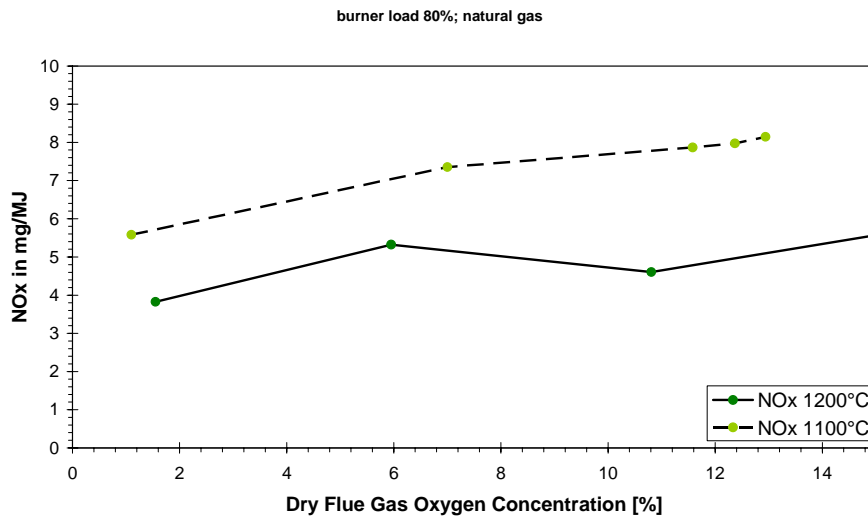


Figure 116. NOx in mg/MJ for Natural gas, 80 % burner load.

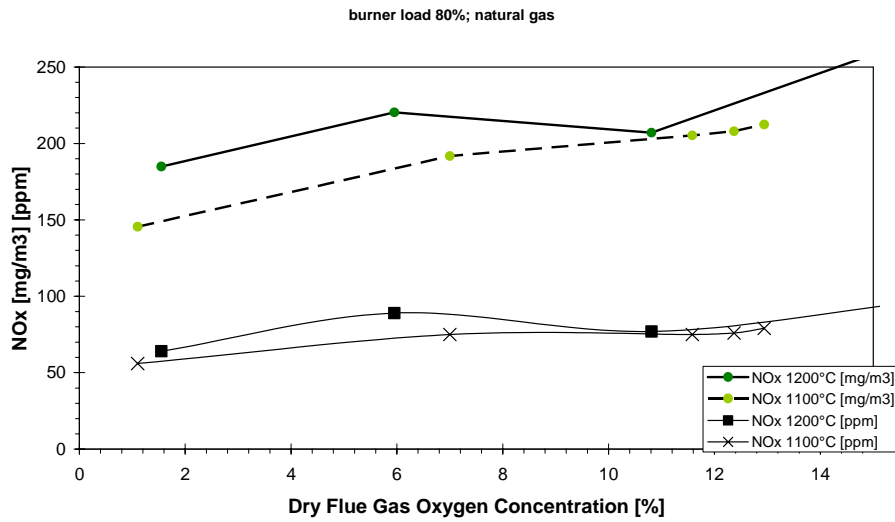


Figure 117. NOx in mg/m³ for Natural gas, 80 % burner load.

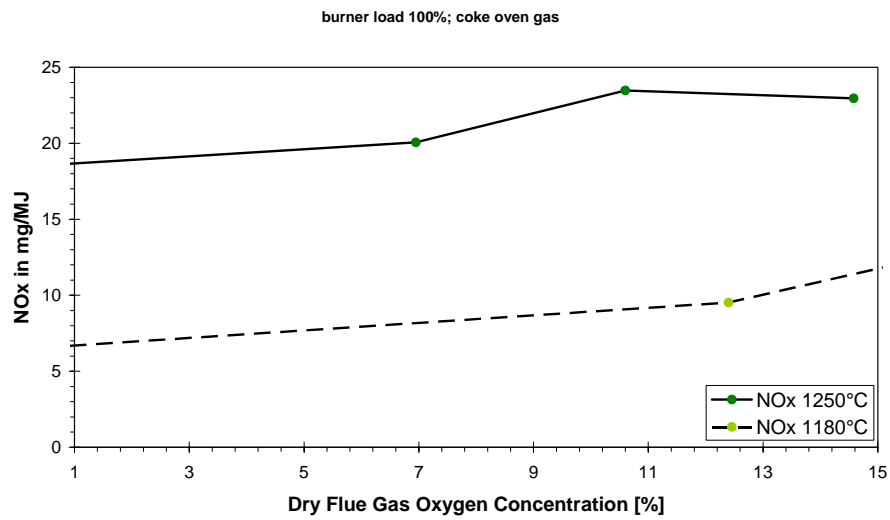


Figure 118. NOx in mg/MJ for Coke Oven gas, 100 % burner load.

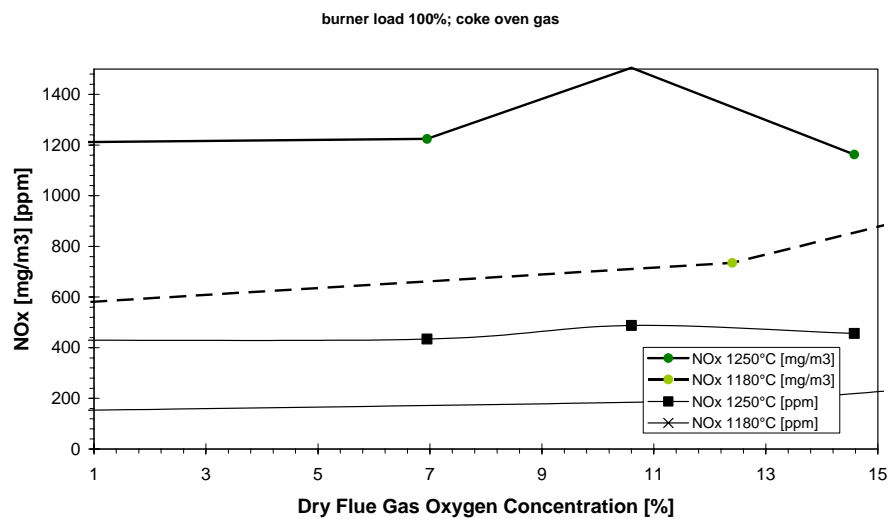


Figure 119. NOx in mg/m³ for Coke Oven gas, 100 % burner load.

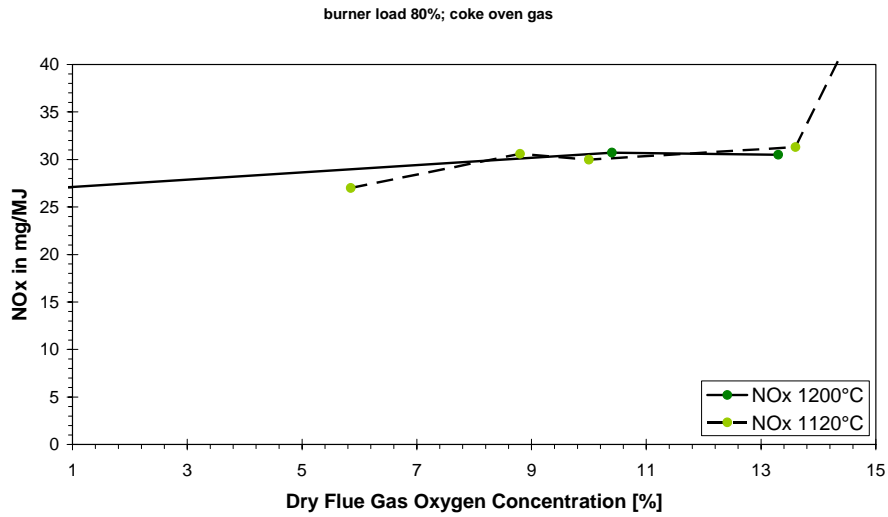


Figure 120. NOx in mg/MJ for Coke Oven gas, 80 % burner load.

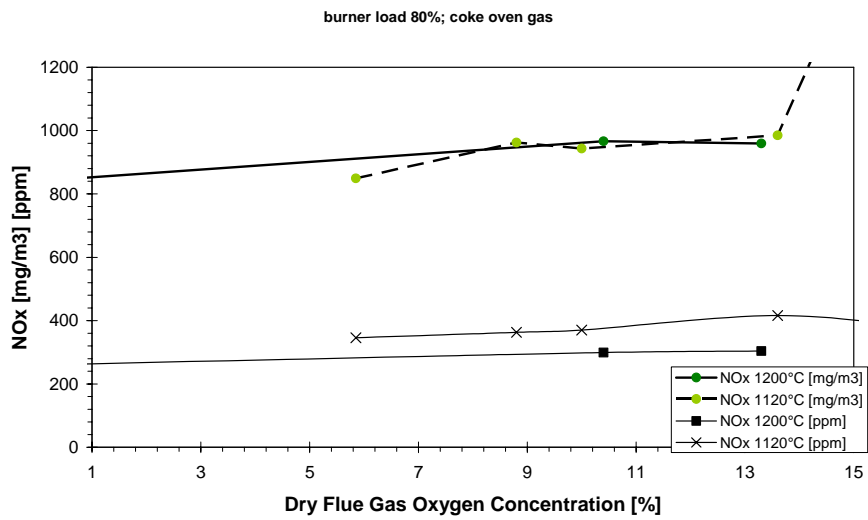


Figure 121. NOx in mg/m³ for Coke Oven gas, 80 % burner load.

2.5 WP 5 - Minimising NO_x emissions by high temperature reduction /HTR

The HTR procedure is based on the effect of NO reduction through the presence of radicals with stoichiometric combustion (air and fuel staging) known from coal combustion in power plants. These radicals have a very high nitrogen oxide reduction potential. The possibility of a transfer and the effectiveness of this effect for reheating furnaces should be examined. Ammonia-radicals should be used for the high temperature reduction instead of fuels by using the fuel staged combustion procedure. So for high temperature reduction the kind of additives - ammonia gas, ammonia aqueous solution or urea solution - is similar to the well known SNCR-process. The stoichiometric boundary condition is similar to the fuel staged process with the advantage of an extensive independence of any small temperature windows. Based on the procedure of the staged air combustion, an additive for the formation of radicals were injected in a purposeful manner into the understoichiometric combustion zone. The complete post combustion of the flue gas is guaranteed by the supply of secondary air. Excess radicals are also oxidized by the secondary air. Therefore, no secondary emissions result in form of ammonia slip. The aim of the investigations is to optimize the reduction procedure and to show the possible methods to install the technique with low capital investment and low emission values. The reduction of the capital investment is achieved by the minimization of the required volume of the reaction chamber. This can be done by having the NO_x-reduction reaction and the post combustion reaction in the available flue pipes of a normal reheating furnace. Figure 122 shows this method of application of HTR for a reheating furnace.

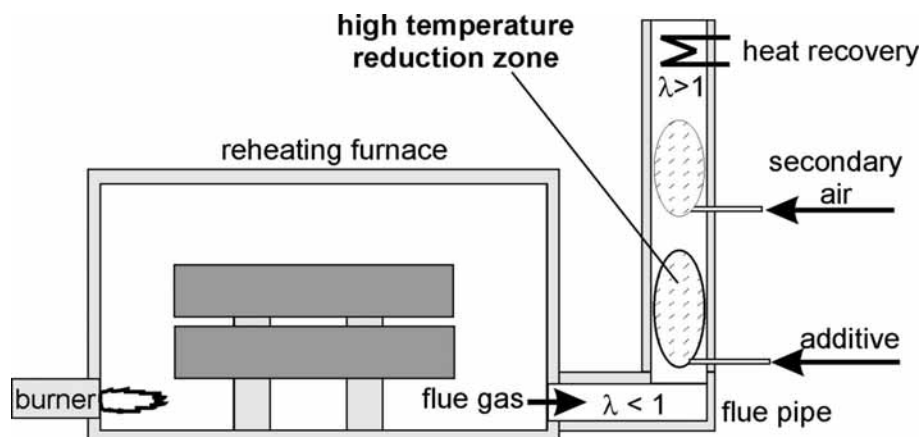


Figure 122. Sketch of the method for application of the high temperature reduction procedure for a reheating furnace.

2.5.1 Task 5.1 Investigation of the parameters of HTR

An example for the possible application of the high temperature reduction for a reheating furnace used data from a 120 t forging furnace with a power input of 2.8 MW and 4 flue pipes (each diameter: 0.5 m). The boundary conditions in one of these flue pipes was reproduced for the examination in the BFI-experimental combustion chamber. Figure 123 shows the experimental set-up with the flue pipe design made of ceramic plates. The flue gas is forced into the channel by means of a front blocking wall. A ceramic foam plate at the front of the flue pipe shall homogenize the flow at the entrance of the flue pipe. In order to minimize leakages, a second blocking at the end of the flue pipe was constructed. Important boundary conditions are described in Table 47 and special data for fluent calculations are given at the end of this report.

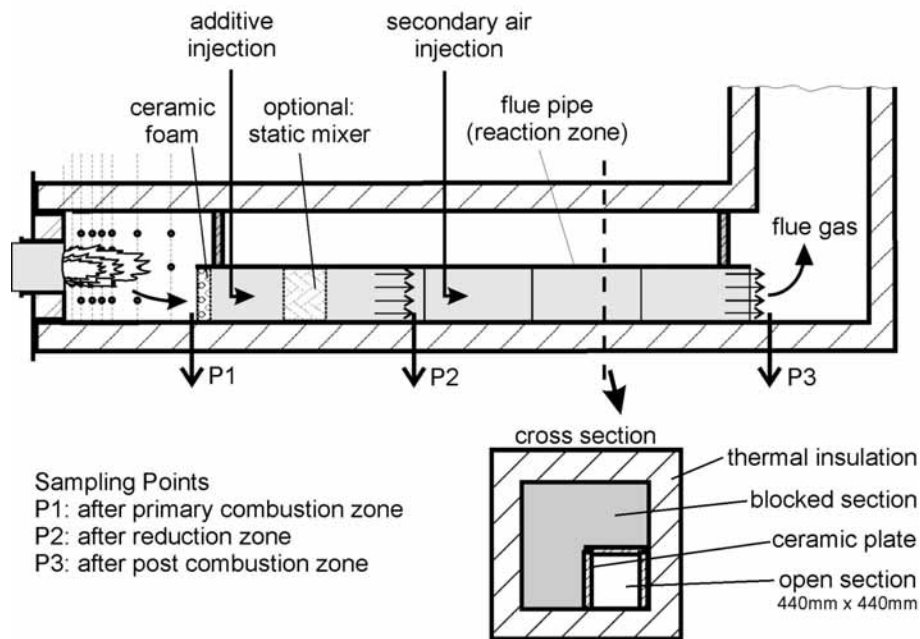


Figure 123. Experimental set-up with constructed flue pipe in the experimental combustion chamber and sampling points.

Table 47. Boundary conditions for the High temperature reduction experimental set-up.

Primary combustion zone	700 kW coke oven gas, 138 m ³ /h (STP) excess air coefficient 0.95 ... 1.02 cooled by cooling plates
flue pipe	square 0.44 m x 0.44 m = 0.19 m ²
HT reduction zone	flue gas mean velocity 5,8 m/s temperature 1000 ... 1200 °C
additives	ammonia gas, 70 ... 700 l/h (STP), additional nitrogen for high-pressure injection urea solution (liquid), injection with pneumatic atomizing nozzle (with nitrogen) 0.35 ... 3.5 l/h
Post combustion zone secondary air	30 ... 70 m ³ /h (STP) temperature 25 °C

Additive injection

Liquid additives must be evaporated in order to achieve an intense mixing and reactivity with nitrogen oxides in the flue gas flow. Therefore the vaporization time and the distance of the droplets are to be considered in the design of the process. The vaporization of a droplet can be separated into two phases. The temperature of the droplet increases during the very short first phase. On account of the small temperature of the droplet, in this phase the vaporization mass flow is neglectable. In the second phase the temperature of the droplets remains constant to a large extent. The vaporization can be described by the temporal constant decrease of the square of the droplet diameter. The vaporization time can be computed with the so-called law of drop vaporization [67].

$$-d(d^2)/dt = \text{constant} \quad (\text{Eq. 9})$$

with d: droplet diameter

On the basis of these fundamentals, the additive nozzle for the HTR procedure was chosen. For the injection of liquid additive BFI bought a lance with a gas atomizing system. In order to avoid an oxidation of the additive, nitrogen is used for the atomization. This system is suitable for a very small

volume flow and produces very small droplet diameters up to 85 micrometer. Figure 124 shows the droplet size distribution of the nozzle. Figure 125 shows the calculated results of the droplet vaporization in the flue gas flue pipe at 1200 °C. The largest drops evaporate completely after a flow path of 250 millimetre. Figures 126 and 127 show the gas atomizing nozzle for urea injection and the secondary air lance each with a principle of operation. Separate injection lances for the gaseous additive ammonia were produced by BFI. The dimensioning data of this lances are tabulated in Table 48.

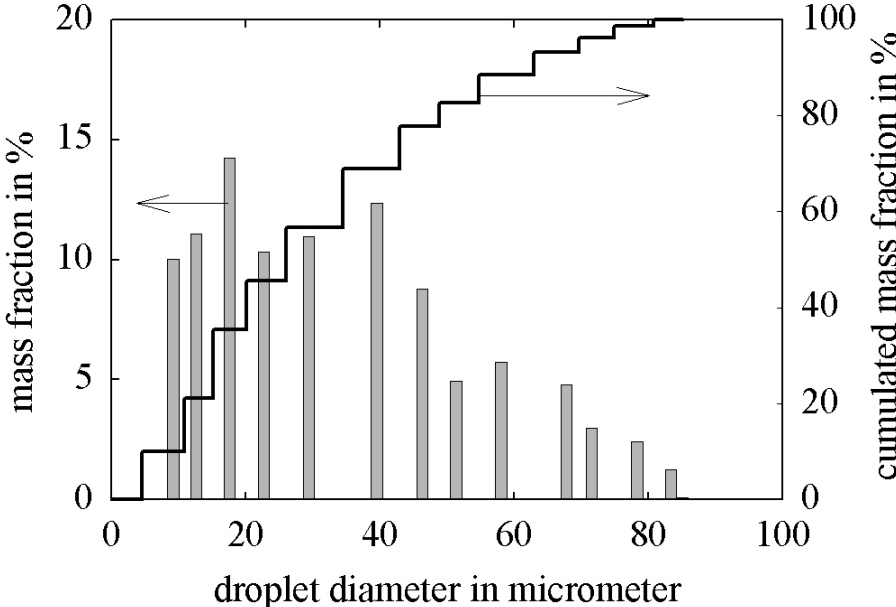


Figure 124. Distribution of the droplet size of the pressure air atomizing nozzle.

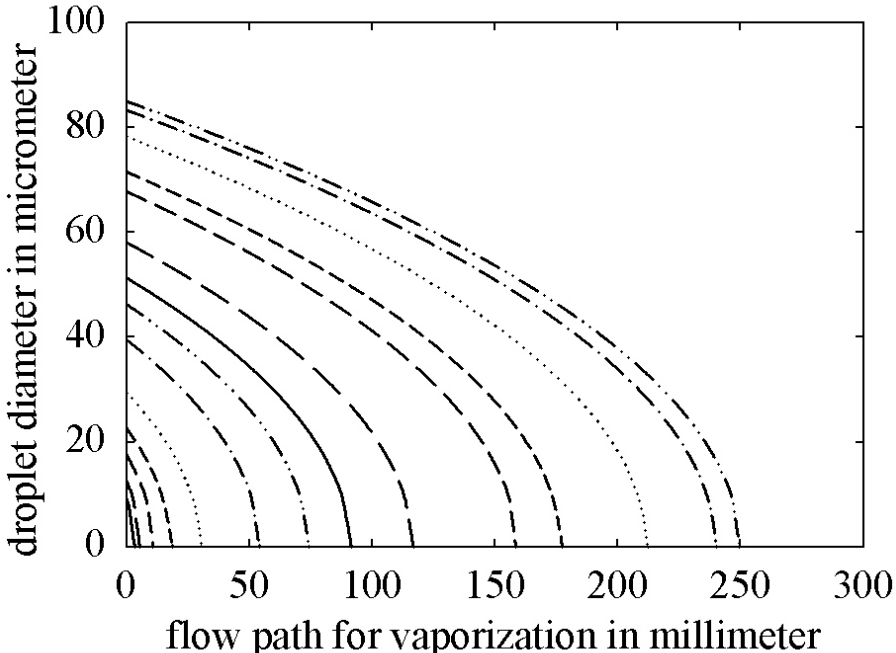


Figure 125. Calculated results of the droplet vaporization in the flue gas flue pipe at 1200 °C.

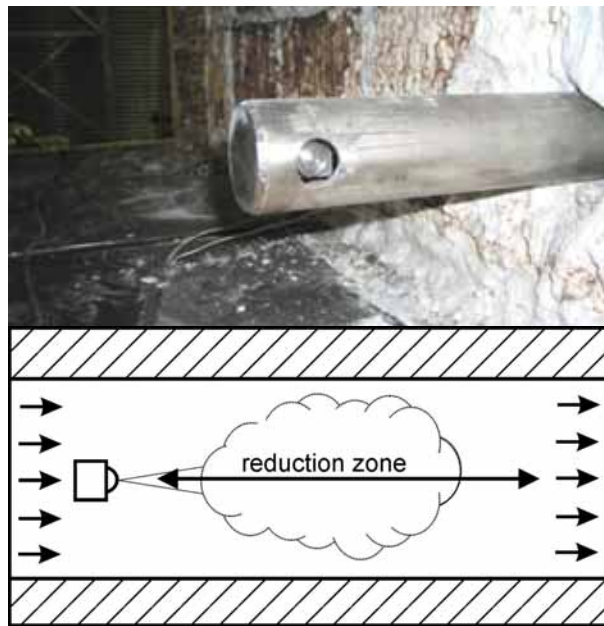


Figure 126a-b. Photo and principle of operation of gas-atomizing nozzle for urea injection.

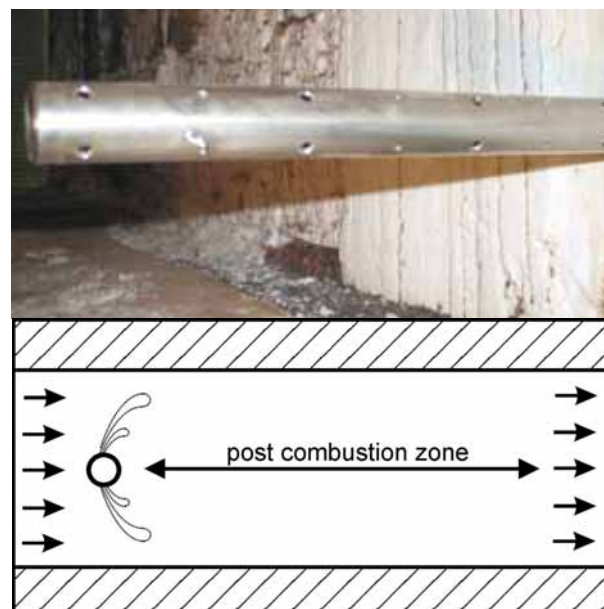


Figure 127a-b. Photo and principle of operation of secondary air lance.

Secondary air injection

The secondary air shall be injected homogeneously into the flue gas with a as short as possible mixing distance in the flue pipe. For this purpose, lances with many nozzles were designed. The secondary air is injected without preheating into the flue gas by cross flow. The secondary air shall approach the opposite flue pipe wall asymptotically after the flow deviation. Therefore, the penetration depth of the air flow must correspond to the half flue pipe width. Then a homogeneous and optimal mixing is achieved between the flue gas and the secondary air. This penetration depth can be computed according to the following conditional equation. The factor 1.224 was determined empirically by experiments [68].

$$\text{penetration depth} = 1.224 \cdot v_2/v_1 \cdot d_2 \cdot (\varphi_2/\varphi_1)^{0.5} \tag{Eq. 10}$$

- v : velocity
- d: pipe diameter
- φ: density
- index 1: flue gas
- index 2: secondary air

Figure 5.7 shows the calculated results of the penetration depth for different operating pressure values depending on the nozzle diameter. Large penetration depths can be achieved with large values of air pressure and nozzle diameter. However it has to be considered, that also the air volume flow increases strongly with the nozzle diameter. Figure 5.8 shows these dependences. For a targeted near-stoichiometric primary combustion, only a small secondary air flow is required. In this respect the requirements for the nozzle design are oppositely directed. A homogeneous distribution and mixing could be achieved with alternating big and small holes with different penetration depth of the air. BFI produced 3 lances with different nozzle geometries. Table 49 shows the parameters of the different lances.

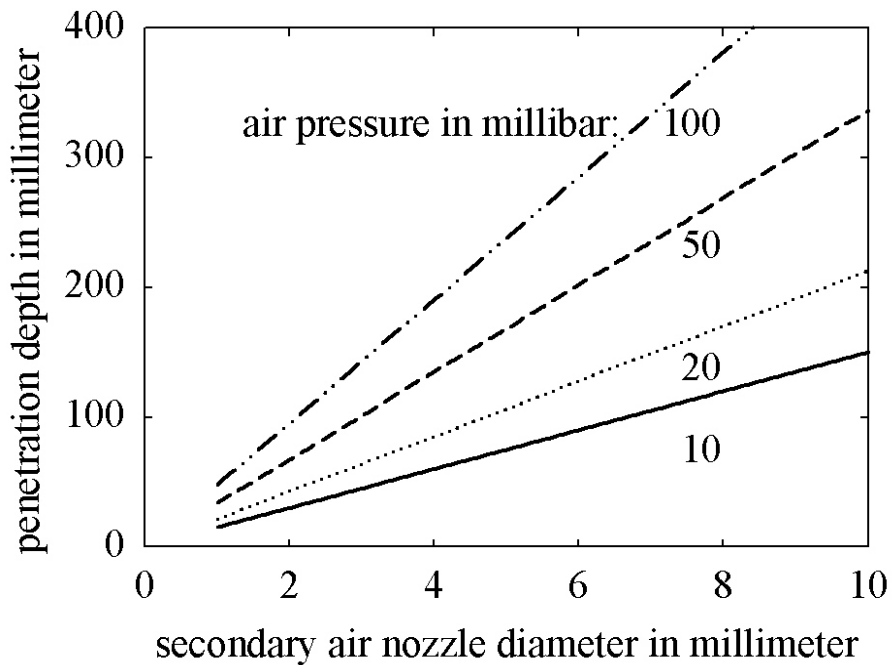


Figure 128. Calculated results of the air penetration depth depending on the nozzle diameter.

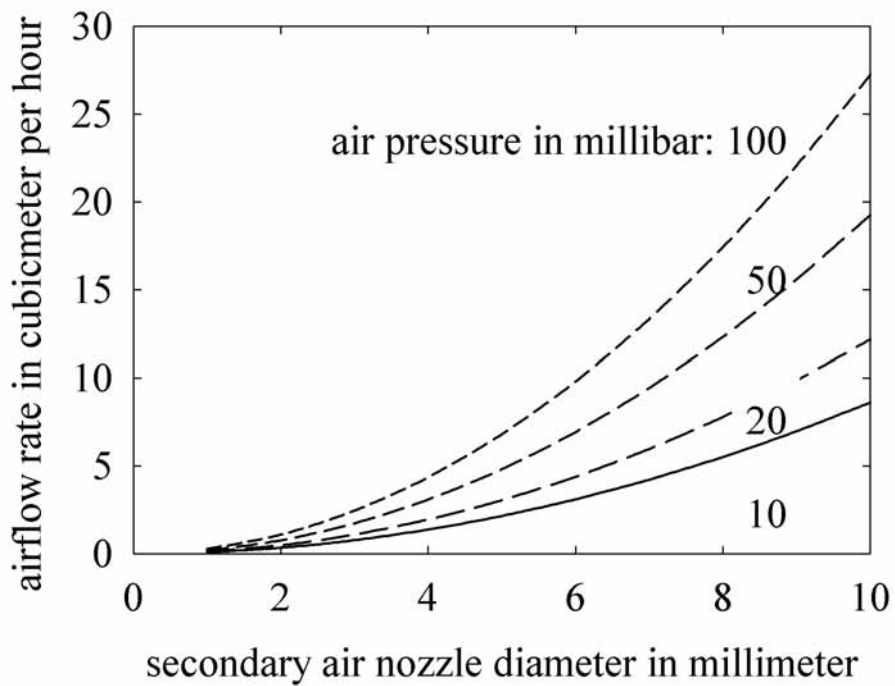


Figure 129. Calculated results of the secondary air- flow rate depending on the nozzle diameter.

Table 48. Geometrical data of the ammonia-additive lances.

lance-system	A	B
number of lances	2	1
design gas pressure	800 mbar	800 mbar
nozzle constellation, angle	180°	-
number and diameter of the nozzles	8 x 0.8 mm	1 x 4 mm
additive and additional gas	NH3 + N2	NH3 + N2

Table 49. Geometrical data of the secondary air lances for the tests.

lance	A	B	C
design air pressure	50 mbar	100 mbar	100 mbar
nozzle constellation, angle	180°	90°	180°
number and diameter of the large nozzles	10 x 6 mm	10 x 6 mm	14 x 4 mm
number and diameter of the small nozzles	8 x 3 mm	8 x 3 mm	12 x 2 mm

The emission values of the burner were measured at operation with coke oven gas. At a low excess of air (coefficient 1.05) the NO_x emission amounts to 670 mg/m³ at 5 % oxygen in dry flue gas. In the case of staged combustion, with a lower primary air, but constant total excess air, the NO_x emission decreases. For the investigation of the high temperature reduction, a comparison of the concentration values with steady unit is required. The flue gas volume fluctuated with different temperatures and different flue gas compositions in the substoichiometric field of the combustion. In the post combustion zone, the emission values (indicated in ppm) are reduced by the dilution of higher excess air. Therefore at these examinations the NO_x emission values were calculated for an oxygen concentration of 0 % and subsequently indicated for simplified comparability. The NO_x emission reference value for the evaluation of the NO_x reduction is for 429 ppm calculated at 0 % O₂ (= 670 mg/m³ at 5 % O₂), which is a relatively high NO_x level.

2.5.2 Task 5.2. Optimisation of HTR using CFD

The problem of the High Temperature Reduction (HTR in advanced) had been described by means of a CHEMKIN reactor network. The general scheme of the HTR and post-combustion zones is shown in Figure 130, with the reactor scheme to describe this treatment of flue gases with reactor network. Shown scheme consists of different elements including three gas inlets: First the Burner (Primary Combustion Zone), that is the inlet with exhaust gases from the burner, Second: gas injection of ammonia (NH_3 gas) or Urea solutions (25 %) where injections are like vapour not like liquids, (Molar fractions Composition NH_2 -0.13325, CO -0.11675 H_2O 0.75), and Third: Secondary Air Injection in post combustion zone.

Two Gas mixer reactors which perform the thermodynamic mixing of gas streams in the absence of chemical reactions. These are the Gas mixer: primary flue gas and additive and Second Gas Mixer: cleaned flue gas and secondary air. Two “Plug Flow Reactors” simulate chemically-reacting flow in a plug-flow reactor, where convection dominates transport in the axial direction and the gas is uniform in the cross-flow direction. The flow takes place in a channel of rectangular geometry (0.4 x 0.4 meters), characterized by flow area (0.16 m^2). Surface chemistry and external heat transfer are not included.

First Plug Flow Reactor (High temperature reduction zone) has a longitude of 3 meters.

Second Plug Flow Reactor (Post Combustion Zone) has a longitude of 1 meters.

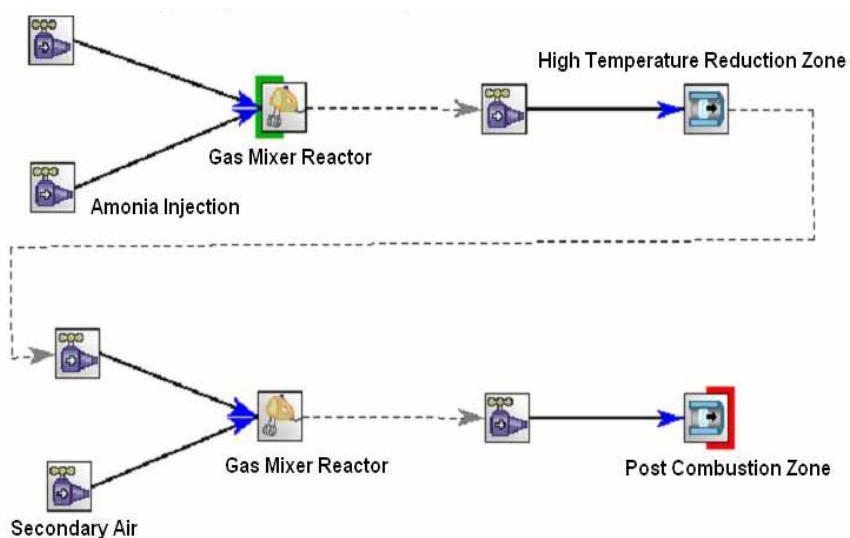


Figure 130. Reactor network solution.

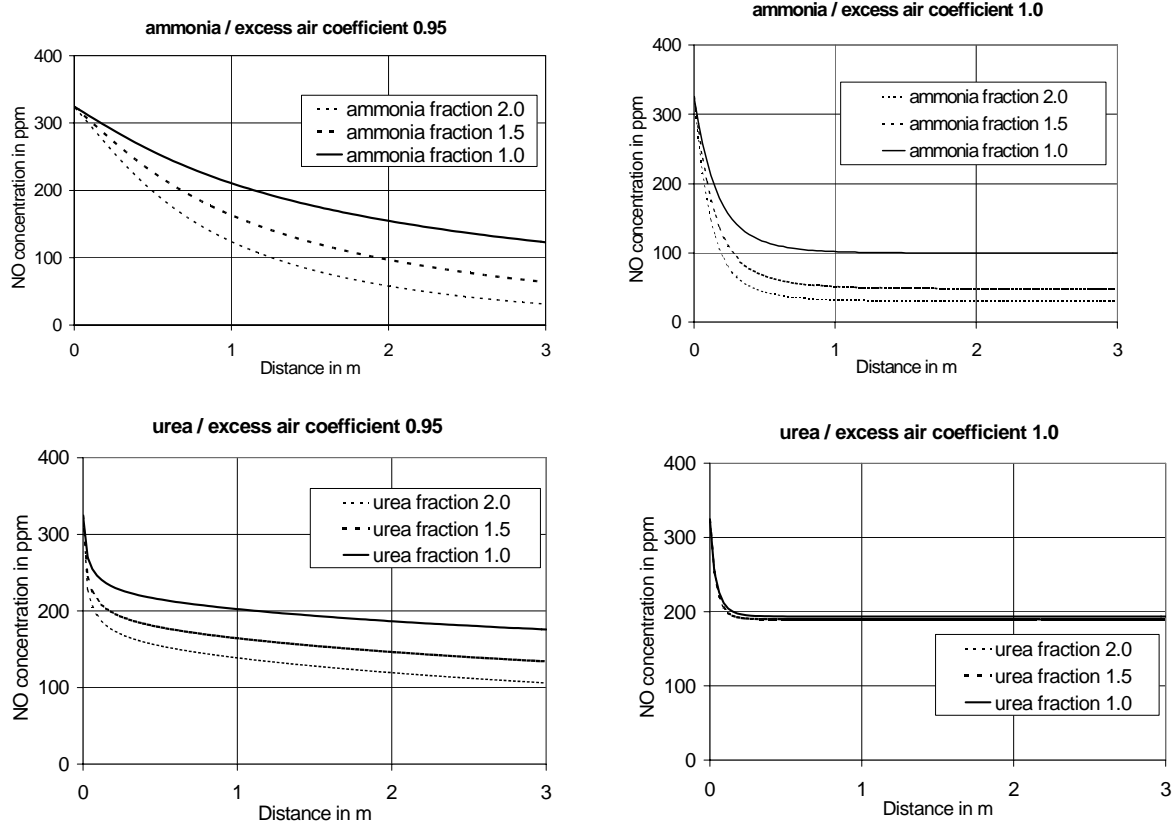


Figure 131a-d. Results of calculations: NO reduction with ammonia and urea at different boundary conditions.

Hypotheses in the network to describe HTR scheme are:

- A perfect mixture exists between primary fuel gas and additive, and also between cleaned flue gas and secondary air.
- It is considered that the reaction zone (HTR Zone and Post Combustion Zone) starts when the mixing process is completed.
- The chemical reactions that occur are described by the Chemical Kinetic Model "Kilpinen 97".
- The simulations were carried out with three molar ratios (1, 1.5 and 2).

Modelling of the HTR zone leads to the observation that the most efficient NO reduction is obtained with ammonia addition. Figures 131 a-d. show the calculated decrease in NO along the flow path in the reduction zone. At substoichiometric condition (0.95) the reactions are slower than at stoichiometric condition (needed flow path: 3 meters/1 meter). An increase in the molar ratio NH_3/NO causes a progressive reduction in NO concentration at substoichiometric condition. At stoichiometric condition the increase in the molar ratio causes a less effective NO reduction when the molar ratio is bigger than 1.5. With ammonia gas the most effective reduction is obtained at stoichiometric condition. Tables 50 and 51 show the detailed results for ammonia and urea as additives. The afterburning of CO will be no problem. No CO emission occurs. Starting with an excess air coefficient 0.95 the temperature increases 120 K in the post combustion zone. In the stoichiometric case the temperature increases 10 K.

Table 50. Calculated results for NO reduction with ammonia at different primary excess air coefficients and initial NO concentrations.

excess air coeff.:	0.95	0.95	1.0	1.0
initial NO:	128	321	128	321
molar ratio	NO in ppm	NO in ppm	NO in ppm	NO in ppm
1	78	123	66	100
1.5	56	64	49	49
2	49	31	38	30

Table 51. Calculated results for NO reduction with urea.

excess air coeff.:	0.95	0.95	1.0	1.0
initial NO:	128	321	128	321
molar ratio	NO in ppm	NO in ppm	NO in ppm	NO in ppm
1	52	176	96	193
1.5	40	134	98	190
2	33	106	101	190

Several series of tests with different primary excess air values and different quantity of additive were carried out at BFI test furnace, at first without a static mixer in the flue pipe to minimize the construction expense and costs. The injection of the liquid additive urea with a gas atomizing system was very problematic. Because of the very high flue gas temperature and a limited heat insulation the nozzle grew hot and the very low additive flow started to boil. Several solutions for an optimized heat protection of the additive nozzle, like thicker external insulation, additional internal insulation and self made internal water-pipe-cooling, were constructed and tested, but with little success. An overheating of the additive with a low formation of vapour bubbles and discontinuous flow couldn't be prevented. Only a fluctuating and very low NO reduction could be obtained because of the discontinuous additive flow. The tests were continued with ammonia because of the easier principle of injection with gas pressure. Figure 132 shows the course of flue gas concentrations upstream and downstream of the secondary air injection respectively after reduction zone and in the chimney for ammonia as additive. Between 10:10 and 10:22 the burner operated over-stoichiometric also in the primary combustion zone. On account of the secondary air flow - which could not be stopped to prevent an air lance overheating - the oxygen values in the chimney are higher than in the reduction zone. The measured (ppm) NO_x values in the chimney are lower than in the reduction zone because of the dilution by secondary air.

At 10:22 the burner was adjusted to a stoichiometric combustion. Unlike the theoretical equilibrium here appear alternating low variations of oxygen- and CO concentrations up to one or two per cent on account of small pressure fluctuations in the coke oven gas fuel pipe. Starting at 10:41 a.m., ammonia was added with increasing quantity. No NO reduction worth mentioning could be measured in the case of oxygen concentrations in the HTR zone above the detection limit. A higher NO reduction was measured in the case of negligible oxygen concentration and CO concentrations above approximately 0.1 %. These results confirm that the reaction scheme for reducing NO by high temperature reduction is different from the reaction scheme for reducing NO by SNCR. The SNCR process doesn't work without any oxygen content in the flue gas [69].

The NO concentration in the reduction zone decreases with higher molar ratio ammonia per NO (Figure 134: 10:46 and 10:56). In contrast with this effect the NO concentration in the chimney increased. The total NO reduction decreased with higher additive molar ratios for values clear over 1.0. This is caused by the oxidation of the excess additive in the post combustion zone. Figure 133 shows the individual NO_x concentration results of the first measurement series in the reducing zone and in the chimney. Partially clear deviations of the NO concentrations in the reducing zone were measured in the case of similar but not identical boundary conditions. In the reduction zone a high NO reduction was achieved at very high additive quantity (molar ratio NH₃/NO up to 3). The lowest NO concentration was 130 ppm. The design of the different tested secondary lances had no fundamental influence on the

results. However, the mounting position of the secondary air lance had a greater effect on the total NO_x reduction. Lower NO_x emissions were measured with enlarged distance between additive and secondary air injection - in accordance with a prolongation of the HTR zone (in the experiment from 2.4 m to 5.3 m). An heterogeneous mixing of the additive with the flue gas was assumed. This would cause fluctuating NO concentrations downstream of the HTR zone and also clearly fluctuating NO_x emissions in the chimney on account of the possible NO increase in the post combustion zone.

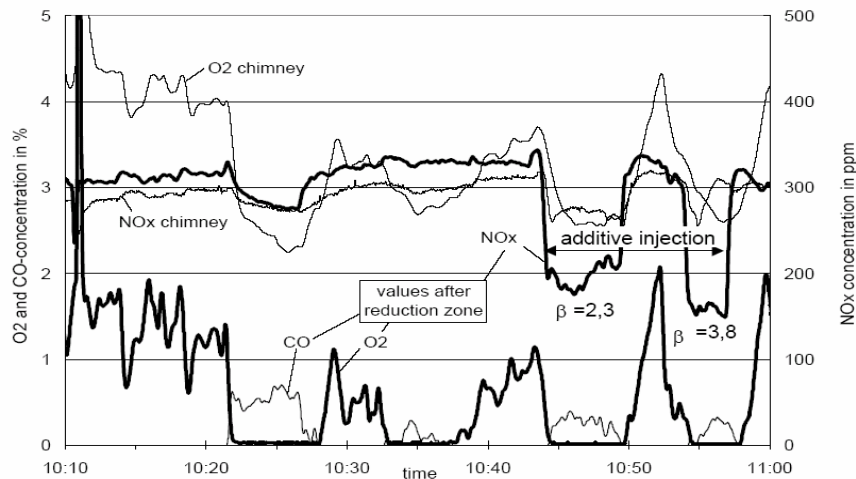


Figure 132. Course of flue gas concentrations after reduction zone and in the chimney for a stoichiometric adjustment with coke oven gas (β = molar ratio NH₃/NO).

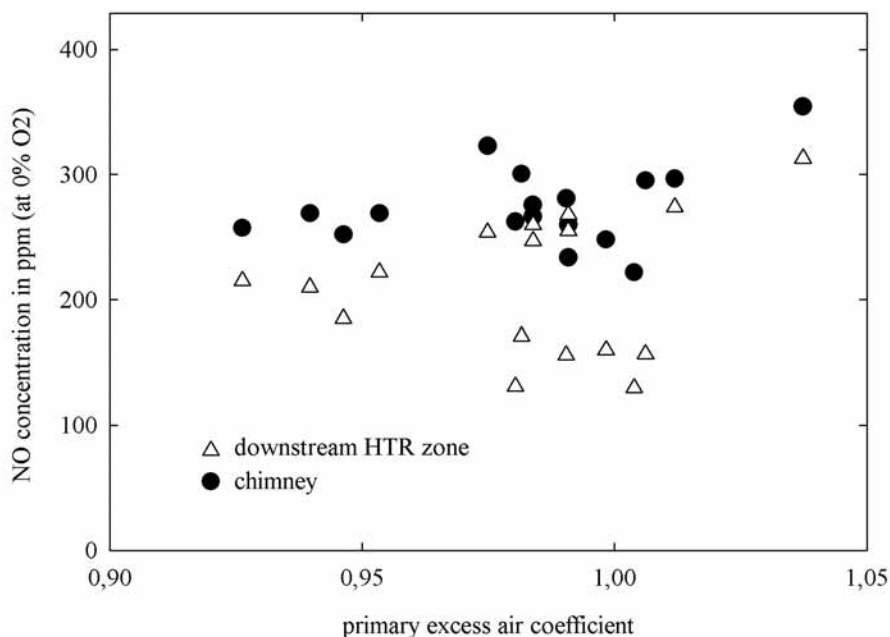


Figure 133. NO_x concentration results of the first HTR measurement series.

CFD calculations were made for optimized of the additive mixing with flue gas. The mixing of additive and flue gas should occur in a short section of the flue pipe. An improved mixing should be achieved by selective fittings in the flue pipe to increase the flow turbulence. CFD flow calculations were performed for getting information about efficient geometries of fittings. These fittings or maybe simple plates could be manufactured of a ceramic material cheaply. The k- ϵ model to calculate the turbulence was used for the tests. An exhaust gas flow from a furnace with a burner output of 500 kW and an air ratio of 0.95 was assumed for the simulation. The ammonia injection was fixed at 174 l/h according to an NH₃/NO_x- mol ratio of 1.5 with an NO_x concentration of 321 ppm in the exhaust gas.

The mixing of the ammonia injected via the lance without gas mixers in the exhaust gas duct were calculated. The concentration distributions of the additive NH_3 with and without mixing fittings at the end of the exhaust gas duct are compared for all designs in Figure 134. It was found that there can be no optimum mixing and thus no great reduction of the NO_x emissions over the entire cross-section without a gas mixer. The injection was carried out via two lances, with 8 bores each. A variety of fittings designs was calculated between the additive injection and the secondary air supply. The influence of these different fitting designs on the increase in turbulence was investigated. Starting from a simple flat plate, more and more complicated and slanted plate combinations were successively calculated for the different fitting designs (from A to E). Whereas the fittings according to designs B to D only lead to a slight turbulence in the direct vicinity of the fittings, the variant E caused a very turbulent flow in the duct and thus a good mixing of the ammonia and exhaust gas over the entire flow cross-section. A turbulent transverse exchange occurs in the flow. The results show that complicated static fittings are needed to create a high turbulence in the exhaust duct. The relatively complex additive injection via two lances with a large number of small bores does not lead to a solution on its own. Therefore, tests followed to see whether it would be possible to dispense with these lances. Unlike the previous results, variant 5 investigates the additive injection through only one laterally arranged nozzle. This design significantly reduces the apparatus needed for the injection since no components protrude into the hot exhaust gas duct and a much lower thermal load on the material can be expected compared to lance injection.

Designs A to C show a better distribution compared to the mixing without fittings, though these designs also display locally higher additive concentrations. An almost equal distribution of the ammonia over the entire cross-section is achieved with variant D. In variant E the omission of the additive injection via two lances does not lead to a deterioration of the quality of the mixing. The calculation results also show a very homogeneous NH_3 concentration profile compared to variant D. The complex geometry of the optimum fittings that was determined roughly corresponds to the geometry of a common "static mixer". It was thus resolved to fit a static mixer for the planned HTR tests in the test combustion chamber. Figure 135 shows the ceramic static mixer that was chosen and fitted in the exhaust gas duct for the next series of tests.

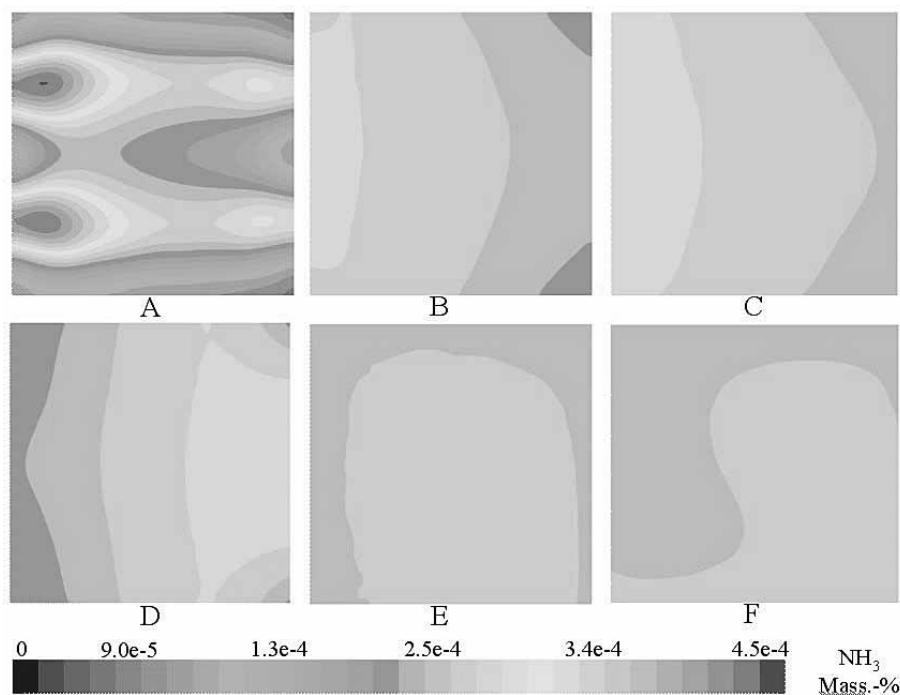


Figure 134. NH_3 concentration distributions at the end of the flue pipe for all variants showing the quality of the mixing without fittings in the exhaust gas duct (A), and with turbulence variant 1 (B), variant 2 (C), variant 3 (D), variant 4 (E) and lateral additive injection with variant 5 (F).



Figure 135. View of the ceramic static mixer fitted in the flue pipe in the combustion chamber.

Measurements were performed inside the furnace chamber at P1; after ammonia addition at P2 and in flue gas before stack at P3 as shown earlier. Extensive tests were done at various flue gas temperatures and types of additive injection. Figure 136 shows the results of the measurements of the efficiency of the HTR method with nozzle injection of the additive using 2 lances, a flue gas temperature of 1000 °C and different additive amounts chosen. This data can be compared with the results of nozzle injection of the additive through only one nozzle in the side of the flue duct at a flue gas temperature of 1200 °C (Figure 137). The static mixer leads to a fast and homogeneous mixing of the additive and flue gases in the area of the HTR zone. The NO_x concentration decreases after additive injection - for all marginal conditions - with an increasing amount of additive. The very high NO_x reduction that can be achieved at over-stoichiometric additive amounts (mol ratio > 1.2) cannot, however, be technically used. Unfortunately, new NO_x is produced by the reaction of the excess additive and oxygen of excess air in the post-combustion area that is always needed with staged combustion for prevention of CO emissions. The measured ammonia slip was negligible in all tests or below 1 mg/m³, Figure 138. The NO_x concentrations in the area of the stack were only slightly dependent on the amount of additive and when converted to ppm NO_x at 0 % oxygen they amounted to around 75 % of the NO_x- concentration in the combustion chamber. Figure 139 summarizes the results of all the measurements and compares the NO_x emissions for air-staged combustion (mol ratio = 0) with the reduced NO_x emissions that can be achieved by using the high temperature reduction procedure at various additive amounts (molar ratio). The procedure can be used over a wide range of temperatures (at least 1000 °C to 1200 °C and higher) and achieves its greatest efficiency with a slightly over-stoichiometric use of additive (molar ratio approx. 1.2). Based on initial NO_x emission values of 380 to 460 mg/m³, the tests proved that the emissions could be reduced to 250 or 300 mg/m³. This corresponds to a mean NO_x reduction of 35 %. Based on the original initial NO_x emission value (670 mg/m³) of the test furnace in combination with the staged combustion - which decreases the initial emission value about 35 % - a total reduction of 60 % was achieved.

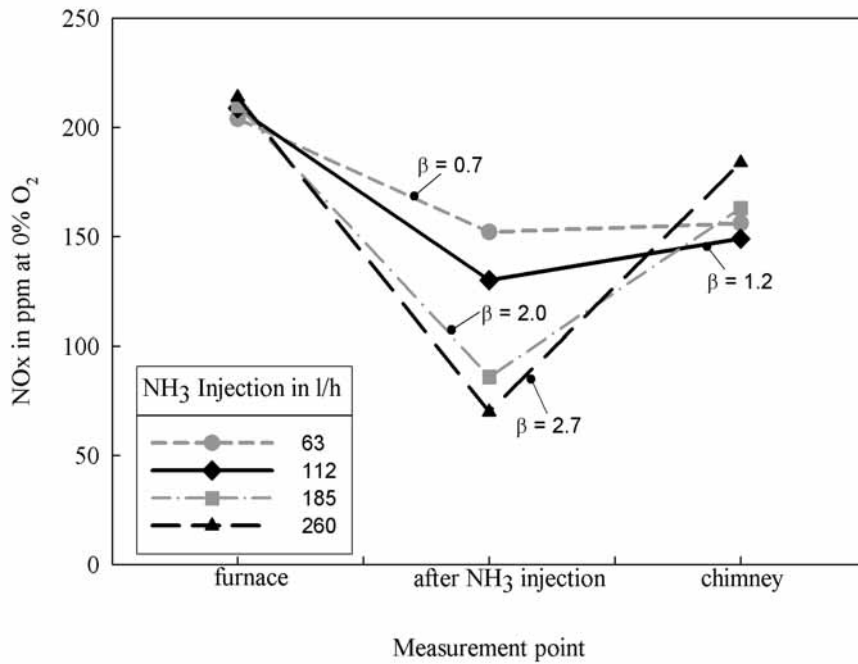


Figure 136. Effect of the high temperature reduction and the post combustion at different additive molar ratios ($\beta = \text{NH}_3 / \text{NO}$) for the additive injection with two lances at 1000 °C.

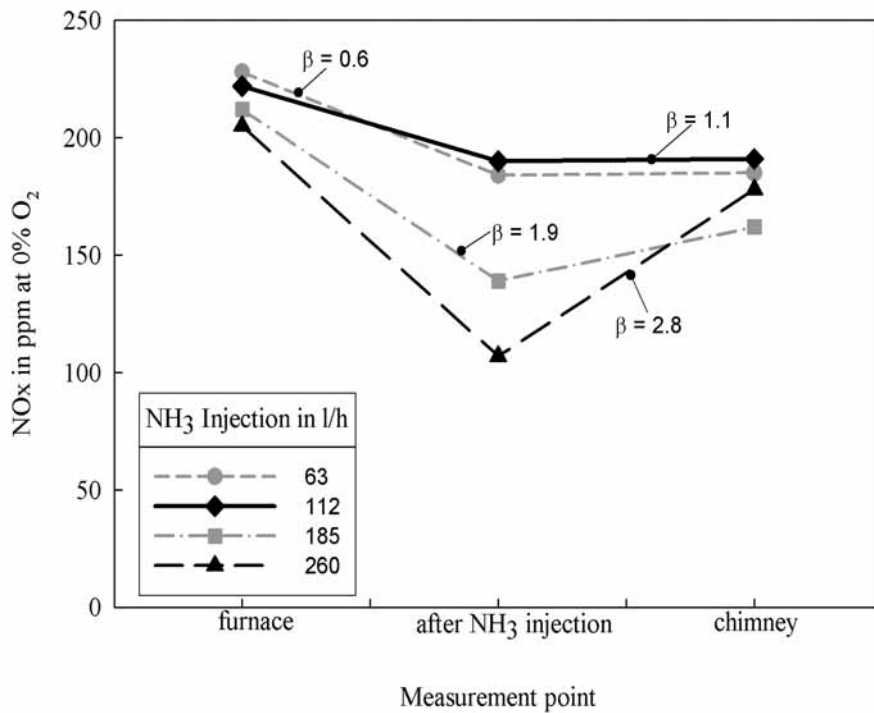


Figure 137. Effect of the high temperature reduction and the post combustion at different additive molar ratios ($\beta = \text{NH}_3 / \text{NO}$) for the additive injection with one side lance at 1200 °C.

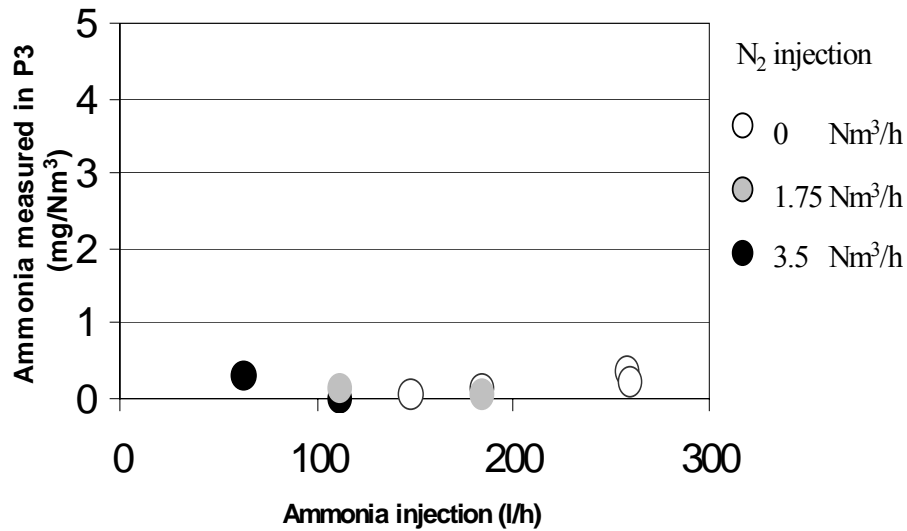


Figure 138. Ammonia concentration measured at position P3 in the HTR process.

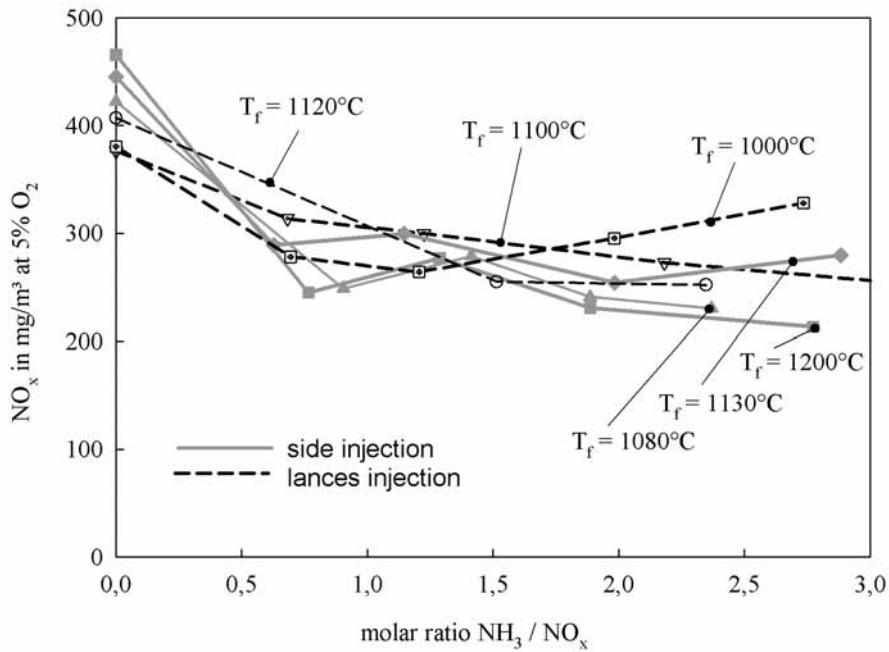


Figure 139. Summary of the total high temperature reduction results (furnace-chimney) with different temperatures and molar ratios.

Aim of the heavy metals measurements was the investigation of the flue gas concentration as a result of coke oven gas impurities. Emissions of Total Suspended Particles (TSP) and heavy metals were measured before stack in P3 by ISQ. Results are presented in Table 52.

Table 52. TSP and heavy metal concentration measured at P3 before stack (sample filters 1 and 2).

Pollutant	Concentration - solution -1 (mg/Nm ³)	Concentration - filter -1 (mg/Nm ³)	Concentration - solution -2 (mg/Nm ³)	Concentration - filter -2 (mg/Nm ³)
TSP		270		1075
As	0.0020	0.19	<0.00073	<0.10
Pb	0.0090	0.34	0.0049	0.081
Cd	0.016	<0.026	0.00047	<0.025
Cr	<0.011	4.8	<0.011	6.0
Fe	<0.075	30	<0.073	130
Cu	<0.019	0.27	<0.018	0.44
Ni	<0.019	23	<0.018	63
V	<0.019	0.19	<0.018	0.10

The results are very different and they showed unexpected very high concentration values which are not only caused by fuel gas impurities. The examination of the boundary conditions at the combustion chamber while testing the high temperature reduction process gave the following explanations: A high content of particles with C- or CH-compounds was caused by the very small combustion chamber for the primary combustion with a quenching in the ceramic foam at the entrance of the flue gas duct. A normal COG-combustion with nearly unlimited reaction zone for carbon- and CO-combustion has typically nearly no emission of unburned particles or gases. The very high contents of Fe, Cr and Ni result from the ammonia pipes/lances (made of Cr-Ni-alloy for a continuous operation maximum temperature of 600 °C, used for the short time of the tests at 1200 °C). The lances were not cooled by water and thus a high scale formation occurred. A direct correlation between TSP or heavy metal and the NO reduction couldn't be detected.

Scale-up and calculation of the HTR process for a reheating furnace

A revamping of an existing reheating furnace with the high temperature reduction procedure is possible, when the furnace is able to operate with a nearly stoichiometric, but substoichiometric combustion. Using stoichiometric combustion, a decrease of the furnace efficiency can be avoided. It should be possible, to mount the systems for additive injection and post combustion injection into the existing flue pipes. Then no additional reaction chambers need to be constructed and a minimization of the investment costs will be achieved. The test results proved, that an optimization of the additive mixing is needed. A ceramic static mixer should advantageously used for this purpose. The investment costs for the static mixer are calculated to 3000 € / MW nominal power. The calculation based on a mixer volume requirement of 0.1 m³/MW and a theoretical purchase price of round about 30000 €/m³. The investment costs for the additive injection are similar to the costs of a simple SNCR procedure without redundant injection levels (pressure tank, piping, lances with nozzles and control unit). For high temperature reduction a first reduction of the initial NO_x emission of 35 % is given by the staged combustion. An example is given in Table 53.

Table 53. Operating costs/required additive (for example: ammonia) for a nominal power of 1 MW, a molar ratio of 1.2 and calculated 8000 operating hours per year; additive costs include costs for delivery.

	high temperature reduction	SNCR
initial emission of the furnace	550 mg/m ³ @ 5 % O ₂	550 mg/m ³ @ 5 % O ₂
first emission reduction through	staged combustion	-
emission upstream of additive injection	≈ 360 mg/m ³ @ 5 % O ₂	550 mg/m ³ @ 5 % O ₂
additive flow rate	≈ 210 l/h	≈ 320 l/h
additive amount per year	≈ 1660 m ³ / (MW · a)	≈ 2560 m ³ / (MW · a)
additive mass per year	≈ 1300 kg / (MW · a)	≈ 2000 kg / (MW · a)
additive costs for 3 MW furnace	≈ 5500 € / a	≈ 8500 € / a
additive costs for 50 MW furnace	≈ 78 T € / a	≈ 120 T € / a

The high temperature reduction procedure is one of several possible ways to reduce the NOx emission of existing reheating plants. A revamping of reheating furnaces with new low-NOx-burners (see results in WP 1) most of the time will give the lowest NOx emission values. A problem of old reheating furnaces with many small burners could be the required high investment costs, depending on the required number of burners. In cases where the planned residual service life of reheating furnaces is limited, the operating company could be reserved against the high investment costs for minimizing the NOx emissions. The common secondary SNCR (selective non catalytic reduction) process is a good solution for combustion systems with constant operating conditions. In reheating furnaces with varying operating conditions it could be difficult to get high NOx reduction values. A comparison of the different best operating conditions for SNCR and high temperature reduction is given in Table 54. In the European community only one steel mill operates with the SNCR procedure: Outokumpu, Avesta with two of their reheating furnaces (called 5BA and 5BB). Outokumpu achieves a NOx reduction up to 71 % and emission values down to 45 mg/MJ by using ammonia as additive. The ammonia slip is between 0.5 and 2.5 mg/m³. The costs are 5-22 SEK/kg NOx (≈ 0.5-2.4 € / kg NOx) depending on the initial NOx level [70]. So it is advantageous for the European environment to place an additional procedure with lower investment costs as temporary solution at disposal.

Table 54. Operating conditions for high temperature reduction and selective non catalytic reduction.

	high temperature reduction	SNCR
NOx reduction potential	60 %	50-70 %
flue gas: temperature	1000 °C - > 1200 °C	950 °C-1050 °C
flue gas: oxygen content	0 %-0.01 %	0.1 %-> 3 %
combustion	air staged	standard
ammonia slip	< 1 mg/m ³	5-30 mg/m ³
additive mixing with flue gas	enhance by static mixer	1 or several of lance-levels
Main problem for application in an existing furnace	Requirement for staged combustion	Continuous operation without large temperature fluctuations at the point of application

3 ECONOMIC ANALYSIS AND CONCLUSIONS

3.1 Oxy-fuel versus air combustion in new furnaces

An economic analysis for the new types of technologies investigated in this NO_x-RF project was not included in the work packages. An example of this type of analysis for low NO_x oxy-fuel technology for various types of new reheating furnace installations was made by Techint Technologies, PA, USA, together with Praxair in a project supported by the DOE [71]. There are many design parameters to consider, so they limited the study to evaluating a 120 t/hr natural gas fired reheating furnace for hot rolling 150 mm (6 inch) square billets reheated to 1175 °C (2150 °F). Fully oxy-fuel reheating with the Praxair Dilute oxygen Combustion (DOC-oxy-fuel) design was compared with several air combustion furnace designs, including a standard reheating furnace (STD-air furnace) with air preheated to 480 °C (900 °F) using recuperative heat recovery, plus a reheating furnace with a longer preheating zone to save energy (STD + long preheat) and a reheating furnace with selective catalytic reduction (SCR) for additional NO_x reduction (STD + SCR). Several hybrid oxy-fuel plus air combustion designs were also considered, but they were primarily for controlling scaling and not for minimizing NO_x or energy consumption. The assumptions used for the cost analysis are critical, since they can vary depending on when and where the furnace is installed. The 10 year net present value (NPV) comparison in the DOE report from 2003 [71] was made assuming capital costs at 12.5 %, a one time NO_x fee of 6000 USD/ton for 1.2 times the annual emission at design capacity, 8000 hrs/yr operation, natural gas cost of 3.75 USD/MMBtu (ca. 9.5 EURO/MWh) increasing at 3 % annually, oxygen at 32 USD/ton (24 EURO/ton at 0.743 EURO/USD) with 1% inflation, and electricity at 40 USD/MWh (30 EURO/MWh) with 2 % inflation. The results of the analysis are shown by the solid bars in Figure 140.

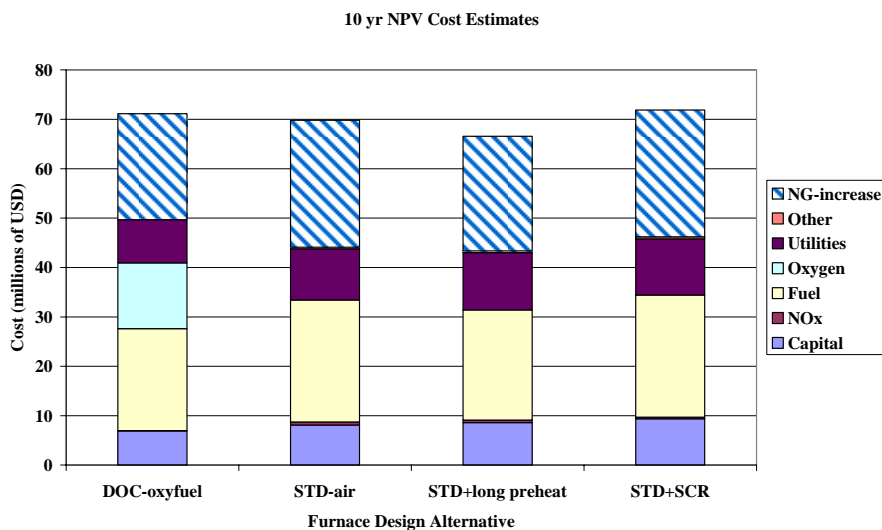


Figure 140. Comparison of a DOC-oxy-fuel with 3 types of recuperative reheating furnaces firing natural gas with air combustion. The solid bars are the original analysis, and the striped bar is for the increase in natural gas price to 2006.

The lowest cost alternative was found to be the conventional furnace with a longer preheating zone, with a total NPV of 43.4 MUSD. The furnace with SCR NO_x removal was also cheaper than DOC-oxy-fuel, but only if the cost of fuel is low. The cost transition favors the oxy-fuel design if fuel prices are over 7 USD/MMBtu (18 EURO/MWh). The price for natural gas has risen significantly recently in both the USA and Europe since the study was made. The average industrial natural gas prices in the USA rose to 7.65 USD/MMBtu already in 2006 (7.88 USD/1000 scf [72]), and the price in Europe was locally much higher in 2006, for example, natural gas for large users rose to over 30 EURO/MWh in Germany (ca. 12 USD/MMBtu [73], see Figure 141). The NPV cost for DOC-oxy-fuel for new furnaces is now lower than with SCR removal as shown in Figure 140 with the striped bars, correcting for the higher fuel costs (by the factor "NPV fuel-2003 * (7.65/ 3.75)"). The comparison is only valid for the assumptions used, so the author pointed out that stricter NO_x limits or higher NO_x emission costs could also favor the DOC-oxy-fuel alternative. The break-even point between DOC-oxy-fuel and a standard recuperative furnace was a natural gas price of 8.89 USD/MMBtu (22.6 EURO/MWh).

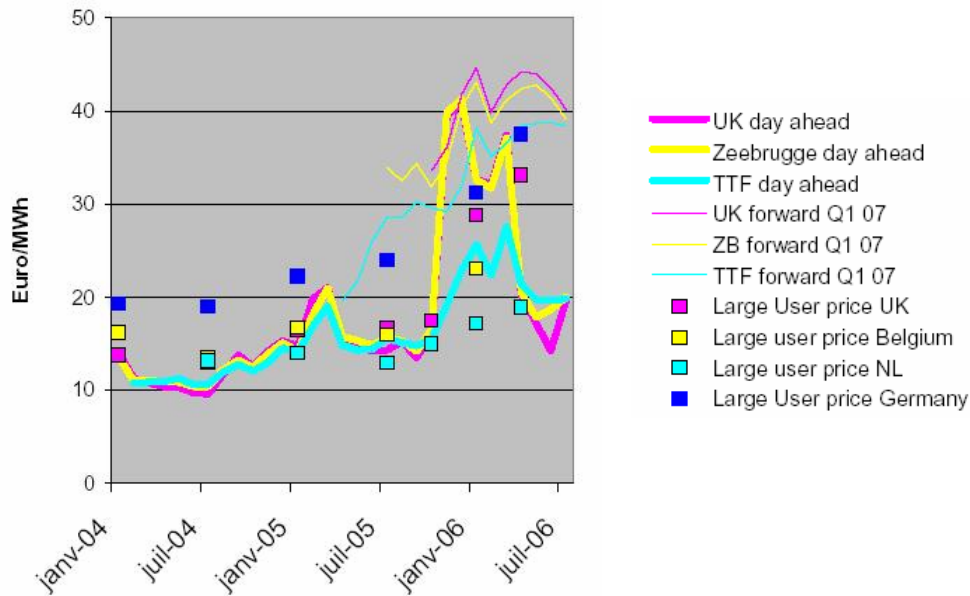


Figure 141. Natural gas prices trends in Europe [73].

There are many questions that are still unanswered, if a steelmill is considering installing oxy-fuel reheating. Weakness in the DOE study [71] include the lack of a comparison with regenerative combustion, the use of cost data for installations in the USA instead of for Europe which is also several years old now and the lack of data from actual installations of fully oxy-fuel combustion. Therefore the conclusion from this DOE study do not necessarily reflect the views of Air Liquide or the other partners in this project.

3.2 Oxy-fuel revamping of furnaces

There are many steel reheating furnaces which have been revamped for oxy-fuel combustion, especially pit furnaces, but the only walking beam steel reheating furnace in Europe revamped to fully oxy-fuel combustion is at the Outokumpu Stainless AB hot rolling mill in Degerfors, Sweden [74]. This furnace had a conventional recuperator, which was removed together with the existing exhaust duct system, when the furnace was converted to oxy-fuel with 16 MW burner power in 2003. The fuel consumption was reduced by 25 %, production capacity increased by 30 % and the NO_x levels were under 70 mg NO_x/MJ [74]. The greatest profitability for the conversion was the increase in furnace capacity of 30 %, because the benefits for the reduction in the fuel consumption are at least partially off-set by the additional cost of oxygen. New oxy-fuel furnace installations should be compared with traditional reheating furnaces using air combustion considering all the local costs and the investment costs using the NPV method. Rebuilding a traditional recuperative reheating furnace like the one assumed in the DOE study to partially or fully oxy-fuel reheating is not normally justified by the energy and NO_x reduction possible. Increased furnace capacity and increased furnace productivity normally are the economic driving forces for rebuilding existing furnaces.

Increased furnace capacity and lower energy costs can be also obtained with regenerative heat recovery instead of oxy-fuel. A list of advantages for oxy-fuel with comments for conventional recuperative or regenerative heat recovery is given in Table 55 below. Advantages of flameless oxy-fuel and flameless air combustion were also given in Table 11 earlier. The issue of scale growth and adhesion should be addressed in a larger study for the two types of technologies. A study at the Royal Institute found that oxy-fuel could give a less adhesive scale, with approximately the same amount of scale as air combustion when the reheating time for oxy-fuel was shortened for the faster reheating cycle [75]. A major advantage for traditional recuperative reheating furnaces is the large variety of well proven and tested designs, while both flameless oxy-fuel and flameless regenerative burners are relative new technologies for industry to install. An article comparing high temperature air combustion (regenerative heat recovery) with oxy-fuel combustion concluded that both gave many of the same advantages over

traditional recuperative furnaces, including high energy savings depending on the exhaust gas temperatures for each system, low NOx emissions and good temperature uniformity [76]. The total costs were not compared, and a comparison should be made for the local conditions and costs for each new or revamped furnace for these new technologies.

Table 55. Comparison of oxy-fuel versus fossil fuel-air fired reheating furnaces.

Advantages of flameless oxy-fuel	Comments relative to air combustion
* Lower investment costs	* Total NPV costs can be lower for air combustion, depending on fuel and oxygen prices (see DOE study above [71])
* Compact burners for compact furnaces and easier retrofitting	* Central regenerators can be considered when regenerative burners are too large
* Faster reheating and higher capacity for the same zone temperatures	* Applies to existing furnaces with limited size, since new furnaces can be built as large as required for high capacity
* Lower fuel consumption than recuperative furnaces	* No oxygen costs weigh against higher fuel costs
* Less CO2 and NOx emissions are possible, even sequestration of exhaust gases	* There is a risk for relatively high NOx when mixing oxy-fuel and air combustion
* Low maintenance costs	* Maintenance costs normally are much lower than other operating costs (Figure 140)

The cost of oxygen is a very important factor in an economic analysis of oxy-fuel. Oxygen production requires energy which must be included in the price to the consumer, plus the size of the air separation plant is critical to the price, since a high volume of oxygen can be sold at a lower unit price. Kobayashi presented a rough comparison for oxygen costs for different production techniques [77]. The price of oxygen can vary from about 15-30 USD/ton for very large cryogenic separation plants producing over 3000 tons per day (TPD) to over 60 USD/ton for under 20 TPD using much smaller vacuum pressure swing adsorption (VPSA) plants, with a price advantage for VPSA for plants under about 200 TPD and an advantage for cryogenic separation for plants producing over 800 TPD. Oxygen production requires about 200 kWh per ton oxygen, so an energy savings of about 9-14 % is required to cover the energy associated with oxygen production [77]. The actual fuel savings required depends on the cost of the fuel and cost of the oxygen, which is dependent on the oxygen consumption at the plant site, etc.

3.3 Conclusions

This NOx-RF project has focused on the technology issues related to flameless oxy-fuel combustion and other low NOx combustion alternatives rather than the economic issues. A separate investigation should be made to further investigate the economic issues comparing oxy-fuel and air combustion. Oxy-fuel technology is still developing, and it has found a niche not only for furnace boosting and revamping, but also for new furnace construction. An example of new furnace construction is the 100 % oxy-fuel fired rotary hearth reheating furnace at Ovako in Hofors, Sweden [78]. The furnace was built with 22 oxy-fuel burners firing with 7.5 MW power reheating up to 22 t/h to 1120-1240 °C. This furnace at Ovako was built based on the advantages of oxy-fuel combustion without flameless low NOx burners. Ovako reported at a conference in 2006 that they are evaluating upgrading to flameless low NOx technology to obtain even lower NOx and better temperature uniformity [79].

Some conclusions for oxy-fuel combustion are:

Oxy-fuel combustion is a technology that in theory can give zero NOx, but the air infiltration must be controlled. An alternative for zero NOx and CO2 emissions is to use sequestration of all the exhaust gases. The relatively high ppm levels of NOx in oxy-fuel exhaust gases should be converted to mg NOx/MJ in regulatory limits.

The greatest energy savings for oxy-fuel combustion is when comparing with cold air combustion, with decreasing savings with increasing combustion air temperatures. The NPV of all the investment and

operating costs should be compared for the location of the furnace installation, when comparing oxy-fuel with alternative technologies.

Higher furnace productivity is a major economic incentive for revamping furnaces with oxy-fuel combustion. Lower capital costs is a major economic incentive for building new oxy-fuel furnaces. Regulations on the emission of pollutants has not been a critical factor for choosing oxy-fuel, but increasingly stringent CO₂ and NO_x regulations could make these factors important in the future.

4 LIST OF FIGURES

- Figure 1. Typical NO_x emissions from side burners for reheating furnaces equipped with a central recuperator based on the research at CSM.
- Figure 2. TSN burner NO_x emission: experiment vs. modelling.
- Figure 3. NO_x, CO₂ and oxygen in the flue gases sampling during oxy-fuel trial in the WBF.
- Figure 4. NO_x with the ALROLL-S burner at BFI firing natural gas (note that for oxy-fuel the NO_x is reported in mg NO_x/MJ).
- Figure 5. Effect of the high temperature reduction and the post combustion at different additive molar ratios ($\beta = \text{NH}_3/\text{NO}$) for the additive injection with two lances at 1000 °C.
- Figure 6. Summary of the total high temperature reduction results (furnace-chimney) with different temperatures and molar ratios.
- Figure 7. Effects on NO_x emission of different combustion techniques [17].
- Figure 8. Techint TSN burner as delivered to CSM.
- Figure 9. Switching valve for Hauck burner.
- Figure 10. External and internal view of CSM's modular furnace.
- Figure 11. CSM's modular furnace schematics.
- Figure 12. Photos of the TRIOX and TSN burners mounted on the furnace.
- Figure 13. Different burner modes operation.
- Figure 14. TSN flame for different burner operating conditions.
- Figure 15. Laser induced fluorescence for OH-radicals at flame and flameless mode [18].
- Figure 16. TSX reaction zone in Low-NO_x mode.
- Figure 17. NO_x emission of Hauck TRIOX, Techint TSN and TSX burners at 1150 °C furnace temperature and different preheated air temperature and burner load.
- Figure 18. NO_x emission of Hauck TRIOX, Techint TSN and TSX burners at 1250 °C furnace temperature and different preheated air temperature and burner load.
- Figure 19. Temperature profiles for the TriOx burner 90/10 operating at 100 % of the thermal capacity (1 MW) at the average temperature of 1250 °C.
- Figure 20. Composition profiles for the TRIOX burner operating at 100 % of the thermal capacity (1 MW) at furnace temperature of 1250 °C and combustion air of 550 °C.
- Figure 21. NO_x emissions for the VTS-NFK HRS burner in the flameless F2 mode with a 1150 °C furnace and varying the excess air and combustion air temperatures.
- Figure 22. NO_x emissions for the VTS-NFK HRS burner in the flameless F2 mode with a 1250 °C furnace and varying the excess air and combustion air temperatures.
- Figure 23. Installation of the Hennig SBLN side burner at the BFI experimental combustion chamber.
- Figure 24. NO_x emissions for the Hennig SBLN side burner tested at BFI varying the combustion air temperature at a burner load of 100 % and 1250 °C furnace temperature.
- Figure 25. NO_x emissions for the Hennig SBLN side burner tested at BFI varying the combustion air temperature at a burner load of 100 % and 1150 °C furnace temperature.
- Figure 26. NO_x emissions for the Hennig SBLN side burner tested at BFI varying the combustion air temperature at a burner load of 50 % and 1150 °C furnace temperature.
- Figure 27. NO_x emissions for the Hennig SBLN side burner tested with coke oven gas at BFI varying the combustion air temperature at a burner load of 100 % and 1150 °C furnace temperature.
- Figure 28. Comparison of NO_x emissions for the Hennig SBLN side burner tested with coke oven gas and natural gas at BFI varying the combustion air temperature at a burner load of 100 % and 1150 °C furnace temperature.
- Figure 29. Tests with oscillating combustion in the F1 central flame mode with a 1150 °C furnace and 450 °C air in the chamber furnace at MEFOS.
- Figure 30. Tests with oscillating combustion in the F1 central flame mode with a 1200°C furnace, 600 °C combustion air and a 40 kW load at MEFOS.
- Figure 31. Burner geometry for the separate air and fuel injection trial at MEFOS. The black centre pipe is for hot air injection and the two small nozzles are for propane injection.
- Figure 32. NO_x with separate propane injection at 1250 °C with preheated air compared with NO_x for cold air with a premix burner in MEFOS chamber furnace.
- Figure 33. NO_x with separate propane injection at 1150 °C and preheated air in MEFOS chamber furnace.

- Figure 34. FBB TriX100 burner as received at CSM.
- Figure 35. FBB TriX100 installation at CSM Modular Furnace # 1.
- Figure 36. CSM Modular furnace schematics after FBB burner installation.
- Figure 37. NO_x emission for different combustion technology and different combustion air temperature. Data for the NFK HRS burner with flameless combustion at 1000 °C is from the IFRF tests.
- Figure 38. NO_x emissions at various R ratios with a furnace temperature of 1150 °C.
- Figure 39. NO_x emissions at various R ratios with a furnace temperature of 1250 °C.
- Figure 40. Air temperature versus R for various cycles.
- Figure 41. NO_x emissions for various R ratios and oxygen concentrations at 1150 °C.
- Figure 42. NO_x emissions for various R ratios and oxygen concentrations at 1250 °C.
- Figure 43. Thermal efficiency versus R for a furnace at 1150 °C (left side figure).
- Figure 44. Thermal efficiency versus R for a furnace at 1150 °C (right side figure).
- Figure 45. Pressure drop in regenerator.
- Figure 46. Scheme of the installation of the FBB TriX regenerative burners at the BFI burner test rig.
- Figure 47. Temperature fluctuation in the furnace and inside of the regenerator top and base (air or flue gas temperatures) at different switching times.
- Figure 48. Temperature fluctuation over the length in the BFI combustion chamber during a half cycle at the operation of one regenerative burner (on the left side).
- Figure 49. Path lines from fuel injection for the oxy-fuel burner model.
- Figure 50. Path lines from secondary oxygen in combustion chamber.
- Figure 51. Temperature profiles (in K).
- Figure 52. NO distribution for the oxy-fuel burner (ppm on a dry basis).
- Figure 53. Geometry and boundary condition for TSN simulation.
- Figure 54. Effect of an obstacle (wall) inside the furnace on recirculation rate (k- ω model).
- Figure 55. Results of TSN simulation for different turbulence models and Arrhenius rates.
- Figure 56. Iso-surface with Da=1 coloured by temperature.
- Figure 57. Near burner zone.
- Figure 58. Geometry, boundary condition and surface mesh for TSX simulation.
- Figure 59. Temperature field generate by Techint TSX burner inside the CSM Modular Furnace.
- Figure 60. Fluid-dynamic behaviour of TSX burner for the base line condition : T_{air}=450 °C, T_{furnace}=1250 °C, 1.25 % O₂ in DFG.
- Figure 61. Comparison between TSN and TSX burner combustion behaviour.
- Figure 62. Temperature and NO_x (thermal + prompt) field for different working conditions of TSN burner.
- Figure 63. TSN burner NO_x emission: experiment vs. modelling.
- Figure 64. NO_x emission for TSN and TSX burner versus peak flame temperature variation.
- Figure 65. Velocity and temperature and NO_x field for TSX burner with different combustion models.
- Figure 66. Temperature profiles inside CSM modular furnace in three positions.
- Figure 67. Specie mass fraction and NO_x field for TSX burner with different combustion models.
- Figure 68. NO_x field for TSN burner with different combustion models.
- Figures 69a-b. Velocities and oxygen concentrations and NO concentration at the centreline of the burner in the CFD model of the DFI trials in the chamber furnace at MEFOS.
- Figures 70. Temperatures at the centreline of the burner in the CFD model of the DFI trials in the chamber furnace at MEFOS for a furnace temperature of 1250 °C, 3 % dry oxygen and 500 °C combustion air.
- Figure 71. NO concentration at the centreline of the burner in the CFD model of the DFI trials in the chamber furnace at MEFOS for a furnace temperature of 1250 °C, 3 % dry oxygen and 500 °C combustion air.
- Figure 72. A comparison of the NO_x calculated with CFD versus the experimental results for DFI with 1250 °C furnace, 500 °C combustion air and varying the excess oxygen.
- Figure 73. Scheme of the Voestalpine slab reheating furnace.
- Figure 74. Full geometric furnace model.
- Figure 75. Grid for the model of half furnace at Voestalpine.
- Figure 76. Grid details of the 1/8 furnace model.
- Figure 77. Reference case: Gas- temperature in the furnace (note, the figure was compressed on the z-axis).

- Figure 78. Inner wall temperatures of the furnace (note, the figure was compressed on the z-axis).
- Figure 79. Velocities in a plane crossing the burners of the lower preheating and heating zones. Vectors corresponding to velocities larger than 10 m/s have been omitted for clarity.
- Figure 80. NO volume fraction in the reference case.
- Figure 81. Temperature in furnace operated with blast furnace gas (note, the figure was compressed on the z-axis).
- Figure 82. NO_x concentration at furnace outlet during burner-on period.
- Figure 83. Temperature field in the furnace equipped with air-staging burners (note, the figure was compressed on the z-axis).
- Figure 84. Measured (mess) and calculated (calc) temperatures at different locations in a slab passing through the furnace. Distance of the measuring sites from the surface: M1 130 mm, M2 102 mm, M3 70 mm with a slab thickness of 207 mm.
- Figure 85. Measured and calculated temperatures at different locations in a slab passing through the surface. For the calculation, the energy input in each zone was averaged only over that period when the slab was actually in that zone.
- Figure 86. Geometry for the 3D volume grid of the regenerative burner and the furnace.
- Figure 87. Velocity field generated by regenerative burner inside the BFI combustion chamber.
- Figure 88. Temperature field generated by regenerative burner inside the BFI combustion chamber.
- Figure 89. NO field generated by regenerative burner inside the BFI combustion chamber.
- Figure 90. The classical two-layer MLP feed forward architecture.
- Figure 91. CBP architecture with two layers of neurons.
- Figure 92. The VQ-based network multiplexing strategy, where the input pattern, x , is detected to belong to the n -th partition of the data space and activates the associated CBP neural estimator.
- Figure 93. Estimated NO_x values versus actual values for run #1.
- Figure 94. Estimated NO_x values versus actual values for run #2.
- Figure 95. Estimated NO_x values versus actual values for run #1.
- Figure 96. Estimated NO_x values versus actual values for run #2.
- Figure 97. NO_x measurements using the mass spectrometer to measure both the NO and NO₂ for VTS-NFK burner in the flameless F2 mode with the furnace at 1250 °C and for 600 °C combustion air (March 31, 2006).
- Figure 98. Universal Stack Sampler Anderson, sampling probe and sampling train.
- Figure 99. Temperature distribution within test slab during heat up process with air burners.
- Figure 100. Temperature distribution within test slab during heat up process with oxygen burners.
- Figure 101. Results from flue gas sampling and flue gas temperature during entire slab heat up process.
- Figure 102. NO_x emissions levels and O₂ levels in flue gas duct during oxygen combustion. [mg/MJ].
- Figure 103. NO_x emissions levels and O₂ levels in flue gas duct during air combustion [mg/m³].
- Figure 104. Detail of flue gas sampling during oxygen case.
- Figure 105. Maximum measured temperature difference in test slab during the two different runs.
- Figure 106. Power distribution in the different zones for the different burners.
- Figure 107. Temperature distribution within test slab during heat up process with air burners.
- Figure 108. Flue gas composition for the air combustion case.
- Figure 109. Flue gas composition for the OXY combustion case 1.
- Figure 110. Flue gas composition for the OXY combustion case 1.
- Figure 111. NO_x emissions levels and O₂ levels in flue gas duct during air combustion [mg/MJ].
- Figure 112. A photo of the oxyburner mounted in the pilot furnace at BFI.
- Figure 113. The pilot furnace at BFI.
- Figure 114. NO_x in mg/MJ for Natural gas, 100 % burner load.
- Figure 115. NO_x in mg/m³ for Natural gas, 100 % burner load.
- Figure 116. NO_x in mg/MJ for Natural gas, 80 % burner load.
- Figure 117. NO_x in mg/m³ for Natural gas, 80 % burner load.
- Figure 118. NO_x in mg/MJ for Coke Oven gas, 100 % burner load.
- Figure 119. NO_x in mg/m³ for Coke Oven gas, 100 % burner load.
- Figure 120. NO_x in mg/MJ for Coke Oven gas, 80 % burner load.
- Figure 121. NO_x in mg/m³ for Coke Oven gas, 80 % burner load.
- Figure 122. Sketch of the method for application of the high temperature reduction procedure for a reheating furnace.

- Figure 123. Experimental set-up with constructed flue pipe in the experimental combustion chamber and sampling points.
- Figure 124. Distribution of the droplet size of the pressure air atomizing nozzle.
- Figure 125. Calculated results of the droplet vaporization in the flue gas flue pipe at 1200 °C.
- Figure 126a-b. Photo and principle of operation of gas-atomizing nozzle for urea injection.
- Figure 127a-b. Photo and principle of operation of secondary air lance.
- Figure 128. Calculated results of the air penetration depth depending on the nozzle diameter.
- Figure 129. Calculated results of the secondary air- flow rate depending on the nozzle diameter.
- Figure 130. Reactor network solution.
- Figure 131a-d. Results of calculations: NO reduction with ammonia and urea at different boundary conditions.
- Figure 132. Course of flue gas concentrations after reduction zone and in the chimney for a stoichiometric adjustment with coke oven gas ($\beta = \text{molar ratio NH}_3/\text{NO}$).
- Figure 133. NO_x concentration results of the first HTR measurement series.
- Figure 134. NH₃ concentration distributions at the end of the flue pipe for all variants showing the quality of the mixing without fittings in the exhaust gas duct (A), and with turbulence variant 1 (B), variant 2 (C), variant 3 (D), variant 4 (E) and lateral additive injection with variant 5 (F).
- Figure 135. View of the ceramic static mixer fitted in the flue pipe in the combustion chamber.
- Figure 136. Effect of the high temperature reduction and the post combustion at different additive molar ratios ($\beta = \text{NH}_3 / \text{NO}$) for the additive injection with two lances at 1000 °C.
- Figure 137. Effect of the high temperature reduction and the post combustion at different additive molar ratios ($\beta = \text{NH}_3 / \text{NO}$) for the additive injection with one side lance at 1200 °C.
- Figure 138. Ammonia concentration measured at position P3 in the HTR process.
- Figure 139. Summary of the total high temperature reduction results (furnace-chimney) with different temperatures and molar ratios.
- Figure 140. Comparison of a DOC-oxy-fuel with 3 types of recuperative reheating furnaces firing natural gas with air combustion. The solid bars are the original analysis, and the striped bar is for the increase in natural gas price to 2006.
- Figure 141. Natural gas prices trends in Europe [73].

5 LIST OF TABLES

- Table 1. Measurements performed by ISQ and measured pollutants.
- Table 2. Classification of side burners for reheating furnaces equipped with a central recuperator.
- Table 3. NO_x reduction (average %) for selected techniques with their advantages and disadvantages.
- Table 4. Examples of some low NO_x burners with some typical NO_x levels firing natural gas for various furnace temperatures and combustion air temperatures.
- Table 5. Techint TSN vs. TSX burner.
- Table 6. Hauck TRIOX 2008 Series burner capacities.
- Table 7. Test matrix for burner characterisation.
- Table 8. Supplier based technical data for the NFK-VTS low NO_x burner.
- Table 9. Gas composition and properties of natural gas and coke oven gas at BFI.
- Table 10. Furnace temperatures and recycle ratio R.
- Table 11. Advantages and disadvantages of flameless low NO_x burners for air and oxy-fuel combustion.
- Table 12. CFD model parameters at CSM.
- Table 13. Arrhenius reaction rate parameters.
- Table 14. Conditions used at CSM for testing the TSX burner.
- Table 15. NO_x measurements and calculated concentrations for trials at CSM.
- Table 16. Physical models and boundary conditions for the CFD model at MEFOS.
- Table 17. Modelling parameters and results.
- Table 18. Data for the Voestalpine slab reheating furnaces.
- Table 19. Arrhenius- Rates and rate (concentration) exponents for the reactions. The parameters are based on data from the project partner CSM.
- Table 20. Gas and air flow-rates of the burners in the reference-case with $\Lambda = 1.05$ in all the zones. If more than 1 burner is modelled, then the flow-rate is the sum over all the burners in this zone of the model.
- Table 21.. Simplified analysis of air, b: simplified analysis of natural gas and c: simplified analysis of coke oven gas.
- Table 22. NO_x in the flue gas calculated for various modes of operation for the furnace.
- Table 23. Slab temperatures for various modes of operation for the furnace.
- Table 24. Flow rates with 100 % coke oven gas.
- Table 25. Gas flows used in the model with blast furnace gas.
- Table 26. Analysis of blast furnace gas.
- Table 27. Heat balance for the gas phase in the model furnace. It is to be noted that the model furnace is only 1/8 of the real furnace, the power is reduced correspondingly.
- Table 28. NO_x concentration with on-off operation corresponding to 70 % power and furnace load of the reference case.
- Table 29. Velocities and corresponding pressure-differences in the Reference case and with air staged burners.
- Table 30. Average actual furnace temperatures from reference case compared with results of the stationary calculation.
- Table 31. NO_x in flue gas in standard case.
- Table 32. Flow rates in the reference case. Indicated are averages over the observed time period.
- Table 33. Measured NO_x in the heating, preheating and convective zones of the Voestalpine slab reheating furnace.
- Table 34. Physical models and boundary conditions at BFI.
- Table 35. Typical NO_x emissions for Techint burners firing natural gas with a furnace temperature of 1250 °C.
- Table 36. Results of the clustering analysis.
- Table 37. Test results on run #1 and run #2.
- Table 38. Test results on run #1 and run #2.
- Table 39. Measurements performed by ISQ and measured pollutants.
- Table 40. Horiba PG-250 specifications.
- Table 41. NO_x reduction for different abatement techniques [64].

- Table 42. Conditions for the different zones of the WBF.
- Table 43. Composition of test slabs.
- Table 44. Scale losses during the experiment.
- Table 45. Compilation of actual operating conditions.
- Table 46. Experimental configurations and flow rates of fuel and oxygen at BFI.
- Table 47. Boundary conditions for the High temperature reduction experimental set-up.
- Table 48. Geometrical data of the ammonia-additive lances.
- Table 49. Geometrical data of the secondary air lances for the tests.
- Table 50. Calculated results for NO reduction with ammonia at different primary excess air coefficients and initial NO concentrations.
- Table 51. Calculated results for NO reduction with urea.
- Table 52. TSP and heavy metal concentration measured at P3 before stack (sample filters 1 and 2).
- Table 53. Operating costs/required additive (for example: ammonia) for a nominal power of 1 MW, a molar ratio of 1.2 and calculated 8000 operating hours per year; additive costs include costs for delivery.
- Table 54. Operating conditions for high temperature reduction and selective non catalytic reduction.
- Table 55. Comparison of oxy-fuel versus fossil fuel-air fired reheating furnaces.

6 LIST OF REFERENCES

- [1] "Int'l Symposium on High Temp. Air Combustion and Gasification", Taiwan, Jan. 1999.
- [2] "4th HATC 2001", Rome, Nov. 2001.
- [3] "6th International Symposium on High Temperature Air Combustion and Gasification", October 17-19, 2005, CityHall Essen, Germany.
- [4] Aguille: Characterisation of burner operating in flameless oxidation mode, IFRF ToTeM25, Stockholm, Sweden, Oct. 2003.
- [5] Quinqueneau A.: InterNOx Project. Integration of new high-performance low-NOx techniques, called "flameless oxidation", into industrial process using natural gas, IFRF ToteM25, Stockholm 2003.
- [6] Blasiak W.: Application of High Temperature Air Combustion in Heat Treatment Furnaces, IFRF ToTeM25, Stockholm, Sweden, Oct. 2003.
- [7] Hasegawa T., Kishimoto S., Suzakawa Y.: "Environmental compatible regenerative combustion heating system", II Int. Seminar on High Temperature Combustion, Stockholm, Jan 2000.
- [8] Wüning J.G.: "FLOX – Flameless combustion", Thermoprocess Symposium, 2003.
- [9] O'Connor S.J. et al. "Performance of the Regenerative Burners in BaoSteel 2050 Hot Strip Mill Furnace Baoshan, China", AISTech 2006.
- [10] D. Szweczyk, J. Sudoh, et. al : "Over Decade of the Industrial Experience in High Temperature Air Combustion Applied with HRS Regenerative Burner", "6th HiTAC, October 17-19, 2005.
- [11] M.Daneri , M. Fantuzzi , E. Malfa , U. Zanusso (2004): "Gas burners technology for iron and steelmaking industry with minimum environmental impact", 59° Congresso ATI, Genova, September 2004.
- [12] M.Daneri et. al "Development of Flameless Gas Burners for Reheating Furnaces", 6th HiTAC, October 17-19, 2005.
- [13] D. Szweczyk and B. Forsberg. "High-cycle regenerative system (HRS burners) and high temperature air combustion technology (HiTAC) – European Industrial Application", ISNGU, September 25-16, 2006, Poznan, Poland.
- [14] J. Niska, A. Rensgard, M. Mörtberg, "NOx-RF Low NOx combustion", Stål 2007, Jernkontoret, Borlänge, Sweden.
- [15] Mörtberg, and R. Tsiava, J. Niska, A. Rensgard, R. Giese and H-P. Gitzinger,"Oxy-combustion – a viable solution for reduced emissions and minimized energy consumption", AFRC International Symposium, Oct. 16-18, 2006, Houston, Texas.
- [16] S.M. Almeida et al; Minimizing NOx emission from reheating furnaces, IFRF members conference 15, Italy, 2007.
- [17] CECA 7210-PR/020 "Optimisation of beam reheating conditions in the reheating furnace", Final Report.
- [18] Flamme, M.et. al "Optimization of Energy Efficiency of Industrial Furnaces", 4th HATC 2001, Rome, Nov. 2001.
- [19] Techint Technologies Furnace: "TS BURNERS: STANDARD SINGLE AIR BURNERS".
- [20] J.G. Wüning, "Flameless Combustion and its Application", IFRF Member Conference Noordwijkerhout, The Netherland, May 2004.
- [21] IFRF Doc N° C108/y/2, Ijmuiden, February 2004.
- [22] B. Cain, T. Robertson, J. Newby, "The development and application of direct fuel injection techniques for emission reduction in high temperature furnace", 2nd International Seminar on High Temperature Combustion 2000, Stockholm, 2000.
- [23] DOE – Industrial Combustion Technology Roadmap April 1999 (at www.oit.doe.gov/combustion)
- [24] M.Daneri , M. Fantuzzi , E. Malfa , U. Zanusso (2004): "Gas burners technology for iron and steelmaking industry with minimum environmental impact", 59° Congresso ATI, Genova, September 2004.
- [25] Funghini, et.al. "Reheating furnace in Germany – Market requirement and technology", MTP International, 5, 2006.
- [26] J. Janicka and W. Kollmann. A Two -Variable Formulation for the Treatment of Chemical Reactions in Turbulent H₂-Air Diffusion Flames. In 17th Symp (int) of Combustion. The Combustion Institute, 1978.

- [27] Glarborg P., Dam–Johansen K., and Kristensen P., Final Report, Gas Research Institute Contract No. 5091–260–2126, Nordic Gas Technology Centre Contract No. 89–03–11, Dec. 1993.
- [28] Glarborg P., Kubel D., Kristensen P., Hansen J., and Dam–Johansen K., Comb. Sc. Tech., 110–111, 461, 1995a.
- [29] Miller, J.A., Glarborg, P. Springer Series in Chemical Physics; Springer-Verlag: Berlin, Germany, 1996.
- [30] Coda Zabetta, E., Hupa, M., A Detailed Kinetic Mechanism with Methanol for Simulating Biomass Combustion and N–Pollutants, submitted to international scientific journal, 2006.
- [31] D. L. Baulch, D. D. Drysdall, D. G. Horne, and A. C. Lloyd (1973) “Evaluated Kinetic Data for High Temperature Reactions”, volume 1,2,3. Butterworth, 1973.
- [32] R. K. Hanson and S. Salimian (1984) “Survey of Rate Constants in H/N/O Systems” In W. C. Gardiner, editor, Combustion Chemistry, page 361, 1984.
- [33] C. P. Fenimore (1971) “Formation of Nitric Oxide in Premixed Hydrocarbon Flames” In 13th Symp. (Int'l.) on Combustion, page 373. The Combustion Institute, 1971.
- [34] B. Binniger, M. Chan, G. Paczkko, and M. Herrmann. Numerical Simulation of Turbulent Partially Premixed Hydrogen Flames with the Flamelet Model. Technical report, Advanced Combustion GmbH, Internal Report, 1998.
- [35] C. M. Muller, H. Breitbach, and N. Peters. Partially Premixed Turbulent Flame Propagation in Jet Flames. Technical report, 25th Symposium (Int) on Combustion, The Combustion Institute, 1994.
- [36] L. Wang, D.C. Haworth, S.R. Turns, M.F. Modest. Interaction among soot, thermal radiation, and NO_x emissions in oxygen-enriched turbulent nonpremixed flames: a computational fluid dynamics modelling study. Combustion and Flame, 2005.
- [37] L. Caracciolo (2004): “Analisi fluidodinamica di getti in ambiente confinato: modello numerico per applicazioni industriali in camera di combustione” 2003-2004, Politecnico di Milano, Dip. Energetica, Relatore Prof. M. Colombo, Co-relatore E.Malfa.
- [38] E.Malfa, E.Colombo, F.Inzoli (2005): “Free Jet in Confined Combustion Chamber: Numerical Model for Industrial Application in Low NO_x Burner”, 2005 Summer Heat Transfer Conference, 17-22/07/2005, San Francisco, USA.
- [39] Malfa E., Venturino M., Macchi E., Tota V. (2002): “Numerical Simulation of Flameless Recuperative Burner”, Fluent User Group Meeting, Maranello, Oct. 2002.
- [40] Tota V. (2002): “Modellazione numerica di un bruciatore a tubo radiante per applicazioni termofotovoltaiche”, Politecnico di Milano, Dip. Energetica, Relatore Prof. E. Macchi, Co-relatore E.Malfa.
- [41] Wilcox D.C. (2000): “Turbulence Modelling for CFD”, DCW Industries Inc., 2000.
- [42] B. F. Magnussen (1981): “On the Structure of Turbulence and a Generalized Eddy Dissipation Concept for Chemical Reaction in Turbulent Flow”, Nineteenth AIAA Meeting, St. Louis, 1981.
- [43] C. Westbrook, F.L Dryer (1981): “Simplified Reaction Mechanisms for the Oxidation of Hydrocarbon Fuels in Flame”, Combustion Science and Rechnology, Vol.27, pp.31-42.
- [44] Yimer, H. A. Becker and E.W. Grandmaison (2001): “The Strng-jet/Weak-jet: New Experiments and CFD”, Combustion and Flame 124:481-502.
- [45] S. B.Pope (1985) :“Pdf methods for turbulent reactive flows” Progress Energy Combustion Science, 11:119, 1985.
- [46] R.H. Hekkerns, M.Mancini (2004): ”Non-isothermal CFD modelof the HEC burner and furnace (Additional Calculation)“, IFRF Doc. No. G108/y/3.
- [47] Yang Weihong and Blasiak Wlodzimierz, “CFD as applied to high temperature air combustion in industrial furnaces”, IFRF Combustion Journal, Nr. 200603, Nov. 2006.
- [48] Marcus Oledal, private communications 2007, ANSYS Sweden/FLUENT Sweden AB, Vestagatan 2B, Göteborg, Sweden.
- [49] D. E. Rumelhart and J. L. McClelland, *Parallel distributed processing*, MIT Press, Cambridge, MA, (1986).
- [50] S. Ridella, S. Rovetta, and R.Zunino, “Plastic algorithm for adaptive vector quantization,” *Neural Computing & Applications*, 7 (1998) 37-51.
- [51] V. Vapnik, *Statistical Learning Theory*, Wiley, New York (1998).
- [52] K. Hornik, M. Stinchcombe and H. White, “Multilayer feed forward networks are universal approximators,” *Neural Networks*, 2(5) (1989) 359-66.

- [53] T. P. Vogl, J. K. Mangis, A. K. Rigler, W. T. Zink and D. L. Alkon, "Accelerating the convergence of the back propagation method," *Biol. Cybern.*, **59** (1988) 257-263.
- [54] Ridella, S. Rovetta, and R. Zunino, "Circular back-propagation networks for classification," *IEEE Trans. on Neural Networks*, **8** (1) (1997) 84-97.
- [55] Bell, Ron D. et al, An overview of technologies for reduction of oxides of nitrogen from combustion furnaces, MPR Associates, Inc., consulted in http://www.mpr.com/pdf_files/nox_control.pdf
- [56] Lambert Darlene et al, NO_x control techniques for the CPI, chemical Engineering, June 1996, pages 98-101.
- [57] Suzanne Shelley, Destroying Emissions with Catalysts, Chemical Engineering, July 1997, pages 57-60.
- [58] Zandaryaa, Sarantuyaa et al, Nitrogen oxides from waste incineration: control by selective non-catalytic reduction, *Chemosphere* 42, 2001, 491-497.
- [59] Lefan, M. et al, "Removal of NO_x from Flue Gas with Iron Filings Reduction Following Complex Absorption in Ferrous Chelates Aqueous Solutions", *Journal of the Air & Water Management Association*, Volume 54, December 2004, pages 1543-1549.
- [60] Grigorios C. Koltsakis, et al, "Storage of Chemical Species in Emission Control Systems: The Role of Mathematical Modelling", presented in the 2001 GLOBAL POWERTRAIN CONGRESS: Detroit, MI, June 5-7, 2001.
- [61] U.S. Environmental Protection Agency, Office of Air Quality Planning and Standards, "Nitrogen Oxides (NO_x), Why and How They Are Controlled", Research Triangle Park, North Carolina, November 1999.
- [62] Rajkumari Kumaraswamy, "Ecophysiological characterization of microbial communities in BioDeNO_x reactors", PhD Thesis Tech. Univ. Delft, The Netherlands, 2005.
- [63] PMF van der Maas, "Chemically enhanced biological NO_x removal from flue gases-Nitric oxide and ferric EDTA reduction in the BioDeNO_x reactors", PhD Thesis, Wageningen, The Netherlands, 2005.
- [64] "NO_x Abatement Techniques", Appendix to draft final report for NO_x-RF project.
- [65] John Niska, Anders Rensgard, Magnus Mörtberg, "NO_x-RF Low NO_x combustion", Stål 2007, Jernkontoret, Borlänge, Sweden.
- [66] Mörtberg, and R. Tsiava, J. Niska, A. Rensgard, R. Giese and H-P. Gitzinger, "Oxy-combustion – a viable solution for reduced emissions and minimized energy consumption", AFRC International Symposium, Oct. 16-18, 2006, Houston, Texas.
- [67] Lefebvre, A. H.: *Atomization and Sprays*. New York: Hemisphere Publishing Corporation, 1989. – ISBN 0-89116-603-3.
- [68] Kolb, T.: *Experimentelle und theoretische Untersuchungen zur Minderung der NO_x-Emissionen technischer Feuerungen durch gestufte Verbrennungsführung*. Dissertation, Technical University Karlsruhe, Germany, 1990.
- [69] Lyon, R.K., Hardy, J.E.: *Discovery and development of the thermal DeNO_x process*. *Ind. Eng. Chem. Fundam.* 1986, 25, 19-24.
- [70] Jönsson, B., Outokumpu, NO_x reduktion i praktiken, Jernkontoret seminar, Stockholm, Sweden, 18 April 2006.
- [71] M. Riley, "Dilute oxygen combustion", DOE, DE-FC36-95ID13331, April 2003.
- [72] U.S. Regional Natural gas prices: Base case, Energy Information Adm. May 2007, at: <http://www.eia.doe.gov/emeu/steo/pub/6ctab.html>
- [73] Quarterly review of European electricity and gas prices, Sept. 2006, Issue 8, at: http://ec.europa.eu/energy/electricity/publications/doc/review/2006_09_qr08.pdf
- [74] REBOX Revamping a walking beam furnace with oxy-fuel combustion, Linde AG, at: http://www.linde-gas.com/international/web/lg/com/likelgcomn.nsf/docbyalias/ind_rebox_publications
- [75] J. Adolfi, T. Ekman, J. von Scheele and W. Blasiak, "Scale formation and surface quality of carbon steel at oxy-fuel heating" presented at Steel Rolling 2006, Paris, France at: www.linde-gas.com
- [76] N. Krishnamurthy, W. Blasiak and A. Lugnet, "Development of high temperature air and oxy-fuel combustion technologies for minimized CO₂ and NO_x emissions in industrial heating", Joint Int'l Conf. on Sustainable Energy and Environment, 1-3 Dec. 2004, Hua Hin, Thailand.

- [77] H. Sho Kobayashi and B. Van Hassel, “CO2 reduction by oxy-fuel combustion: Economics and opportunities”, presented at the GCEP Advanced Coal Workshop, Provo, Utah, March 15, 2005.
- [78] “Oxy-fuel combustion in a rotary hearth heating furnace”, sales literature Linde Gas Division, Linde AG at www.linde-gas.com
- [79] P. Fredriksson, E. Claesson, P. Vesterberg, A. Lugnet and O. Ritzen, “Application of oxy-fuel combustion in reheating at Ovako, Hofors works, Sweden – Background, solutions and results”, Steel Rolling 2006, Paris, France.